University of Nottingham
UK | CHINA | MALAYSIA

Evaluating human Induced Pluripotent Stem Cell-Derived Cardiomyocytes for Commercial Drug Testing

Submitted by

Puspita Anggraini Katili, MD, MSc

4255054

Thesis submitted to The University of Nottingham
for the degree of Doctor of Philosophy

School of Medicine
Department of Stem Cell Biology

December 2019

Acknowledgements

I would like to thank my supervisor, Prof. Chris Denning, for his constant guidance and support throughout my studies at The University of Nottingham over the last 3 years. I would also like to thank my previous supervisor, Dr. Vinoj George, for his guidance and support during my studies in the first year. My gratitude extends to Dr. Alexander Thompson for his support as second supervisor over the last 3 years, and Assoc. Prof. Lopa Leach for her support during the first and second year viva as my internal assessor.

I would like to thank Dr. Karl Firth for his guidance, support, and training to introduce me to Crack-IT project before his leave. My huge appreciation goes to Ms. Nurul Mohd Yusof, for being my work partner during the Crack-IT project Tier 2 phase and thereafter, sharing the joy and pain during the process. An enormous thank you to Mr. James Awford, Mr. Jayson Bispham, and Ms. Maria Barbadillo-Mũnoz for their big assistance during the Crack-IT project Tier 2 phase. Many thanks as well to Dr. James Smith, Dr. Diogo Mosqueira, Dr. Jamie Bhagwan, and Ms. Ana Tellechea-Lopez for their assistance during the process.

I am grateful to Dr. Robert Markus for training of super resolution microscopy, as well as Ms. Denise McLean for training of transmission electron microscopy, both in the School of Life Sciences Imaging and Microscopy (SLIM) facility. I am also grateful to Ms. Katarzyna Lis-Slimak for training of high content image analysis.

Big thank you should also go to Ms. Caroline Reffin, Ms. Penny Gwynne, Dr. Alexander Kondrashov, Dr. Divya Rajamohan, Dr. Spandan Kalra, Dr. Minh Duc Hoang (Harry), and Ms. Ngoc Vo Thi (Kate) for their enormous support and some occasions of having good time together. I would like to thank my housemates Afsaneh, Asma, and Deborah for their patience and support during the writing process of this thesis. I am very thankful to my friends Jeir and Katie for their willingness to proofread this thesis.

Greatest appreciation to my workplace at Department of Biochemistry and Molecular Biology, Faculty of Medicine, Universitas Indonesia, and from my sponsor Indonesia Endowment Fund for Education (LPDP). Both of them provided opportunity for me to be enrolled for this PhD studies.

Finally, I would like to dedicate this thesis to my parents Irwan and Hendri, my younger brother Adrian, and my sister-in-law Xandratysta for their unwavering love and selfless devotion.

Declaration

I hereby declare that this thesis has been composed by myself and has not been submitted for any other degree previously. Acknowledgements of specific procedures not performed by myself are stated; otherwise, the work described is my own.

Puspita Anggraini Katili _____

Date: 20 December 2019

Abstract

The cost of developing new drugs has increased by ~100 fold in recent decades, largely due to high attrition rate in clinical development caused by cardiotoxicity. Since the recent discovery of human induced pluripotent stem cell–derived cardiomyocytes (hiPSC-CMs), it has been developed as a novel, promising *in vitro* research tool in preclinical testing of drug-induced cardiotoxicity. However, major limitation of currently available hiPSC-CMs is their immature phenotype, which can hinder evaluation of contractile dysfunction.

Existing contractility monitoring on hiPSC-CMs is currently being done at low throughput or by using surrogate markers (e.g. impedance). In addition, there has been no detailed cross-site validation study to evaluate the effect of drugs on hiPSC-CMs contractility. A multinational consortium was established with the University of Nottingham as the academic lead, in order to address the CRACK-IT InPulse Challenge. The Challenge consisted of two phases that lasted for 3.5 years.

This project was part of the consortium aimed to develop medium throughput technology platform that could measure contractility in hiPSC-CMs as a physiologically-relevant functional output for use in preclinical drug safety evaluation. The University of Nottingham utilised CellOPTIQ® platform, a medium-high throughput screening platform to measure contractility and electrophysiology.

Protocols were unified across all academic partners via a drug training set in phase 1, allowing subsequent blinded multi-centre evaluation of drugs with known positive, negative, or neutral inotropic effects in phase 2. Accuracy ranged from 44% to 85% across the platform-cell configurations. Refinement to test conditions was addressed after blinded testing, which resulted in increased accuracy to 85% for 2D monolayers and 93% for 3D EHT system.

Through this study, hiPSC-CMs cultured in 2D and 3D platform have been shown to considerably have a value in predictive safety pharmacology despite their immaturity status and current technology evolution.

Table of Contents

List of Figures

List of Tables

Abbreviations

Abbreviation	Description
AC	adenylyl cyclase
ACE	angiotensin converting enzyme
ACh	acetylcholine
AKAP	A kinase anchoring protein
ANOVA	Analysis of variance
ATP	adenosine triphosphate
CA	contraction amplitude
cAMP	cyclic adenosine monophosphate
CICR	Calcium-induced calcium release
CM	Cardiomyocyte
CO	CellOPTIQ
CT	contraction time
cTnT	cardiac troponin-T
Cx43	connexin 43
DAPI	Di-amino phenyl-indole
DMEM	Dulbecco's (Modified Eagle's) minimal essential medium
DMSO	Dimethyl sulfoxide
E8	Essential 8 medium
EC50	half maximal effective concentration
EHT	Engineered Heart Tissue
FTCP	free therapeutic plasma concentration
GTP	guanosine triphosphate
hERG	human eag-related gene
hESC	Human embryonic stem cell
hESC-CM	Human embryonic stem cell-derived cardiomyocyte
hiPSC	Human induced pluripotent stem cell
hiPSC-CM	Human induced pluripotent stem cell-derived cardiomyocyte
hPSC	Human pluripotent stem cell
hPSC-CM	Human pluripotent stem cell-derived cardiomyocyte
IC50	half maximal effective inhibitory concentration
iPSC	Induced pluripotent stem cell
M2-Rec	M2-muscarinic receptor
MLC2a	Myosin Light Chain Atrial
MLC2v	Myosin Light Chain Ventricular
n.d	not defined
NE	no effect

NI	negative inotrope
PDE	phosphodiesterase
PI	positive inotrope
PKA	Protein kinase A
PLB	phospholamban
Reg	PKA regulatory subunit
ROCKi	Rho-associated kinase inhibitor
RT	relaxation time
RyR	ryanodine receptor
SD	Standard deviation of the mean
SEM	Standard error of the mean
SERCA	Sarcoplasmic reticulum Ca^{2+}-ATPase
SR	Sarcoplasmic reticulum
SSR inhibitor	selective serotonin reuptake inhibitor
TTM	Triple Transient Measurement
β-AR	β-adrenergic receptor
%	Percentage
^{0}C	Degree Celsius
RMP	Resting Membrane Potential
AP	Action Potential
TdP	Torsades de Pointes
ECG	Electrocardiogram
EB	Embryoid bodies
HCN	Hyperpolarization-activated cyclic nucleotide-gated channels

1 Introduction

1.1 Thesis rationale

The pharmaceutical industry is facing a significant challenge as the ever-increasing cost of drug discovery and development is largely caused by high attrition rate in clinical development due to cardiotoxicity. Although the number of animals used in preclinical drug development remains extremely high, the accuracy of predicting toxicity in human is limited by species difference, particularly in cardiac structure and function. The discovery of human induced pluripotent stem cell–derived cardiomyocytes (hiPSC-CMs) has led to the development of a novel *in vitro* platform in preclinical testing of drug-induced cardiotoxicity. However, a major concern is immature phenotype of hiPSC-CMs, which can hinder evaluation of contractile dysfunction.

Although large-scale efforts to evaluate drug-induced electrophysiological (proarrhythmia) toxicity using hiPSC-CMs have been made, similar initiatives on other aspects of cardiotoxicity such as changes in cardiac contractility have lagged behind. This is surprising, as altered function of the contractile myocardium is usually the first clinical manifestation of drug-induced cardiotoxicity.

CRACK-IT InPulse Challenge specified that hiPSC-CMs should be used as a source of physiologically-relevant cells for development of a new *in vitro* assay. The hiPSC-CMs with an enhanced/matured phenotype were to be integrated into a technology platform that could allow recording (potentially simultaneously) of electrophysiology, Ca^{2+} handling and contractility. To answer the challenge, a multinational consortium was established between pharmaceutical company (GlaxoSmithKline; GSK), a UK funding agency (National Centre for the Replacement, Refinement and Reduction of Animals in Research; NC3Rs), and 4 academic labs in the UK, Netherlands, and Germany. (The University of Nottingham as the academic lead, followed by the University of Glasgow, Leiden University Medical Center, and the University Medical Center Hamburg-Eppendorf), with focus on contractility assay. Parallel or simultaneous measures for electrophysiology and/or Ca^{2+} handling were done as optional parameters

in order to compliment and/or help on interpretation of drug's inotropic effect responses tested on hiPSC-CMs.

Chapter 3 outlines the first phase of the project, which was a Tier 1 'training set' of 8 unblinded drugs from GSK to rationalise which platforms and cell configurations, as well as unification of standard operating procedures, between the partner sites that would be taken forwards into the final testing. This ran concurrently with evaluating methods for improved hiPSC-CMs maturation.

Chapter 4 outlines the second, which is also the final phase of the project, aimed to evaluate the predictivity of Tier 2 'test set' of 28 blinded drugs from GSK. Results demonstrated the lack of accurately predicted positive inotropic drug responses on hiPSC-CMs, in particular on 2D platform.

Chapter 5 outlines the follow up study with simple refinement of the test conditions involving change of culture medium and/or use of the pacemaker I_f current blocker, ivabradine, and prolonged exposure of the drugs for the chronic toxicants, which increased the predictivity with an accuracy of 85-93%, comparing favourably with *in vivo* animal models.

1.2 Drug development process

In the drug development pipeline, large compound libraries are narrowed down through a series of assays in order to identify and characterise pharmacological activity associated with molecular target(s), off-target(s), and safety liabilities (Moffat et al., 2017). These assays involve *in silico* screens, heterologous cell lines, primary cells, organotypic models and preclinical assessment in animals, before candidate drugs are taken into Phase I-III clinical trials.

However, drug development is cumbersome with a long and costly process. Costs are rising exponentially particularly in late, clinical stages of drug development. On average, 37 new drugs are launched to market each year over the last 20 years (Moffat et al., 2017, Denning et al., 2016), yet cost of development has now increased from ~$14M per drug in the 1960s to ~$1.5Bn (**Figure 1-1**), inflation adjusted (Catapult, 2018, IFPMA, 2017).

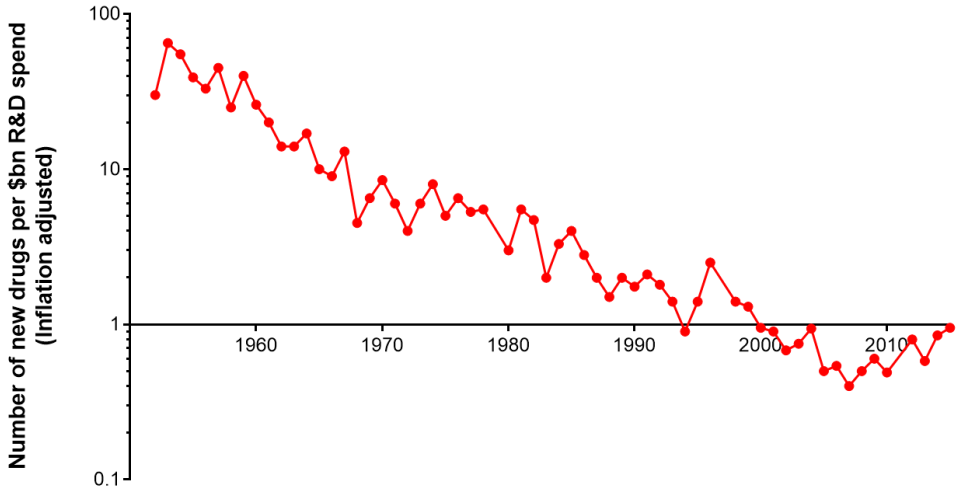

Figure 1-1. Long term productivity of drug discovery is in decline. The cost of developing new drugs has increased by ~100 fold as depicted in inflation adjusted graph for drug discovery between 1953 and 2014. Adapted from (Catapult, 2018).

Attrition rates remain high, with only ~2% of the drugs entering Phase 1 clinical trials actually proceeding to be used in patients. A key concern is cardiovascular toxicity with an estimated ~45% of all drug withdrawals (Laverty et al., 2011), with 79 (17%) of the 462 drugs withdrawn from market (Onakpoya et al., 2016) and 41% of the top 200

prescribed drugs being labelled with adverse drug reaction or 'black box' warnings (Fuentes et al., 2018). Therefore, many pharmaceutical companies follow a 'fail early, fail cheap' approach, with the risk of wasting potentially valuable drugs.

Between 1990 and 2006, 13 drugs were withdrawn from the market due to altered cardiac electrophysiology (Shah, 2006). This led to establishment of International Conference on Harmonization (ICH) S7B guidelines for pro-arrhythmic risk detection using simplified *in vitro* assays to measure blockade of the rapid component of the delayed rectifier potassium I_{Kr} current, commonly known as the human Ether-à-go-go-Related Gene (hERG) (Food and Drug Administration, 2005b). Inhibition of hERG-dependent current I_{Kr} is a common cause of severe ventricular arrhythmias, such as "Torsades-des-Pointes" (TdP) arrhythmias (Del Rosario et al., 2010). Combined with the ICH E14 guidelines (Food and Drug Administration, 2005a) on electrocardiogram (ECG) monitoring, drug withdrawal due to altered electrophysiology has reduced, with no reported incidences since 2007. These approaches have improved safety, but the relatively poor specificity for predicting human outcomes and oversimplification of the assays has raised concern that promising drug candidates may be abandoned too early due to either false negatives or positives (Gintant, 2011). Example is shown in multi-channel blocking drug, verapamil (Redfern et al., 2003), which is marked as potentially harmful in single ion channel assays and yet is safe in humans. This is representation of the inability of these assays to detect interactions with other ion channels (e.g. calcium, sodium) or multichannel blocks, due to not replicating the complexity of the native cardiomyocytes.

1.2.1 Animal model in drug screening

It is well-known that animal models may not accurately represent human cardiotoxicity because of species differences in cardiac structure and function. The heart beat rate in rats and mice (300–400 and 500–700 bpm, respectively) (Gintant et al., 2019) is ~10 times faster compared with human cardiomyocytes (60 bpm) (Denning et al., 2016, Davis et al., 2011). Increases in heart rate are associated with increased force of contraction in humans but decreased force in mice (Doevendans et al.,

1998). Ion currents for depolarisation (I_{Na} and I_{CaL}) are comparable between mouse and human cardiomyocytes. For repolarisation, in mouse it is driven primarily by I_{to} as a predominant current, yet this role is achieved by the potassium channels, I_{Kr} and I_{Ks} in humans (Salama and London, 2007) (**Figure 1-2**). The role of ion channels in electrophysiology will be explained further in section 1.3.3.

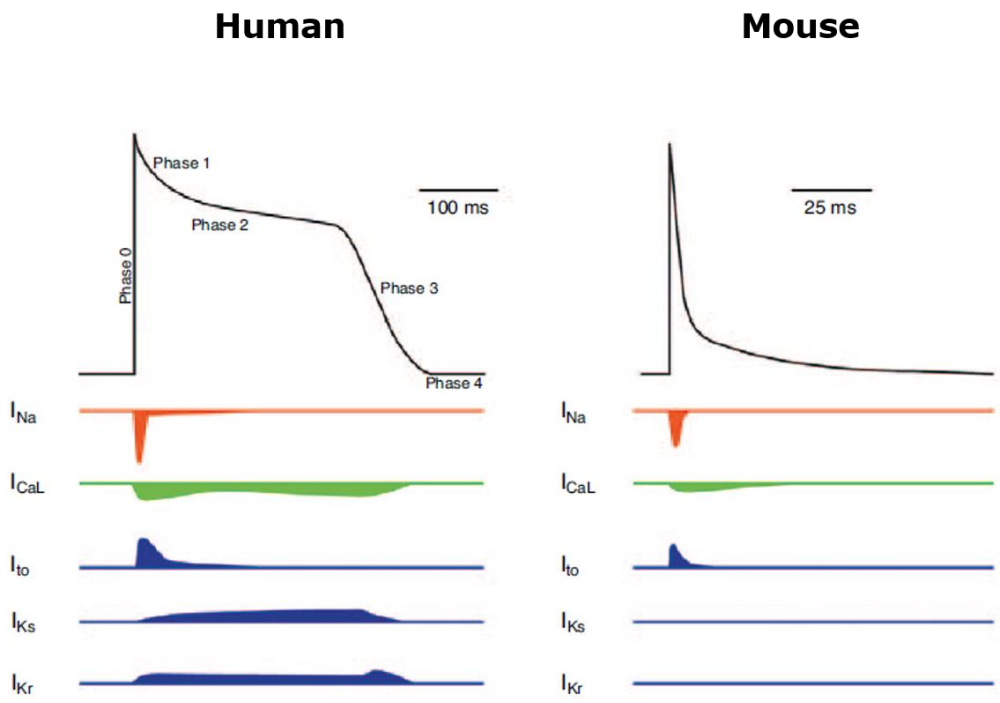

Figure 1-2. Schematic illustration comparison of electrophysiology properties between adult human and mouse cardiomyocytes. Action potential (AP) durations and shapes of the ventricular cardiomyocytes are distinctively different between these two species due to their ionic currents. Abbreviation: ms, millisecond. Adapted from (Davis et al., 2011).

The differences, as mentioned previously, mean that mice are at least 10× more tolerant to 37% of drugs than humans (Denning et al., 2016). Issues applied as well to rats and larger animals such as dogs, which tolerate 4.5- to 100-fold the concentration of various chemotherapeutic agents than humans, such as ThioTEPA, Myleran, Actinomycin-D, Mitomycin C, Mithramycin, and Fludarabine (Price et al., 2008).

More than 6000 candidate drugs are in preclinical development stage in 2015, using millions of animals at a total cost of $11.3Bn, a financial value only surpassed by Phase 3 clinical trials, with a total cost of $15.3Bn.

Only ~1700 drugs (~30%) proceeded to Phase 1 clinical trials, and yet only 56 (<1%) made it to market (Moffat et al., 2017, Denning et al., 2016). Reducing drug attrition in Phase 1 clinical trials by 5% could reduce development costs by 5.5–7.1% (Schachter and Ramoni, 2007), with total savings of about $100M.

Thus, there is a pressing need in developing alternative, human-based models for drug safety assessment, which include human pluripotent stem cell–derived cardiomyocytes (hPSC-CMs). Human embryonic stem cells (hESCs) are derived from the inner cell mass of the preimplantation embryo and thus raise ethical issues, whereas human induced pluripotent stem cells (hiPSCs) are derived from epigenetic reprogramming of human somatic cells. Therefore, although both cell types have similar properties, hiPSCs are more preferred by industry. Furthermore, hiPSCs can be generated from a wide variety of sources, including skin fibroblasts, mononuclear blood cells, and urinary cells (Raab et al., 2014, Xue et al., 2013).

1.2.2 hiPSC-CMs for drug screening

Primary human cardiomyocytes is the ideal tool for predicting cardiotoxicity from drug effects. However, their large-scale use is hindered by near non-existent proliferation and/or almost immediate de-differentiation in culture, whilst limited availability and poor consistency are additional burdens (Denning et al., 2016, Eschenhagen et al., 2015). Since the discovery of human induced pluripotent stem cell-derived cardiomyocytes (hiSPC-CMs) (Takahashi et al., 2007), these cells have emerged as promising tools for cardiac research. Recent studies have documented efficient production of hiPSC-CMs of >85% purity at scale (Smith et al., 2018, Mosqueira et al., 2018), both in academic and commercial laboratories.

Therefore, the attraction of using hiPSC-CMs to complement or replace existing model systems are several-fold with several advantages as follow: (1) overcoming the issue of primary cardiomyocytes as hiPSC-CMs can be maintained for months, and in extreme cases 1-2 years, in culture and can be shipped between labs in either live or cryopreserved formats; (2) representing human heart physiology compared to animal

model (as described in previous section), therefore enhancing the translation between basic research and clinical science; (3) more accurate in predicting hERG assay compared to recombinant cells highly expressing I_{Kr}-carrying ion channels; (4) able to integrate population- and disease-based variability in drug responses (Matsa et al., 2016) as hiPSC-CMs retain the genetic identity of the individual donor; (5) providing no ethical and practical concerns as well as being compliant with the 3R principles (reduce, refine, and replace animal experimentation), and (6) reducing costs compared with animal experiments (as described in previous section).

However, despite the numerous advantages offered, there are also several limitations of the hiPSC-CM models: (1) have immature phenotype with fetal (~week 16) characteristic (Yang et al., 2014a, Chen et al., 1999), raising the question whether using hiPSC-CMs provides higher validity compared to experiments using animal, (2) still have heterogeneous population with atrial- or nodal-like phenotypes despite predominant ventricular phenotype in most of generated hiPSC-CMs (Moretti et al., 2010), (3) confounding factors found in cultured cells such as cellular heterogeneity, batch-to-batch variations of medium supplements, the risk of karyotypic abnormalities, and (4) could not evaluate systemic effects of drugs *in vitro*.

1.2.2.1 Current status of hiPSC-CMs in cardiac electrophysiology assays

The most prominent of studies investigating the impact of drugs on the electrophysiology of hiPSC-CMs is the Comprehensive *in vitro* Proarrhythmia Assay (CiPA), and recently followed by a complimentary approach from the Japan iPS Cardiac Safety Assessment (JiCSA) initiatives (Sager et al., 2014, Fermini et al., 2016, Kanda et al., 2018). CiPA was aimed at providing a framework for proarrhythmic risk assessment of new drugs *in vitro* with improved specificity compared to the assays currently recommended by ICH-S7B. These included: 1) assessment of several major ion channels in transfected cell lines; 2) *in silico* modelling of the ion channel effects; 3) proarrhythmic assessment in hiPSC-CMs; and 4) clinical assessment of electrocardiograms (ECGs) from phase I human studies.

Meanwhile, JiCSA established a multi-electrode array (MEA) protocol using 60 drugs which largely overlapped with the 28 drugs used in CiPA.

Data that emerged from CiPA show that optical- and multi electrode array-based platforms using commercially-sourced hiPSC-CMs play a significant role for validation and implementation of hiPSC-CMs in cardiac safety pharmacology. These platforms enable an 87% accuracy in predicting proarrhythmic liability across geographically diverse testing laboratories (Blinova et al., 2018) with similar studies being reported by others (Bot et al., 2018).

1.2.2.2 Current status of hiPSC-CMs in cardiac contractility assays

Despite large-scale studies on evaluating altered electrophysiology on hiPSC-CMs, investigation on other aspects of cardiotoxicity such as changes in cardiac contractility are lagging behind. Data from a large pharmaceutical company, GlaxoSmithKline (GSK), revealed direct damage to the myocardium and cardiac electrophysiology accounts for 30% and 22%, respectively, of the cardiovascular liability. Assessing changes in contractility is recommended within the ICH-S7A guidelines (Food and Drug Administration, 2001), although as part of the follow-up/supplementary studies.

Changes in cardiac contractility can be assessed clinically in altered left ventricular ejection fraction (LVEF) (Marwick, 2018). Preclinical assessments involve isolated cardiomyocytes, *in vivo* studies, isolated whole heart models (Guo et al., 2009), or *ex vivo* heart tissue, which are limited in throughput. Therefore, there is an increased focus on the development of novel *in vitro* models with higher throughput. Cardiac myocyte function is described by changes in contraction force (inotropy), contraction time (clinotropy, time to peak contraction), relaxation time (lusitropy, time to relaxation), and beat rate (chronotropy). However, translation of *in vitro* contractility parameters to clinically relevant data is not always straightforward.

Most of hiPSC-CM-based approaches are using indirect measurements of contractility, such as impedance signals, Ca^{2+} flux, sarcomere shortening, image-based contractile motion, and video-based cell geometry technologies (Scott et al., 2014, Pointon et al., 2015).

Subsequent studies (Pointon et al., 2017, Archer et al., 2018) showed that predictivity of detecting inotropic effects could be enhanced by using 3D cardiac microtissues composed of hiPSC-CMs, cardiac endothelial cells, and cardiac fibroblasts. The first study demonstrated that improvements in contractility were due to higher expression of genes for calcium handling, myofilaments and beta-adrenergic signalling, yet not due to morphological maturation and anisotropy. The second study demonstrated that the approach was able to detect changes at clinically relevant concentrations and provide insights into the phenotypic mechanisms of this liability.

However, there is still a need for improved methods in predicting changes in cardiac contractility. Moreover, there has been no detailed cross-site validation study to evaluate the inotropic drug effects on hiPSC-CMs contractility.

1.3 Characteristics of human cardiomyocytes

Native cardiac cells are under constant physical and electromechanical stimulation. This leads to activation of mechanosensitive signalling pathways, which affects cardiomyocytes phenotype (Salameh et al., 2010, Trepat et al., 2007, Zhuang et al., 2000).

Native heart ECM network is predominantly composed of collagen type I (80%) (Kai et al., 2011), which during development accumulates in the environment of the cardiomyocytes and results in increased tissue elasticity. Adult human heart tissue has elastic modulus value ranging from 0.02 to 0.5 MPa (Tallawi et al., 2015), 10 to 20 kPa (Sommer et al., 2015, Handorf et al., 2015). This increased elasticity affects the sensitivity of cardiomyocytes, demonstrated by increase in expression of myofibril protein and sarcomere alignment (Capulli et al., 2016, Yang et al., 2014a). This ECM network directs the anisotropic alignment and maintains the rod-like architecture of cardiomyocytes (Fleischer and Dvir, 2013).

1.3.1 Morphology of cardiomyocytes

Adult cardiomyocytes are large, elongated anisotropic rod-shaped cells with highly organised sarcomeres (Gerdes et al., 1998). They have length-to-width ratio (also known as aspect ratio) within a range of 7 to 9.5:1 in mammalian species (Gerdes, 2002, Gerdes and Capasso, 1995, Gerdes et al., 1992). Conversely, fetal and early phase hPSC-CMs (first month after contraction is initiated) are known to have small, circular or polygonal, disorganised sarcomeres and have lower aspect ratio of 2 to 3:1 (Hartman et al., 2016, Yang et al., 2014a, Robertson et al., 2013, Kuo et al., 2012) (***Figure 1-3***). In addition, 25-30% of mature cardiomyocytes are marked by binucleation phenotype, while hPSC-CMs are mostly mononucleated (Zhang et al., 2015, Bergmann et al., 2009). Cell surface area is significant for action potential depolarisation velocity and total contractile force (Spach et al., 2004). However, hPSC-CMs has been reported to have cell surface area 9- to 13-fold smaller compared to adult cardiomyocytes (Ribeiro et al., 2015).

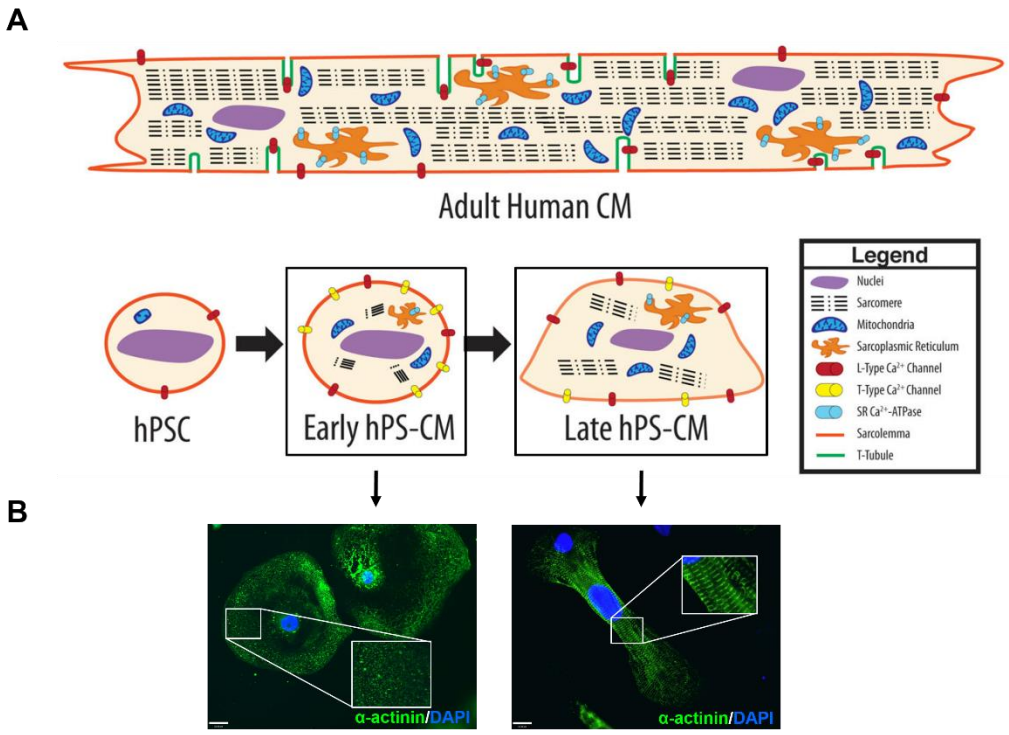

Figure 1-3. Illustrations depicting morphology of early, late, and adult hPSC-CMs. (A) Adult hPSC-CMs have distinct structure with larger, elongated shape and have multinucleation, highly organised sarcomere with large sarcomere area and abundant mitochondria. In contrast, hPSC-CMs have smaller, circular shape with mononucleation, poorly organised sarcomeres. (B) Representative images of early (left) and late (right) stage of hPSC-CMs. (A) is adapted from (Robertson et al., 2013). Scale bar: left 31 μm; right 15 μm.

1.3.2 Sarcomere

Sarcomere is the contractile unit of cardiomyocytes, defined as the region between two Z-discs that form the boundaries of each sarcomere unit. Adult cardiomyocytes have sarcomere length of average 2.2 μm while hPSC-CMs have shorter sarcomere length (~1.6 μm) (Yang et al., 2014a). Each sarcomere consist of thick (myosin) and thin (actin) filaments. Ultrastructural images by electron microscopy in adult cardiomyocytes show sarcomere unit as banding pattern (***Figure 1-4***). Cytoskeletal protein α-actinin is expressed in Z-discs. Extending from Z-discs is the I-band, an area with only actin filaments (where regulatory proteins troponin and tropomyosin are interlocked with). Located between two I-bands in the middle of sarcomere is the A-band, consisting of interdigitating actin and myosin filament, and in the middle of the A-band lies the H-zone containing only myosin filament, and in the centre of the H-zone is the M-band, which

contains M-band proteins (myomesin, M-protein). During heart development, sarcomerogenesis, a process in which sarcomeric proteins assemble into a highly organised structure, develops first from Z-dics and I-bands, followed by the generation of H-, A-, and M-bands (Veerman et al., 2015).

In majority of hPSC-CMs however, H-, A-, and M-bands are not observed in ultrastructural images. Study by Kamakura et al., 2013, of hPSC-CMs differentiated using embryoid bodies (EBs) method, after 360 days on 2D culture showed the presence of M-bands, however the gene expression level of M-band-specific protein myomesin 1 (MYOM1), myosin heavy chain 7 (MYH7), and myosin regulatory light chain 2 (MYL2) are still considerably lower compared to adult cardiomyocytes. M-bands are known to be indicative of sarcomeric structure maturation; however, from this study, the presence of M-bands alone is not sufficient to determine final stage of maturation.

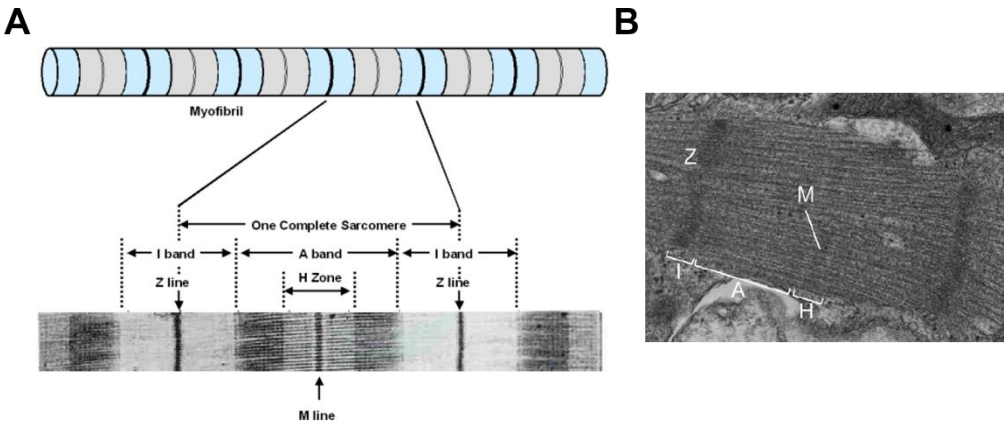

Figure 1-4. Ultrastructure of cardiomyocytes. (A) Myofibril is a contractile element and sarcomere is the functional unit of a myofibril, with banding pattern A-, H-, I-, M-, and Z-bands in each one sarcomere unit found in adult cardiomyocytes. (B) Transmission electron microscopy image of 1-year old hiPSC-CMs showing ultrastructural maturation, indicated by M-band presence. Adapted from (Blaber, 2001, Kamakura et al., 2013).

1.3.3 Physiology of cardiac function

1.3.3.1 Cardiac rate and rhythm

The normal cardiac rhythm is initiated by pacemaker impulses that occur in the sinoatrial (SA) node and are conducted in sequence through the atria, the atrioventricular (AV) node, bundle of His, Purkinje fibres and ventricles. SA nodal cells depolarise automatically in which basal rate (known as heart rate) is modulated by the autonomic nervous system. Increased sympathetic activity will increase the rate, whilst increased parasympathetic activity will decrease the rate. AV nodal conduction is slow and also modulated by the autonomic nervous system. Increased sympathetic activity, resulting in higher heart rate, will accelerate AV nodal conduction and shorten the PR interval on the electrocardiogram (ECG). In contrast, increased parasympathetic activity, resulting in lower heart rate, will slow AV nodal conduction and prolong the PR interval. The delay between atrial and ventricular electrical activity, enacted by the AV node, allows sufficient time for atrial contraction to affect diastolic filling of the ventricles (Vetulli et al., 2018, Vassalle, 1971). These structures have electrical excitability to voltage-sensitive sarcolemma (striated muscle cell membrane) channels selective for several ions, including Na^+, K^+, and Ca^{2+}, with electrophysiological features described further in section **1.3.5**.

Cardiac rhythm is related to Ca^{2+} currents, as it involves a slow inward Ca^{2+} current which initiates action potentials (APs) in SA and AV nodes, and during the plateau there is an influx of Ca^{2+} (Lakatta et al., 2010, Maltsev et al., 2006). The heart contains voltage-dependent calcium channels in the sarcolemma, which are important in controlling cardiac rate and rhythm. The main type of voltage-dependent calcium channel in adult ventricular cardiomyocytes is L-type Ca^{2+} channel (LTCC), $Ca_v1.2$, or DHPR (encoded by gene *CACN1C*). LTCC is the main pathway for Ca^{2+} entry into adult cardiomyocytes (Harvey and Hell, 2013). T-type Ca^{2+} channel expression is lower in adult ventricular cardiomyocytes compared to those found in embryonic and neonatal cardiomyocytes (Louch et al., 2015), but is expressed mainly in conducting and pacemaker cells (Bers, 2008). $Ca_v1.2$ expression level gradually increases at a later stage of human heart development and increases further in adult (Qu and Boutjdir, 2001). In hPSC-CMs, $Ca_v1.2$ levels have been reported to increase with prolonged

time culture (>60 days), similar to those observed in adult ventricular cardiomyocytes (Otsuji et al., 2010, Magyar et al., 2000). Unlike in pacemaker cells, LTCC does not contribute substantially to the rapid rising phase of the AP in ventricular cardiomyocytes (Bers, 2008).

Cardiac rhythm can be disrupted either by heart disease or by the action of drugs or circulating hormones. The most common cause of cardiac arrhythmia is ischaemic heart disease, with ventricular fibrillation following after myocardial infarction (Jalife, 2016, Demidova et al., 2012). Fibrillation is a condition where chaotic electrical activity causes heart chambers to stop contracting in a coordinated way, leading to rapid uncoordinated contractions within ventricles or atria that do not support output from the affected chambers (Weiss et al., 2005).

Arrhythmia are classified according to: (1) the site of origin of the abnormality (atrial, junctional, or ventricular) and (2) rate change (tachycardia as increased and bradycardia as decreased). The most common types of tachyarrhythmia are atrial fibrillation (completely irregular) and supraventricular tachycardia (SVT; rapid but regular) (Narayan and Zaman, 2016). Less common but more severe tachyarrhythmia are ventricular tachycardia and ventricular fibrillation (completely chaotic electrical activity in the ventricles and ceased cardiac output) (Jalife, 2016). Bradyarrhythmia includes several heart blocks (e.g. at the AV or SA node) and asystolic arrest (complete cessation of electrical activity) (Barstow and McDivitt, 2017).

The mechanism underlying cardiac arrhythmia are: (1) delayed after-depolarisation, (2) re-entry, (3) ectopic pacemaker activity, and (4) heart block. The main cause of delayed after-depolarisation is abnormally raised intracellular Ca^{2+} by spontaneous sarcoplasmic reticulum (SR) Ca^{2+} release events. This SR Ca^{2+} release activates Na^{+}/Ca^{2+} exchange which accounts fully for transient inward current that depolarises membrane potential toward threshold for an AP (Pogwizd et al., 2001, Bers et al., 2002). Raised intracellular Ca^{2+} concentration also contributes to opening of non-selective cation channels in the sarcolemma. Altogether, these trigger inward current and thus a wave of abnormal APs (Bers, 2008, Wit and Cranefield, 1977). Re-entry occurs when the electrical wave repetitively excites the atria or ventricles after the refractory period has subsided, which is often

found after myocardial damage. Ectopic pacemaker activity which occurs during myocardial damage is caused by increased sympathetic activity resulting from released epinephrine due to pain, and by partial depolarisation resulting from ischaemic damage. Heart block refers to a condition where electrical impulse fails to propagate in its normal direction and in sequence depolarise the myocardium. Heart block may result from ischaemic damage especially in the AV node. In complete heart block, atrial and ventricles beat independently, with the ventricles beating at a slow rate as affected by the pacemaker picks up distal to the block (Wagner et al., 2015).

1.3.3.2 Cardiac contractility

The mechanisms underlying the myocardial force production is the actomyosin crossbridge interaction. The activation of crossbridges, which underlies cardiac contraction, is initiated by Ca^{2+} binding to troponin C (TnC) with the subsequent conformational changes of troponin/tropomyosin complex (tropomyosin, troponin I (TnI), and troponin T (TnT)) to allow actomyosin interaction. The cardiac relaxation occurs when Ca^{2+} is pumped back into the sarcoplasmic reticulum (SR) by the sarcoplasmic reticulum Ca^{2+} -ATPase pump (SERCA) and transported outside the cell by the Na^{+}–Ca^{2+} exchanger (NCX) (Bers, 2008). This is further explained in **section 1.3.6**.

The myosin head attaches to actin and the resulting crossbridge rotates to produce force for a certain amount of time (force-producing state duration), before detaching again back to basal rate (non-force-producing state duration). The formation of a crossbridge facilitates the formation of crossbridges at neighbouring actin sites and the binding of Ca^{2+} at neighbouring TnC sites. The crossbridge binding and force generation enhance the affinity of Ca^{2+} binding to TnC, therefore slowing Ca^{2+} dissociation and thus prolonging the active state. Contractile force depends on the number of crossbridges attached per unit of time (Hasenfuss and Teerlink, 2011). Therefore, inotropy, i.e. the number of cross-bridges activated, depends upon: (i) Ca^{2+} concentration to bind to TnC, (ii) affinity of Ca^{2+} to TnC, and (iii) alterations at the level of the cross-bridge cycle.

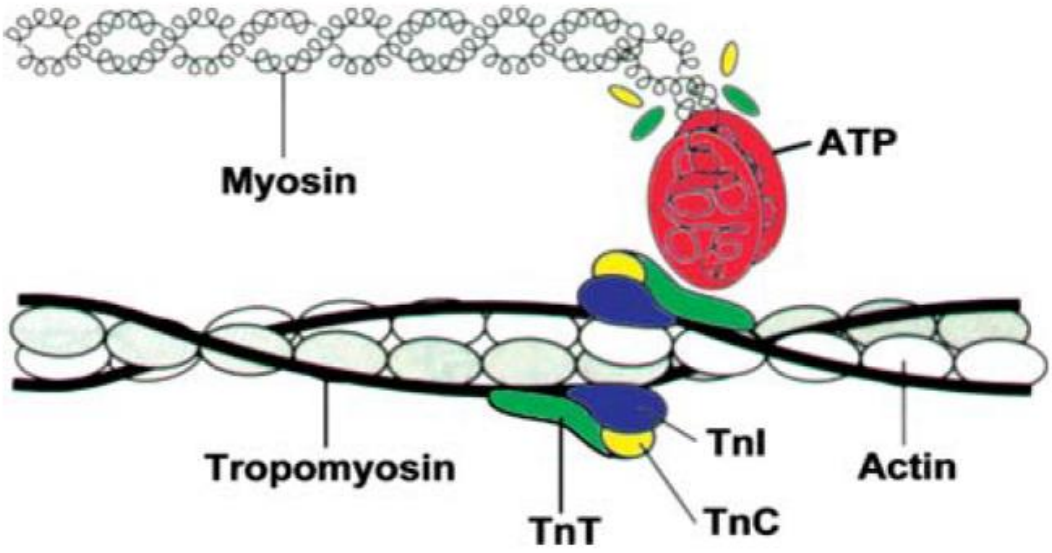

Figure 1-5. **Actomyosin crossbridge interaction as the mechanisms underlying the cardiac contractility machinery**. The myosin head carrying the ATPase site attaches to actin in order to produce force. This mechanism is facilitated by the binding of Ca^{2+} to troponin C (TnC) which leads to a conformational change of tropomyosin, troponin I (TnI), and troponin T (TnT). Adapted from (Hasenfuss and Teerlink, 2011).

The most crucial mechanism to regulate the basal heart contractile force is length-dependent activation of crossbridges, which is achieved by increasing sarcomere length. This condition allows for more optimal overlap of thick and thin filaments, thereby allowing more formation of crossbridges and greater force production. Myofilament overlap contributes to the Frank-Starling law, in which greater diastolic filling leads to stronger contraction (Sequeira and Van Der Velden, 2015, Konhilas et al., 2002). At increased heart rate, efflux of Ca^{2+} via the NCX is slower than influx of Ca^{2+} via LTCC. This contributes to accumulation of intracellular Ca^{2+} entering the cardiomyocyte that is sequestered into the SR by SERCA, in which later is released in greater amounts on the following beat. Altogether, this 'Bowditch-Treppe' effect (positive chronotropy) recruited more crossbridges and increased contractile force (Hasenfuss and Pieske, 2002). Another endogenous inotropic mechanism to increase contractile force include catecholamine via the β-adrenoceptor-adenylyl cyclase system or via stimulation of α-receptors. Mechanism involving β-adrenoceptors are further explained in **section 1.3.4** and **section 1.3.7**.

1.3.4 Autonomic control of the cardiovascular system

Autonomic control of the cardiovascular system is defined by the sympathetic and parasympathetic inputs, which regulate cardiac chronotropy (heart rate), inotropy (myocardial contraction), and lusitropy (myocardial relaxation).

1.3.4.1 Sympathetic (adrenergic) control

The sympathetic nervous system controls the release of the catecholamines epinephrine and norepinephrine, which then travel through the systemic circulation, where they act on adrenoreceptors throughout the body. Epinephrine and norepinephrine act as agonists for α- and β-receptors in the vasculature and the myocardium. Adrenergic receptors in myocardium are primarily of the β subclass (Bristow et al., 1988, Feldman, 1993), with composition of 65% β_1 and 20% β_2 in the nonfailing heart (Bristow, 1993). Norepinephrine is the dominant endogenous cardiac neurotransmitter and has 30 to 50 times greater affinity for the β_1 compared with the β_2 receptor. Therefore, β_1 is the predominant regulator of contractility and heart rate in the nonfailing heart (Gilbert et al., 1993).

Stimulation of the β-adrenoceptor on myocardium leads to increased heart rate (positive chronotropic effect), increased force of contraction (positive inotropic effect), and more rapid atrioventricular (AV) conduction (Motomura et al., 1990). The positive chronotropic effect results from an increased slope of the pacemaker potential (Hutter, 1956). The mechanism underlying positive inotropic effect is stimulation of adrenergic receptors in the sarcolemma leading to an increase in intracellular Ca^{2+} concentration. This process is initiated and amplified by a membrane-bound transduction system, which consist of: (1) adrenergic receptors, (2) guanine nucleotide-binding proteins (G proteins), and (3) the effector enzyme adenyl cyclase (AC) (Lambert, 1993), which will be further described in section **1.3.7**. The increase in intracellular Ca^{2+} concentration has effect on the transient inward current. The resulting increase after-depolarisation following single stimulus leads to increased AV conduction (Wit and Cranefield, 1977). Activation of β_1-adrenoceptors stimulates the Na^+/K^+ pump (NKA) which can repolarises damaged myocardium following myocardial infarction.

Therefore, epinephrine is one of the most important drugs used during cardiac arrest.

α_1-adrenoceptors constitute 13% to 15% of the adrenergic receptors in ventricular myocardium (Bristow, 1993). Stimulation of α_1-adrenoceptors also has a positive inotropic effect. α_2-adrenoceptors are found primarily in vascular smooth muscle and in the central nervous system (CNS) (Ruffolo, 1985). Whereas stimulation of α_2-adrenoceptors leads to vasoconstriction, α_2 agonist such as clonidine has sympathetic inhibition effect due to decreased norepinephrine secretion from the CNS. Therefore, clonidine is frequently used in the management of hypertension (Giovannitti et al., 2015).

1.3.4.2 Parasympathetic control

The parasympathetic innervation to the heart is mediated by the neurotransmitter acetylcholine which then travels to the sinus node, atrioventricular node, and cardiomyocytes. Muscarinic receptors in myocardium are predominantly of the M_2 subtype, and the density is 2- to 2.5-fold greater in the atria than in the ventricles in contrast to the uniform distribution of β receptors (Brodde et al., 1992). In contrast to adrenergic stimulation, cholinergic stimulation reduces heart rate (negative chronotropic effect), force of contraction (negative inotropic effect) in atria only, and block of AV conduction. The negative chronotropic effect results from opening of G protein-activated inward rectifying K^+ channel (GIRK) by M_2 receptors, increasing K^+ permeability. This leads to hyperpolarising current which opposes the inward pacemaker current (Hutter, 1956). The mechanism underlying negative atrial inotropic effect is activation of inhibitory receptors in the sarcolemma, limiting the accumulation of intracellular Ca^{2+}. Both the increased K^+ permeability and reduced intracellular Ca^{2+} concentration contribute to conduction block at the AV node, where propagation depends on the Ca^{2+} current.

1.3.5 Cardiac electrophysiology in cardiomyocytes

Ion channels are pore-forming, transmembrane proteins taking part in establishing and controlling voltage gradients through the selective and directional flow of ions. The 'action potential' (AP) in cardiomyocytes is created by the balance between depolarising and repolarising ion currents through these ion channels (Nerbonne, 2004).

Cardiac action potential (AP) is the event where changes of transmembrane electrical potential in cardiomyocytes happen in a time-dependent manner, which is characterised by 5 phases (0-4) (Garg et al., 2018, Liu et al., 2016a) (***Figure 1-6***). Phase 4 is the resting state with resting membrane potential (RMP) ~-90 mV. Phase 0 is initiated when cardiomyocytes are electrically stimulated through gap junctions, elevating the RMP to the threshold at which voltage-gated sodium channels (Na_v, that mediate I_{Na}) open. This is the rapid depolarisation phase that is marked by a rapid influx of Na^+, shifting the membrane potential toward the Na^+ equilibrium potential of +40 mV. Phase 0 is then followed by time-dependent inactivation of Na^+ channel that resulted in a brief activation of the transient outward potassium current (I_{to}), which is phase 1 (brief repolarisation). This is subsequently followed by an influx of Ca^{2+} by activation of voltage-gated L-type Ca^{2+} channels (LTCC). The following phase 2 (plateau phase) is a period when there is a near equal influx of Ca^{2+} and efflux of K^+, with the inward currents mediated by LTCC ($I_{Ca,L}$) and the sodium calcium exchanger (I_{NCX}), and outward currents (I_{Kr} and I_{Ks}) mediated by 2 different voltage-gated delayed rectifier potassium channels. Phase 3 is the rapid repolarisation phase when efflux of K^+ dominate influx of Ca^{2+} after LTCC inactivate late in the plateau phase. Inwardly rectifying potassium channels (Kir2.1, that mediate I_{K1}) contribute to late phase 3 and phase 4, which is when membrane potential is close to equilibrium, thus called diastolic phase.

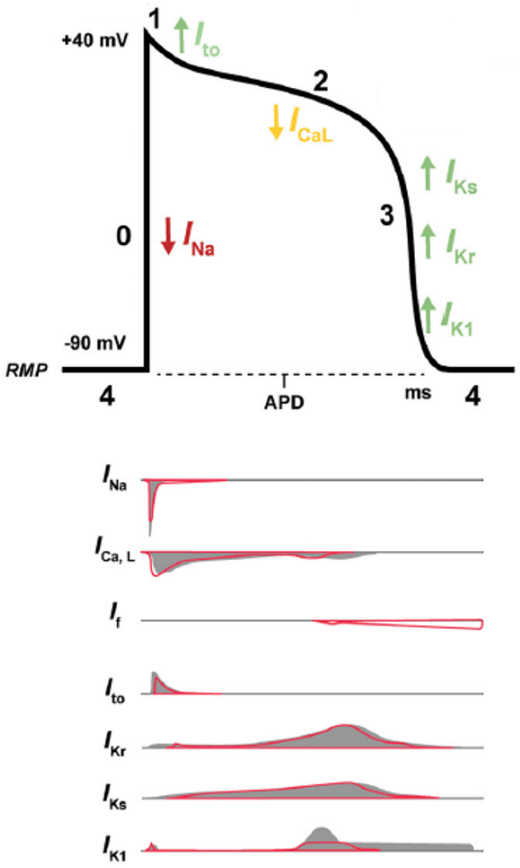

Figure 1-6. Schematic illustration of electrophysiology properties in ventricular cardiomyocytes. Different phases (0-4) of action potential with various depolarising (arrows down) and repolarising (arrows up) ion currents are shown in top figure, whereas relative amount of various ion currents in adult ventricular cardiomyocytes (grey) vs hiPSC-CMs ventricular subtype (red) are shown in bottom figure. Abbreviation: APD, action potential duration; ms, millisecond; RMP, resting membrane potential. Adapted from (Garg et al., 2018).

Modest changes of the inward and outward conductances during plateau phase can lead to different action potential morphologies, such as spike-and-dome shape in ventricular subtype cardiomyocytes and triangular shape in atrial subtype cardiomyocytes. Atrial cardiomyocytes have more prominent expression of I_{to} yet lesser expression of I_{K1} compared to ventricular cardiomyocytes (Shibata et al., 1989). Pacemaker cells have a hallmark feature different from that of ventricular and atrial cells; that is, spontaneous beating in the absence of an external stimulus. The automaticity involves the funny current (I_f), mediated by the hyperpolarization-activated cyclic nucleotide-gated channels (HCN) (Lakatta et al., 2006). The RMP is more depolarised (-50 to -65 mV),

causing the Na^+ channels to be mostly inactivated. This resulted in low upstroke velocity due to phase 0 only mediated by slowly activating I_{CaL}. Since I_{to} is absence in pacemaker cells, phase 1 is non-existent. I_f activates at the end of phase 3 and contribute to phase 4 (Biel et al., 2009).

1.3.6 Excitation-contraction coupling and calcium homeostasis

Heart contraction-relaxation involves a calcium-related feedback mechanism in excitation-contraction coupling (ECC). In adult cardiomyocytes, contraction is initiated with an extracellular Ca^{2+} influx during membrane depolarisation through L-type Ca^{2+} channel (LTCC), $Ca_v1.2$ channels at invagination of t-tubular network, which triggers the release of stored Ca^{2+} from the sarcoplasmic reticulum (SR) via ryanodine receptor 2 (RyR2) (Lai et al., 1988), a process called Ca^{2+}-induced-Ca^{2+} release (CICR) (Fabiato, 1983). This combination of Ca^{2+} influx and Ca^{2+} release from SR results in increased Ca^{2+} in cytosol about 10-fold in only tens of milliseconds (Louch et al., 2015), by binding of Ca^{2+} to myofilament protein troponin C (TNNC1). The binding allows translocation of tropomyosin (release of inhibition induced by troponin I (TNNI3)), followed by the attachment of myosin to actin filaments. The filaments slide past one another resulting in shortening of sarcomere, thus leading to contraction of myofilaments. Ca^{2+} storage capacity in SR is regulated by calreticulin in embryonic stage (Mesaeli et al., 1999), whose expression reduces during development and is later replaced with calsequestrin in adult cardiomyocytes (Ioshii et al., 1994). Together with triadin and junctin, calsequestrin forms a complex that take part in regulation of Ca^{2+} associated with RyR-dependent SR release (Gyorke et al., 2009) (***Figure 1-7***).

Relaxation begins when a negative feedback mechanism occurs to stop further Ca^{2+} influx by removing Ca^{2+} from cytosol. There are two events to retrieve resting Ca^{2+} level: (1) Ca^{2+} is re-sequestered into SR via the sarcoplasmic-endoplasmic reticulum Ca^{2+} -ATPase (SERCA) that are regulated by phospholamban (PLN), and (2) Ca^{2+} is extruded to the extracellular space via the Na^+ -Ca^{2+} exchanger (NCX) or Ca^{2+} ATPase pump. These allow Ca^{2+} to be released from binding to troponin C. The

changes in Ca^{2+} level, rise and then decay, is known as Ca^{2+} transient (Bers, 2002).

Ca^{2+} handling properties in hPSC-CMs resemble those of human fetal cardiomyocytes, and thus are known to have robust yet slower rate Ca^{2+} transient kinetics (Lee et al., 2011, Hwang et al., 2015). hPSC-CMs have smaller amplitudes and slower Ca^{2+} transients kinetics compared to adult cardiomyocytes (Li et al., 2013). Studies in hPSC-CMs have reported lack of presence of transverse tubules (t-tubules) (Parikh et al., 2017, Knollmann, 2013, Gherghiceanu et al., 2011), resulting in entry of calcium mainly via sarcolemma instead of from SR release (Dolnikov et al., 2006), with calcium release being slow and spatially inhomogeneous (Lee et al., 2011).

T-tubules are invaginations in sarcolemma, and is located between adjacent sarcomeres (Z-disc) (Flucher et al., 1993). T-tubules contain ion channels that are important for excitation–contraction coupling (ECC; signal transmission from sarcolemma to actin/myosin filaments mediated by Ca^{2+}) (Orchard et al., 2009). This structure is critical for effective, rapid ECC in adult cardiomyocytes as a majority of Ca^{2+} influx that triggers intracellular sarcoplasmic reticulum (SR) Ca^{2+} release enters via t-tubules, $Ca_v1.2$ density being higher in t-tubules compared to sarcolemma (Brette and Orchard, 2003).

The spatial separation between $Ca_v1.2$ and RyR2 due to lack of presence of t-tubules in hPSC-CMs results in inefficiency of CICR (Lieu et al., 2009, Zhang et al., 2013). Increased level of Ca^{2+} occurs initially at the cell periphery, and then diffuses to the central region of the cell, thus delaying activation of RyR2. This explains how the Ca^{2+} wavefront observed in hPSC-CMs is non-uniform and exhibits a U-shape with the rise of calcium in the periphery being faster than centre (Li et al., 2013, Lieu et al., 2009).

In hPSC-CMs, Ca^{2+} release from non-SR calcium stores is suggested to be predominant and Inositol-3-phosphate receptor (IP_3R) is suggested to have a role in that part (Itzhaki et al., 2011, Dolnikov et al., 2006). Furthermore, hPSC-CMs is shown to be sensitive to IP_3 and IP_3R antagonists in contraction rate (Itzhaki et al., 2011) although this might be due to relation with RyRs inhibition (Kim et al., 2010). It is currently

still unclear the relationship of IP_3-mediated Ca^{2+} release with other Ca^{2+} handling pathways (Kane et al., 2015).

A study using thyroid hormone T3 (triiodothyronine; 100 nmol/L) and glucocorticoid Dex (dexamethasone; 1000 nmol/L) in hiPSC-CMs during days 16 to 30 of differentiation was conducted to observe t-tubule development and improved excitation-contraction coupling (Parikh et al., 2017). hiPSC-CMs were then dissociated and cultured as single cells on Matrigel mattress, an extracellular matrix with physiological stiffness, for an additional 5 days. The study found that the combination of T3+Dexamethasone on a Matrigel mattress contributed to the formation of t-tubules. This was done by cellular staining for regulators of t-tubule genesis: BIN1 (bridging integrator 1), JP2 (junctophilin-2), and Cav3 (caveolin-3) (Manfra et al., 2017, Ziman et al., 2010). However, the t-tubules remained sparser and less organised compared to adult human ventricular cardiomyocytes. The formed t-tubules by treatment of T3+Dexamethasone on Matrigel mattress enhanced excitation-contraction coupling by greater contribution of SR Ca^{2+} release to CICR and spatially and temporally uniform Ca^{2+} release. Furthermore, RyR2 structural organisation was found as clusters, suggestive of dyad formation which is found in adult ventricular myocardium. The resulting increased coupling between the RyR2 and LTCC allowed more efficient negative feedback of SR Ca^{2+} release on LTCC (i.e. increased Ca-dependent inactivation of LTCC). Combination of T3+Dexamethasone without Matrigel mattress however gave same results with control cells. This study therefore emphasised on the importance of extracellular matrix for hiPSC-CMs maturation in addition of chemical compounds.

Evidence of immature t-tubule formation is also demonstrated in a previous study using 3D engineered heart tissues (EHTs) during days 30 to 35 of differentiation with 2-3 weeks of culture before measurements (Mannhardt et al., 2016), with punctual yet irregular staining pattern and poorly organised of Cav3- and JP2-positive structures. More recent study from a different group used a combination of EHTs and electrical stimulation by dissociating hiPSC-CMs on day 12 of differentiation to form 3D tissue, followed by increasing frequency for two weeks from 2 to 6 Hz followed by one week at 2 Hz. EHTs were cultured for 4 weeks before

measurements, and this study demonstrated robust t-tubules with spacing optimised for calcium handling and its positioning near to SERCA2A and NCX1 (Ronaldson-Bouchard et al., 2018).

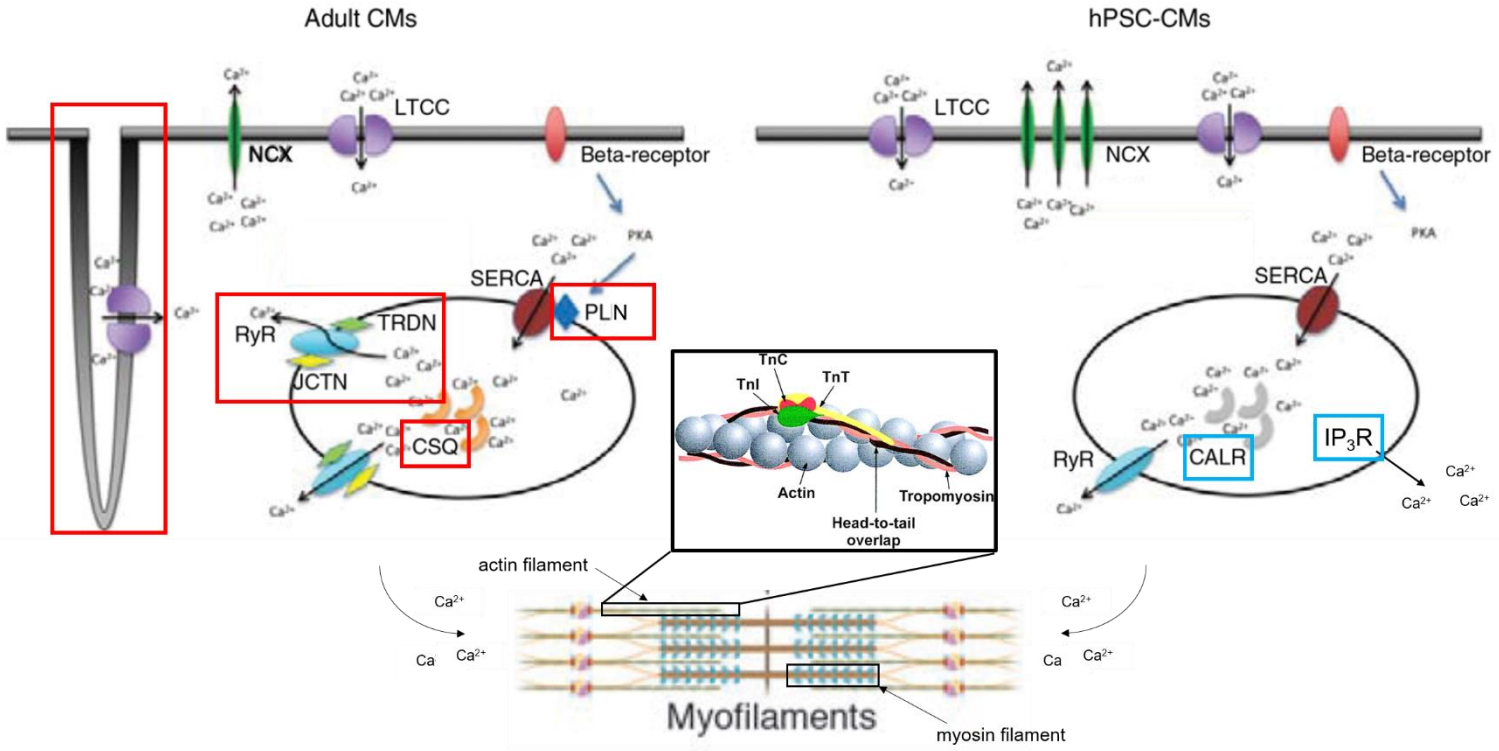

Figure 1-7. Schematic of Ca^{2+} handling in comparison between adult cardiomyocytes (red box) and hPSC-CMs (blue box). hPSC-CMs has been characterised by (1) lack of t-tubules and dyads, (2) lack of ryanodine receptor (RyR) and its associated protein junctin (JCTN) and triadin (TRDN), (3) lack of calsequestrin (CSQ) that is replaced by calreticulin (CALR), (4) lack of phospholamban (PLN), and (5) dominance distribution of IP_3R along SR membrane. Adapted from (Li et al., 2013, Jurkat-Rott and Lehmann-Horn, 2005, Gordon et al., 2000).

1.3.7 Regulation of β-adrenergic signalling in calcium homeostasis

Physiological sympathetic release of noradrenaline (NA) in the myocardium stimulates β_1-adrenergic receptors, which leads to increased contraction force (positive inotropy), decreased relaxation time (positive lusitropy), and decreased Ca^{2+} in cytosol (Bers, 2002). These 7-transmembrane receptors activates a GTP-binding protein (Gs), which stimulates adenylyl cyclase (AC) to produce cyclic adenosine monophosphate (cAMP) from adenosine triphosphate (ATP). cAMP then activates cAMP-dependent protein kinase A (PKA), which phosphorylates several proteins involved in ECC coupling (phospholamban, PLN; L-type Ca^{2+} channels, LTCC; ryanodine receptors, RyRs; troponin I and myosin binding protein C) (**Figure 1-8**).

Phosphorylation of PLN and troponin I leads to decreased relaxation time (positive lusitropy) by increasing the sarcoplasmic reticulum (SR) Ca^{2+} re-uptake via SERCA and dissociation of Ca^{2+} from the myofilaments, respectively. Increased SR Ca^{2+} reuptake contributes to increased SR Ca^{2+} content. Combination of increased I_{Ca} and SR Ca^{2+} leads to increased contraction force (positive inotropy). This combination affects the increase in Ca^{2+} transient amplitude and decrease in myofilament calcium sensitivity due to phosphorylation of troponin I. However, PKA-dependent phosphorylation altering RyRs behaviour during rest or ECC is inconsistent by showing an increase, decrease, or no effect (Bers, 2002, Winslow et al., 2005).

In ventricular subtype cardiomyocytes, the activation of β1-adrenergic receptors leads to robust inotropic and lusitropic effects, which is paralleled by phosphorylation of LTCC, PLN and troponin I. On the contrary, the activation of β2-adrenergic receptors may be more limited to increased I_{Ca} (Kuschel et al., 1999), and β2-adrenergic receptors are located almost exclusively in caveolae, a specialised sarcolemmal invaginations (Rybin et al., 1999).

M_2-muscarinic receptor activation by β1-adrenergic receptors leads to decreased cAMP, whereas said activation by β2-adrenergic receptors leads to increased cAMP (Aprigliano et al., 1997). This may be partly because of the relative exclusion of M_2-muscarinic receptors from caveolae.

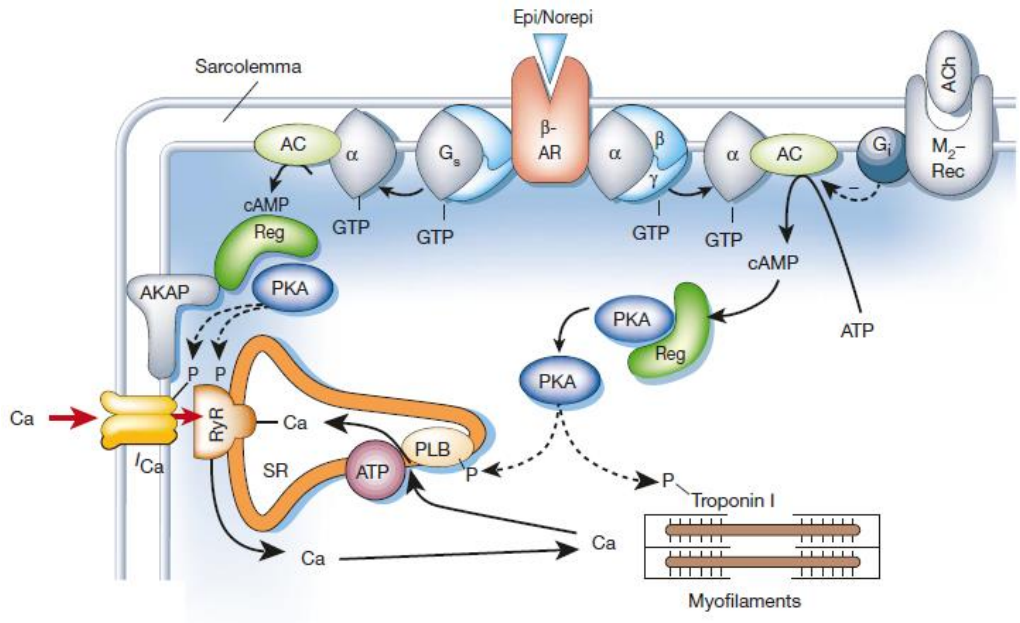

Figure 1-8. β-adrenergic receptor-mediated regulation of excitation-contraction coupling by activation and phosphorylation of target proteins. Abbreviations: AC, adenylyl cyclase; ACh, acetylcholine; AKAP, A kinase anchoring protein; ATP: adenosine triphosphate; β-AR, β-adrenergic receptor; cAMP, cyclic adenosine monophosphate; Epi: epinephrine; Norepi: norepinephrine; GTP: guanosine triphosphate; M_2-Rec, M_2-muscarinic receptor; PKA: Protein kinase A; PLB, phospholamban; Reg, PKA regulatory subunit; RyR: ryanodine receptor; SR, sarcoplasmic reticulum. Adapted from (Bers, 2002).

Phosphodiesterase (PDE) breaks down cAMP by hydrolysing it and therefore hindering the positive inotropic effects of β-adrenergic stimulation (Kiuchi et al., 1993, Brodde, 1993, Guellich et al., 2014). Thus, PDE inhibitors can sensitise the cardiomyocytes to β-adrenergic stimulation and are used as positive inotropic compounds. PDE3 has been identified as the dominant isoforms in the adult human heart (Richter et al., 2011) and confirmed by another study done in human ventricular trabeculae (Eschenhagen, 2013), whereas the other isoform PDE4 is also involved in rodent (Johnson et al., 2012). However, recent study on blinded drug screening using hiPSC-CMs in engineered heart tissues (EHTs) demonstrated positive lusitropic effect with no inotropic effect of PDE4 inhibition (by rolipram) and yet no effect of PDE3 inhibition (by milrinone) (Mannhardt et al., 2017), suggesting the immature cardiomyocyte phenotype, despite in 3D platform. As comparison, the human atrial trabeculae in the same study showed no effect after treated with rolipram,

and both positive inotropic and lusitropic response after treated with milrinone.

1.4 Physiology and clinical use of common antiarrhythmic drugs in cardiovascular disease

Despite the wide used in cardiovascular disease, antiarrhythmic drugs remain of modest efficacy. Furthermore, antiarrhythmic drugs have also been hindered by proarrhythmic actions as well as other adverse effects (Lafuente-Lafuente et al., 2015). Nevertheless, antiarrhythmic drugs are still an essential part of managing patients with atrial and ventricular arrhythmias. Antiarrhythmic drug development has been slow due to currently limited understanding of the role of ionic currents in arrhythmogenesis (Kumar and Zimetbaum, 2013).

Based on modernised version of the Vaughan Williams system (Lei et al., 2018), antiarrhythmic drugs are further classified as:

- Class 0 – HCN channel blockers (e.g. ivabradine)
- Class I – voltage-gated Na^+ channel blockers (e.g. quinidine, lidocaine, flecainide)
- Class II – autonomic inhibitors and activators (e.g. atenolol, isoprenaline, atropine, digoxin, adenosine)
- Class III – K^+ channel blockers and openers (e.g. amiodarone, dofetilide, nicorandil)
- Class IV – Ca^{2+} handling modulators (e.g. bepridil, verapamil)
- Class V – mechanosensitive channel blockers (e.g. *N*-(p-amylcinnamoyl) anthranilic acid)
- Class VI – gap junction channel blockers (e.g. carbenoxolone)
- Class VII – upstream target modulators (e.g. captopril, enalapril, valsartan, pravastatin)

This section will focus on antiarrhythmic drugs that will be used in further result chapters, with a summary of their mechanisms of action and clinical applications as depicted in **Figure 1-9** and **Table 1-1**.

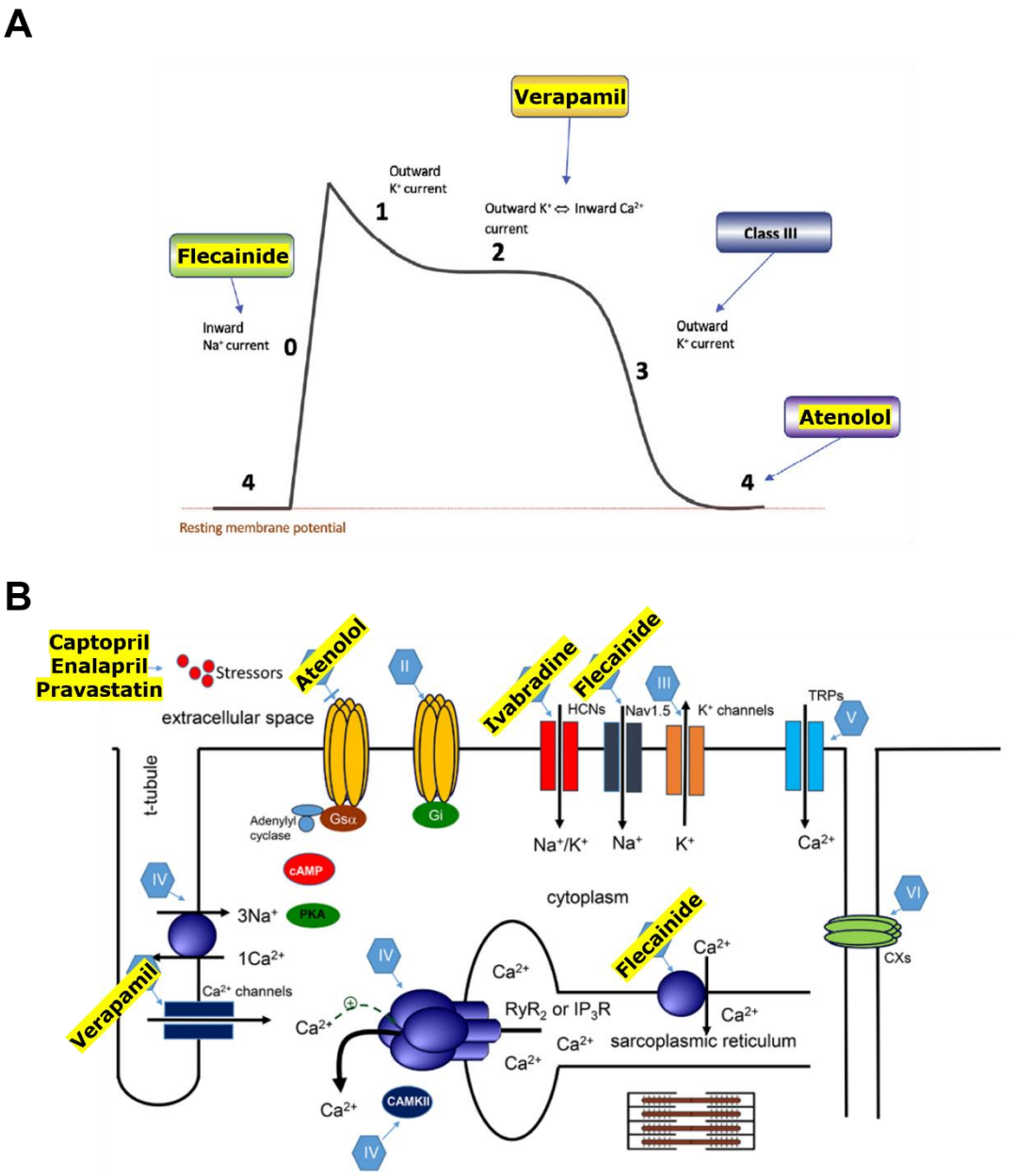

Figure 1-9. **Antiarrhythmic drugs and their mechanisms of action**. (A) Schematic illustration of action potential in ventricular cardiomyocytes and role of various antiarrhythmic drugs in each AP phases. (B) Cellular mechanism of electrophysiological and inotropic effect of antiarrhythmic drugs in cardiomyocytes. Abbreviations: CaMKII, calcium/calmodulin kinase II; Cx, connexin; G_i, inhibitory G protein; G_s, stimulatory G-protein; HCN, hyperpolarization-activated cyclic nucleotide-gated channel; Nav1.5, cardiac Na^+ channel protein; PKA, protein kinase A; RyR2, cardiac ryanodine receptor type 2; and TRP, transient receptor potential channel. Adapted from (Mankad and Kalahasty, 2019, Lei et al., 2018).

1.4.1 HCN channel blockers

Ivabradine acts through blockade of "funny current" (I_f) carried by hyperpolarisation-activated cyclic nucleotide (HCN)-gated channels in the sinoatrial node (SAN) cells (Difrancesco, 2006). The blockade in the pacemaker cells reduces the Na^+ and K^+ flow, thereby flattens the spontaneous depolarisation slope. This results in heart rate reduction when initial heart rate is high, without direct effect on contractility or on the vascular (Komajda, 2017). Furthermore, ivabradine reduces myocardial oxygen demand without inducing hypotension (Guha et al., 2016). In patients with systolic heart failure, chronic stable angina, and potential management of sinus tachycardia, ivabradine has been shown to give no clinically significant adverse effects (Koruth et al., 2017).

1.4.2 Voltage-gated Na^+ channel blockers

Flecainide acts by slowing conduction in the atria, His-Purkinje system, ventricles, and accessory pathways (Kowey et al., 2000). In addition, flecainide also prolongs, in particular, atrial refractoriness. At higher heart rates, these actions are more marked, thereby effective in ceasing atrial fibrillation, despite it sometimes resulted in atrial flutter (Naccarelli et al., 1996). Moreover, flecainide also might cause ventricular arrhythmias, specifically in patients with ischaemic cardiomyopathy (Cardiac Arrhythmia Suppr Tial, 1989).

1.4.3 β-adrenergic receptor inhibitors

Atenolol is a non-vasodilating with β_1-selectivity-adrenoceptor antagonist which decrease the heart rate by inhibiting sympathetic activity on Ca^{2+} channels. β-blockers prolong sinus node recovery time, the AV node refractoriness, and atrial-His intervals (Kowey et al., 2000). Therefore, atenolol is used in patients with cardiac fibrillation (Morganroth, 1986, Tamariz and Bass, 2004). β-blockers were originally used in patients with angina and later also had been used as first-line drugs in the treatment of hypertension (Erdine and Arı, 2006). Atenolol is often used as a reference drug in randomised controlled trial studies of hypertension. However, a meta-analysis study showed that atenolol is associated with

higher mortality rate, arrhythmias, and peripheral vascular resistance compared to non-atenolol β-adrenergic blockers (Aursnes et al., 2007).

1.4.4 L-type Ca^{2+} channel blockers

Verapamil is a nondihydropyridine Ca^{2+} channel blocker which affects Ca^{2+}-dependent slow APs by diastolic depolarisation in the SA and AV nodes, thereby slowing the heart rate. In addition, verapamil also prolongs the refractory period of the AV node, thus slowing the ventricular rate during atrial fibrillation and may also prevent ventricular tachycardia or fibrillation (Kowey et al., 2000).

1.4.5 Angiotensin-converting enzyme inhibitors

Captopril and enalapril are angiotensin converting enzyme inhibitors (ACEIs) which act by targeting a pluripotent zinc metalloproteinase which catalyses the conversion of angiotensin I to angiotensin II, thereby inhibiting the formation of angiotensin II. These drugs decrease total peripheral resistance and blood pressure, whilst heart rate and cardiac output remain unchanged (Jackson et al., 2018). A meta-analysis study mentioned ACEIs as the most effective antihypertensive drugs to reduce left ventricular hypertrophy compared to Ca^{2+}-channel blockers, diuretics and β-blockers (Klingbeil et al., 2003). ACEIs are associated with cough and very low risks of angioedema (Messerli et al., 2018).

1.4.6 Statins

Statins are the most widely prescribed, cholesterol-lowering drugs worldwide (Demasi, 2018). Statin acts by selectively inhibiting the enzyme hydroxymethylglutaryl-CoA (HMG-CoA) reductase, which is important in the sterol biosynthetic pathway. Pravastatin is a second generation of statins with open ring structures and is a hydrophilic agent unlike other statins (Sirtori, 2014). Adverse effect of liver failure occurred in statin-treated patients was reported to be equal to the background rate in the general population (Tolman, 2002).

Table 1-1. Antiarrhythmic drugs: mechanisms of action and their clinical applications. Adapted from (Mankad and Kalahasty, 2019, Lei et al., 2018, Laurent, 2017, Sirtori, 2014, Kumar and Zimetbaum, 2013)

Drug	Cellular mechanism of electrophysiological effect	Cellular mechanism of inotropic effect	Clinical indication (aside arrhythmia)	Medications by arrhythmia type		Adverse effects (aside arrhythmia)	Proarrhythmic actions	Proarrhythmic mechanisms
				Atrial	Ventricular			
Ivabradine	Decrease in SAN phase 4 pacemaker depolarisation rate	Decrease in Ca^{2+} transient peak	Stable angina	Potential application for tachyarrhythmias		N/A	Sinus bradycardia	Reduction in SAN automaticity
Flecainide	Decrease in AP generation with increased excitation threshold	Decreased Na^{+} influx	N/A	Yes	in CPVT	N/A	Ventricular tachycardia (in cardiac ischaemia or old myocardial infarction)	Slowing of conduction in the ventricle or myocardial scar areas
Atenolol	Inhibition of G_s protein-mediated effects of increased adenylyl kinase activity and cAMP	N/A	N/A	Yes	idiopathic VT	Hypotension	Sinus bradycardia; AV block Sinus tachycardia	β-blockade β-adrenoceptors upregulation in long-term therapy; β-blocker withdrawal
Verapamil	Inhibition of SAN pacing, inhibition of AVN conduction, increased AP recovery time	Decreased Ca^{2+} influx	N/A	Yes	idiopathic VT	Hypotension	Sinus bradycardia; AV block	Reduction in SAN automaticity
Captopril Enalapril	N/A	N/A	Hypertension Symptomatic heart failure	Potential application for reducing arrhythmic substrate		Cough Angioedema	N/A	N/A

Pravastatin	N/A	N/A	Myocardial infarction Stroke	Abnormal cardiac rhythms	Liver toxicity	N/A	N/A

Abbreviations: AP, action potential; AV, atrioventricular; cAMP, cyclic adenosine monophosphate; CPVT, catecholaminergic polymorphic ventricular tachycardia; N/A, not available; SAN, sinoatrial node; VT, ventricular tachycardia.

1.5 Physiology and clinical use of common inotropic drugs in cardiovascular disease

Exogenous inotropic agents have been fundamental for the management of cardiovascular disease. In heart failure, abnormal Ca^{2+} accumulation of the SR occurs due to Ca^{2+} leak from the SR via RyR, decreased Ca^{2+} re-uptake due to decreased levels of SERCA, and increased Ca^{2+} efflux due to increased levels of the NCX (Bers, 2006). Consequently, this event is the main mechanism underlying the negative force-frequency relation, which is a decline of contractile force at higher heart rates (Hasenfuss and Pieske, 2002, Mulieri et al., 1992). Altogether, in heart failure, higher heart rates *in vivo* resulted in decreased left ventricular ejection fraction (LVEF) and cardiac output (the product of heart rate and stroke volume) (Hasenfuss et al., 1994).

Positive inotropic drugs to increase cardiac output have been used to treat patients with heart failure; however, older drugs such as catecholamines and phosphodiesterase (PDE)-inhibitors which act by increasing intracellular Ca^{2+}, are pro-arrhythmic and related to increased mortality. Therefore, newer drugs such as levosimendan and omecamtiv mecarbil target sarcomeres in order to improve systolic function without increasing intracellular Ca^{2+} (Ponikowski et al., 2016, Maack et al., 2019). This section will focus on inotropic drugs that will be used in further result chapters, with a summary of their mechanisms of action as depicted in **Figure 1-10**.

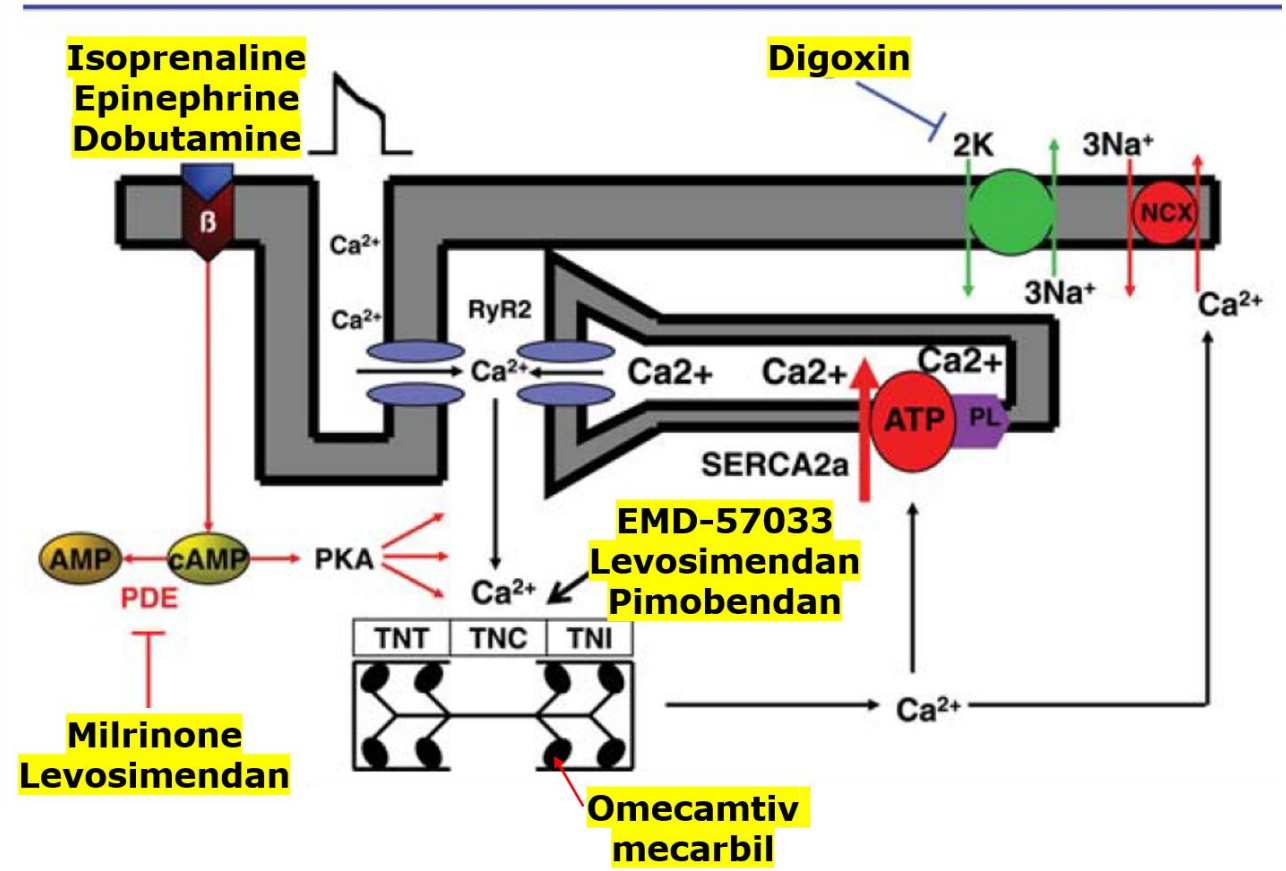

Figure 1-10. **Inotropic drugs and their mechanisms of action**. Catecholamines (isoprenaline, epinephrine, dobutamine) activates β-adrenoceptors, which stimulates adenylyl cyclase (AC) to produce cyclic adenosine monophosphate (cAMP). This activates protein kinase A (PKA) to phosphorylate intracellular calcium handling proteins. Phosphodiesterase (PDE)-inhibitors (milrinone, levosimendan) impede degradation of cAMP by PDE. Digitalis (digoxin) inhibits transport of 3 Na^+ for 2 K^+ through NA^+/K^+-ATPase. Ca^{2+} sensitisers (levosimendan, pimobendan) increase the affinity of troponin C to bind Ca^{2+}, whilst another Ca^{2+} sensitiser EMD-57033 directly binds to the myosin motor domain. Cardiac myosin activators (omecamtiv mecarbil) promote crossbridges to force-producing state. Abbreviations: ATP, adenosine triphosphate; NCX, Na^+–Ca^{2+} exchanger; PL, phospholamban; RyR2, ryanodine receptor 2; SERCA, sarcoplasmic reticulum Ca^{2+} -ATPase pump; TnC, troponin C; TnI, troponin I; TnT, troponin T. Adapted from (Hasenfuss and Teerlink, 2011).

1.5.1 Conventional inotropic drugs

With catecholamines on chronic stimulation, desensitisation and downregulation of β-adrenoceptors occurs via protein kinase A (PKA), G-protein coupled receptor kinase 2 (GRK2), and β-arrestin (Lohse et al., 2003, Rockman et al., 2002). Despite desensitization of β-adrenoceptors from PKA-mediated inotropy, β-arrestin activates Ca^{2+}/Calmodulin-dependent protein kinase II (CaMKII), in which sustains contractility (Tilley, 2011), yet the major cause of cardiac arrhythmia (Wagner et al., 2015). In contrast, digitalis as the oldest inotropic drug is safe to be used in patients with failing heart and improves morbidity (Digitalis Investigation, 1997). Details of these drugs are described further in **Table 1-2**.

1.5.1.1 Digoxin

Digoxin is a digitalis-derived cardiac glycoside that inhibits Na^+ efflux via the sarcolemmal Na^+/K^+ ATPase (NKA) in the cardiomyocyte. The increased intracellular Na^+ concentration affects the NCX activity by slowing the Ca^{2+} efflux, which in turn raises the intracellular Ca^{2+} concentration (positive inotropic effect). The ability of digoxin to drive the NCX may be inadequate in the immature heart (Phoon et al., 1997). In heart failure, digoxin improves haemodynamics without affecting heart rate or blood pressure (Gheorghiade et al., 1987). However, the increase in activator calcium is responsible for the arrhythmogenic effects of cardiac glycosides (Liu et al., 2010). In general, digoxin levels between 0.5-0.9 ng/mL are optimal (McMurray et al., 2012).

1.5.1.2 Isoprenaline

Isoprenaline is a synthetic catecholamine with high affinity for both β_1- and β_2-receptors and very low affinity for α-adrenergic receptors. It functions as both potent chronotrope and inotrope. Isoprenaline increases stroke volume, however, due to β_2-mediated effect on reduced systemic vascular resistance, it has neutral impact on cardiac output (Overgaard and DžAvíK, 2008).

1.5.1.3 Epinephrine

Epinephrine is an endogenous catecholamine with high affinity for both β_1- and β_2-receptors at low concentration, and α_1-receptors at higher concentration. It functions as both chronotrope and inotrope. In septic shock where hypotension is underlied by vasodilation, epinephrine acts via α_1-adrenergic-mediated vasoconstriction (Maack et al., 2019). High and prolonged concentrations can cause direct cardiac toxicity through direct stimulation of cardiomyocyte apoptosis and damage to arterial walls (Singh et al., 2001). In cardiogenic shock after acute myocardial infarction, epinephrine contributes to five-fold more frequent refractory shock compared to norepinephrine according to a recent study (Levy et al., 2018). This is due to its strong β_2-adrenergic activation, thereby increased heart rate, and elevated myocardial O_2 consumption, thereby increased lactate.

1.5.1.4 Dobutamine

Dobutamine is a synthetic catecholamine with higher affinity (~10-fold) for β_1- compared to β_2- and α_1-receptors (Williams and Bishop, 1981). Due to that selectivity, it functions as a weaker chronotrope and potent inotrope. In cardiogenic shock where neuroendocrine activation induces tachycardia and vasoconstriction, dobutamine acts as positive inotrope without having significant effect on systemic vascular resistance (Tuttle and Mills, 1975), which is ideal. Concentrations up to 15 µg/kg/min increase contractility without significantly affecting vascular resistance, due to α_1-mediated vasoconstriction and β_2-mediated vasodilatation (Ruffolo, 1987). However, despite its mild chronotropic effects at low to medium concentrations, dobutamine significantly increases myocardial O_2 consumption (Tuttle and Mills, 1975, Ruffolo, 1987) and arrhythmias.

Table 1-2. **Catecholamines (endogenous and synthetic): mechanisms of action and effects on haemodynamics**. Adapted from (Maack et al., 2019, Overgaard and DžAvíK, 2008)

Drug	Receptor binding			Cellular mechanism of inotropic effect	Heart rate	Stroke volume	Systemic vascular resistance	Clinical indication	Adverse effects	Arrhythmias
	α_1	β_1	β_2							
Isoprenaline	0	++++	++++	Increase in cAMP, Ca^{2+} influx, SR Ca^{2+} uptake and SR load	++++	+++	---	Bradyarrhythmia	Ventricular arrhythmia Cardiac ischemia	+++
Epinephrine	++++	+++	++++	Increase in cAMP, Ca^{2+} influx, SR Ca^{2+} uptake and SR load	+++	++++	++	Cardiac arrest Symptomatic bradycardia or heart block	Ventricular arrhythmia Cardiac ischemia Sudden cardiac death	+++
Dobutamine	++	+++	+	Increase in cAMP, Ca^{2+} influx, SR Ca^{2+} uptake and SR load	+	++++	-/0/+	Low cardiac output (decompensated heart failure, cardiogenic shock) Symptomatic bradycardia	Tachycardia Ventricular arrhythmia Cardiac ischemia	+

Abbreviations: α_1, α_1 receptor; β_1, β_1 receptor; β_2, β_2 receptor; 0, neutral effect; - through ----, increasing negative effects; + through ++++, increasing positive effects; IV, intravenous; IM, intramuscular.

1.5.2 Nonadrenergic inotropic drugs

Phosphodiesterase (PDE) 3 is an intracellular enzyme that breaks down cyclic adenosine monophosphate (cAMP), a second messenger regulating intracellular Ca^{2+}, and is associated with the sarcoplasmic reticulum (SR) in cardiomyocytes and vascular smooth muscle. Therefore, PDE-inhibitors increase cAMP level, which increases Ca^{2+} influx into cardiomyocytes as well as its efflux, which in turn leads to increased myocardial contractility. They function as potent inotropes, cAMP-mediated vasodilators due to increased Ca^{2+} efflux from vascular smooth muscle, as well as improving diastolic relaxation (lusitropy), thereby reducing preload, afterload, and systemic vascular resistance (Overgaard and DžAvíK, 2008). This is beneficial for patients with acute heart failure, but not for patients with cardiogenic shock due to decreased blood pressure. PDE-inhibitors were developed in order to overcome desensitisation and downregulation of cardiac β-adrenoceptors, as well as their blockade through β-blockers (Maack et al., 2019). In human failing ventricular myocardium, PDE3-inhibition facilitates β-adrenoceptor-mediated positive inotropic effects for controlling intracellular cAMP (Molenaar et al., 2013). Conversely, in human atrial myocardium, PDE4-inhibition facilitates arrhythmias induced by both β_1- and β_2-adrenoceptor stimulation, whilst PDE3-inhibition only facilitates β_1-adrenoceptor-induced arrhythmias (Molina et al., 2012). Calcium sensitisers have mechanism of actions in which are Ca^{2+} sensitisation of contractile proteins and the opening of ATP-dependent K^+ channels. Ca^{2+} sensitiser affects the relationship between intracellular Ca^{2+} and force development of sarcomeres (i.e. the pCa-force relationship) by shifting it to the left, thereby increasing systolic contractility force at any given intracellular Ca^{2+} concentration. However, this shift of pCa-force curve to the left also slows relaxation following the decrease in intracellular Ca^{2+} concentration (Maack et al., 2019). The opening of ATP-dependent K^+ channels on vascular smooth muscle leads to vasodilation which may protect myocardium during ischemia (Lehtonen and Poder, 2007). Details of these drugs are described further in **Table 1-3**.

1.5.2.1 Milrinone

Milrinone is a PDE-inhibitor which increases contractility (inotropy) and improves diastolic function (lusitropy), as well as peripheral vasodilation. Milrinone increases heart rate but not to the same extent as dobutamine (Francis et al., 2014). This drug is particularly useful if adrenergic receptors are desensitised or downregulated in the setting of chronic heart failure, or after chronic β-agonist administration (Overgaard and DžAvíK, 2008). Milrinone is widely used in patients with acute decompensated heart failure. However, milrinone was shown to be associated with adverse effects such as atrial fibrillation and ventricular tachycardia (Cuffe et al., 2002).

1.5.2.2 EMD-57033

EMD-57033 is a calcium sensitiser which acts differently from levosimendan and pimobendan. This drug affects the actomyosin interaction by direct binding to the myosin motor domain (Radke et al., 2014). EMD-57033 increases crossbridge attachment time, resulting in negative lusitropy and increased diastolic force (Teramura and Yamakado, 1998, Brixius et al., 2002), therefore levosimendan is much preferred for treatment of patients with heart failure. EMD-57033 does not affect pacemaker currents, and thereby does not increase sinus rate (Lakhe et al., 1998).

1.5.2.3 Levosimendan

Levosimendan is a calcium sensitiser, and also a potent PDE3 inhibitor at higher concentrations, with ~1000-fold lower affinity for PDE4 (Szilagyi et al., 2004, Hasenfuss et al., 1998, Todaka et al., 1996). It increases the affinity of troponin C (TnC) to bind intracellular Ca^{2+} (Schlecht et al., 2016, Pollesello et al., 1994), thereby enhancing crossbridge formation (positive inotropic and lusitropic effect) (Givertz et al., 2007). Unlike pure Ca^{2+} sensitiser, levosimendan has unique mechanism in which it binds to TnC only during systole when Ca^{2+} is high and not on diastole when Ca^{2+} is low, thereby not impairing diastolic relaxation (i.e. does not increase relaxation time) (Hasenfuss et al., 1998). Furthermore, as a PDE3 inhibitor,

levosimendan increases cAMP with similar potency as it increases contractility force (Boknik et al., 1997).

The inotropic effects of levosimendan in human myocardium require β-adrenergic prestimulation and/or increase of intracellular Ca^{2+} concentration, which can be prevented by PDE3-inhibition (Orstavik et al., 2014, Hasenfuss et al., 1998). As a result, at higher β-adrenoceptors pre-activation via catecholamines, the inotropic effect of levosimendan is mediated by its PDE3-inhibition, whilst at low β-adrenoceptors pre-activation (such as with the use of β-blocker), the inotropic effect of levosimendan is mediated by its Ca^{2+} sensitisation.

In addition, levosimendan activates adenosine triphosphate (ATP)-dependent K^+ channels in smooth muscle cells, thereby causing peripheral vasodilatation (Yokoshiki and Sperelakis, 2003), which is beneficial for both acute and chronic heart failure. In heart failure, haemodynamic profile improves with concentrations ranging from 0.1-0.4 μg/kg/min (titrated upward over 4h) (Slawsky et al., 2000). A meta-analysis study of patients with acute severe heart failure suggested that compared to dobutamine, levosimendan was associated with lower mortality (Delaney et al., 2010), as with the case pre-treated with β-blocker (Kivikko et al., 2016, Mebazaa et al., 2009). However, in patients with septic shock pre-treated with catecholamines, levosimendan was associated with higher rates of supraventricular tachycardia (Gordon et al., 2016).

1.5.2.4 Pimobendan

Pimobendan is a calcium sensitiser that is mainly used for veterinary medicine (Boyle and Leech, 2012), with exception of human use in Japan (Koizumi and Taguchi, 2016, Kawano et al., 2014). With mechanism of Ca^{2+} sensitisation same as levosimendan, pimobendan increases the affinity of troponin C (TnC) to bind intracellular Ca^{2+} (Schlecht et al., 2016, Fujino et al., 1988).

Table 1-3. **Nonadrenergic agents: mechanisms of action and their clinical applications**. Adapted from (Maack et al., 2019, Overgaard and DžAvíK, 2008).

Drug	Cellular mechanism of inotropic effect	Increasing cAMP	Myofilament Ca^{2+} sensitisation	Clinical indication	Adverse effects
EMD-57033	Myofilament sensitisation to Ca^{2+}	(+)	+++	N/A	N/A
Levosimendan	Increase in cAMP Myofilament sensitisation to Ca^{2+}	++	++	Decompensated heart failure	Tachycardia
Milrinone	Increase in cAMP, Ca^{2+} influx, SR Ca^{2+} uptake and SR load	+++		Low cardiac output (decompensated heart failure)	Ventricular arrhythmia Cardiac ischemia

Abbreviations: + through ++++, increasing positive effects; N/A, not available.

1.5.3 Emerging inotropic drugs

1.5.3.1 Omecamtiv mecarbil

Omecamtiv mecarbil (formerly known as CK-1827452) is a selective cardiac myosin activator. It directly influences the crossbridge cycle by selectively activates the main component (the S1 domain) of myosin (Planelles-Herrero et al., 2017) and accelerates actin-dependent phosphate release of the actomyosin crossbridge. Consequently, this increases the number of myosin bound to actin filaments while the intracellular Ca^{2+} transients remain unchanged (Malik et al., 2011). The increase in cardiac contractility and subsequent prolongation of systolic ejection time increases left ventricular stroke volume in patients with chronic heart failure. This leads to raised blood pressure, which then reduce endogenous sympathetic activation. Altogether, omecamtiv mecarbil cause modest decrease in heart rate and relatively no change in cardiac output. At plasma concentrations above 1200 ng/mL, omecamtiv mecarbil was reported to cause chest pain, tachycardia, and myocardial ischaemia in patients with heart failure (Cleland et al., 2011, Teerlink et al., 2011).

1.6 Current hiPSC-CMs platforms used in drug screening

Whether hiPSC-CM technologies are fit-for-purpose might be due to the maturity status. Improved cardiomyocytes maturation are seen by using T3 hormone, metabolic maturation, 3D constructs, mechanical load, electrical training, long-term culturing and auxiliary cell types (e.g. cardiac fibroblasts and cardiac vascular endothelial cells). This section will focus more on 3D constructs.

The aim of utilising 3D cell culture is to provide a biomimetic microenvironment that is expected to enhance maturation of hPSC-CMs. Although previous studies tend to show that 3D cell culture improved structural maturation of hPSC-CMs mimicking native human heart, functionally they still resemble embryonic state reviewed in (Yang et al., 2014a). A complex 3D cell culture with artificial tissues is crucial, especially for regenerative medicine application, where there is a need to provide mechanical support and to replace lost tissue. Additionally, for drug screening and disease modelling, the goal is to create *in vitro* model systems that represent human disease (Zuppinger, 2016).

1.6.1 Muscular thin films (MTFs)

Muscular thin films (MTFs) is a pseudo 3D platform that incorporates micro-patterned polydimethylsiloxane (PDMS) scaffolds with tuneable stiffness and flexibility in order to mimic desired heart conditions, either healthy or diseased (Palchesko et al., 2012). This platform allows measurement of contraction force and can be combined with electrical stimulation and microfluidic platform (Grosberg et al., 2012). However, due to two-step SU-8 lithography that is used in the fabrication of MTFs, this hinders parallelisation (carrying out multiple experiments simultaneously) and mass production (Boudou et al., 2012, Legant et al., 2009). Furthermore, MTFs require handling thermosensitive ECM gels that limits experimental throughput.

1.6.2 Biowire and its next generation systems

Biowire is a 3D system culture combined with electrical stimulation from 1 to 6 Hz, with cells seeded in collagen gel around a surgical suture placed in a PDMS mould (Nunes et al., 2013). Under the 6-Hz regimen,

this study demonstrated improved alignment of cardiomyocytes, enhanced ultrastructural sarcomeric organisation, elevated conduction velocity, improved electrophysiology and Ca^{2+} handling properties. However, Biowires depends on differentiation protocol which produce interline variability in Ca^{2+} handling properties. Furthermore, Biowire maturation is incomplete, shown by low membrane conductance, and thus needs to be supplemented by other maturation strategies.

Its next generation systems are now providing bioreactor with ventricular-assist capabilities (MacQueen et al., 2018), as well as commercial offerings such as Biowire II (TARA Biosystem) and 'Heart-in-a-Jar' (Novoheart) (Li et al., 2018). In study using Biowire II, electrical conditioning showed to improve structural maturation as in sarcomeric organisation, and increased gene expression associated with electrophysiology, Ca^{2+} handling, contractility, and lipid metabolism. Positive inotropic drug effect was also detected with milrinone (Zhao et al., 2019). The Heart-in-a-Jar concept embeds ventricular-like subtype hiPSC-CMs in collagen-based extracellular matrix (ECM) hydrogel. This creates a miniature 3D engineered electro-mechanically coupled cardiac organoid chamber, which is capable of ejecting fluid to mimic pumping action that is found in native heart.

1.6.3 Engineered heart tissues (EHTs)

Engineered heart tissues (EHTs) at present are the most established 3D *in vitro* heart model. The cells are embedded in extracellular matrix (ECM) gel, forming a construct that is attached to rigid boundaries (such as posts or mesh) that pin EHTs to the ECM (Tulloch et al., 2011, Hansen et al., 2010). However, despite the promise of EHTs as physiologic *in vitro* model, this system has disadvantages because the culture requires a large number of cells (>1 million per tissue) (Thavandiran et al., 2013), and is composed of mixed population of both cardiomyocytes and fibroblasts. Therefore, the need for large cell numbers has a challenge in: (1) producing different lines of hiPSC-CMs for drug screening and disease modelling, and (2) overcoming diffusion-limited mass transport of oxygen and nutrient through the thick tissue (Vollert et al., 2014). Furthermore,

the requirement of handling ECM gels in EHTs limits experimental throughput.

Hirt et al., 2014 conducted a study using EHTs combined with electrical stimulation, demonstrating improved sarcomere structure and ultrastructure, reduced spontaneous beating activity, and stronger inotropic response to β-adrenergic stimulation (isoproterenol) (Hirt et al., 2014). However, EHTs still produce less mature cardiomyocytes, indicated by lower twitch forces and electrophysiology properties compared to native human heart tissue (Tzatzalos et al., 2016). Therefore, to boost maturation of cardiac tissues, combination of mechanical and electrical stimulation has been reported in 3D culture (Kurokawa and George, 2016, Stoppel et al., 2016).

1.6.4 Micro-Heart Muscles (μHMs)

A recent study has developed a mini version of EHTs, named Micro-Heart-Muscle (μHMs) (Huebsch et al., 2016). This platform was developed to resolve the limitation found in EHTs such as requirement of large cell numbers (only needs <10,000 cells), rigid boundaries, handling ECM gels, and lack of accessibility to contractile force measurement. Huebsch et al., 2016 showed that μHMs allowed robust sarcomere assembly, robust Frank-Starling response to external stretch, and inotropic response to β-adrenergic stimulation (isoprenaline), thus indicating improved structural and functional maturation in hPSC-CMs. μHMs allow massive parallelisation and smaller size system for high-throughput studies in application for drug screening and disease modelling. However, μHMs need to be manually moved to an organ bath for force measurements (Weinberger et al., 2017).

1.7 Screening tools for drug testing

In safety pharmacological studies, it is beneficial to have a high throughput technology platform *in vitro* that is capable of measuring simultaneous key cardiac readouts: electrophysiology, calcium handling, and contractility. At present, there are several techniques for the evaluation of hiPSC-CMs phenotypes. This section will focus more on the relevant methods that involve electrophysiology, optical measurements, and contraction force.

The gold standard approach to evaluate cardiac electrophysiology is manual patch-clamp by measuring cardiac action potential (AP). However, this assay has limitations: very low throughput, labour intensive, and requires a skilled operator (Denning et al., 2016). Therefore, efforts have been made to develop automated version of patch-clamp platform as a more high throughput assay and useful to record individual ion channels, although it is not yet for measuring AP (Rajamohan et al., 2016).

Multielectrode arrays (MEAs), a medium throughput technology platform as alternative method to measure electrophysiology and ion channel properties, is starting to be extensively used by academia, pharmaceutical, and biotechnology companies in cardiac drug safety (Asakura et al., 2015, Mulder et al., 2018). Instead of recording AP as in patch clamp electrophysiology, MEAs record the cardiac field potential (FP). FP duration (FPD) is considered as the equivalent of AP duration at 90% of repolarisation (APD_{90}) (Braam et al., 2010); however, it is a challenge to translate other parameters (AP amplitude, RMP, maximal rate of depolarisation (V_{max}), APD_{50}) from FPs. A recent study demonstrated computational simulation to convert those parameters, providing more valuable information for assessing potential drug safety risk (Tertoolen et al., 2018).

Other recording techniques rely on optical-based approaches, utilising fluorescence-based voltage- or calcium-sensitive dyes. The combined dyes with microscope-based, high-content imaging system allows simultaneous imaging of electrical and calcium dynamics as described in a previous study (Lee et al., 2012). The nature and properties of the voltage-sensitive dyes can affect the optical AP recording. Organic electrochromic dyes such as Di-4-ANEPPS are fast response membrane potential fluorescent probes and

use ratiometric measurements that, unfortunately, yields rather low signal-to-noise ratio (SNR) and are more sensitive to motion artefact. FluoVolt™ is the next generation in voltage-sensitive dyes that is also a fast response probe but with higher sensitivity (magnitude of response) up to 25% per 100 mV (Bedut et al., 2016), compared to Di-4-ANEPPS which is up to 10% per 100 mV (Herron et al., 2012). Despite that, both Di-4-ANEPPS and FluoVolt™ demonstrated immediate cellular phototoxicity at the highest concentration that occurs linearly to the duration and intensity of the illumination (Bedut et al., 2016). Genetically encoded dyes, such as ArcLight, requires transfection phase and has slow response kinetics (Leyton-Mange et al., 2014).

As mentioned above, aside from cellular phototoxicity, one of the challenges in optical mapping studies using a voltage-sensitive dye for monitoring cardiac membrane potential is motion artefact due to myocardial contraction, which results in a low SNR and poor quality AP recordings (Li and Nattel, 2007). Pharmacological method using an excitation-contraction uncoupler (ECU) are widely used in order to eliminate myocardial contraction, such as 2,3-butanedione monoxime (BDM; a non-competitive inhibitor of myosin ATPase) and cytochalasin-D (cyto-D; agent impairing F-actin filament polymerisation). However, both BDM and cyto-D are known to significantly alter cardiac electrophysiology and calcium handling in rabbit (Kettlewell et al., 2004) and mice (Baker, 2004). Blebbistatin (BB) emerged as the new ECU, which is an ATPases inhibitor associated with class II myosin isoforms (Limouze et al., 2004, Allingham et al., 2005), that has been reported in several studies to have minimal effect on electrophysiology and calcium handling (Dou et al., 2007, Fedorov et al., 2007, Farman et al., 2008, Jou et al., 2010). However, more recent study focusing on perfusion pressure (PP), electrical restitution property, and ventricular fibrillation threshold (VFT) in isolated rabbit heart reported that BB at 5 μM significantly affected cardiac electrophysiology and induced ventricular fibrillation (VF), which is shown by prolonged ventricular monophasic action potential duration (MAPD) mirrored by QT interval prolongation, and significant increase in APD restitution slope and VF threshold (Brack et al., 2013). This study proposed that the prolonged

APD might be caused by increased Ca^{2+} released into the cytosol leading to an increase in the Ca^{2+} transient.

Cardiac contractility is one of key readouts that are affected in many cardiac diseases: positive inotropic drugs (increase in cardiac contractility) is harmful for ischemic heart disease patients, whilst negative inotropic drugs (decrease in cardiac contractility) is harmful for heart failure patients (Wallis et al., 2015). Measurements of contraction force are performed either in individual cardiomyocytes or on cell clusters, with 3D engineered heart tissues (EHTs) demonstrated value that is similarly found in native cardiac tissue (Eschenhagen et al., 2015). However, these contractility assays are low throughput (van Meer et al., 2016). Therefore, the method was adapted to a standard 24-well format, and newer systems are starting to work in 96-wells with hμMs (Mills et al., 2019).

1.8 Hypothesis and Aims

The central hypothesis of this thesis is that hiPSC-CMs can predict inotropic drug responses reliably. Simpler 2D and 3D systems can be used in up to high throughput primary screens and discovery work. Advancing this further will require international collaboration between regulatory agencies, academia and industry. To answer the need for improved methods for predicting changes in cardiac contractility, a public-private partnership was established between a pharmaceutical company (GlaxoSmithKline; GSK), a UK funding agency (National Centre for the Replacement, Refinement and Reduction of Animals in Research; NC3Rs), and 4 academic labs in the UK, Netherlands, and Germany. (The University of Nottingham as the academic lead, University of Glasgow, Leiden University Medical Center, University Medical Center Hamburg-Eppendorf).

In order to test the hypothesis, the following objectives will need to be achieved:

- Perform 'training' testing of drugs known to be positive- or negative-inotropes or have no effect on heart function in smaller scale, in order to do the next objective.
- Establish the protocols to be used on platforms used by academic labs.
- Perform blinded testing of drugs known to be positive- or negative-inotropes or have no effect on heart function in larger scale, with adult cardiomyocytes as comparator.
- Refine test conditions to improve predictivity.

2 Materials and Methods

2.1 Materials and General Culture

Culture media and reagents were purchased from Life Technologies and chemicals were from Sigma-Aldrich unless otherwise stated. Cell cultures were maintained in incubator at 37°C, 5% CO_2.

2.2 Maintenance of human induced pluripotent stem cells & differentiation into cardiomyocytes

The human induced pluripotent stem cell (hiPSC) line, NCRM5, was used in these experiments, and cultured in xeno-free and feeder-free Essential 8™ (E8) Medium in Matrigel™-coated (BD Biosciences) T25 flasks over a period of <15 passages from thaw, with medium exchange every day. Cells were passaged every 2-3 days using our in-house cell dissociation method (CDS) for 4 minutes. This consisted of 40% Roswell Park Memorial Institute (RPMI), 40% Cell Dissociation Buffer, and 20% trypsin. Cardiac differentiation was performed using our novel in-house monolayer differentiation method (Smith et al., 2018, Mosqueira et al., 2018) (**Figure 2-1**) with cells seeded in Matrigel™-coated 24-well plates in: TCPS (Nunclon delta surface; Thermo Scientific) and electrospun aligned nanofibers (NanoAligned™; Nanofiber Solutions), with a density 85,000 cells/cm^2 in TCPS and 95,000 cells/cm^2 in nanofibers.

When the cells reached >80% confluence state, usually achieved in 2-3 days after seeding, differentiation preconditioning was conducted by replacing medium with StemPro-34 complete medium supplemented with 1 ng/mL recombinant human bone morphogenetic protein-4 (BMP-4; R&D Systems) and Matrigel™ (1:100 dilution). Within 12-18 hours after preconditioning, differentiation was initiated (day 0) by replacing medium with StemPro-34 complete medium supplemented with 10 ng/mL BMP-4 and 8 ng/mL recombinant human Activin-A. After 48 hours (day 2), the medium was changed to RPMI-B27 minus Insulin, supplemented with small molecules 10 μM of KY02111 and XAV939 (R&D Systems). On day 4 of differentiation, medium was switched to RPMI-B27 and supplemented with the same small molecules. From day 6 of differentiation onwards, the cells

were subsequently maintained in RPMI-B27 with media exchange every 2-3 days.

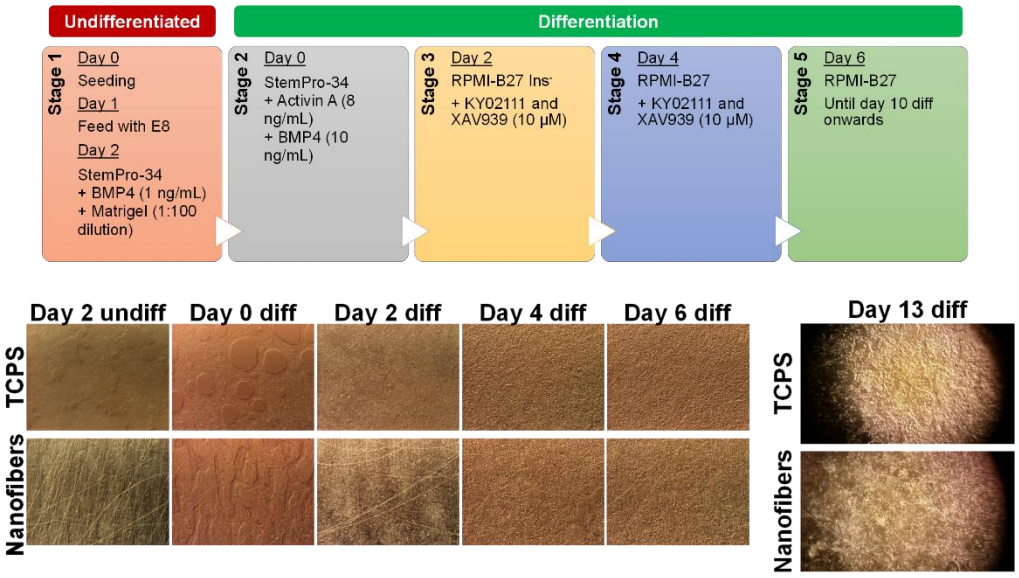

Figure 2-1. Schematic workflow of in-house monolayer cardiac differentiation protocol.

After day 10-13 of differentiation, when beating sheets of cardiomyocytes were observed under microscope, cardiomyocytes were harvested using the CDS method and reseeded on vitronectin-coated plates and afterwards maintained in RPMI-Panexin NTA (PAN-Biotech) media, composed of purified proteins, lipids, salts, amino acids, trace elements, attachment factors and hormones.

2.3 Maturation of human induced pluripotent stem cells

After 3 days following cardiomyocyte dissociation (at least 15 days from start of differentiation), maturation in the different substrates were initiated with either 10 µM dexamethasone or 20ng/mL triiodothyronine hormone (T3) (**Figure 2-2**), and left for 48 hours followed by a washout with RPMI-Panexin NTA for 1 day. This cycle was repeated for 4 more cycles (total 5 cycles over 15 days) while untreated plates were maintained throughout in RPMI-Panexin NTA. Afterwards the plates were processed as indicated.

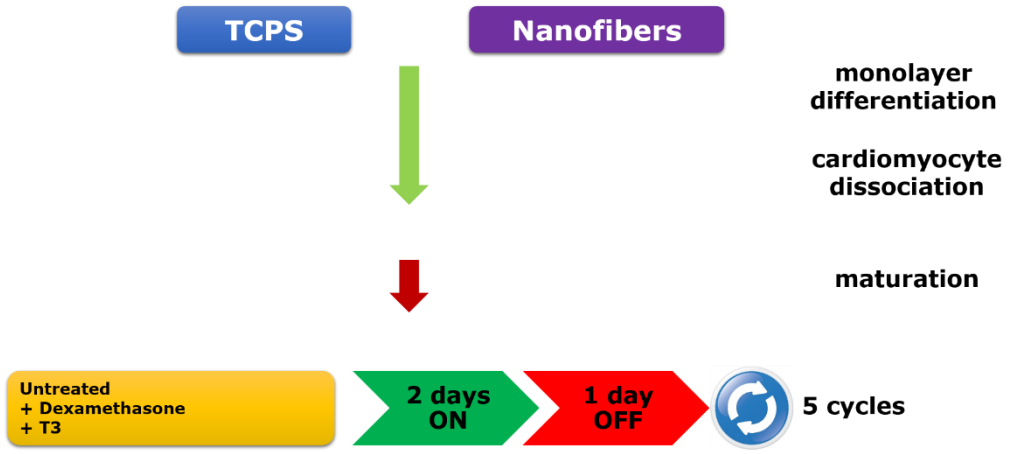

Figure 2-2. Strategic approach for hPSC-CM maturation. NCRM5 hiPSC line were seeded in TCPS or 3D aligned nanofiber scaffolds and differentiated into cardiomyocytes. Beating sheets of cardiomyocytes were then dissociated and replated before initiation of 5 cycles of maturation treatment with Dexamethasone, or T3.

2.4 Immunocytochemistry

Cells were fixed in 4% paraformaldehyde (PFA) for 15 minutes at room temperature, permeabilised with 0.05% Triton X-100 for 15 minutes, washed with 0.5% Tween-20 (Fisher), blocked with 5% human serum in PBS for 30 minutes at room temperature and incubated for 1 hour at room temperature or overnight at 4°C with primary antibody (**Table 2-1**). Cells were then washed twice with 0.5% Tween-20 (15 minutes wash) and incubated with secondary antibody at optimal concentration (**Table 2-1**) for 1 hour at room temperature in the dark, washed again twice with 0.5% Tween-20 for 15 minutes followed by PBS wash. Afterwards, cells were counterstained with DAPI for 15 minutes before refreshed with PBS. Cell morphology was visualised using a high-throughput confocal plate reader, Operetta® High Content Imaging System (PerkinElmer).

Table 2-1. List of primary and secondary antibodies used in immunocytochemistry. Abbreviations: cTnT, cardiac troponin-T; Cx43, connexin 43; MLC2a, Myosin Light Chain Atrial; MLC2v, Myosin Light Chain Ventricular.

Type		Species	Dilution	Company	Catalogue No
Primary antibody	α-actinin	mouse	1:800	Sigma	a7811
	cTnT	rabbit	1:400	Abcam	ab45932
	Cx43	rabbit	1:1000	Abcam	ab11370
	MLC2a	mouse	1:300	Abcam	ab68086
	MLC2v	Rabbit	1:4000	Abcam	ab79935
Secondary antibody	Alexa Fluor™ 488	Goat anti-mouse	1:1000	Life Technologies	A11001
	Alexa Fluor™ 488	Goat anti-rabbit	1:1000	Life Technologies	A11008
	Alexa Fluor™ 633	Goat anti-mouse	1:400	Life Technologies	A21052
Nucleic acid staining	DAPI	N/A	1:500	Sigma	D9542

2.5 Imaging analysis

Aspect ratio measurements were made using the program Icy (Institut Pasteur). For quantification measurement of immunocytochemistry result, images derived from Operetta® High Content Imaging System (PerkinElmer) were processed and analysed using Harmony® High Content Imaging and Analysis Software (PerkinElmer).

2.6 Transmission Electron Microscopy

Transmission electron microscopy was performed on 45- and ~120-day hiPSC-CMs in Thermanox™coverslips and nanofiber 24-well plate inserts (NanoAligned™; Nanofiber Solutions). hiPSC-CMs were fixed with 3% glutaraldehyde in 0.1M cacodylate buffer for 1 h at 37°C followed by two washes with 0.1M cacodylate buffer. All samples were then post fixed with 1% OsO_4 for 30 mins at RT, washed twice for 2 mins each with distilled water before dehydrated in graded series of ethanol (2x 5 min 50%, 2x 5 min 70%, 2x 5 min 90%, 3x 10 min 100% ethanol). Acetone was used as

a transitional agent post dehydration before infiltration with resin in a glass vial. This consisted of following steps: 1:3 resin:acetone mix for 30 minutes, followed by 1:1 resin:acetone mix for another 30 minutes, then in pure resin three times for 1h each in embedding oven (TAAB) at 45°C, 600 millibar (**Table 2-2**). This was followed by embedment in plastic moulds to be polymerised in oven for 48 h at 60°C. Ultrathin sections were obtained using a 2.1 mm diamond knife (Diatome) attached to an ultramicrotome (Leica EM UC6) and obtained samples were put in a copper hexagonal 100 mesh grids (Agar; G2410C) and stained with saturated uranyl acetate in 50% ethanol for 5 minutes followed by lead citrate stains for another 5 minutes. Images were taken using TEM (Tecnai™ G2 Spirit BioTWIN; FEI) at resolution in the range of 1000-2000 nm.

Table 2-2. List of components in making resin used in processing for transmission electron microscopy.

Reagent	Volume	Used for	Company	Catalogue No
Araldite CY212 resin	25 mL	Resin component	TAAB	E006
Agar 100 resin	15 mL	Resin component	Agar	R1043
DDSA	55 mL	Resin component	TAAB	D025
Dibutyl phthalate	2 mL	Resin component	Agar	R1071
DMP 30	1.5 mL	Resin component	TAAB	D035

2.7 Electrophysiology and Contractility

The hiPSC-CMs used were R-PAT (derived and differentiated in house as described previously) (Smith et al., 2018, Mosqueira et al., 2018), and iCell^2 and Pluricyte (purchased from Cellular Dynamics International and Ncardia). Manufacturer instructions were followed for the commercial hiPSC lines. For iCell^2, seeding was at 25,000 cells into each well of 96-well plates (Nunclon™ Delta Surface; Thermo, 167008) and then maintained for 10 days before use in drug evaluation studies. The same plates were used for R-PAT hiPSC-CMs, which were seeded at 40,000 cells/well and maintained until day 20-21 of differentiation before use. For Pluricyte hPSC-CMs, seeding was at 35,000 cells into each well of 96-well plates (Greiner Bio-One; 655087) and then maintained for 8 days before use. Confluent monolayers of R-PAT and iCell^2 hiPSC-CMs were changed into serum-free medium (SFM) (Dulbecco's Modified Eagle Medium (Gibco, 21969035) + 10mM galactose (Sigma-Aldrich, G0750) and 1 mM sodium

pyruvate (Sigma-Aldrich, P2256) 24h before testing. Pluricyte hiPSC-CMs were changed into 50% SFM and 50% Pluricyte Cardiomyocyte Medium (serum-free) 24 h before day of testing, and on the day of testing were changed into SFM. For the refined conditions described for R-PAT hiPSC-CMs, plating and maintenance were as before but cells were received fresh RPMI-B27 medium 24 h before testing instead of SFM.

Human iPSC-CMs in 96-well plate were transiently loaded in 50 µL/well of SFM containing FluoVolt™ (1:200 part B, 1:2000 part A; Life Tech, F10488) for 20 min at 37 °C and 5% CO2. After incubation, the medium was replaced with 200 µL/well of SFM. Plates were then incubated at 37 °C and 5% CO2 for 15 min before recording, which were made using a 40x (NAO.6) objective at 10 KHz. To apply electric field stimulation, a custom-made 8 channel electrode StimStrip (Clyde Biosciences was placed in a row of a 96-well plate and connected externally to a box (DC power supply; Lavota). Human iPSC-CMs were paced at a frequency of 1.2-1.7 Hz (or 0.7-1 Hz in the refined conditions) with an amplitude of 8 Volts and a pulse width of 20 msec. Recordings of 10 sec were made for each well (contractility was 100 frames/sec, hence 1000 frames). Baselines and drug addition were as described for the TTM system. Electrophysiology data were analysed using CellOPTIQ® proprietary software of Clyde Biosciences and were normalised to a maximum amplitude of 1 and minimum of 0 to standardise height for comparison of traces created in OriginPro (OriginLab version 7.5). Contractility data were analysed based on pixel displacement using an ImageJ plug-in. This plug-in use a sum of absolute differences (SAD) algorithm.

2.8 Statistical analysis

Data are reported as mean ± SEM unless otherwise stated and presented as graphs using GraphPad Prism version 7.01+. All statistical tests were performed with either one-way ANOVA (to compare all groups) or Student's unpaired t test (for 2 groups). $p<0.05$ or less was considered statistically significant. p-values are displayed in graph as follows: * $p<0.05$, ** $p<0.01$, *** $p<0.001$, **** $p<0.0001$, ns = not significant.

3 Cardiovascular Safety Liabilities Screening – Initial Phase

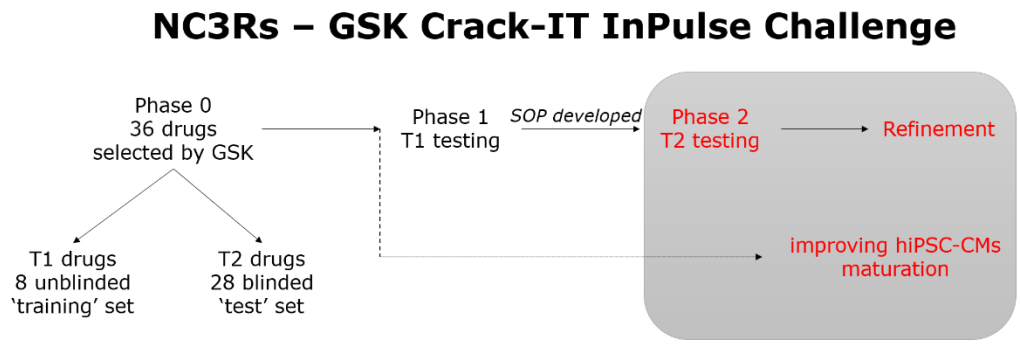

3.1 Introduction

To generate physiologically-relevant hiPSC-CMs in order to predict potential cardiovascular liabilities in drug testing, a project called the CRACK-IT Challenge 13: InPulse was raised and aimed to develop medium to high throughput technology platform for assessment of key cardiac readouts: electrophysiology, calcium handling, and contractility. To answer the challenge, a consortium consisting of 4 academic labs (The University of Nottingham, Leiden University Medical Center, University Medical Center Hamburg Eppendorf, University of Glasgow), a UK-based funding organisation (National Centre for the Replacement, Refinement, & Reduction of Animals in Research; NC3Rs), a global healthcare company (GlaxoSmithKline; GSK), and private biotechnology companies (Clyde Biosciences, Glasgow and Ncardia, The Netherlands) was established in 2014.

The challenges were then sequenced into several phases: (1) evaluating methods to improve hiPSC-CMs maturation that ran simultaneously with (2) Tier 1, which is a 'training set' stage of 8 unblinded drugs provided by GSK in order to established standard operating procedures (SOPs), allowing progression to final phase (3) Tier 2, which is a 'test set' of 28 blinded drugs, also provided by GSK.

The choice of 36 drugs in this study was based on (1) commercial availability, (2) range of positive inotropes (PI), negative inotropes (NI), and no effect drugs (NE) with approximate balance in numbers, (3)

inclusion of false positive or negative drugs, (4) previous data on cardiomyocytes and/or heart function both in preclinical and clinical setting, (5) previous data on free therapeutic plasma concentrations (FTPC), (6) solubility in DMSO with maximum concentration of 0.1% v/v to avoid toxicity in hiPSC-CMs, and (7) modes of action relevant to interest of the pharmaceutical industry.

To answer the need of system with integrations of readouts for contractility, electrophysiology, and calcium handling, academic labs in the CRACK-IT Challenge 13: InPulse have introduced Triple Transient Measurement (TTM), CellOPTIQ®, and EHTs. TTM was developed by Leiden (van Meer et al., 2019) and has the capability of measuring electrophysiology, calcium handling, and contractility in both single cells and monolayers of hiPSC-CMs. This platform has the advantage of true interlaced cardiomyocyte function parameters measurement (contractility → calcium handling → electrophysiology → back to contractility, etc.). CellOPTIQ® was developed by Glasgow/Clyde Biosciences and has the capability of measuring contractility, electrophysiology, and calcium handling in sequentially manner (with contractility first). Due to toxicity from calcium-sensitive dyes in the initial optimisation before Tier 1 phase, only electrophysiology and contractility were measured. 3D EHTs were developed by Hamburg and have the capability of measuring contraction force (based on the deflection extent of two silicon posts) and calcium handling (using genetically encoded calcium indicator; GECI with lentiviral mediated expression of GCaMP6f).

3.2 Chapter Aims

- To investigate the effect of Tier 1 drugs on hiPSC-CMs cultured in standard cell culture 2D monolayers and 3D engineered heart tissues (EHTs).
- To determine the positive control and negative control drugs from Tier 1 phase for Tier 2 phase.
- To identify protocols to determine optimal conditions which improve assessment of hiPSC-CMs in Tier 2 phase.
- To establish unified SOPs between the partner sites for Tier 2 phase.

3.3 Results

3.3.1 Cardiotoxicity screening in Tier 1 phase

During early stages of the project, 8 hiPSC-CM lines (in house: NCRM1, NCRM5 (NIH Center for Regenerative Medicine (NIH CRM), obtained from RUDCR Infinite Biologics at Rutgers University), AT1 and R-PAT derived as described in previous study (Mosqueira et al., 2018), ERC18 derived as described in previous study (Breckwoldt et al., 2017); commercial: Pluricytes (Ncardia; https://ncardia.com/product/pluricyte-sup-sup-cardiomyocyte-kit.html), iCell^2 (Cellular Dynamics International; https://fujifilmcdi.com/products-services/icell-products/icell-cardiomyocytes2/) were proposed based on: (1) cell culture and differentiation efficiency, (2) viability during assays, (3) cost consideration, and (4) unification of the cell lines between the partners. In addition, 4 cell configurations (2D single cells, 2D monolayer, 2.5D muscular thin films, and 3D EHTs) were tested, all with the intention of defining the cell lines and configurations suitable for the project.

To demonstrate the ability of 3 technology platforms in evaluating drug responses provided by GSK in both standard cell culture 2D monolayers and 3D EHTs, 8 drugs as a 'training set' were assessed (**Table 3-1**). These are selected because they represent the positive and negative inotropes commonly investigated in drug cardiotoxicity study. Concentration range of 5 x ½ log was chosen based on the literature review and/or free therapeutic plasma concentration (FTPC).

Table 3-1. List of Tier 1 compounds with known positive or negative inotropic effects in order to standardise the procedures across the platform-cell combinations within the study. Abbreviations: FTCP; free therapeutic plasma concentration; n.d, not defined; RyR2, ryanodine receptor 2; SR, sarcoplasmic reticulum.

Class	Drug	Mechanism of action	Concentration range (μM)	FTPC (μM)	References
Positive inotropes	Isoprenaline	Non-selective β adrenoceptor agonist	0.0003-0.1	0.0095	(Reyes et al., 1993)
	Digoxin	Na^+/K^+ ATPase inhibitor	0.01-10	0.00075-0.0015	(Lullmann and Ravens, 1973)
	Bay K 8644	L-type Ca^{2+} channel agonist	0.03-3	n.d.	(Aass et al., 1988)
	EMD 57033	Calcium sensitizer	0.01-30	16	(Hajjar et al., 1997, de Zeeuw et al., 2000)
	Caffeine	Opener of RyR2 (at high concentration)	100-10,000	20-40	(Chaban et al., 2017)
Negative Inotropes	Nifedipine	L-type Ca^{2+} channel blocker	0.003-0.3	0.02	(Angus et al., 2000)
	Ryanodine	Inhibitor of RyR2	1-30	n.d.	(Sutko and Willerson, 1980, Fedorov et al., 2002)
	Thapsigargin	Inhibitor of SR Ca^{2+} ATPase	0.3-30	n.d.	(Kirby et al., 1992, Baudet et al., 1993)

Preparation of hiPSC-CMs for Tier 1 phase experiment were conducted as depicted in **Figure 3-1**. After several meetings held between investigators, in house R-PAT cell line was selected for the Nottingham site in the project due to reproducibility of differentiation and electrophysiology response observed in baseline. Production of CMs derived from hiPSC using in house monolayer protocol is previously described in Methods section. Beating sheets of R-PAT cardiomyocytes were harvested and replated in a 96-well and left for 3-5 days to allow recovery and observe sign of monolayer beating cells (**Figure 3-1**A).

Quality control for R-PAT CMs used in Tier 1 phase experiment was done as shown in **Figure 3-1**B. Cells were fixed for immunocytochemistry procedure as described in Materials and Methods section (section 2.4) and stained for cardiac marker α-actinin. The 96-well plate were then scanned in a high-content imaging system Operetta (PerkinElmer). Unstained cell population were used as negative control and its intensity was quantitatively measured using proprietary software Harmony (PerkinElmer) as previously described in Materials and Methods section (section 2.4). Purity of cardiomyocytes as α-actinin positive cells was obtained by calculating percentage of number of cardiomyocytes compared to total cells, which is >90%.

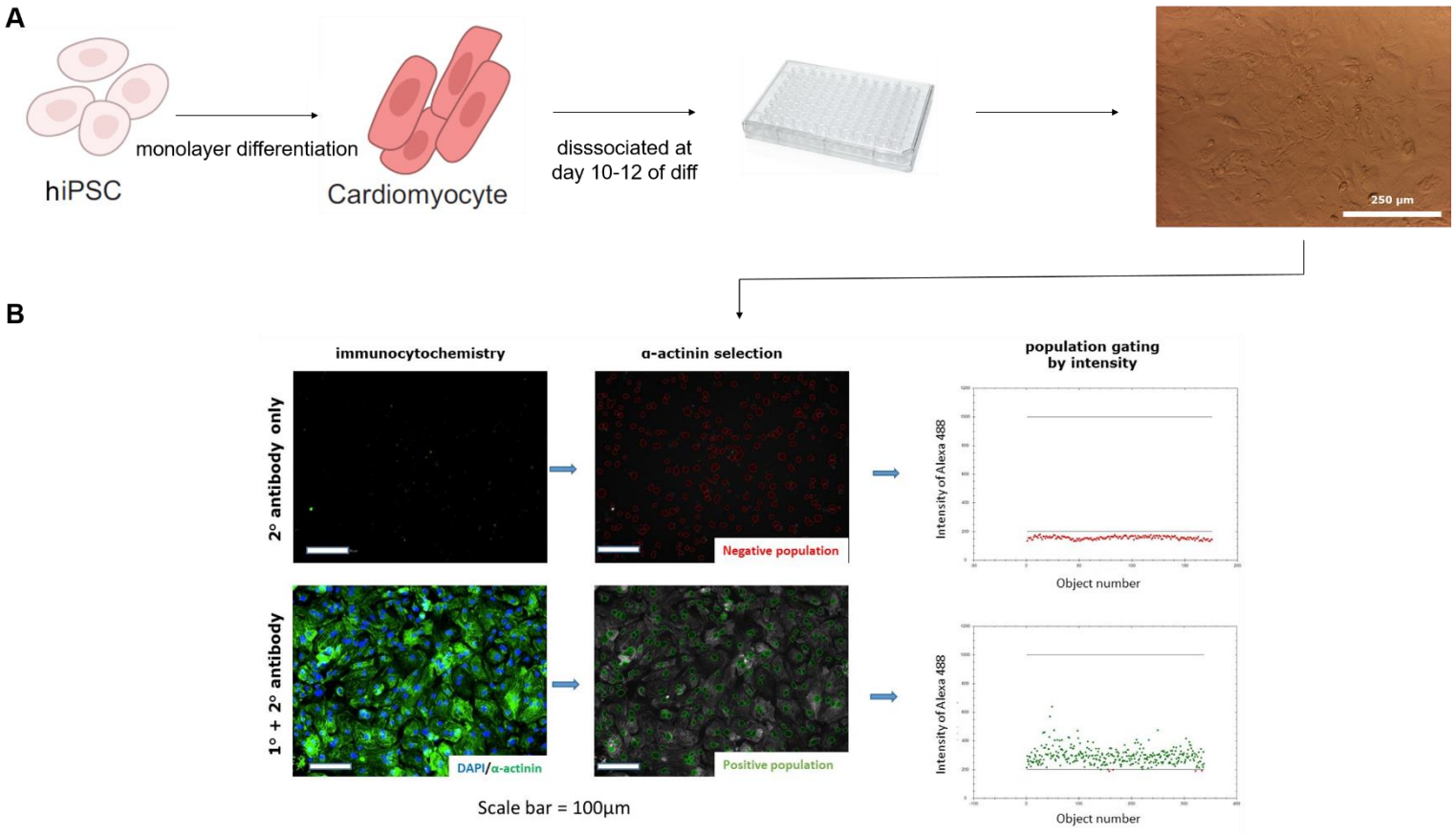

Figure 3-1. Workflow for production of in house hiPSC-CMs and quality control for Tier 1 phase. (A) Using in house monolayer differentiation protocol, cardiomyocytes derived from hiPSC were dissociated and then replated into a 96-well. (B) Immunocytochemistry with α-actinin and subsequent quantitative analysis using proprietary software were performed as quality control in order to acquire percentage of cardiomyocyte purity. Cell illustration in (A) was adapted from (Spaeter et al., 2014).

The CellOPTIQ® system (Clyde Biosciences Ltd) was used to measure the electrophysiology and contractility properties of hiPSC-CMs cultured on our screening platform. As can be seen in **Figure 3-2**A, the platform consists of: (1) a microscope with a 40x (NAO.6) objective, (2) an electrophysiology unit with fluorescence box and PC embedded with proprietary software to analyse voltage traces generated after recording at 10KHz as depicted in **Figure 3-2**C, and (3) a contractility unit with high-speed camera to analyse contraction traces after recording at 100 frames per second as shown in **Figure 3-2**E.

Principle work of voltage-sensitive dyes (VSDs) can be found in **Figure 3-2**B. Once bounded to the cell membrane's lipid bilayer, the VSDs becomes fluorescent (depicted as red). The electronic structure of the dye as well as the fluorescence properties are affected by the changes in the membrane action potential. The emitted fluorescence is measured when cardiomyocytes are excited with a 470nm light-emitting diode. The emitted fluorescence is then detected through the use of two photomultiplier tubes (PMT1 for wavelength < 585nm and PMT2 for > 585nm).

Principle work of contraction image analysis can be found in **Figure 3-2**D. Obtained 1000 images per recording were analysed offline based on pixel displacement using an ImageJ plugin. This plugin use a sum of absolute differences (SAD) algorithm, which is a measure of similarity between images. The changes in pixel intensity were acquired by comparing the absolute difference between pixels in the original frame against the pixels in the corresponding frame.

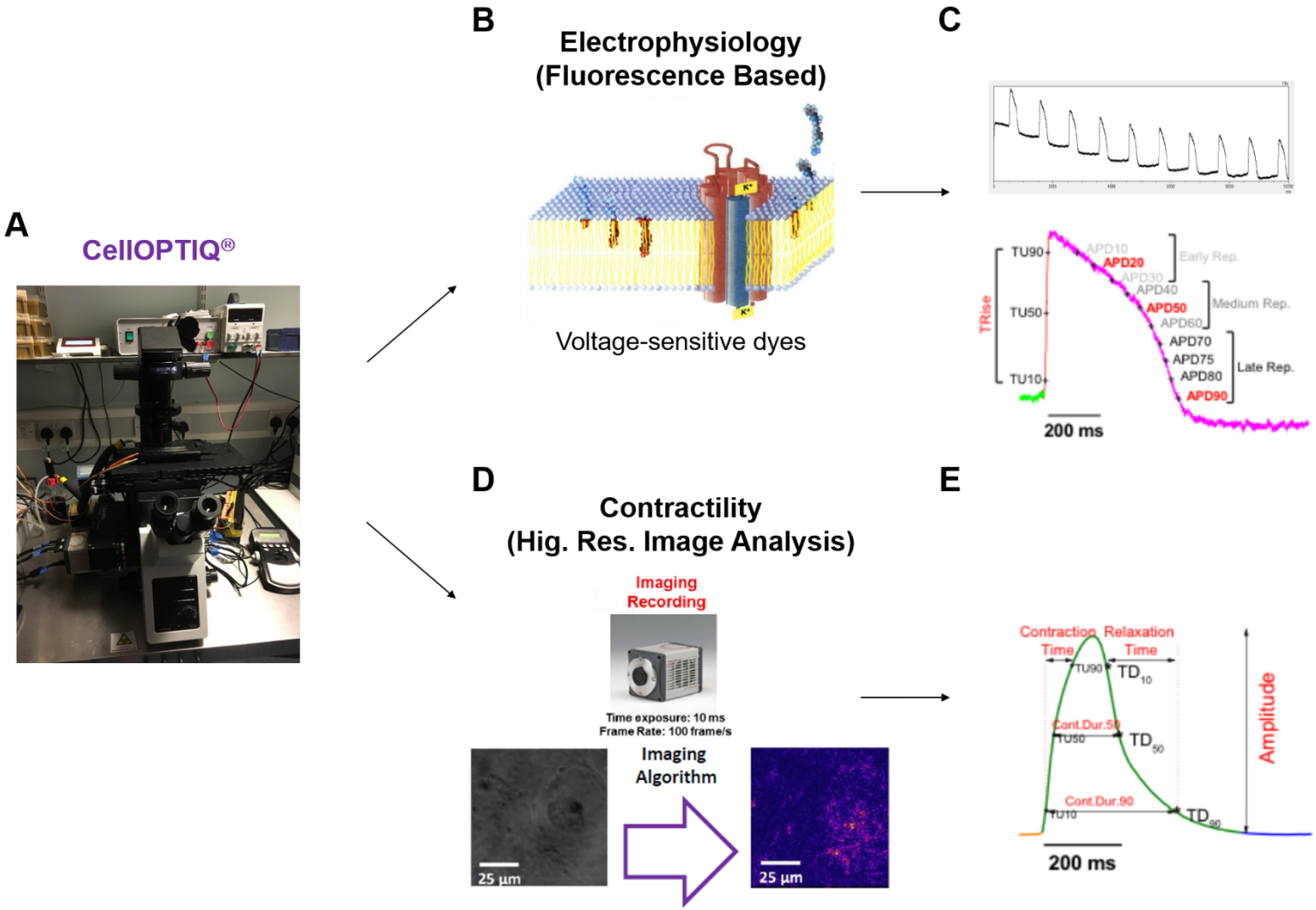

Figure 3-2. Schematic illustration of CellOPTIQ® platform. **(A)** CellOPTIQ® is a custom-built platform by Clyde Biosciences for electrophysiology, calcium handling, and contractility measurements. **(B-E)** CellOPTIQ® allows for subsequential measurement of hiPSC-CMs seeded in multiwell plates, and proprietary software generates data on a wealth of kinetic measurements. Image from **(B)** was adapted from Grinvald A. et al. (1999) In-vivo Optical Imaging of Cortical Architecture and Dynamics. In: Windhorst U., Johansson H. (eds) Modern Techniques in Neuroscience Research. Springer, Berlin, Heidelberg.

On the day of experimentation, cell and drug preparations are described as in Materials and Methods section (section 2.7). Baseline recordings were all done under spontaneous beating for both contractility and electrophysiology during Tier 1 phase. hiPSC-CMs were incubated with the indicated compound for 30 mins before treatment recordings to observe acute response. Results were calculated as percentage of change from baseline by the formula ([drug / drug baseline] / [vehicle / vehicle baseline])*100-100.

Summary of the effects of Tier 1 drugs for the positive inotropes, isoprenaline and digoxin, and the negative inotrope, nifedipine, is in **Figure 3-3**. Consistent with the mode of action of these drugs, there is a trend or significant response for positive inotropy (increased contraction amplitude) in hiPSC-CMs treated with isoprenaline and digoxin, and for negative inotropy (decreased contraction amplitude) in hiPSC-CMs treated with nifedipine.

Electrophysiology	Isoprenaline	Nifedipine
	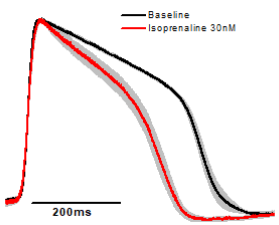	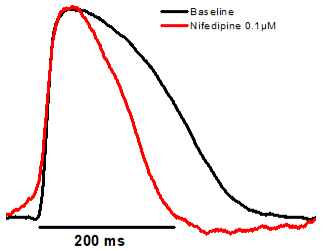
	APD shortening at highest concentration	Concentration dependent shortening of APD
Contractility	Isoprenaline	Nifedipine
	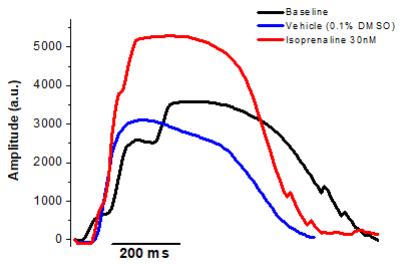	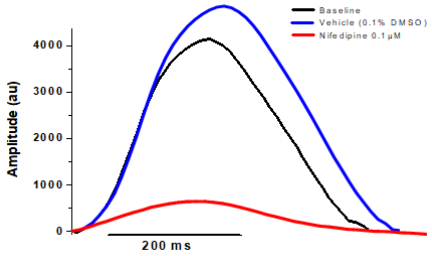
	Increased contraction amplitude at highest concentration and shortening of contraction time	Dose dependent decrease in contraction amplitude and shortening of contraction time

Figure 3-3. Summary of the effects of the representative electrophysiology and contractility data for positive (isoprenaline) and negative (nifedipine) inotropes evaluated in hiPSC-CMs using CellOPTIQ® platform during Tier 1 phase.

3.3.1.1 Isoprenaline treatment

Readouts representing hiPSC-CMs in response to treatment were plotted as mean ± SEM. Traces for voltage showed shortening of APD for the treatment (red) at highest concentration compared to baseline (black) (***Figure 3-4***A). The data were plotted as percentage of change from baseline. There was no significant difference noted for voltage TRise, APD_{20}, APD_{50}, APD_{90} in vehicle vs baseline, as well as all isoprenaline treated conditions. There was trend decrease for APD_{20}, APD_{50}, APD_{90} at 30 nM condition (69.7 ± 6.7%, 70.3 ± 4.2%, 77.3 ± 3.2%) (***Figure 3-4***C-E).

Traces for contraction amplitude showed increase as well as shift in peak maximum to the left for treatment (red) at highest concentration (as indicated by a trend concentration dependent decrease in time to 90% contraction (upstroke time)) (***Figure 3-5***A). There was no significant difference noted for contraction amplitude, Up_{90}, and Dn_{90} in vehicle control vs baseline, as well as all isoprenaline treated conditions. There was trend increase for contraction amplitude at 30 nM condition (135.4 ± 17.7%) (***Figure 3-5***B). A trend concentration dependent decrease was evident for Up_{90} (109.8 ± 23.2% [1 nM], 94.4 ± 14.9% [3 nM], 90.6 ± 8.4% [10 nM], and 82.5 ± 6.2% [30 nM]) (***Figure 3-5***C). A slight trend concentration dependent increase was observed for Dn_{90} (116.5 ± 7% [1 nM], 114.2 ± 17.8% [3 nM], 120.2 ± 8.7% [10 nM], and 125.3 ± 29.2% [30 nM]) (***Figure 3-5***D).

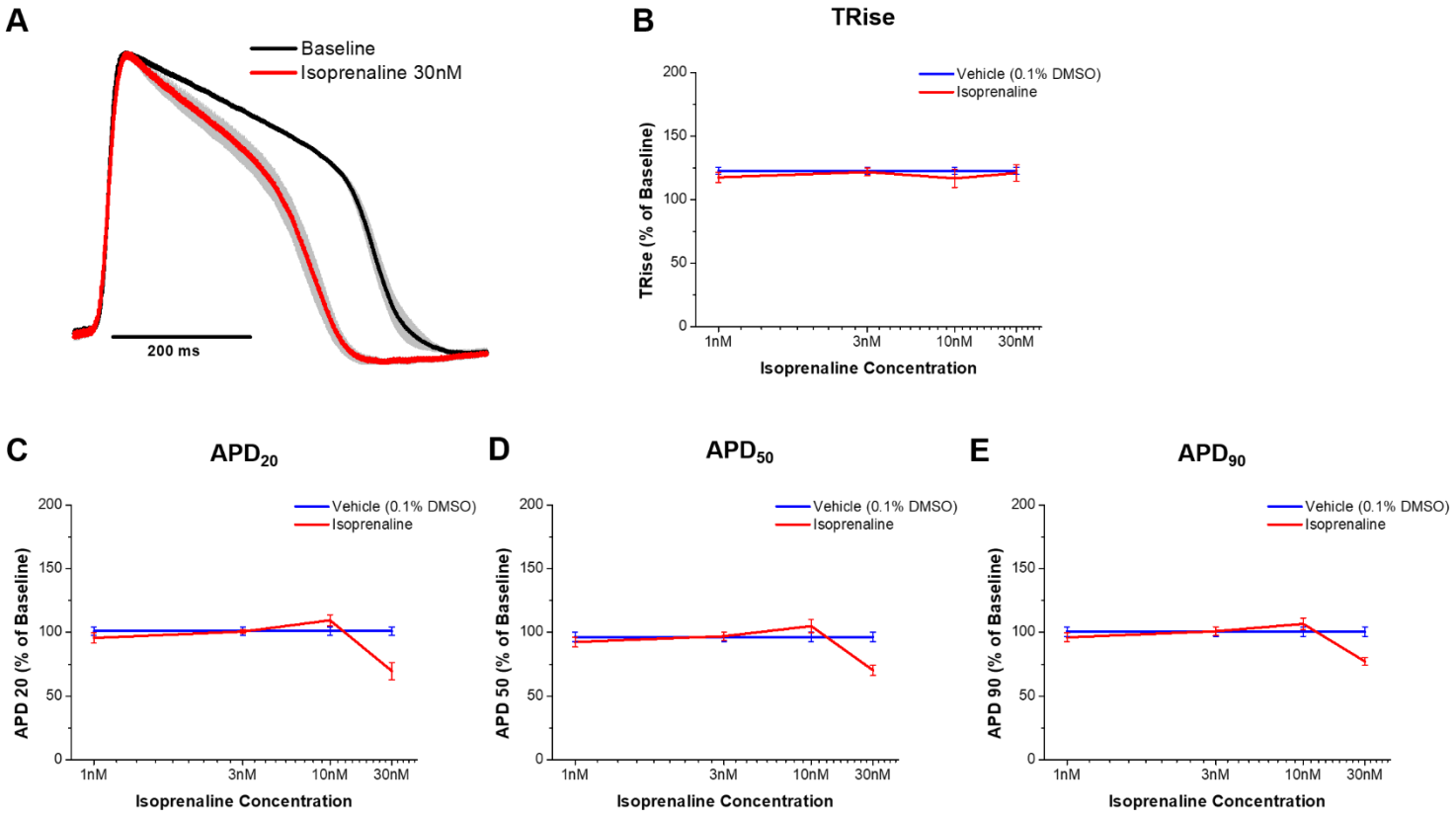

Figure 3-4. Electrophysiology analysis of hiPSC-CMs on 2D monolayers treated with isoprenaline. (A) Representative voltage traces at highest concentration for action potential duration at 90% of repolarisation (APD_{90}). **(B)** Data in TRise showed no significant difference after treatment. **(C-E)** Data in action potential duration at 20, 50, and 90% of repolarisation showed trend decrease at highest concentration. hiPSC-CMs were analysed using CellOPTIQ® as previously described. Baseline (black), vehicle control (blue), and treatment (red). One data point per well was recorded (n=5 per concentration). Data are displayed as mean ± SEM. One-way ANOVA followed by post hoc Tukey's test (p ⩽: * 0.05, ** 0.01).

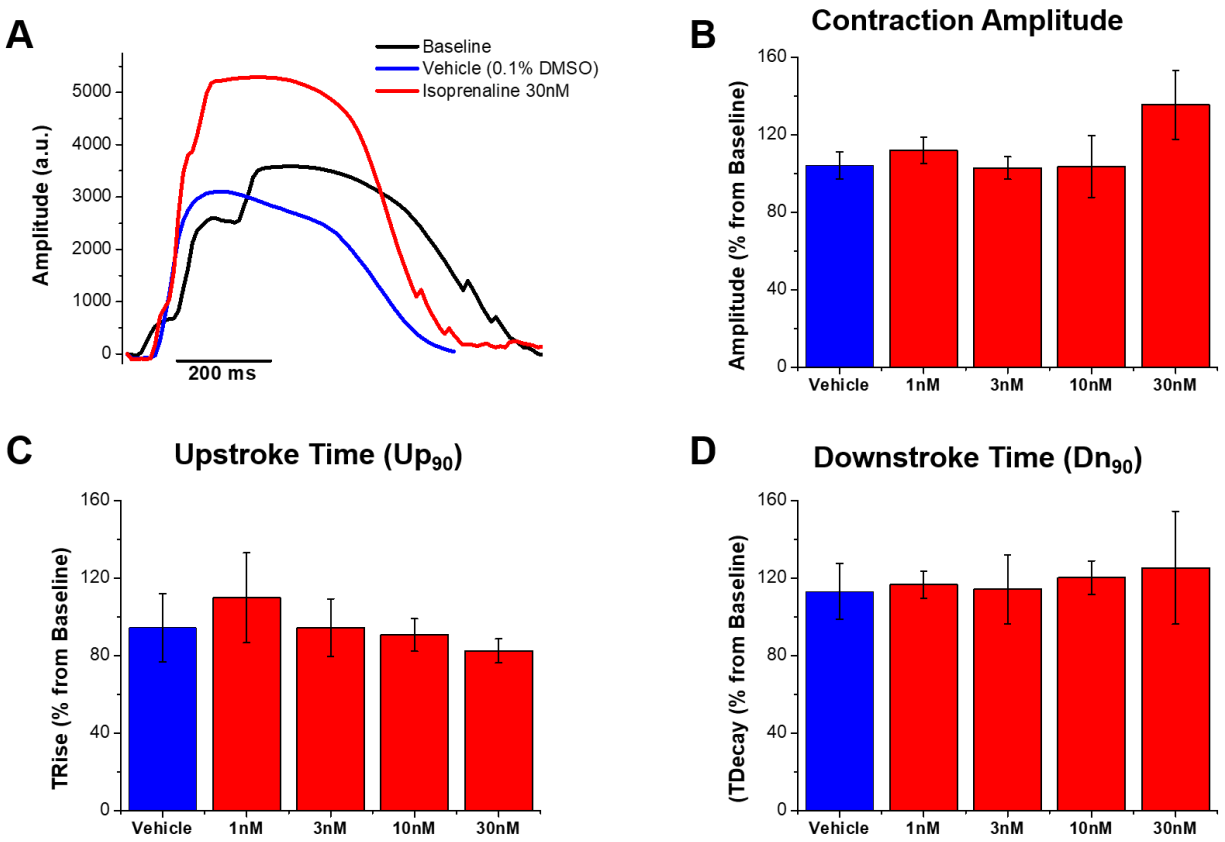

Figure 3-5. Contractility analysis of hiPSC-CMs on 2D monolayers treated with isoprenaline. (A) Representative contractility traces at highest concentration for amplitude. **(B)** Data in contraction amplitude showed trend increase at highest concentration. **(C)** Data in time to 90% contraction (upstroke time) showed trend concentration dependent decrease. **(D)** Data in time to 90% relaxation (downstroke time) showed trend concentration dependent increase. hiPSC-CMs were analysed using CellOPTIQ® as previously described. Baseline (black), vehicle control (blue), and treatment (red). One data point per well was recorded (n=5 per concentration). Data are displayed as mean ± SEM. One-way ANOVA followed by post hoc Tukey's test ($p \leqslant$: * 0.05, ** 0.01).

3.3.1.2 Digoxin treatment

Readouts representing hiPSC-CMs in response to treatment were plotted as mean ± SEM. Traces for voltage showed quiescent at highest concentration (***Figure 3-6***A). There was significant decrease for voltage TRise at 0.3 (85.1 ± 12.2%) (***Figure 3-6***B). Same trend of significant decrease was also observed in APD_{20} at 0.1-0.3 μM (91.2 ± 6.3%, 86 ± 2.1%) (***Figure 3-6***C). In APD_{50}, significant decrease was noted at 0.3 μM (88.2 ±1.9%) (***Figure 3-6***D). In APD_{90}, there are no significant difference compared to baseline (***Figure 3-6***E).

Traces for contraction amplitude showed no change in vehicle (blue) vs baseline (black), and increase as well as shift in peak maximum to the right in peak amplitude for treatment (red) at highest concentration (as indicated by a concentration dependent increase in time to 90% contraction (upstroke time)) (***Figure 3-7***A). There was significant difference noted for contraction amplitude in digoxin treated conditions at 0.3-3 μM (127.4 ± 11.3%, 174.1 ± 16% & 156 ± 12.2%) (***Figure 3-7***B). A similar trend in significance was observed for Up_{90} for all digoxin treated conditions (156 ± 15%, 147.6 ± 8.7%, 219.8 ± 18.4% & 223.5 ± 23%) (***Figure 3-7***C). However, there was no significant difference observed for Dn_{90} in vehicle control vs baseline, as well as all digoxin treated conditions (***Figure 3-7***D).

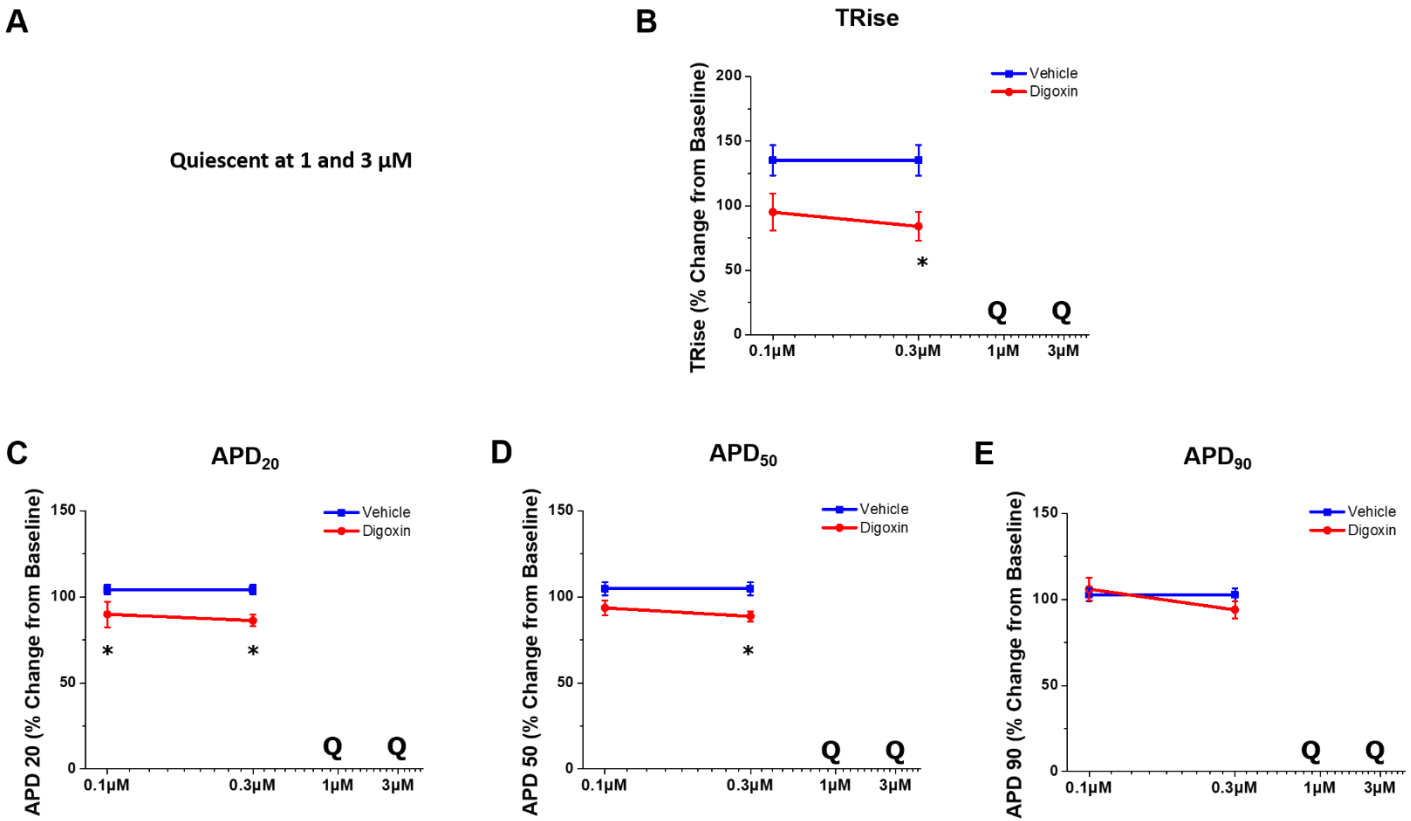

Figure 3-6. Electrophysiology analysis of hiPSC-CMs on 2D monolayers treated with digoxin. (A) Representative voltage traces at highest concentration for action potential duration at 90% of repolarisation (APD90). **(B)** Data in TRise showed slight decrease. **(C-E)** Data in action potential duration at 20, 50, and 90% of repolarisation showed concentration dependent decrease. hiPSC-CMs were analysed using CellOPTIQ® as previously described. Baseline (black), vehicle control (blue), and treatment (red). One data point per well was recorded (n=5 per concentration). Data are displayed as mean ± SEM. One-way ANOVA followed by post hoc Tukey's test ($p \leqslant$: * 0.05, ** 0.01).

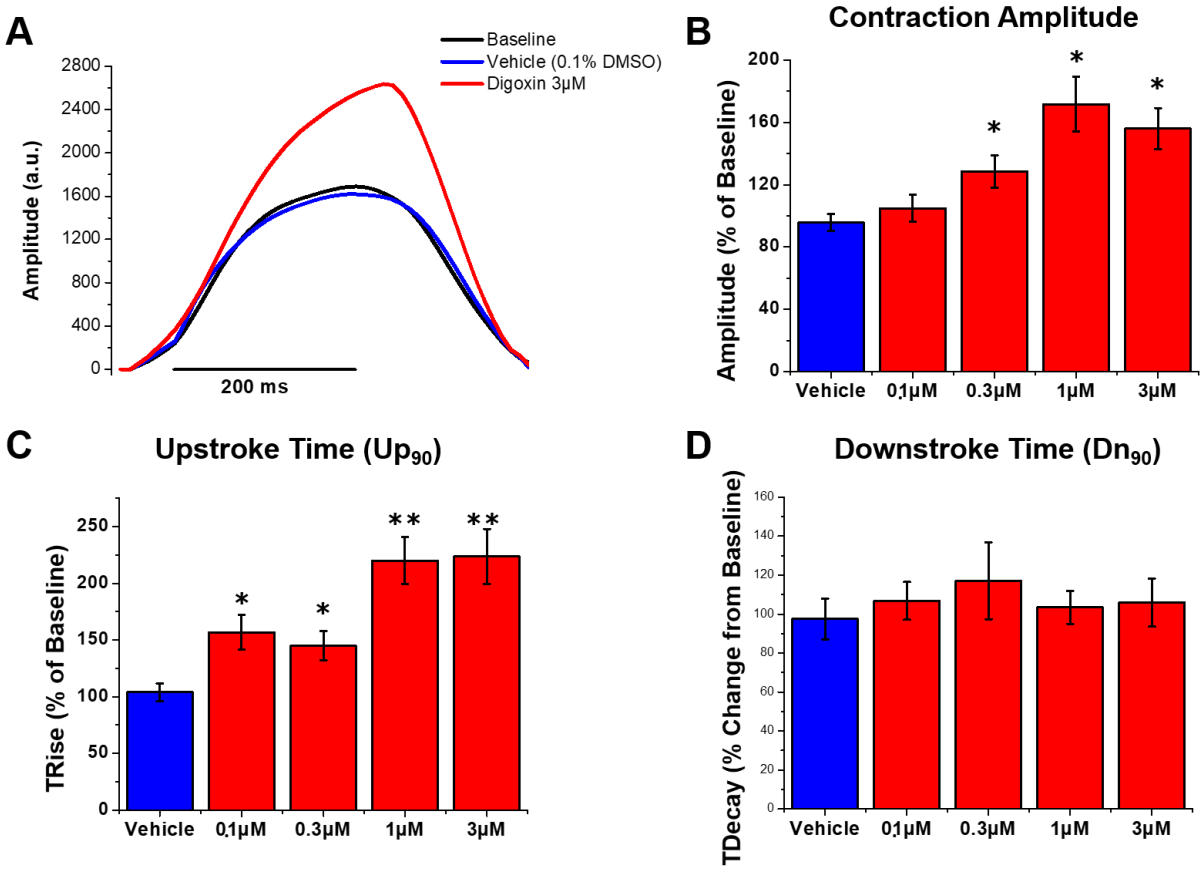

Figure 3-7. Contractility analysis of hiPSC-CMs on 2D monolayers treated with digoxin. **(A)** Representative contractility traces at highest concentration for amplitude. **(B)** Data in contraction amplitude showed concentration dependent increase. **(C)** Data in time to 90% contraction (upstroke time) showed concentration dependent increase. **(D)** Data in time to 90% relaxation (downstroke time) showed no significant difference after treatment. hiPSC-CMs were analysed using CellOPTIQ® as previously described. Baseline (black), vehicle control (blue), and treatment (red). One data point per well was recorded (n=5 per concentration). Data are displayed as mean ± SEM. One-way ANOVA followed by post hoc Tukey's test ($p \leqslant$: * 0.05, ** 0.01).

3.3.1.3 Bay K 8644 treatment

Readouts representing hiPSC-CMs in response to treatment were plotted as mean ± SEM. Traces for voltage showed prolonged APD for the treatment (red) at highest concentration compared to baseline (black) (***Figure 3-8***A). There was trend increase for voltage TRise at all conditions (139.1 ± 3.4%, 151 ± 3.5%, 134.3 ± 5.4% & 135.4 ± 4.7%) (***Figure 3-8***B). Same trend increase was also observed in APD_{20} for all Bay K 8644 treated conditions (145.9 ± 3.6%, 141.8 ± 3.4%, 152.2 ± 3.6% & 148.2 ± 2.9%) (***Figure 3-8***C). In APD_{50}, trend increase was also noted at all conditions (158.1 ± 3.2%, 159.4 ± 4.1%, 159.6 ± 3.9%, & 152.8 ± 1.1%) (***Figure 3-8***D). In APD_{90}, trend increase was noted at all conditions (156.7 ± 2.6%, 160.3 ± 4%, 157.2 ± 3.7%, & 152.6 ± 0.7%) (***Figure 3-8***E).

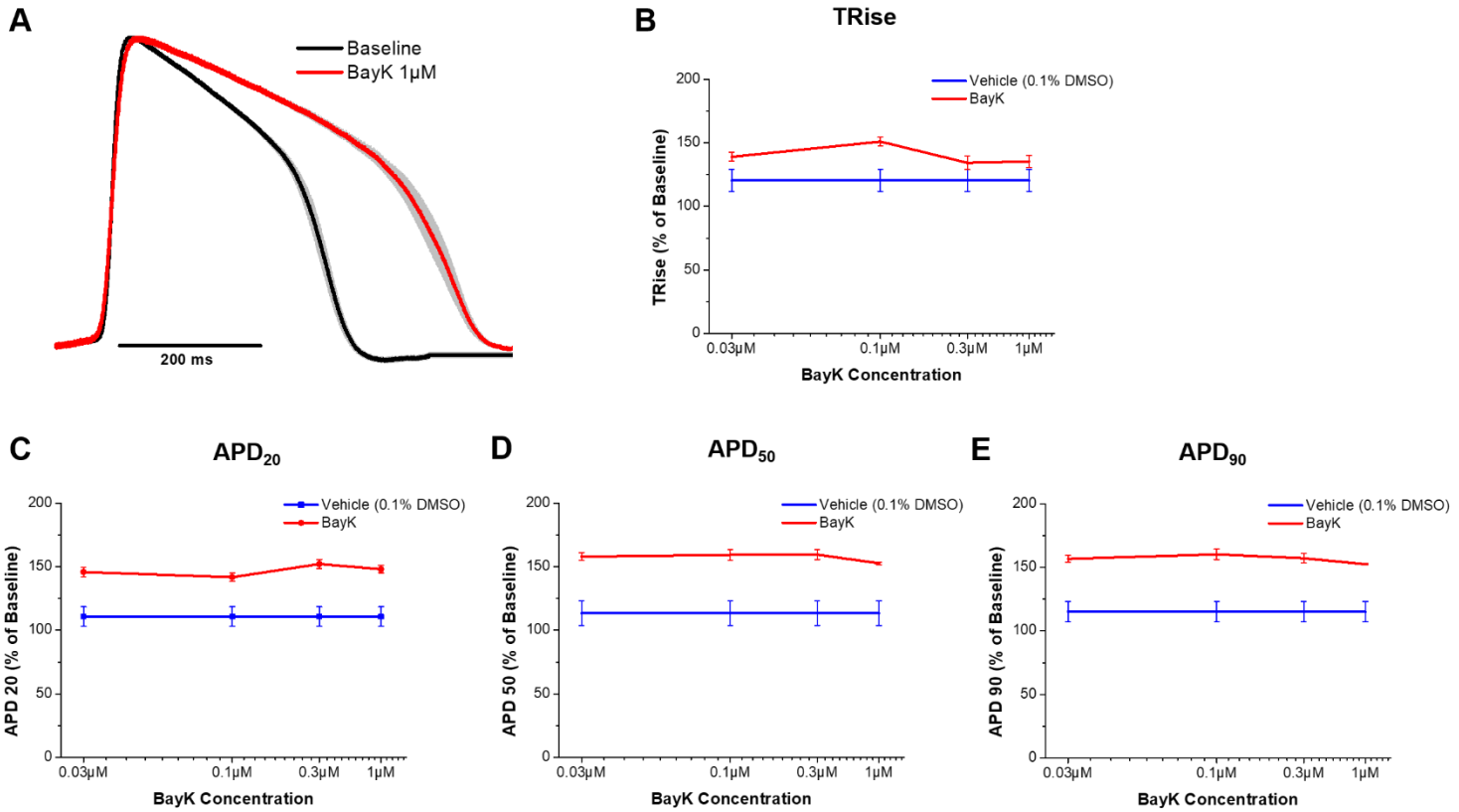

Figure 3-8. Electrophysiology analysis of hiPSC-CMs on 2D monolayers treated with Bay K 8644. (A) Representative voltage traces at highest concentration for action potential duration at 90% of repolarisation (APD90). **(B)** Data in TRise showed increased yet no significant difference after treatment. **(C-E)** Data in action potential duration at 20, 50, and 90% of repolarisation showed increased yet no significant difference after treatment. hiPSC-CMs were analysed using CellOPTIQ® as previously described. Baseline (black), vehicle control (blue), and treatment (red). One data point per well was recorded (n=5 per concentration). Data are displayed as mean ± SEM. One-way ANOVA followed by post hoc Tukey's test (p ⩽: * 0.05, ** 0.01).

3.3.1.4 EMD 57033 treatment

Readouts representing hiPSC-CMs in response to treatment were plotted as mean ± SEM. Traces for voltage showed shortening APD for the treatment (red) at highest concentration compared to baseline (black) (***Figure 3-9***A). There was slight trend increase for voltage TRise at all conditions (112.1 ± 1.1%, 141 ± 16.7%, 114.8 ± 3.9% & 132.2 ± 9.9%) (***Figure 3-9***B). There was slight trend decrease in APD_{20} particularly at 1 and 10 µM (91.5 ± 1.9%, 76.4 ± 3.1%, respectively) (***Figure 3-9***C). Similar trend was found in APD_{50} particularly at 1 and 10 µM (90 ± 3.3%, 85.9 ±2.9%, respectively) (***Figure 3-9***D). In APD90, trend decrease was more prominent only at 1 µM (95.1 ± 3.1%) (***Figure 3-9***E).

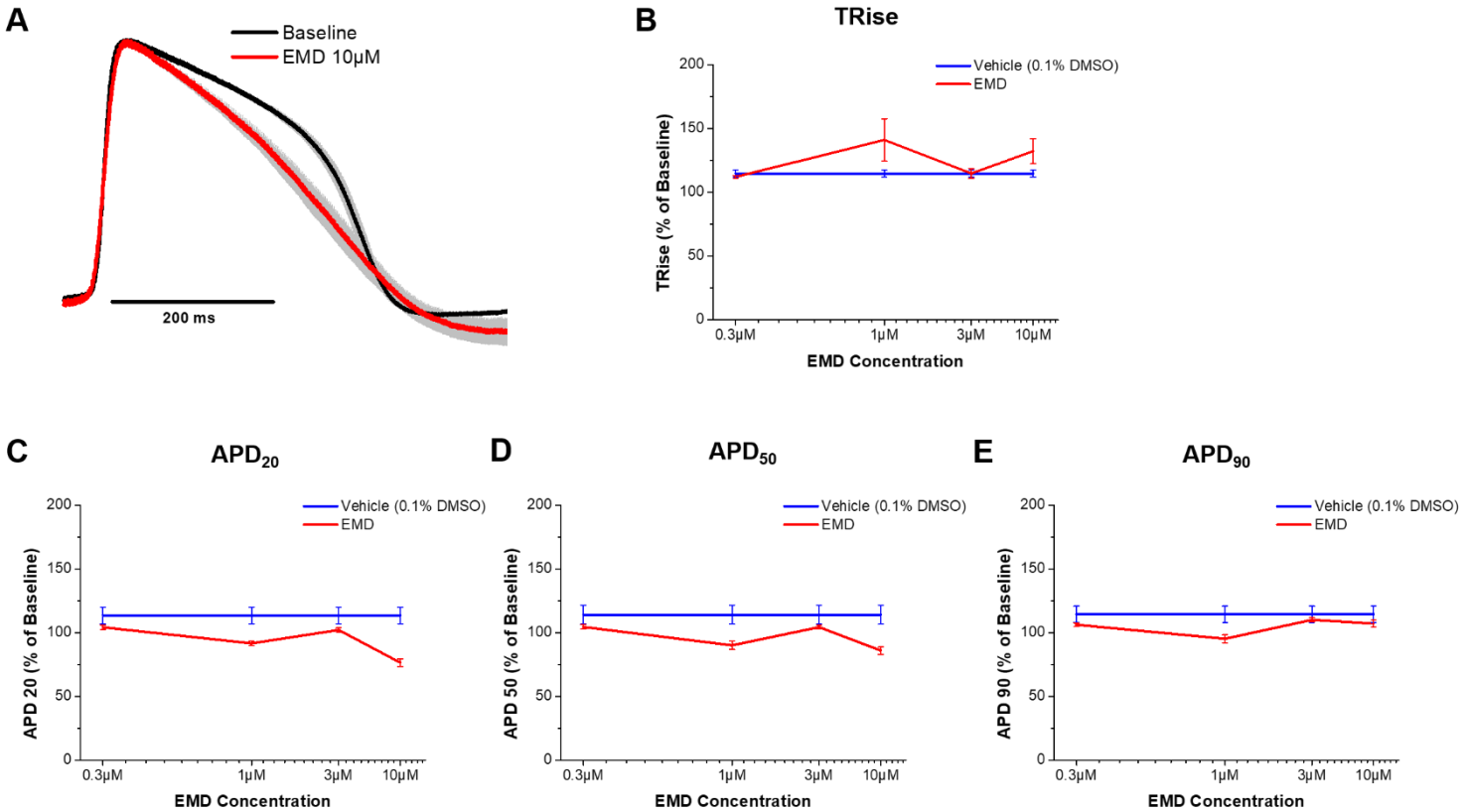

Figure 3-9. Electrophysiology analysis of hiPSC-CMs on 2D monolayers treated with EMD 50377. (A) Representative voltage traces at highest concentration for action potential duration at 90% of repolarisation (APD90). **(B)** Data in TRise showed trend increase yet no significant difference after treatment. **(C-E)** Data in action potential duration at 20, 50, and 90% of repolarisation showed trend decrease yet no significant difference after treatment. hiPSC-CMs were analysed using CellOPTIQ® as previously described. Baseline (black), vehicle control (blue), and treatment (red). One data point per well was recorded (n=5 per concentration). Data are displayed as mean ± SEM. One-way ANOVA followed by post hoc Tukey's test (p ⩽: * 0.05, ** 0.01).

3.3.1.5 Nifedipine treatment

Readouts representing hiPSC-CMs in response to treatment were plotted as mean ± SEM. Traces for voltage showed shortening APD for the treatment (red) at highest concentration compared to baseline (black) (***Figure 3-10***A). There was significant evident concentration dependent increase for voltage TRise at 0.03 and 0.1 μM (119 ± 14.5% & 138.1 ± 17.9%, respectively) (***Figure 3-10***B). Significant concentration dependent decrease was observed in APD_{20} at 0.01-0.1 μM (65.3 ± 5.8%, 59.4 ± 1.3% & 53 ± 0.06%) (***Figure 3-10***C). In APD_{50}, similar significant concentration dependent decrease was noted at 0.01-0.1 μM (81.5 ± 8.4%, 70 ± 2.5% & 58 ± 1.3%) (***Figure 3-10***D). In APD_{90}, significant concentration dependent decrease was noted at 0.03 and 0.1 uM (74.6 ± 3.4% & 59.8 ± 2.8%) (***Figure 3-10***E).

Traces for contraction amplitude showed shift in peak maximum to the right for the vehicle control (blue) compared to baseline (black) yet no significant difference, and showed evident decrease as well as shift in peak maximum to the left for treatment (red) at highest concentration (as indicated by a significant concentration dependent decrease in time to 90% contraction (upstroke time)) (***Figure 3-11***A). There was significant evident concentration dependent decrease noted for contraction amplitude in nifedipine treated conditions at 0.01-0.1 μM (70.1 ± 8%, 45.4 ± 0.8% & 15.4 ± 1.3%) (***Figure 3-11***B). A significant trend was also observed for Up_{90} at 0.03 and 0.1 μM (89.6 ± 3.5% & 84.5 ± 11%, respectively) (***Figure 3-11***C). Significant evident concentration dependent increase for Dn_{90} was observed particularly at 0.003 and 0.1 uM (69.2 ± 0.7%, 133 ± 6%, respectively) (***Figure 3-11***D).

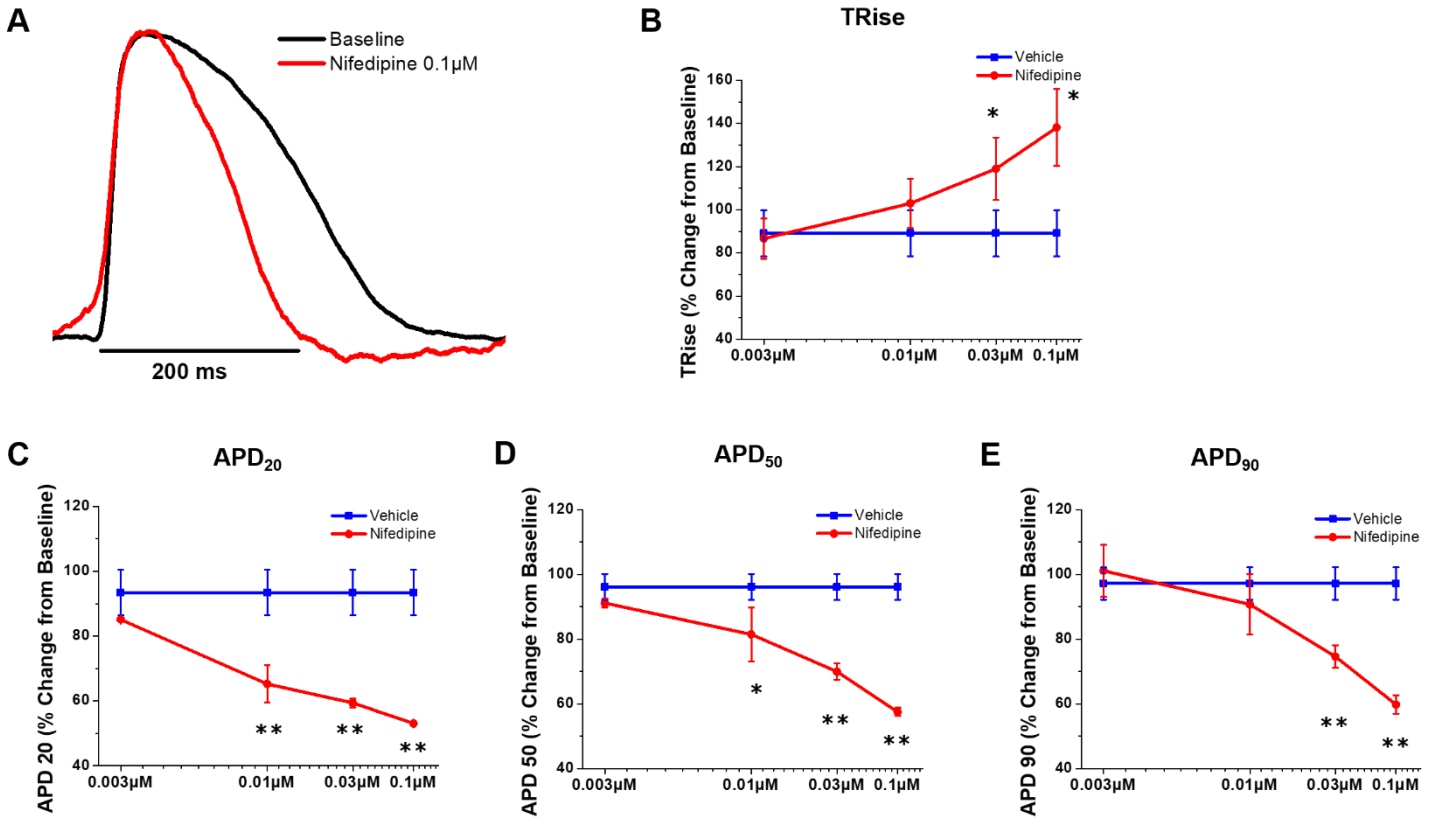

Figure 3-10. Electrophysiology analysis of hiPSC-CMs on 2D monolayers treated with nifedipine. (A) Representative voltage traces at highest concentration for action potential duration at 90% of repolarisation (APD90). **(B)** Data in TRise showed significant concentration dependent increase. **(C-E)** Data in action potential duration at 20, 50, and 90% of repolarisation showed significant concentration dependent decrease. hiPSC-CMs were analysed using CellOPTIQ® as previously described. Baseline (black), vehicle control (blue), and treatment (red). One data point per well was recorded (n=5 per concentration).

Data are displayed as mean ± SEM. One-way ANOVA followed by post hoc Tukey's test (p ⩽: * 0.05, ** 0.01).

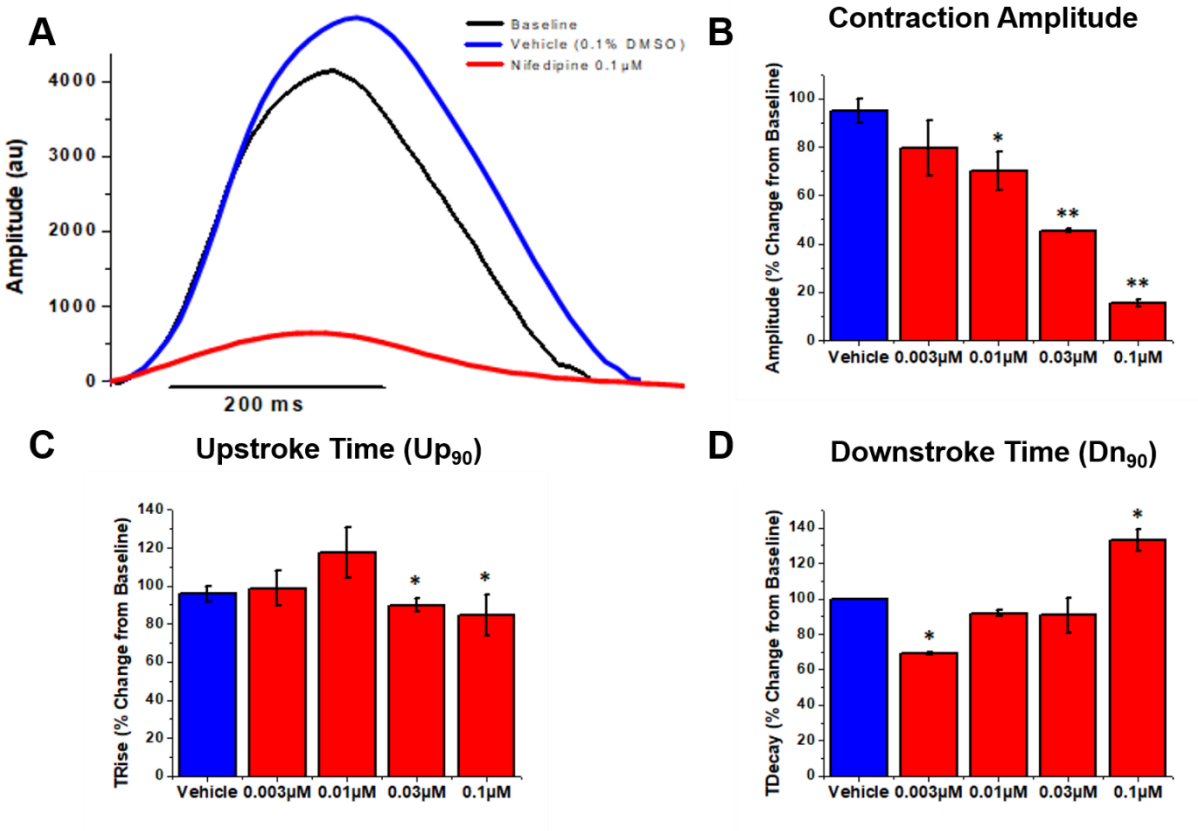

Figure 3-11. Contractility analysis of hiPSC-CMs on 2D monolayers treated with nifedipine. (A) Representative contractility traces at highest concentration for amplitude. **(B)** Data in contraction amplitude showed significant concentration dependent decrease. **(C)** Data in time to 90% contraction (upstroke time) showed significant decrease at higher concentrations. **(D)** Data in time to 90% relaxation (downstroke time) showed significant concentration dependent increase. hiPSC-CMs were analysed using CellOPTIQ® as previously described. Baseline (black), vehicle control (blue), and treatment (red). One data point per well was recorded (n=5 per concentration). Data are displayed as mean ± SEM. One-way ANOVA followed by post hoc Tukey's test ($p \leqslant$: * 0.05, ** 0.01).

3.3.1.6 Ryanodine treatment

Readouts representing hiPSC-CMs in response to treatment were plotted as mean ± SEM. Traces for voltage showed shortening APD for the treatment (red) at highest concentration compared to baseline (black) (***Figure 3-12***A). There was significant increase for voltage TRise at all conditions (142 ± 13.9%, 151.3 ± 17.4%, 147.7 ± 18.7% & 150 ± 14.8%) (***Figure 3-12***B). In APD_{20} and APD_{50}, an increase in lowest concentration at 1 µM was noted (108.6 ± 4.3% & 111 ± 4.7%, respectively). Significant concentration dependent decrease was observed in APD_{20} at 3-30 µM (79.3 ± 3.9%, 78.4 ± 1.3% & 77.9 ± 2.2%) (***Figure 3-12***C). In APD_{50}, similar significant concentration dependent decrease was noted at 3-30 µM (85.2 ± 7.1%, 80.4 ± 5.7% & 78.7 ± 2.9%) (***Figure 3-12***D). In APD_{90}, significant concentration dependent decrease was noted at 3-30 µM (82.3 ± 2%, 73.6 ± 1.3% & 71.1 ± 4%) (***Figure 3-12***E).

Traces for contraction amplitude showed no significant difference for the vehicle control (blue) compared to baseline (black), as well as for treatment (red) at highest concentration (***Figure 3-13***A). There was no significant difference noted for contraction amplitude, Up_{90}, and Dn_{90} in vehicle control vs baseline, as well as all ryanodine treated conditions. A slight trend increase was observed for Up_{90} at 30 µM (114.1 ± 17.8%) (***Figure 3-13***C).

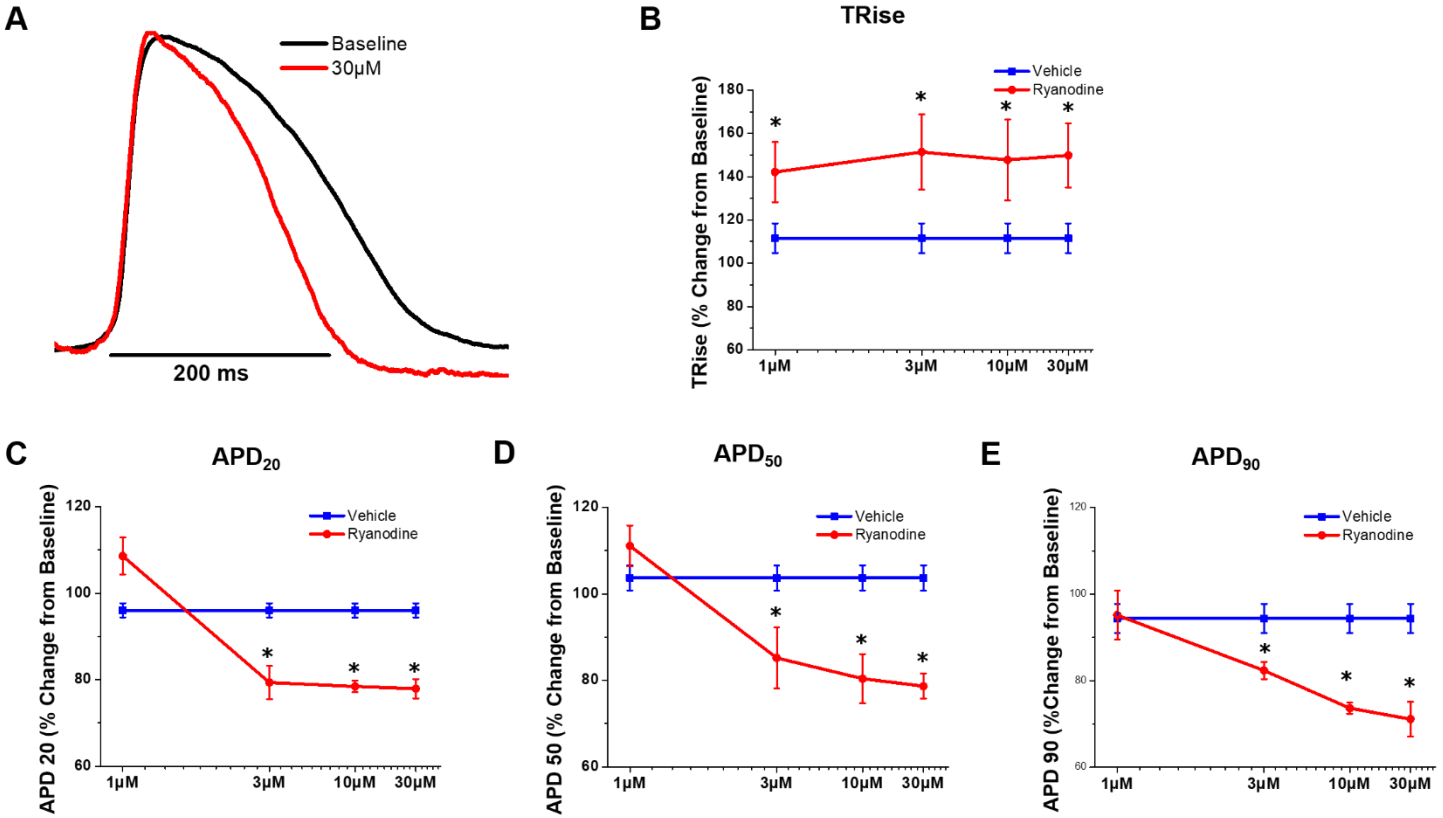

Figure 3-12. Electrophysiology analysis of hiPSC-CMs on 2D monolayers treated with ryanodine. (A) Representative voltage traces at highest concentration for action potential duration at 90% of repolarisation (APD90). **(B)** Data in TRise showed significant increase. **(C-E)** Data in action potential duration at 20, 50, and 90% of repolarisation showed significant concentration dependent decrease. hiPSC-CMs were analysed using CellOPTIQ® as previously described. Baseline (black), vehicle control (blue), and treatment (red). One data

point per well was recorded (n=5 per concentration). Data are displayed as mean ± SEM. One-way ANOVA followed by post hoc Tukey's test (p ⩽: * 0.05, ** 0.01).

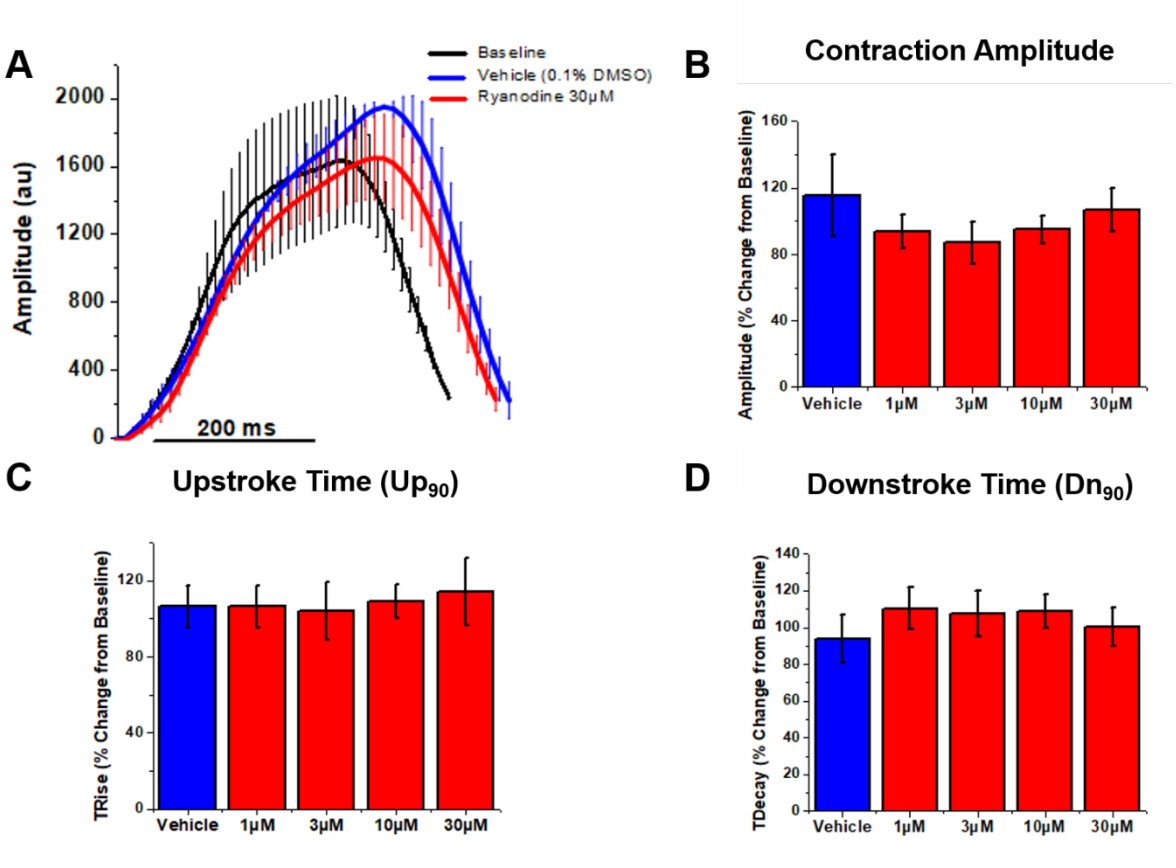

Figure 3-13. Contractility analysis of hiPSC-CMs on 2D monolayers treated with ryanodine. (A) Representative contractility traces at highest concentration for amplitude. **(B)** Data in contraction amplitude showed no significant difference after treatment. **(C)** Data in time to 90% contraction (upstroke time) showed trend increase at highest concentration. **(D)** Data in time to 90% relaxation (downstroke time) showed no significant difference after treatment. hiPSC-CMs were analysed using CellOPTIQ® as previously described. Baseline (black), vehicle control (blue), and treatment (red). One data point per well was recorded (n=5 per concentration). Data are displayed as mean ± SEM. One-way ANOVA followed by post hoc Tukey's test (p ⩽: * 0.05, ** 0.01).

3.3.1.7 Thapsigargin treatment

Readouts representing hiPSC-CMs in response to treatment were plotted as mean ± SEM. Traces for voltage showed prolonged APD for the treatment (red) at highest concentration compared to baseline (black) (***Figure 3-14***A). There was no significant difference observed for voltage TRise at all conditions (***Figure 3-14***B). There was trend increase in APD_{20}, APD_{50}, and APD_{90} particularly at 30 μM (157.3 ± 6%, 170.5 ± 4.5%, & 173.8 ± 3.8%, respectively) (***Figure 3-14***C-E).

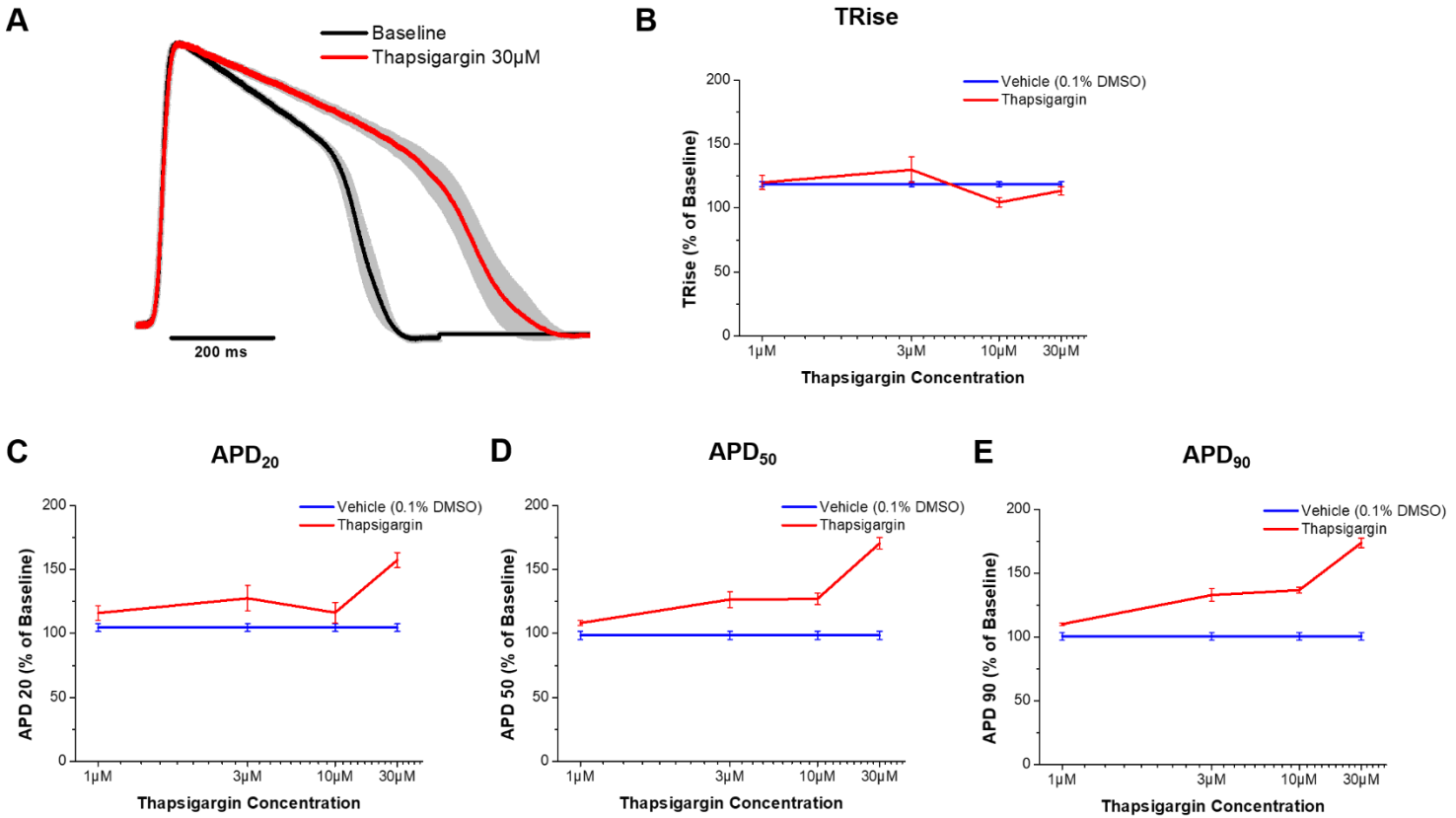

Figure 3-14. Electrophysiology analysis of hiPSC-CMs on 2D monolayers treated with thapsigargin. (A) Representative voltage traces at highest concentration for action potential duration at 90% of repolarisation (APD90). **(B)** Data in TRise showed no significant difference after treatment. **(C-E)** Data in action potential duration at 20, 50, and 90% of repolarisation showed trend increase at highest concentration. hiPSC-CMs were analysed using CellOPTIQ® as previously described. Baseline (black), vehicle control (blue), and treatment (red). One data point per well was recorded (n=5 per concentration). Data are displayed as mean ± SEM. One-way ANOVA followed by post hoc Tukey's test (p ⩽: * 0.05, ** 0.01).

3.3.1.8 Discussion

The results presented from T1 phase demonstrate the ability of hiPSC-CMs on 2D monolayers assessed with CellOPTIQ® to predict cardiac safety when treated with varying pharmaceutical compounds. CMs treated with isoprenaline (adrenergic stimulation) revealed a positive inotrope response, as indicated by increase in contraction amplitude at highest concentration (30 nM). Shift to the left in peak amplitude is consistent with hiPSC-CMs on 3D EHTs (**Figure 3-16**A), and is related with decrease in upstroke time. A previous contractility study of isoprenaline in isolated rat cardiomyocytes demonstrated an increase in contractile force by 9.75% at 1 μM (You et al., 2014), whilst another similar study revealed no effect at 1 nM, a slight increase in contractility at 10 and 100 nM, and a slight decrease in contractility at 1 and 10 μM (Boudou et al., 2012). Previous studies utilising hiPSC-CMs have shown that the addition of isoprenaline increased the amplitude and rate of contraction (Germanguz et al., 2011, Yokoo et al., 2009). Effective concentration has been reported to be ranging from 10 to 1000 nM (Navarrete et al., 2013, Nozaki et al., 2017). Electrophysiological analysis showed trend decrease in APDs at highest concentration (30 nM).

CMs treated with digoxin (Na^+/K^+ ATPase inhibitor) also revealed a positive inotrope response, as indicated by increase in contraction amplitude at higher concentrations (0.3-3 μM). Again, shift to the right peak amplitude is consistent with hiPSC-CMs on 3D EHTs, although it is less prominent (**Figure 3-16**B), and is related with increase in upstroke time. Previous contractility studies of digoxin in isolated rat cardiomyocytes demonstrated an increase in contractile force by 19.3% and 22% both at 1 μM, respectively (You et al., 2014, Boudou et al., 2012). Electrophysiology analysis showed a significant decrease in APDs and voltage TRise, with quiescent cells detected at concentration of 1 and 3 μM. A previous electrophysiology study of digoxin using hiPSC-CMs reported occurrence of arrhythmic beats at concentrations ≥0.3 μM, with transient acceleration of spontaneous beats described as ventricular tachycardia (VT)-like beats at 1 μM, followed by rapidly decline rate of synchronous beats and the development of rapid asynchronous, small-amplitude with high-frequency waves described as ventricular fibrillation

(VF)-like beats at 10 μM (Guo et al., 2011). This study reported that no arrhythmic events were observed in hiPSC-CMs exposed to the vehicle. Another electrophysiology study of digoxin in hiPSC-CMs at 1 μM showed ~20% decrease in APD_{50} yet ~20% increase in TRise and APD_{90} (Dempsey et al., 2016).

CMs treated with Bay K 8644 (L-type Ca^{2+} channel agonist) demonstrated prolonged APDs and increase in voltage TRise, which is consistent with Glasgow site. A previous electrophysiology study of Bay K 8644 in isolated mouse cardiomyocytes demonstrated a concentration-dependent increase in APD (Tertoolen et al., 2018). Although contractility was not performed on Nottingham site and therefore could not be directly compared to, hiPSC-CMs on 3D EHTs showed increase in peak amplitude as shown in **Figure 3-16**C. A previous contractility study of Bay K 8644 in isolated rat cardiomyocytes demonstrated an increase in contractile force by 23.81% at 100 nM (You et al., 2014).

CMs treated with EMD 57033 (calcium sensitizer) demonstrated shortened APDs and trend increase in voltage TRise, which is consistent with Glasgow site (data not shown). Although contractility was not performed on Nottingham site and therefore could not be directly compared to, hiPSC-CMs on 3D EHTs showed increase and shift to the right in peak amplitude as shown in **Figure 3-16**D. A previous contractility study of EMD 57033 in neonatal rat cardiomyocytes exhibited increased twitch forces by 20–25% at 10 mM (Rodriguez et al., 2013).

CMs treated with nifedipine (L-type Ca^{2+} channel antagonist) revealed a negative inotrope response, as indicated by evident concentration dependent decrease in contraction amplitude at 0.01-0.1 μM. Shift to the left in peak amplitude is consistent with hiPSC-CMs on 3D EHTs, although it is less prominent (**Figure 3-16**E), and is related with increase in downstroke time. A previous contractility study of nifedipine in human papillary muscle strips showed a decrease in contractile force (Schwinger et al., 1990). Electrophysiological analysis showed a significant concentration dependent decrease in APDs and concentration dependent increase in voltage TRise. A previous electrophysiology study of nifedipine in hiPSC-CMs at 0.01 μM showed ~20% decrease in APD_{50} and APD_{90} and ~20% increase in TRise (Dempsey et al., 2016). Other electrophysiology

studies showed a decrease in APD at 30 nM (Harris et al., 2013, Peng et al., 2010).

CMs treated with ryanodine (RyR2 inhibitor) unsuccessfully predicted a negative inotrope response, with no significant change in contraction amplitude, upstroke time, and downstroke time. hiPSC-CMs on 3D EHTs showed slight decrease and shift to the right in peak amplitude (***Figure 3-16***F). Studies using animal myocytes (rat, rabbit, cat, and dog) showed a decrease in contractile force as well as an increase in time to peak. In some species, at lower concentrations ryanodine exhibited negative inotropic effects, whilst at higher concentrations exhibited positive inotropic effects, termed a biphasic response (Sutko and Willerson, 1980). Previous study have shown that ryanodine decreased peak contraction amplitude and maximum rates of contraction and relaxation (Germanguz et al., 2011). Another previous contractility study of ryanodine in rabbit ventricular cardiomyocytes showed a decrease of RyR2 Ca^{2+} release at 30 μM (Zhang et al., 2018). As previously mentioned in the introduction, hiPSC-CMs lack expression of RyR2 and instead rely on IP_3R for SR Ca^{2+} release (Itzhaki et al., 2011), which may explain the lack of negative inotrope response. Electrophysiological analysis showed a significant concentration dependent decrease in APDs and increase in voltage TRise.

CMs treated with thapsigargin (SR Ca^{2+} ATPase inhibitor) demonstrated prolonged APDs, which is consistent with Glasgow site (data not shown). Although contractility was not performed on Nottingham site and therefore could not be directly compared to, hiPSC-CMs on 3D EHTs showed slight decrease and shift to the right in peak amplitude as shown in ***Figure 3-16***G, therefore confirmed a negative inotrope response. A previous contractility study of thapsigargin in rabbit ventricular cardiomyocytes showed depletion of SR Ca^{2+} store at 1 μM (Zhang et al., 2018).

Caffeine has long been used for studying ryanodine receptor (RyR)-mediated Ca^{2+} release from intracellular Ca^{2+} stores, and a unique feature of caffeine-induced Ca^{2+} release from RyR2 is the "quantal" Ca^{2+} release. This phenomenon is when multiple additions of caffeine at submaximal concentrations can each induce a partial and transient Ca^{2+} release in a

heterologous expression system (Kong et al., 2008, Cheek et al., 1993). However, concentration range of caffeine in this study is relatively high. At first experiment performed by Dr. Karl Firth resulted in unexpected effect and thereby abandoned. This is due to a special technique, temporally-limited puffs of caffeine (20 mM, <2s) applied by pressure-ejection, needed to be performed in order to overcome the technical issue of the rate of caffeine delivery to the cells (Satin et al., 2008).

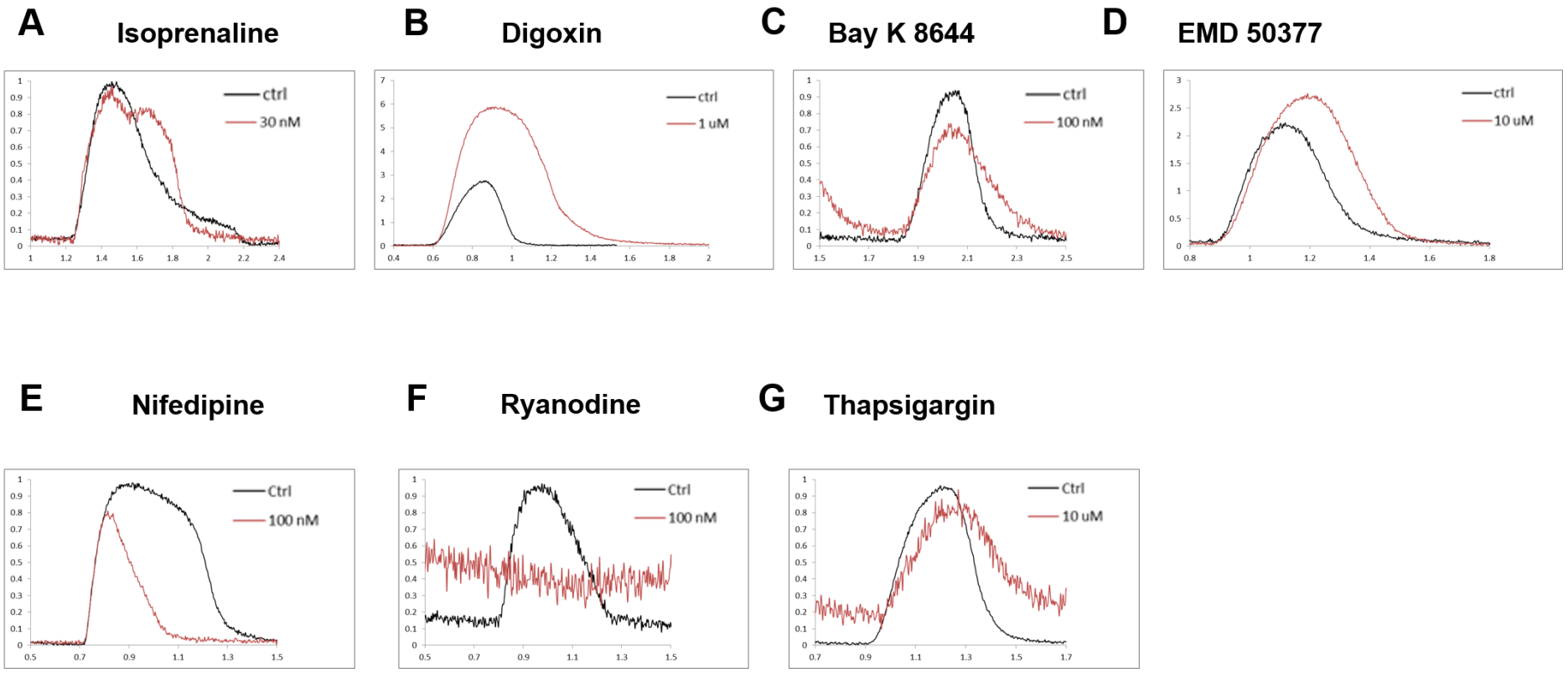

Figure 3-15. **Representative contraction force traces of hiPSC-CMs on 2D TTM. (A-D)** showed positive inotrope drugs whilst **(E-G)** showed negative inotrope drugs. Baseline (black) and treatment (red). Data were generated by Berend J van Meer (Leiden University).

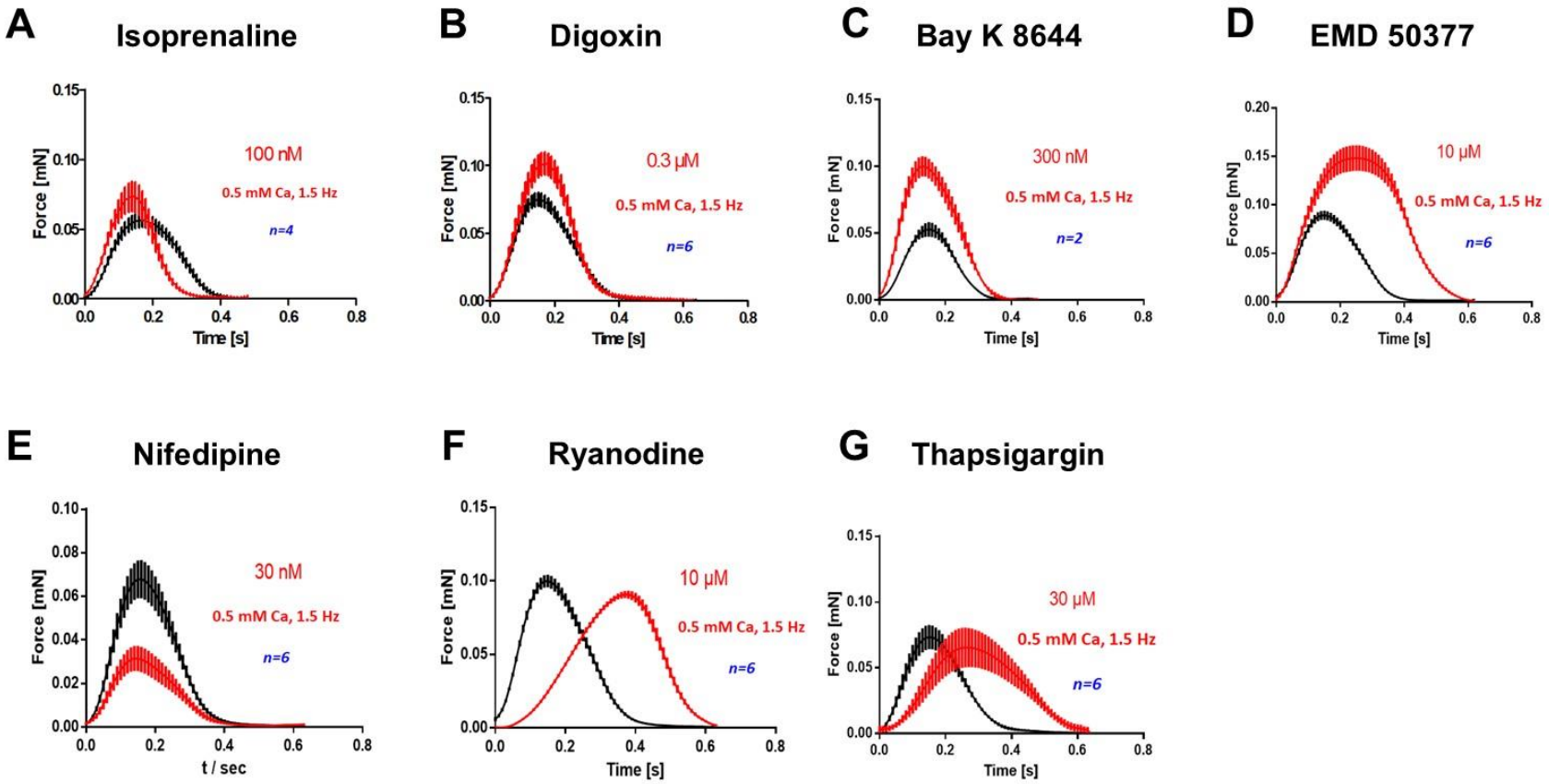

Figure 3-16. Representative contraction force traces of hiPSC-CMs on 3D EHTs. (A-D) showed positive inotrope drugs whilst **(E-G)** showed negative inotrope drugs. Baseline (black) and treatment (red). Data were generated by Umber Saleem and Ingra Mannhardt (University of Hamburg).

3.3.1.9 Conclusion

hiPSC-CMs on 2D monolayers in Tier 1 phase were both treated with both positive inotrope drugs (isoprenaline, digoxin, Bay K 8644, EMD 50377) and negative inotrope drugs (nifedipine, ryanodine, thapsigargin) as a training set that allows progress to Tier 2 phase. Aside ryanodine, hiPSC-CMs on 2D monolayers correctly predicted T1 compounds, allowing 85% accuracy. Possible explanation is due to immature phenotype of hiPSC-CMs cultured on 2D monolayers have low level of RyR2 receptors compared to adult cardiomyocytes (Denning et al., 2016).

It was concluded from the consortium meeting that positive inotrope drugs digoxin at 0.3 μM and negative inotrope drugs nifedipine at 0.03 μM should be used as positive and negative controls, respectively, in Tier 2 phase.

3.3.2 Optimisation for Tier 2

3.3.2.1 Cryopreservation of R-PAT cardiomyocytes

Large scale studies using hPSC-CMs often demand their long-term storage, as: (1) it benefits for later investigations, (2) inexpensive and simple maintenance compared to time-consuming and resource-intensive of differentiating cardiomyocytes from hPSC every time. Cryopreservation of hPSC-CMs is commonly achieved by slow cooling the vials at rate of 1^{o}C/min to a temperature of -80^{o}C before transferred to liquid nitrogen storage (Preininger et al., 2016). During slow cooling, ice crystals formed in the extracellular environment, causing an increase in osmolality. To compensate, the intracellular water passes through cell membrane to the extracellular environment. These events cause cellular dehydration and damage in cell membrane and organelles.

Addition of cryoprotective agent (CPA) prevents intracellular ice crystals formation and therefore reduces cellular dehydration (Fuller, 2004). Currently there is no consensus for best strategy in cryopreservation of hPSC-CMs. CPAs for cryopreserving hPSC-CMs are similar to those for adult stem cells, with dimethyl sulfoxide (DMSO) at a concentration of 10% and fetal bovine serum (FBS) with lower percentage (<30%) if used with hPSC-CMs culture media such as RPMI 1640 containing B27 supplement (Kim et al., 2011, Hwang et al., 2015, Preininger et al., 2016).

To minimise the formation of ice crystals by maximising the cell exposure to CPA, it is crucial to dissociate hPSC-CMs into a single-cell suspension. Addition of Y-2763, a pro-apoptotic protein Rho-associated kinase (ROCK) inhibitor, reduces dissociation-induced apoptosis (Watanabe et al., 2007) and improves post-thaw survival of hPSC-CMs as shown in previous studies (Kim et al., 2011, Chen et al., 2015). The mechanism of Y-2763 in reducing apoptosis is by suppressing the caspase activation through upregulation of interleukin (IL)-1β and its receptor IL-1R, and transforming growth factor (TGF)-β and its receptor ACVR1C (Ichikawa et al., 2012).

Anoikis, a subtype of apoptosis induced by cell detachment from the extracellular matrix (Taddei et al., 2012), has also been proposed as the cause of cell loss after cryopreservation (Li and Ma, 2012). ROCK inhibitor

(Y-2763) can prevent anoikis by: (1) disrupting extracellular cues responsible for apoptosis, and (2) increasing the cell-cell interactions for cell reaggregation by modulating cadherins and gap junctions (Krawetz et al., 2009). Addition of FBS which contains growth factor, such as the basic fibroblast growth factor (bFGF), can also prevent anoikis by activation of Akt and the extracellular-regulated kinase (ERK) signalling pathway, and inhibition of Bcl-2-interacting mediator of cell death and the caspase-ROCK1-myosin signalling (Wang et al., 2009).

To further increase post-thaw viability and recovery of hPSC-CMS, previous studies have investigated the use of commercially available cryopreservation kit and/or cryopreserving hPSC-CMs at younger age. Commercial thawing and maintenance medium have at least one undisclosed component, allowing the cells to have higher percentage of survivability after thawing. The percentage of cell viability after cryopreservation of hPSC-CMs ranges from 60 to 88%, whilst cell recovery is from 55% to 90%, using commercial CPAs (Xu et al., 2011, Chen et al., 2015). Previous research showed that younger cryopreserved hPSC-CMs from day 12 of differentiation has higher post-thaw viability rate (Chong and Murry, 2014, Chong et al., 2014, Kim et al., 2011) compared to older hPSC-CMs cryopreserved later than day 30 of differentiation (Hwang et al., 2015). A direct comparison study showed that cryopreserved hPSC-CMs at day 16 of differentiation exhibited more micro- and ultrastructural damage (disruption of cellular membrane, mitochondria, and nuclear membrane) compared to day 12 of differentiation (Kim et al., 2011). These studies suggested the possibility of improved outcomes achieved when hPSC-CMs are cryopreserved at earlier days of differentiation.

The initial plan had been to use common in house hiPSC-CM line to unify SOPs across partner sites. From the result in section 3.4.1, it was concluded that R-PAT from Nottingham site would be distributed across partners for experimentation, along with optional in house hiPSC-CMs from each partner. It is highly challenging to use freshly dissociated CMs from differentiation in order to conduct the experimentation of 28 Tier 2 compounds in similar timescale across partner sites; therefore, cryopreserved CMs was selected as the option.

Hence, the plan is to test possibility combination of in house (Nottingham) vs commercially available medium from Pluricyte, with schematic as described in **Figure 3-17**. With seeding density of 40,000 per well in a 96-well plate and 40 wells of conditions during experimentations, it would require at least 1.6 million of hiPSC-CMs. Therefore, cryovial was prepared at 2x density (3.2 million), which was based on the observation of 50% viability post thaw.

R-PAT CMs at day 10 or day 20 of differentiation was harvested following Hamburg's CMs dissociation protocol. Cryovials preserved in Nottingham's medium mix consisted of RPMI-B27 + 10% FBS + 1:1000 ROCKi + 10% DMSO. Nottingham's thawing mix consisted of RPMI-B27 + 10%FBS + 1:1000 ROCKi. Day 1 post thaw, medium was replaced with fresh RPMI-B27. There are 4 different scenarios: Nottingham cryo mix (RB) – Nottingham thaw mix (RB); (RB – RB), Nottingham cryo mix (RB) – Pluricyte thaw mix; (RB – PL), Pluricyte cryo mix (PL) – Pluricyte thaw mix; (PL – PL), and Pluricyte cryo mix – Nottingham thaw mix (PL – RB), as well as control (without cryopreservation – thawing process).

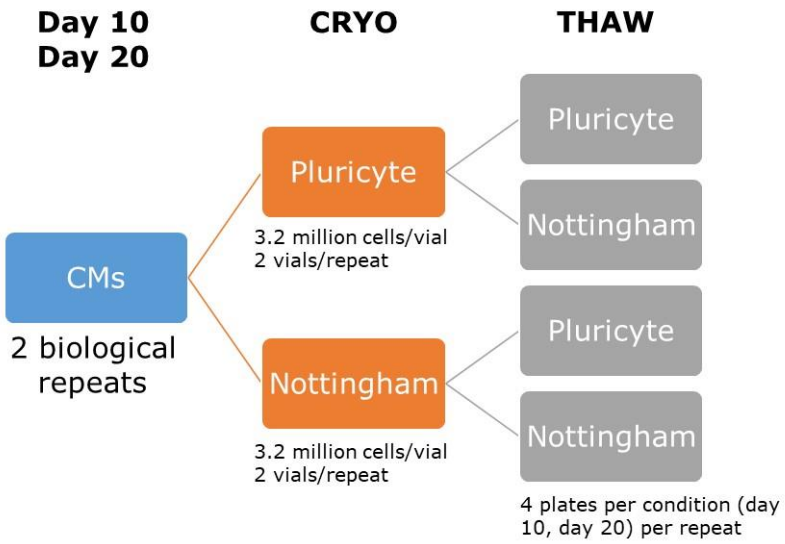

Figure 3-17. Schematic plan of cryopreservation testing for Tier 2 phase. R-PAT CMs were harvested at day 10 and 20 of differentiation before cryopreserved. Cell concentration in cryovials was prepared at 2x of intended seeding density. 4 different scenarios as previously described.

In order to determine plating efficiency of R-PAT CMs harvested at day 10 of differentiation under different conditions, CMs were replated on a 96-well plate and maintained for 3-5 days before being fixed for immunocytochemistry and stained with a cardiac marker α-actinin. Representative of R-PAT CMs under different conditions are shown in **Figure 3-18**A-D. Control wells are CMs without cryopreservation – thawing process. The aim of the experiment was to find condition that gives no significant difference compared to control, thereby reduce the amount of cell death. RB – RB and RB – PL condition demonstrated no change from control, whilst PL – PL had significant increased cell density compared to control, and PL – RB had significant decreased cell density compared to control (**Figure 3-18**E). Cardiomyocytes purity in all conditions showed ≥90% efficiency, with control (97.2 ± 0.5%), RB – RB (97.1 ± 0.2%), RB – PL (95.6 ± 0.3%), PL – PL (93.1 ± 1.4%), and PL – RB (94.5 ± 0.8%) (**Figure 3-18**F).

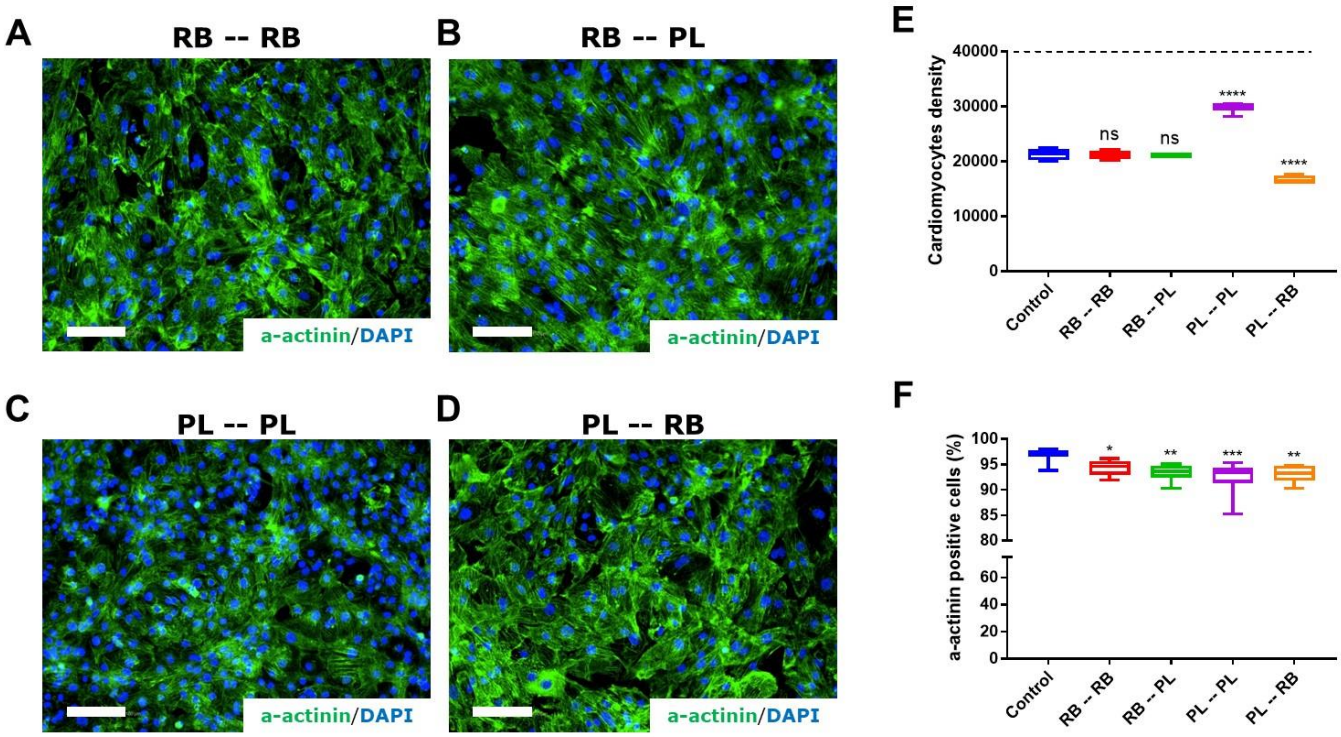

Figure 3-18. Representative R-PAT cardiomyocytes plating efficiency harvested from day 10 of differentiation with intended density of 40,000/well under different conditions. **(A-D)** R-PAT cardiomyocytes stained with α-actinin by immunocytochemistry in RB – RB, RB – PL, PL – PL, and PL- RB condition. **(E)** Cell number was obtained from DAPI quantification only with α-actinin staining to extract cardiomyocytes density information. **(F)** Cardiomyocytes purity was analysed from percentage of α-actinin positive cells. Data are displayed as mean ± SEM. One-way ANOVA with Dunnett's multiple comparison ($p \leqslant$: * 0.05, ** 0.01, *** 0.001, **** 0.0001). Scale bar: 100 µm. n = 4.

To observe the physiological effect of cryopreservation – thawing medium mix conditions, R-PAT CMs harvested at day 10 of differentiation were maintained for 3-5 days before assayed with CellOPTIQ® for electrophysiology and contractility. Electrophysiology analysis showed no prominent difference in voltage trace's shape in RB – RB (**Figure 3-19**B) and PL – RB (**Figure 3-19**E) compared to control (**Figure 3-19**A), while arrhythmic pattern was evident in RB – PL (**Figure 3-19**C) and PL – PL condition (**Figure 3-19**D). A comparison of traces for all conditions can be found in **Figure 3-19**F, indicating ~5x prolonged APDs compared to control. Analysis on APD_{90} showed no difference of RB – RB and PL – RB compared to control, whilst demonstrated significant increase for RB – PL and PL – PL (**Figure 3-19**G).

Contractility analysis showed no difference in beating pattern in RB – RB and PL – RB condition compared to control as indicated in Brightfield video (**Figure 3-20**A, B, E). However, RB – PL condition demonstrated prominent increase in relaxation time (**Figure 3-20**C). Same case was noted on PL – PL condition, in addition to "arrhythmic activity" (**Figure 3-20**D). For statistical analysis purpose, the data were plotted as percentage of change from baseline. Analysis on contraction amplitude and upstroke time (Up_{90}) showed no significant different among conditions (**Figure 3-20**F-G). Significant increase was noted in downstroke time (Dn90) for both RB – PL and PL – PL condition.

Due to the nature of cardiomyocyte differentiation, CMs need to be harvested between day 10-13 of differentiation to be replated before harvested again at day 20 of differentiation. During the process, some cell loss were unavoidable; thus, the number of CMs needed from differentiation for day 20 of differentiation needs to be higher (~2x) compared to day 10 of differentiation harvested CMs. Since results from CMs harvested at day 10 of differentiation looks promising, the experiment for day 20 of differentiation were discontinued.

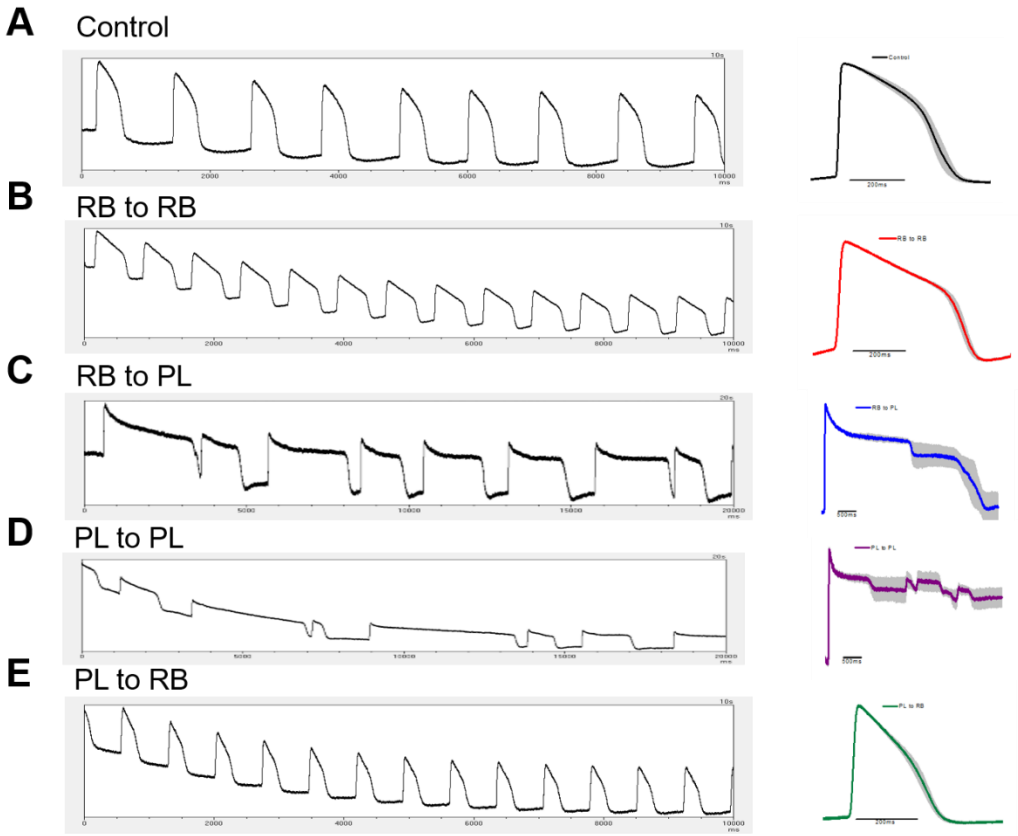

Figure 3-19. Electrophysiology analysis of R-PAT cardiomyocytes harvested from day 10 of differentiation under different conditions. (A-E) Representative voltage traces showed prolonged APDs and arrhythmic event in RB – PL and PL – PL compared to control. **(F)** Comparison of voltage traces in all conditions. **(G)** Analysis showed significant prominent increase in APD_{90} for RB – PL and PL – PL condition. Data are displayed as mean ± SEM. One-way ANOVA with Dunnett's multiple comparison ($p \leqslant$:

* 0.05, ** 0.01, *** 0.001, **** 0.0001). n = 5.

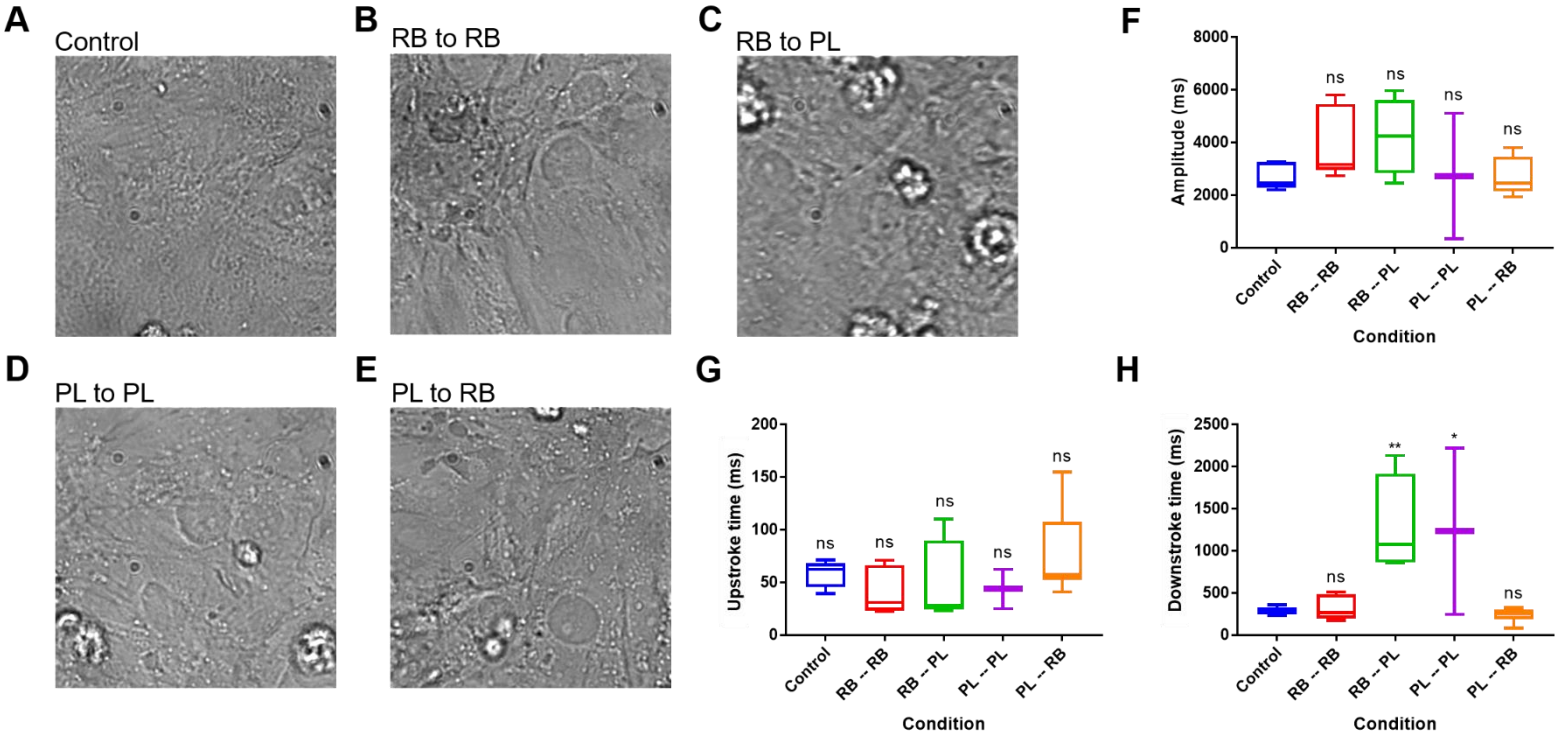

Figure 3-20. Contractility analysis of R-PAT cardiomyocytes harvested from day 10 of differentiation under different conditions. (A-E) Brightfield videos of R-PAT cardiomyocytes showed increased relaxation time in RB – PL and PL – PL condition, whereas PL – PL condition also showed "arrhythmic activity". **(F-G)** Both contractility amplitude and upstroke time showed no significant difference among conditions. **(H)** Downstroke time was noted to be significant in RB – PL and PL – PL condition. Data are displayed as mean ± SEM. One-way ANOVA with Dunnett's multiple comparison (p ⩽: * 0.05, ** 0.01, *** 0.001, **** 0.0001). n = 5.

3.3.2.2 Discussion

This section described the effect of cryopreservation – thawing medium mix on plating efficiency and physiological characteristics of R-PAT CMs in order to improve cryopreserved conditions for the purpose of Tier 2 phase work. It was observed that any medium combination that has RPMI-B27 in cryopreservation mix (RB – RB and RB – PL) resulted in no difference in plating efficiency compared to control. Interestingly, any medium combination that has Pluricyte in thawing mix (RB – PL and PL – PL) resulted in increased relaxation time and arrhythmic events, as well as excessive prolonged APDs. This later finding is consistent with previous experiments done in Pluricyte cell line, which is characterised by increased relaxation time and prolonged APDs.

The majority of cryopreserved hPSC-CMs demonstrated recovery and retained contractility 1-5 days post-thawing (Kim et al., 2011, Xu et al., 2011, Chen et al., 2015). Contractility study showed that cryopreserved hPSC-CMs at 3-5 days post-thaw retained a functional sarcoplasmic reticulum (SR) and robust intracellular Ca^{2+} handling (Hwang et al., 2015). Another study examined thawed hPSC-CMs in extended culture (>5 days post-thaw) and noted increased beating rate up to 1.8 Hz compared to 0.33-0.66 Hz in control (non-cryopreserved cells) at day 6 post-thaw, that became irregular day 8 post-thaw until completely arrested at day 12 post-thaw (Kim et al., 2011). Electrophysiology study showed that cryopreserved hPSC-CMs still retained cardiac action potential characteristics (Chen et al., 2015).

3.3.2.3 Conclusion

As the aim of the section work is to find condition that has no difference compared to control (without cryopreservation – thawing process), it is concluded that based on plating efficiency and functional assay results, RB – RB showed to be the best condition.

3.3.2.4 Reducing beat rate by utilising different matrix

During consortium meeting in November 2017, it was revealed that samples of cryopreserved R-PAT CMs send to partners had (1) beating rate with frequency ~≥1.2Hz at basal rate, resulting in no drug response observed due to CMs being paced at 2Hz, and (2) arrhythmic beating pattern in some cryovial batch banks. Therefore, it was proposed to use different matrix to replace Matrigel®.

Although single-cell or monolayer cultures are widely used for such screening system, some studies have suggested that cardiomyocytes cultured in a three-dimensional (3D) environment play a crucial role in pharmacologically induced responses (Huebsch et al., 2016). In addition to the 3D structure, an extracellular matrix (ECM) is crucial to the function of the heart (Oberwallner et al., 2014).

The cardiac extracellular matrix (ECM) is a complex mesh-work of fibers that is largely composed of collagen, fibronectin, and laminin (Wu et al., 2010). Interactions between cardiac ECM and resident cells are mediated through integrins, transmembrane ECM receptors, to ensure communication between extracellular and intracellular environment (Corda et al., 2000, Bowers et al., 2010). In cardiomyocytes, integrins are majorly localised in costameres, where Z-disc are connected to the sarcolemmal membrane (Samarel, 2005). Integrin linkage to the Z-disc of the sarcomeres via cytoskeleton proteins, such as α-actinin, are important for mechanotransduction pathway that supports iPSC-CMs maturation (Li et al., 2017). Integrins are also found in intercalated discs, which is essential for both mechanical and electrical coupling (Israeli-Rosenberg et al., 2014). β1 integrins subunit are abundant in the adult heart and play a role in hypertropic response in ventricular cardiomyocytes (Ross et al., 1998), which is part of the natural maturation process (Yang et al., 2014a). Integrin activation can regulate a range of cellular receptors including L-type Ca^{2+} channel (LTCC) and potassium (K^{+}) channel (Gui et al., 2010).

Fibronectin is one of the major ECM glycoproteins secreted by cardiac fibroblasts and smooth muscle cells, and shown to promote adhesion of cardiomyocytes (Corda et al., 2000). α3β1-integrin and α5β1-integrin are two important adhesion receptors for fibronectin (Ross and Borg, 2001),

and that adhesive interactions with these integrins are modulated by the contractile state in cardiomyocytes.

Matrigel® is a protein mixture extracted from the Engelbreth-Holm-Swarm mouse sarcoma cells, a tumor enriched in extracellular matrix proteins found in basement membrane (Kleinman et al., 1982). This matrix consists of laminin, collagen IV, proteoglycans, and a number of growth factors, and is widely used in stem cell culture support (Hughes et al., 2010).

In this study, the hiPSC-CMs electrophysiology response using different matrix was observed using negative inotrope verapamil which is a L-type Ca^{2+} channel blocker (at that time was blinded under code INP017 or CPD17) at highest concentration (1 μM) as depicted in **Figure 3-21**. The experiment was based on preliminary data from Hamburg showing complete quiescent of hiPSC-CMs on contractility analysis at 0.3 and 1 μM (**Figure 3-21**C). R-PAT CMs seeded in fibronectin and vitronectin-coated plate showed completely quiescent cardiomyocytes, consistent with data found in 3D EHT. Electrophysiology measurement revealed both fibronectin and vitronectin contributed to significant electrically quiescence hiPSC-CMs compared to Matrigel® (**Figure 3-21**A). Changes in frequency were analysed and showed lower basal heart rate in fibronectin (1.2±0 Hz) followed by vitronectin (1.26±0.06 Hz) and Matrigel® (1.74±0.06 Hz) (**Figure 3-21**B).

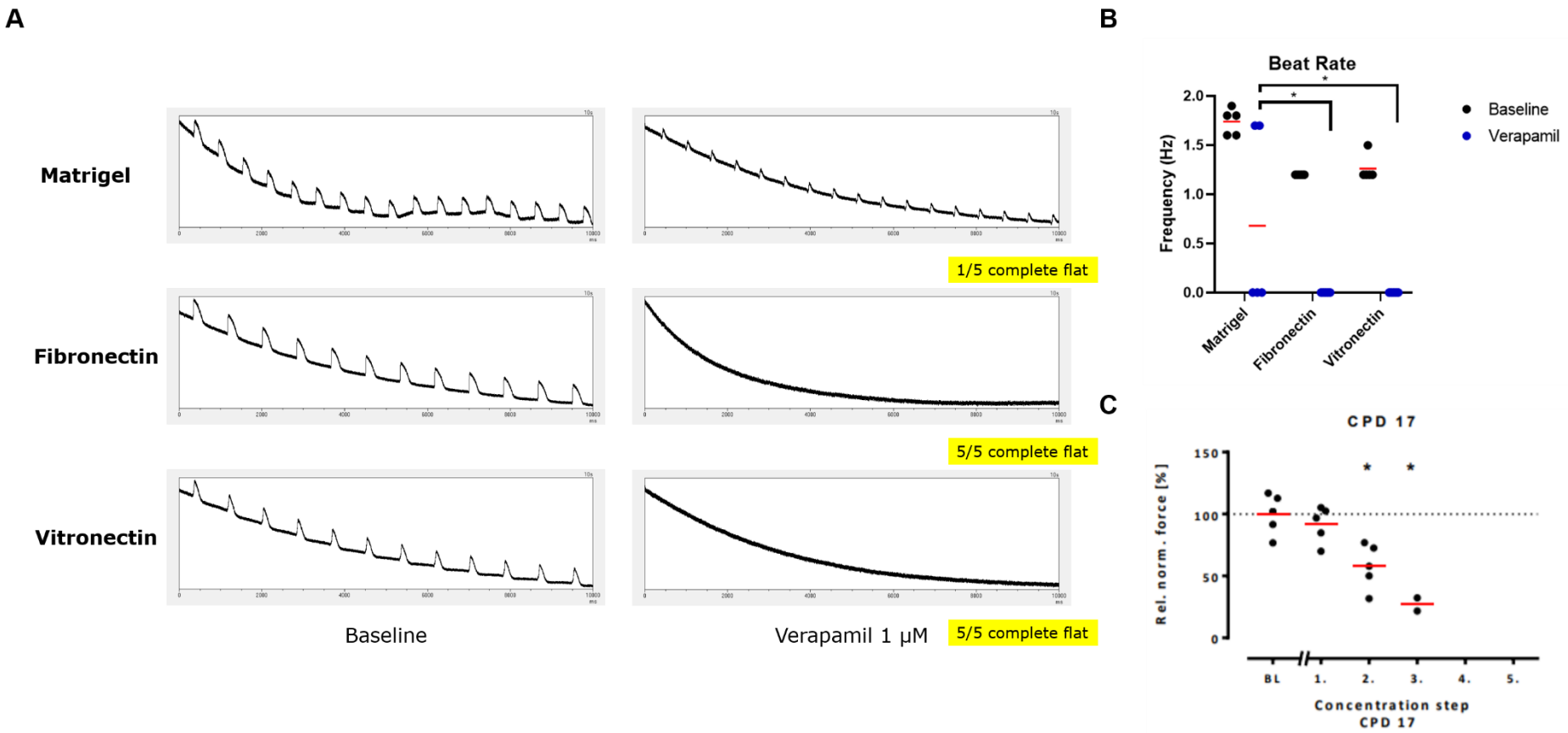

Figure 3-21. **Selection of extracellular matrix in order to reduce basal beat rate ~≥1.2 Hz**. (A) Electrophysiology response of R-PAT CMs after treated with negative inotrope, verapamil (CPD17), at 1 µM demonstrating both fibronectin and vitronectin caused electrically quiescence hiPSC-CMs. (B) Quantification analysis on beat rate showed lower basal heart rate (1.2 Hz) in fibronectin followed by vitronectin and Matrigel®. (C) Preliminary data from Hamburg by Umber Saleem demonstrating complete quiescent of hiPSC-CMs on contractility analysis at 0.3 and 1 µM. Voltage traces were obtained from proprietary software of CellOPTIQ®. Two-way ANOVA with Dunnett's multiple comparison (p ⩽: * 0.05, ** 0.01, *** 0.001, **** 0.0001). n = 5.

3.3.2.5 Discussion

Previous study has shown that α5β1-integrin receptors for fibronectin is induced in the maturation process (Herron et al., 2016). Integrin signaling is a dynamic and complex process in cardiomyocytes depending on the ECM components and mechanical activity (Traister et al., 2014). The experiment showed that fibronectin reduce basal beat rate as low as 1.2 Hz compared to vitronectin and Matrigel® in baseline measurement, and gave completely quiescent hiPSC-CMs after treatment of verapamil.

Due to time limitation in the project, the exact role of extracellular matrix on frequency rates and maturation is still undiscovered. From the literature and preliminary results, it is suggested that fibronectin indeed affecting maturation of hiPSC-CMs via enhanced contractile response, which in turn affecting the beating rate. Existing study based on Matrigel® demonstrated the relationship between the extracellular matrix and hiPSC-CMs maturation (Feaster et al., 2015).

3.3.2.6 Conclusion

Fibronectin was chosen due to lower basal beat rate compared to other extracellular matrix, as well as the similar response with 3D EHT after treatment of a potent negative inotrope. Furthermore, commercial cell line iCell^2 and Pluricyte use fibronectin in their cell culture maintenance, therefore, the data derived from drug testing can be cross-compared.

3.3.3 Establishing protocol across academic partners

The training set of 8 drugs was used to test and refine protocols. Consistent with the mode of action of these drugs, in all cases there was a trend or significant response for positive inotropy (increased contraction amplitude) in hiPSC-CMs treated with digoxin/isoprenaline but negative inotropy (decreased contraction amplitude) for those treated with nifedipine. These studies allowes unification of SOPs, although physical and technical constraints between the platforms meant that some unavoidable differences remained (**Table 3-2**).

Table 3-2. Comparison and unification of standard operating procedures. In house means the conditions or assays used for hiPSC-CMs derived from in house hiPSC lines using in house differentiation methods. Commercial means use of Pluricyte and/or iCell^2 hPSC-CMs that were purchased from Ncardia and Cellular Dynamics International, respectively.

	Protocol	Triple Transient Measurement (TTM)	CellOPTIQ® (CO)	Engineered Heart Tissues (EHTs)
Starting conditions	Format	• 96-well plate	• As for TTM	• 1 million hiPSC-CMs / EHT
	Age	• Thawing + 5-7 days	• As for TTM (commercial) • Differentiation time + 10 days (in house)	• Differentiation time + 14-30 days
	Culture medium	• Manufacturer instructions	• As for TTM (commercial) • Standard culture medium (in house)	• As for CO (in house)
	Quality control	• Response to 100 nM digoxin; 30 nM nifedipine	• Response to 30 nM nifedipine • Cell purity >90% by a-actinin (in house) • Spontaneous beat rate ≤1.5 Hz (in house)	• Response to 100 nM isoprenaline and 30 nM nifedipine • Cell purity >70% by cTnT (in house) • Minimum force: 0.1 mN
Experimental set-up	Medium	• Commercial medium (serum free)	• As for TTM (commercial) • 1.8 mM Ca^{2+} (serum/protein free) (in house)	• 1.8 mM Ca^{2+}-Tyrode (serum/protein free)
	Cell loading	• ANINNE-6 plus, Rhod 3 AM and CellMask Deep Red	• FluoVolt™	• Lentiviral mediated expression of GCaMP6f in EHTs (transduction during EHT fabrication)
	Recording: Baselines	• Paced at 1.2 Hz; 7 sec/area	• Paced at 1.2-1.7 Hz; 10 sec/area	• Paced at 1.5x basal rate; 10 sec/EHT
	Recording: Conc-response curves	• Replicates: 5 wells/compound and 3 areas/well + time matched vehicle controls	• Replicates: 5 wells/compound + time matched vehicle controls	• Replicates: 6 EHTs/compound + time matched vehicle controls
		• Solvent: max 0.1% DMSO	• As for TTM	• As for TTM
		• Treatment duration: 30 mins	• As for TTM	• As for TTM
		• Single concentration/well	• As for TTM	• Cumulative concentrations/EHT
		• Paced at 1.2 Hz; 7 sec/area	• Paced at 1.2-1.7 Hz; 10 sec/well	• Paced at 1.5x basal rate; 10 sec/EHT
Follow-up	Analysis	• Analysis performed offline	• As for TTM	• Analysis performed online and offline
	Recovery	• n/a	• n/a	• Rest and recreation for ≥2 days in standard medium
	Additional testing	• n/a	• n/a	• Baseline at 1.8 mM Ca^{2+}-Tyrode (spontaneous; 20 sec/EHT), compare to prior baseline to evaluate permanent damage
	Repeat testing	• No repeated use of cells	• As for TTM	• As for TTM

4 Cardiovascular Safety Liabilities Screening – Final Phase

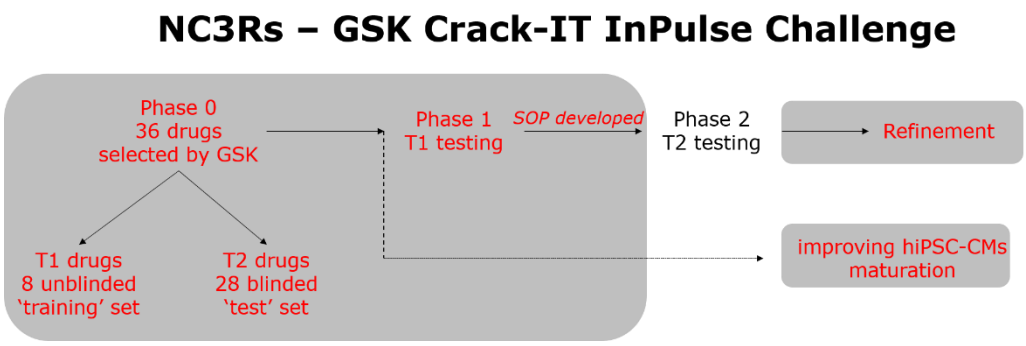

4.1 Introduction

Previous work in chapter 3 described the unblinded training set of 'Tier 1' drugs and the optimisation afterwards in order to develop and fine-tune each academic partner's platform during the first two years since the CRACK-IT InPulse Challenge was established. These provided the SOPs needed to commence the Tier 2 blinded drug set. Up to 28 blinded drugs were chosen during meetings in 2015-2016, with the first 10 ranked drugs as first priority predefined by GSK. The compounds were ordered from commercial suppliers and the powder were aliquoted by GSK for blinded analysis. The aliquoted compounds for Tier 2 phase were then sent in September 2017 with predefined procedure to reconstitute and dilute to working concentrations from stock concentration. During period October 2017 until April 2018, the academic partners tested the Tier 2 blinded drug set. The process is described further in **Figure *4-1***.

Within the drug evaluation project, the primary aim of the CRACK-IT Challenge 13: InPulse was to predict whether the drugs were positive, negative, or neutral inotropes (no effect). Thus, contractility was the parameter common to all platforms and will be discussed in more detail in this section.

Production of cardiomyocytes derived from in-house hiPSC lines, R-PAT and ERC18 were sufficient enough to test all the drugs provided by GSK on CellOPTIQ® and EHTs platform. Due to time and/or resources limitation for adult rabbit cardiomyocytes (as control) and commercial

hiPSC-CMs (Pluricyte and iCell^2), testing was restricted to 10 drugs on CellOPTIQ® (for rabbit cardiomyocytes) and TTM platform.

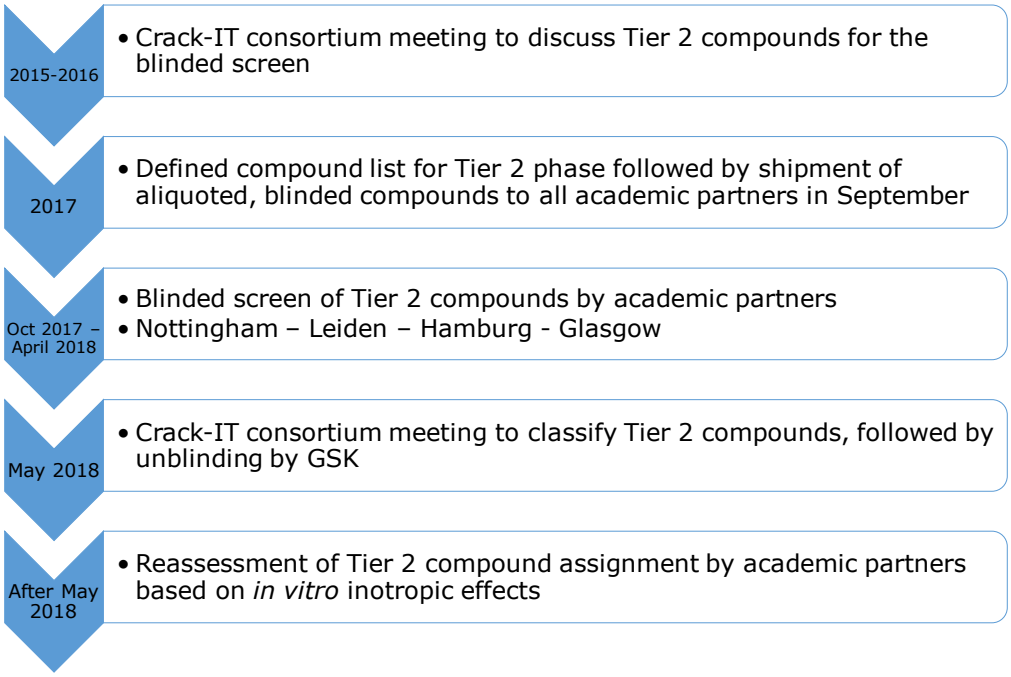

Figure 4-1. Flow chart depicting the Tier 2 compound testing phase.

4.2 Chapter Aims

- To investigate the effect of T2 drugs on hiPSC-CMs cultured in standard cell culture 2D monolayers and 3D engineered heart tissues (EHTs).
- To determine which platform has the greatest accuracy and sensitivity in predicting outcome of drug effect.
- To investigate whether further improvement can be done.

4.3 Results

4.3.1 Cardiotoxicity screening in Tier 2 phase

Presentation, analysis, and inotropy prediction of the Tier 2 data were done at a 2-day meeting between all partners with GSK as observers before the drugs were unblinded. Before the unblinding process, a consensus was reached for the outcome using the parameter as in **Figure *4-2*** and terminology as in **Figure *4-3***.

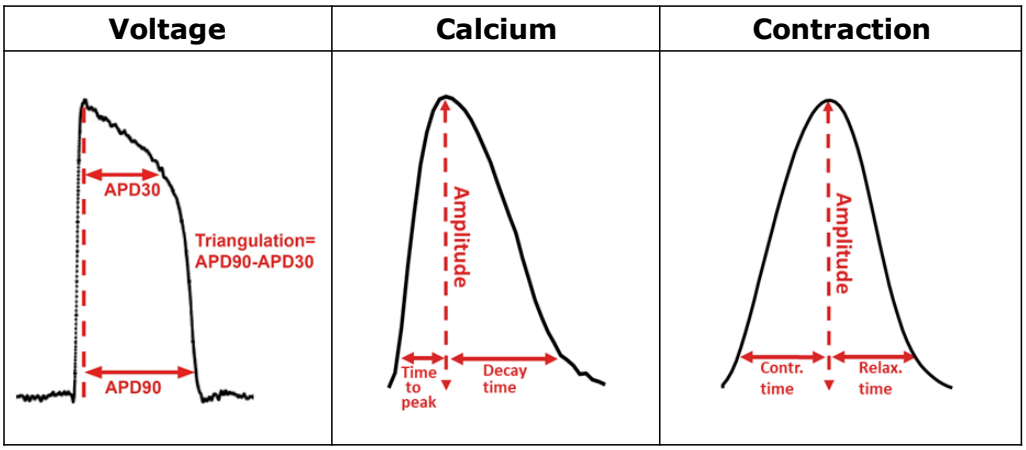

Figure 4-2. Schematic of parameter used in the experimentation across all platforms to quantify drug effect in hiPSC-CMs. Abbreviation: APD, action potential duration.

Action potential duration (APD_{30}, APD_{90}) and triangulation (APD_{90}-APD_{30}) were derived from voltage waveforms in order to detect presence of altered electrophysiology, including arrhythmia. For calcium handling experiment, parameters include amplitude, time to peak, and decay time, whilst for contractility experiment, similar parameters which are amplitude, contraction time, and relaxation time, were derived. In contraction, inotropy is defined as change in peak force, clinotropy as change in contraction time (time-to-peak force from 20% above baseline), and lusitropy as change in relaxation time (time from peak force to 80% before reaching baseline).

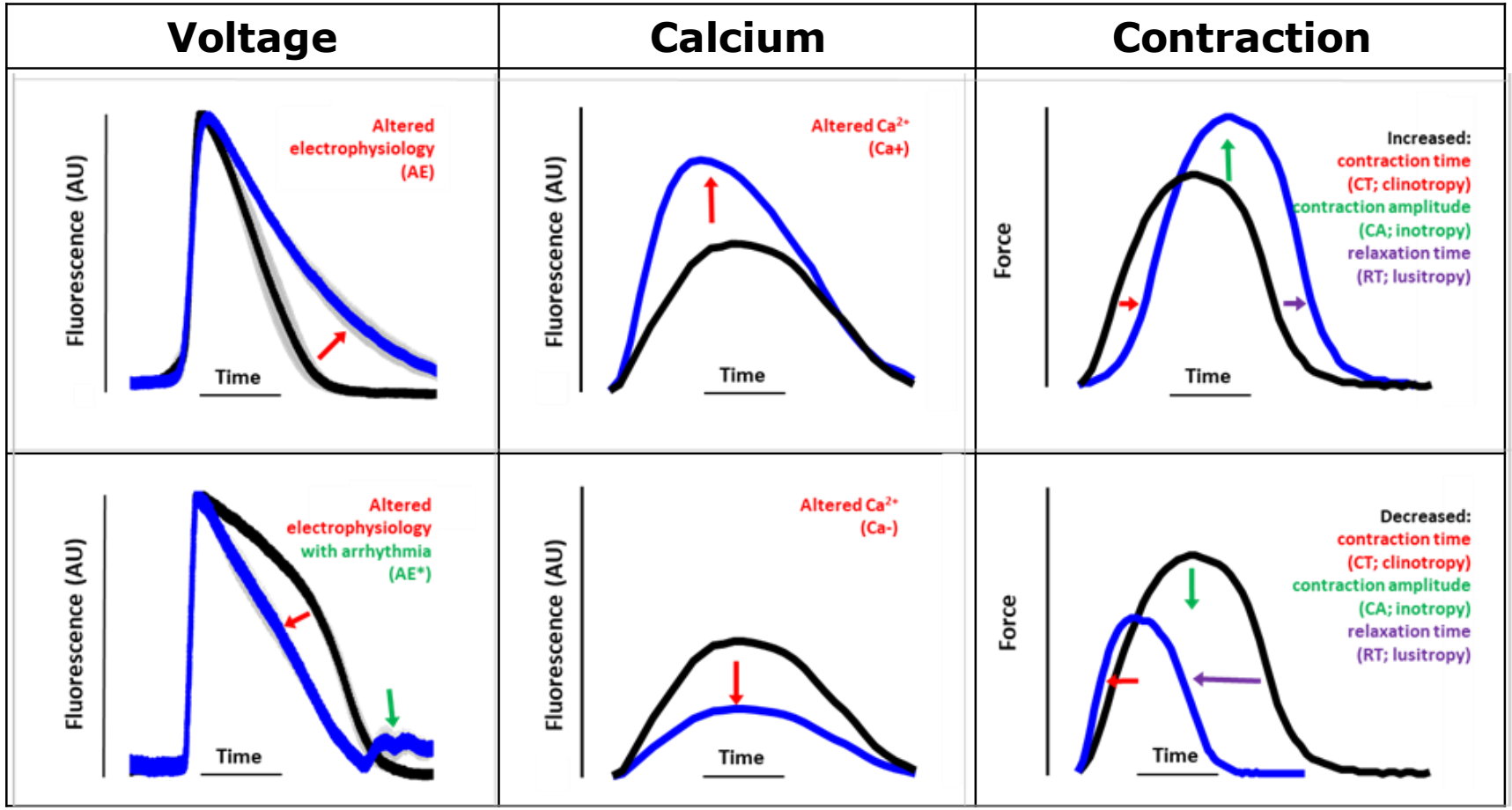

Figure 4-3. Terminology used in the experimentation across all platforms. Baseline readings are represented in black traces, while post-treatment readings are represented in blue traces. Coloured texts are to match coloured arrows.

After all data were presented during the meeting, all 28 Tier 2 compounds were unblinded by GSK representation lead by Peter Clements. The unblinding process was based on contractility data, mainly *in vitro* and some *in vivo* (atenolol, clonidine, glibenclamide). Based on a common agreement by the partners, the assignment was later revised for few compounds, in order to better reflect in vitro contractility analysis data (Crack IT assignments). List of assignment is in **Table *4-1***.

Table 4-1. List of 28 Tier 2 compounds with known positive (8), negative (10) inotropic, and no effects (10) in relation to cardiomyocytes contractility alteration response. Abbreviations: inotropy is defined as change in peak force, FTCP; free therapeutic plasma concentration; n.d, not defined; EC_{50}, half maximal effective concentration; IC_{50}, half maximal effective inhibitory concentration; hERG, human eag-related gene; SR, sarcoplasmic reticulum; SSR inhibitor, selective serotonin reuptake inhibitor; * indicates lack of clarity in literature on inotropic effect.

Class (Crack-IT)	Drug	Mechanism of action	Concentration range (μM)	FTPC (μM)	References
Positive inotropes	Epinephrine GSK: PI	Non-selective α1-,β1- and β2-adrenoceptor agonist	0.01-1	0.0002-0.050	(Molenaar et al., 2007, Wortsman et al., 1984)
	Forskolin GSK: PI	Adenylyl cyclase stimulator	0.1-10	0.012-0.024 (colforsin)	(Bristow et al., 1984, Kikura et al., 2004)
	Levosimendan GSK: PI	Calcium sensitizer PDE3 inhibitor (IC_{50} 25 nM) K_{ATP} channel agonist	0.01-1	0.026-0.35	(Boknik et al., 1997, Hasenfuss et al., 1998, Mebazaa et al., 2007, Papp et al., 2012, Orstavik et al., 2014, Abi-Gerges et al., 2013, Puttonen et al., 2008)
	Pimobendan GSK: PI	Calcium sensitizer PDE inhibitor (partial)	1-100	0.005-0.01	(Honerjager et al., 1984, Berger et al., 1985, Chu et al., 1995)
	Dobutamine GSK: PI	α1-,β1- and β2-adrenoceptor agonist	0.1-10	0.07-1	(Ishihata et al., 1988, Brown et al., 1987,

					Mahoney et al., 2016)
	Milrinone GSK: PI	PDE3 inhibitor	1-100	0.1-0.15	(Brown et al., 1986, Bailey et al., 1994)
	Omecamtiv mecarbil GSK: PI	Cardiac specific myosin activator	0.01-1	0.05-0.42	(Cleland et al., 2011, Planelles-Herrero et al., 2017, Horvath et al., 2017, Teerlink et al., 2011, Liu et al., 2016b)
	Terbutaline GSK: PI	B2-adrenoreceptor agonist	0.1-10	1.3	(Schafers et al., 1994, Dyreborg et al., 2016)
Negative Inotropes	Verapamil GSK: NI	L-type Ca^{2+} channel blocker, hERG blocker	0.01-1	0.05	(Angus et al., 2000, Giacomini et al., 1984)
	Doxorubicin GSK: NI	Impairs Ca^{2+} transport mechanism in sarcoplasmic reticulum	0.1-10	1-2	(Temma et al., 1993, Hofling and Bolte, 1981, Matsushita et al., 2000, Danesi et al., 1999)
	Sunitinib GSK: NI	Multi-targeted TK inhibitor	0.1-10	0.003	(Mooney et al., 2015, Abi-Gerges et al., 2013, Bello et al., 2006)
	Citalopram GSK: NI	SSR inhibitor, hERG & L-type Ca^{2+} channel inhibitor	1-100	0.05	(Witchel et al., 2002, Mannhardt et al., 2017, Rao, 2007)
	Itraconazole GSK: NI	Triazole antifungal, inhibitor of Na^{+} channels and mitochondrial voltage-dependent anion channel 1	0.1-10	0.00086 (higher in tissues)	(Head et al., 2015, Qu et al., 2013, Bellmann, 2007)
	Sorafenib GSK: NI	Multi-targeted kinase inhibitor	0.1-10	0.03 (higher	(Henderson et al., 2013, Duran

				tissue levels)	et al., 2014, Abi-Gerges et al., 2013, Kim et al., 2013)
	Ivabradine* GSK: NE	I_f inhibitor	0.1-10	0.01-0.1	(Perez et al., 1995, Boldt et al., 2010, Bois et al., 1996, Mesirca et al., 2014, Choi et al., 2016)
	Flecainide GSK: NI	Na+ channel blocker, hERG blocker	0.1-10	0.2-0.4	(Abi-Gerges et al., 2013, McQuinn et al., 1988)
	Phentolamine GSK: NI	Non-selective α adrenoceptor agonist, Na^+ and Ca^{2+} channel blocker at high conc.	1-100	2.25	(Sada, 1978, Rosen et al., 1971)
	Zimelidine* GSK: NE	SSR inhibitor	1-100	0.78	(Lindbom and Forsberg, 1981, Forsberg and Lindbom, 1983, Naranjo et al., 1984)
No Effect	Acetylsalicylic acid GSK: NE	Cyclooxygenase inhibitor	1-100	0.3-2	(Abi-Gerges et al., 2013)
	Atenolol GSK: NI	β1>β2 adrenoreceptor antagonist	0.1-10	1	(Lemoine et al., 1988, Kaumann and Blinks, 1980)
	Captopril GSK: NE	ACE inhibitor	1-100	1-2	(Abi-Gerges et al., 2013, Giudicelli et al., 1987)
	Glibenclamide GSK: PI	K_{ATP} channel antagonist	0.1-10	0.02-0.06	(Satoh et al., 1990, Murakami et al., 1992, Pogatsa and Dubecz, 1977, Rydberg et al., 1997)
	Enalapril GSK: NE	ACE inhibitor	1-100	0.12	(Stage et al., 2017)

	Clonidine GSK: NI	α2-adrenoreceptor agonist	0.01-1	0.002-0.004	(Jarrott et al., 1979, Kleiber et al., 2017)
	Paracetamol GSK: NE	Prostaglandin synthesis inhibitor	10-1000	50	(Marks et al., 2012, Kamali et al., 1993, Brown et al., 1992)
	Tolbutamide GSK: NE	K_{ATP} channel antagonist, weak adenylyl cyclase stimulator	1-100	20-30	(Levey et al., 1971, Lasseter et al., 1972, Abi-Gerges et al., 2013, Whiting et al., 1981)
	Pravastatin GSK: NE	HMG CoA reductase inhibitor	1-100	0.018	(Costantine et al., 2016)
	Sildenafil GSK: NE	PDE5 inhibitor	0.3-30	0.02	(Sugiyama et al., 2001, Walker et al., 1999)

Data are accessible in a webtool https://bjvanmeer.shinyapps.io/crackit/. From the top 10 ranked drugs, only 9 drugs were evaluated in common, due to Glasgow and Hamburg didn't receive the 9th ranked drug, doxorubicin, due to limitation in supply provided by GSK.

Overall prediction for 9 drugs in common yield accuracy ranging from 44-78%. All platforms mainly correctly predicted no effect (NE) drugs and negative inotrope (NI) drugs, being up to 100%. However, positive inotrope (PI) drugs were poorly predicted, with range from 0-50% accuracy (**Table *4-2***).

Table 4-2. Cross comparison of predictivity between platform-cell combinations in all 9 drugs tested in common and all drugs evaluated. Shading describes predictivity percentage in green (>75%), orange (50-74%), and red (<50%). Abbreviations: CO, CellOPTIQ® (Glasgow, Nottingham); TTM, Triple Transient Measurement (Leiden); EHT, Engineered Heart Tissue (Hamburg); Rb, rabbit adult cardiomyocytes (Glasgow); Pluricyte (Ncardia); iCell^2 (Cellular Dynamics International); R-PAT (Nottingham); ERC18 (Hamburg); PI, positive inotropes; NI, negative inotropes, NE; no effect drugs.

Platform: Cell	Config.	9 drugs in common				All drugs assessed			
		PI	NI	NE	Total	PI	NI	NE	Total
CO: Rb	2D	2/4 (50%)	2/2 (100%)	2/3 (67%)	6/9 (67%)	2/4 (50%)	2/2 (100%)	3/4 (75%)	7/10 (70%)
TTM: Pluricyte	2D	2/4 (50%)	2/2 (100%)	3/3 (100%)	7/9 (78%)	2/4 (50%)	2/3 (67%)	3/3 (100%)	7/10 (70%)
CO: Pluricyte	2D	0/4 (0%)	2/2 (100%)	3/3 (100%)	5/9 (56%)	0/4 (0%)	2/3 (67%)	3/3 (100%)	5/10 (50%)
CO: iCell^2	2D	1/4 (25%)	2/2 (100%)	3/3 (100%)	6/9 (67%)	1/4 (25%)	2/3 (67%)	3/3 (100%)	6/10 (60%)
CO: R-PAT	2D	0/4 (0%)	1/2 (50%)	3/3 (100%)	4/9 (44%)	0/8 (0%)	5/9 (56%)	10/10 (100%)	15/27 (56%)
EHT: R-PAT	3D	2/4 (50%)	1/2 (50%)	3/3 (100%)	6/9 (67%)	6/8 (75%)	8/9 (89%)	9/10 (90%)	23/27 (85%)
EHT: ERC	3D	2/4 (50%)	1/2 (50%)	3/3 (100%)	6/9 (67%)	6/8 (75%)	8/9 (89%)	8/10 (80%)	22/27 (81%)

From up to 28 drugs tested, overall prediction was similar with the top 10 ranked drugs, ranging from 50-85%. Consistent with the trend, NE and NI drugs were predicted most accurately (up to 100%). It is noted that the 3D EHT platform has highest accuracy (75%) for predicting PI drugs compared to the rest of platform (0-50%) (**Table *4-2***).

As mentioned in chapter 3, two compounds from Tier 1 phase, digoxin and nifedipine, were selected as positive inotrope control and negative inotrope control, respectively. Hamburg used isoprenaline instead, due to the nature of the EHT platform. Based on the Tier 1 phase result, Nottingham with CellOPTIQ® platform used concentration of 0.3 μM for digoxin and 0.03 μM for nifedipine. Leiden with TTM (Triple Transient Measurement) platform used 1 μM for digoxin and same concentration with Nottingham for nifedipine. After treatment readings were compared to their respective vehicle control and showed expected results (**Figure *4-4***). Digoxin and isoprenaline exhibited increased contraction amplitude, whilst nifedipine exhibited decreased contraction amplitude.

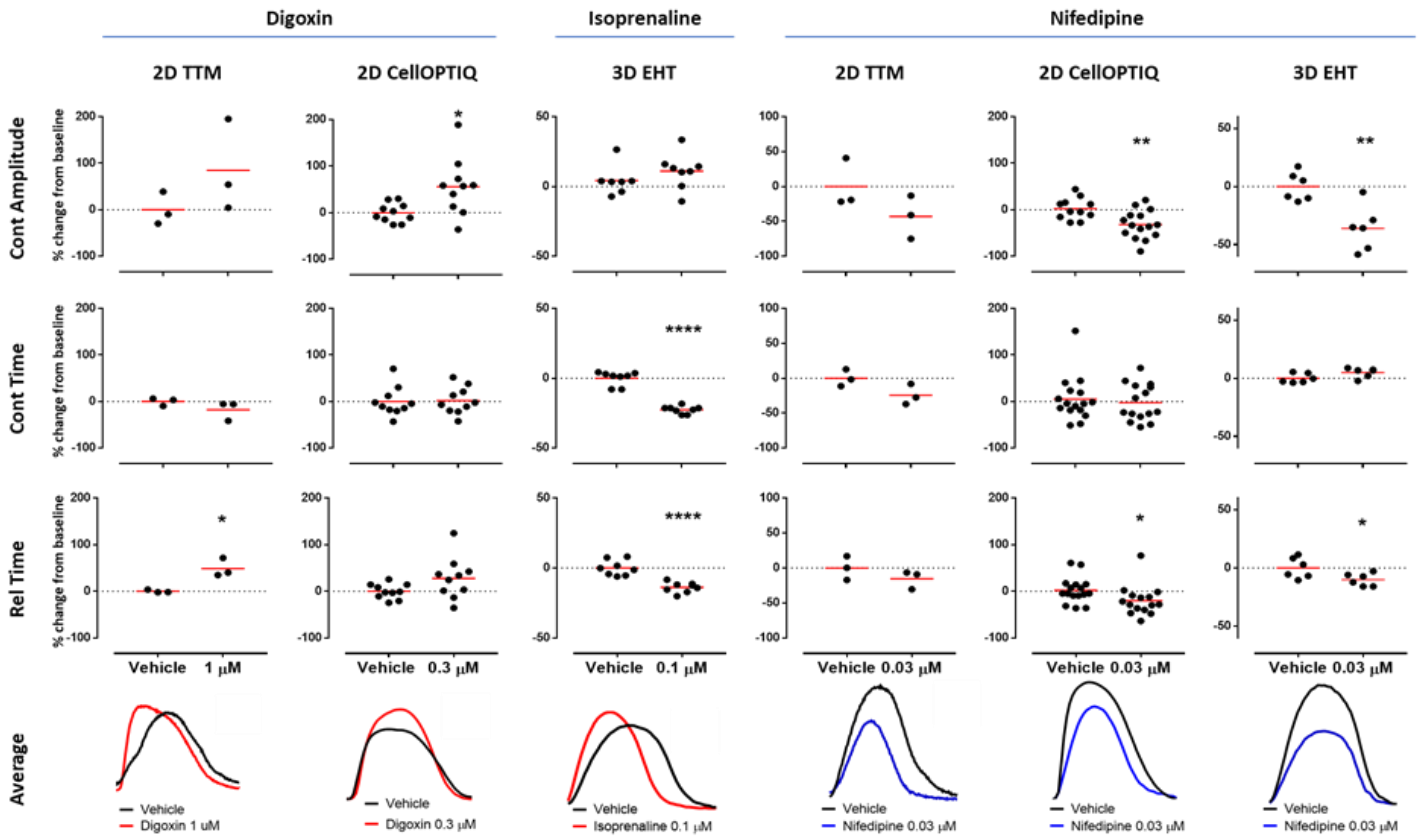

Figure 4-4. Quality control during Tier 2 phase. Representative contractility traces and data are shown for positive (red: digoxin, 2D; isoprenaline, 3D) and negative (blue: nifedipine 2D, 3D) inotropes evaluated in hiPSC-CMs using the TTM (Triple Transient Measurement), CellOPTIQ® and EHT (engineered heart tissue) platforms. The percentage change in drug treated samples is relative to their respective vehicle control. Unpaired T-test. * $p<0.05$; ** $p<0.01$; *** $p<0.001$; **** $p<0.0001$

Summary of the representative effects of Tier 2 compounds for the positive inotropes, negative inotrope, and no effect drugs as performed in Nottingham (CellOPTIQ®) is in **Figure *4-5***. Overall, during Tier 2 phase as screened by Nottingham, all positive inotrope drugs were not able to be predicted correctly, most negative inotrope drugs were correctly predicted, and all no effect drugs were correctly predicted.

Due to large amount of data, only individual data of top 10 compounds tested on CO:R-PAT platform-cell combination will be presented. All 28 compounds during Tier 2 phase will be presented together as comparison between partners in later figures and tables.

4.3.1.1 Epinephrine treatment

Epinephrine is categorised a positive inotrope compound and its mechanism of action is indicated in **Table *4-1***. Readouts representing R-PAT-CMs in response to treatment were plotted as mean ± SEM. Traces for voltage showed no significant effect after treatment (**Figure *4-6***A). The data were plotted as percentage of change from baseline. There was no significant difference noted for voltage Triangulation, APD_{30}, APD_{90} in vehicle vs baseline, as well as all epinephrine treated conditions (**Figure *4-6***B-D).

Traces for contraction amplitude showed trend decrease after treatment, with large variation of distributed data (**Figure *4-7***A). There was no significant difference noted for contraction amplitude, contraction time, and relaxation time in vehicle control vs baseline, as well as all epinephrine treated conditions (**Figure *4-7***B-D).

4.3.1.2 Forskolin treatment

Forskolin is categorised a positive inotrope compound and its mechanism of action is indicated in **Table *4-1***. Readouts representing R-PAT-CMs in response to treatment were plotted as mean ± SEM. Traces for voltage showed no significant effect after treatment (**Figure *4-8***A). The data were plotted as percentage of change from baseline. There was no significant difference noted for voltage Triangulation, APD_{30}, APD_{90} in vehicle vs baseline, as well as all forskolin treated conditions (**Figure *4-8***B-D).

Traces for contraction amplitude showed trend decrease after treatment, with large variation of distributed data (**Figure *4-9***A). There was no significant difference noted for contraction amplitude, contraction time, and relaxation time in vehicle control vs baseline, as well as all forskolin treated conditions (**Figure *4-9***B-D).

Electrophysiology	Epinephrine	Verapamil	Acetylsalicylic acid
	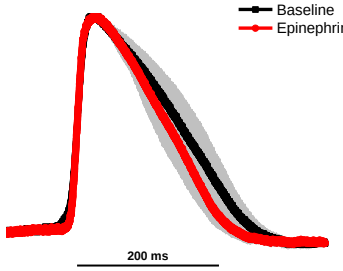	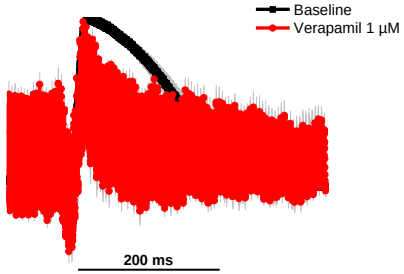	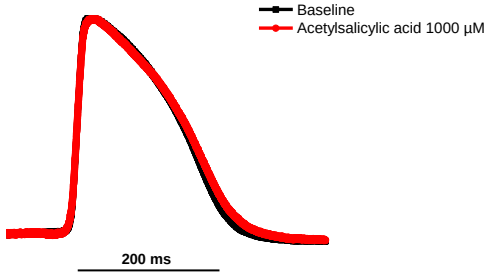
	No significant effect	Concentration dependent shortening of APD	No effect
Contractility	Epinephrine	Verapamil	Acetylsalicylic acid
	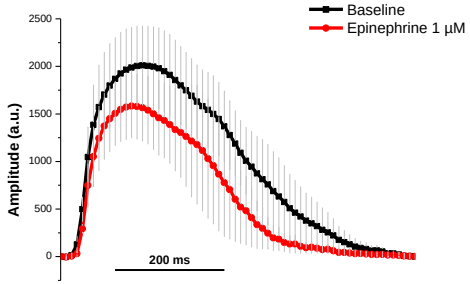	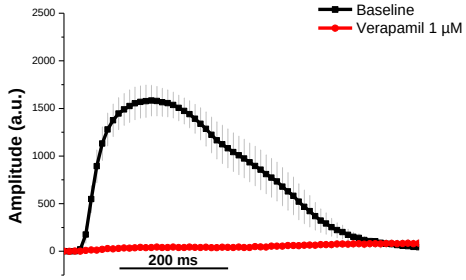	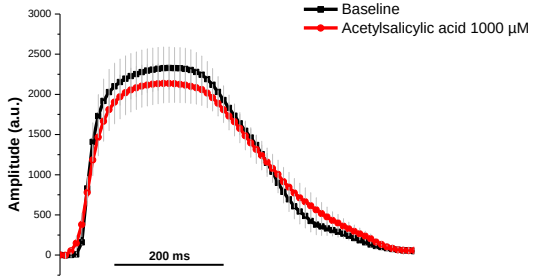
	No significant effect	Concentration dependent decrease in contraction amplitude and contraction time	No effect

Figure 4-5. Summary of the effects of the representative electrophysiology and contractility data for positive (epinephrine), negative (verapamil) inotropes, and no effect (acetylsalicylic acid) compound evaluated in hiPSC-CMs using CellOPTIQ® platform during Tier 2 phase. Black traces represent baseline reading, whilst red traces represent after treatment reading. Concentration used were the highest concentration: epinephrine (1 µM), verapamil (1 µM), acetylsalicylic acid (1000 µM).

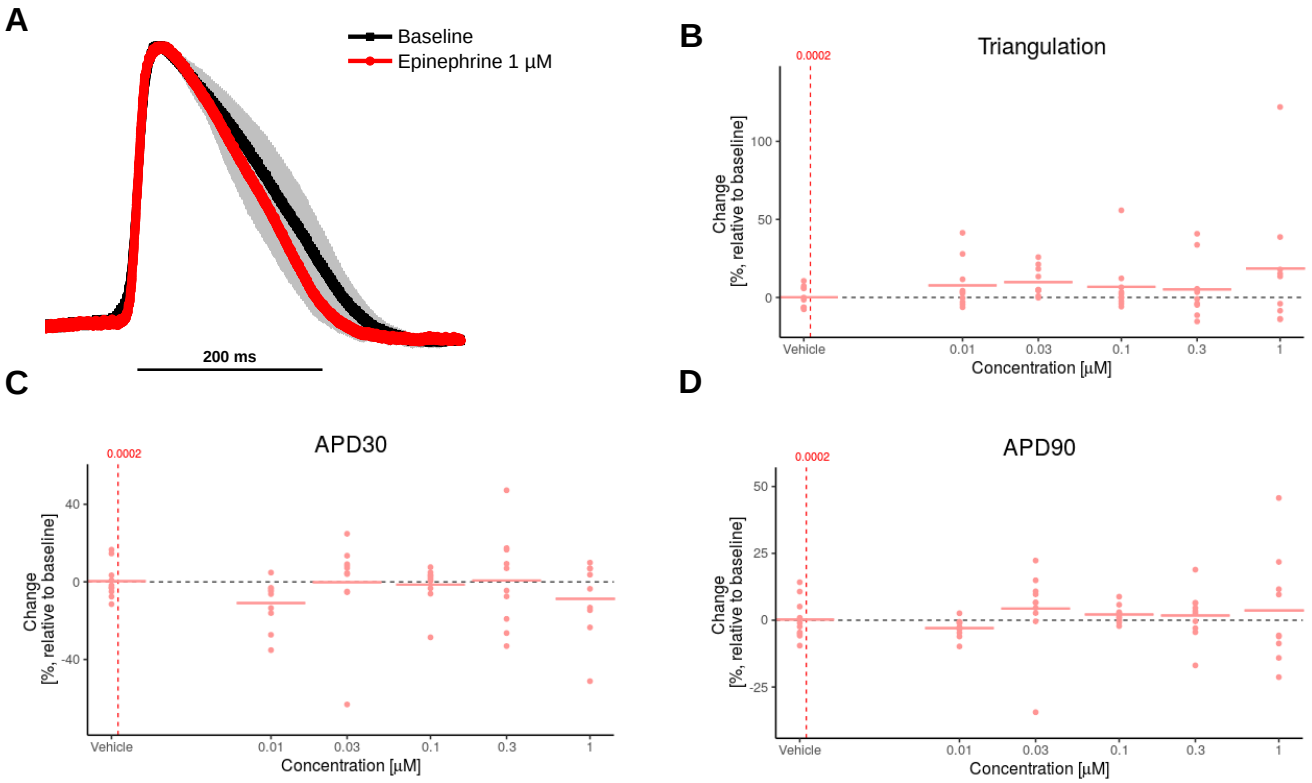

Figure 4-6. Electrophysiology analysis of hiPSC-CMs on 2D monolayers treated with epinephrine. (A) Representative voltage traces at highest concentration (1 µM). (B) Data in Triangulation (APD90-APD30) showed no significant difference after treatment. (C-D) Data in action potential duration at 30 and 90% of repolarisation showed no significant difference after treatment. hiPSC-CMs were analysed using CellOPTIQ® as previously described. Baseline (black) and treatment (red). One data point per well was recorded (n=5 per concentration). Concentration range: 0.01-1 µM. Data are displayed as mean ± SEM. Red dotted line is free therapeutic plasma concentration (FTPC). One-way ANOVA followed by Dunnett's multiple comparisons test vs vehicle control (p ⩽: * 0.05, ** 0.01, *** 0.001, **** 0.0001).

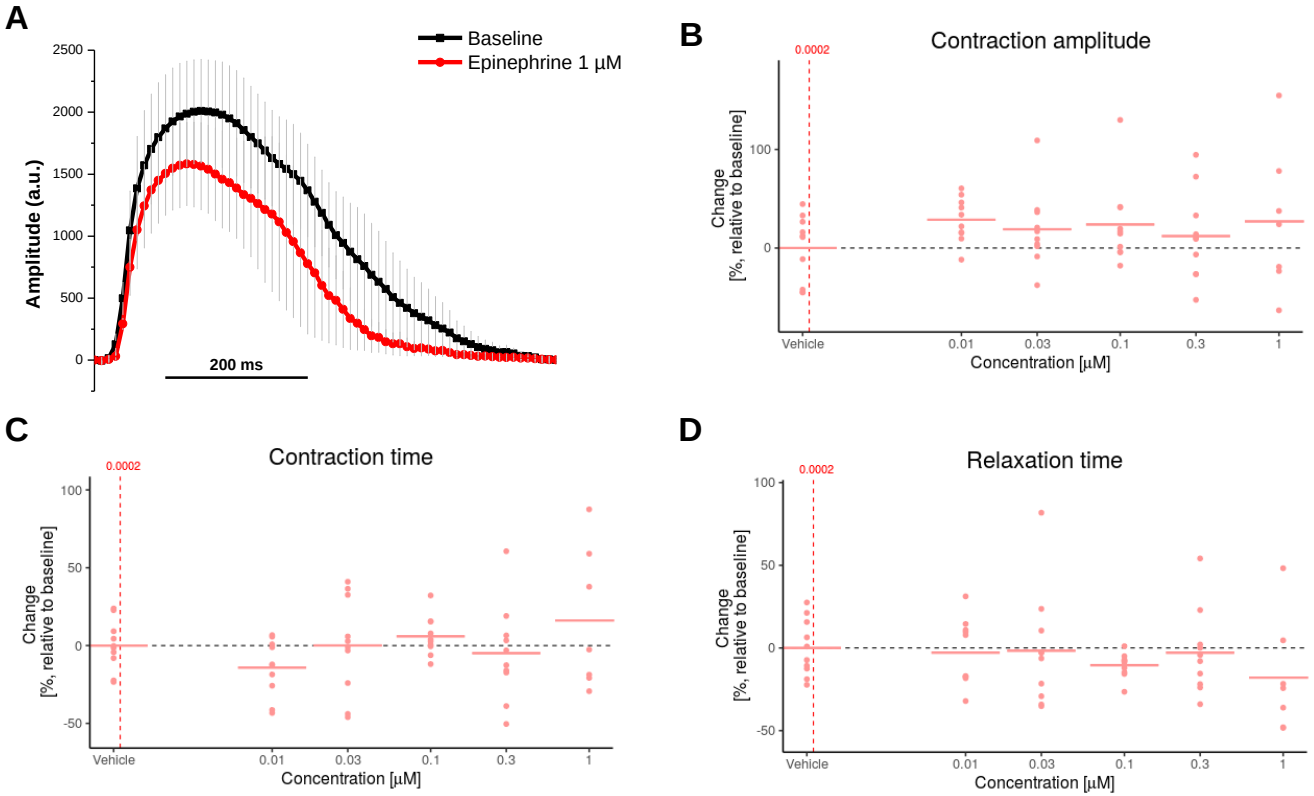

Figure 4-7. Contractility analysis of hiPSC-CMs on 2D monolayers treated with epinephrine. (A) Representative contractility traces at highest concentration (1 µM). (B) Data in contraction amplitude showed no significant difference after treatment. (C) Data in contraction time showed no significant difference after treatment. (D) Data in relaxation time showed no significant difference after treatment. hiPSC-CMs were analysed using CellOPTIQ® as previously described. Baseline (black) and treatment (red). One data point per well was recorded (n=5 per concentration). Concentration range: 0.01-1 µM. Data are displayed as mean ± SEM. Red dotted line is free therapeutic plasma concentration (FTPC). One-way ANOVA followed by Dunnett's multiple comparisons test vs vehicle control (p ⩽: * 0.05, ** 0.01, *** 0.001, **** 0.0001).

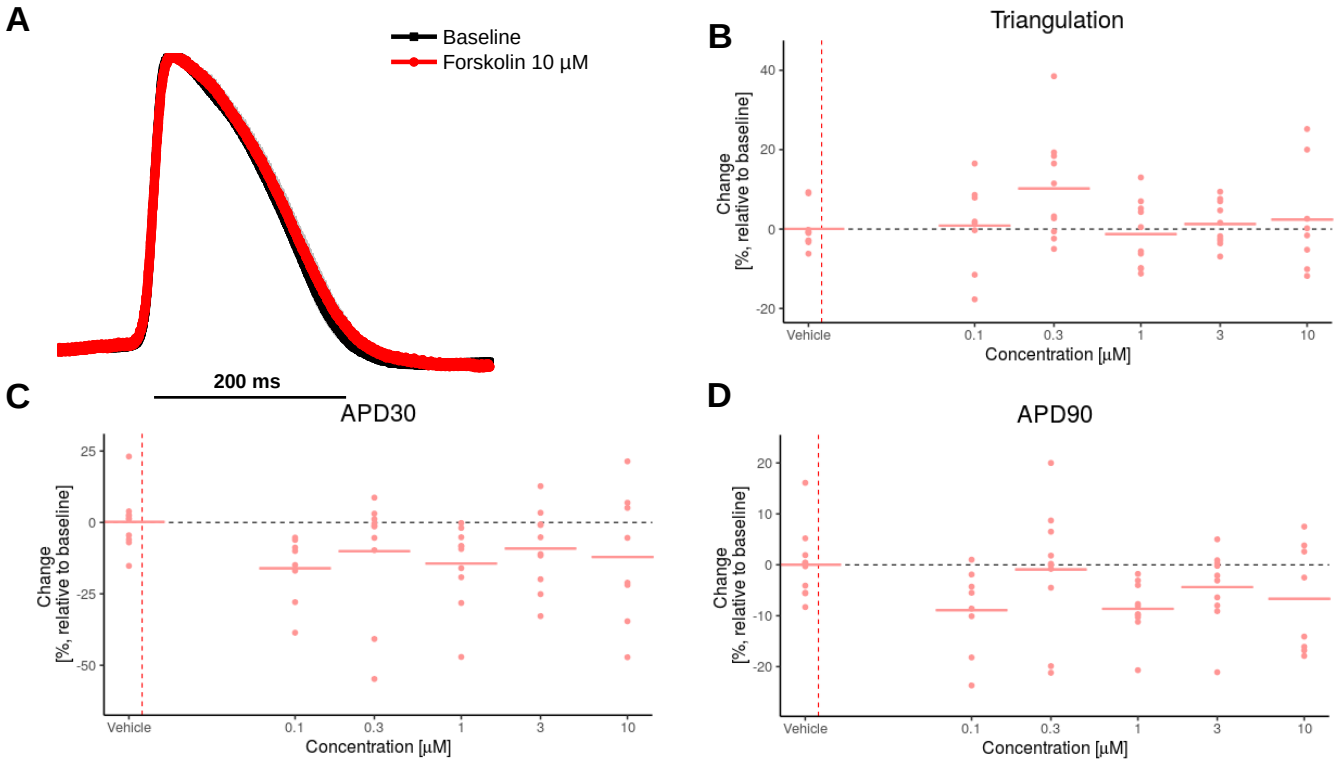

Figure 4-8. Electrophysiology analysis of hiPSC-CMs on 2D monolayers treated with forskolin. (A) Representative voltage traces at highest concentration (10 µM). (B) Data in Triangulation (APD90-APD30) showed no significant difference after treatment. (C-D) Data in action potential duration at 30 and 90% of repolarisation showed no significant difference after treatment. hiPSC-CMs were analysed using CellOPTIQ® as previously described. Baseline (black) and treatment (red). One data point per well was recorded (n=5 per concentration). Concentration range: 0.1-10 µM. Data are displayed as mean ± SEM. Red dotted line is free therapeutic plasma concentration (FTPC). One-way ANOVA followed by Dunnett's multiple comparisons test vs vehicle control (p ⩽: * 0.05, ** 0.01, *** 0.001, **** 0.0001).

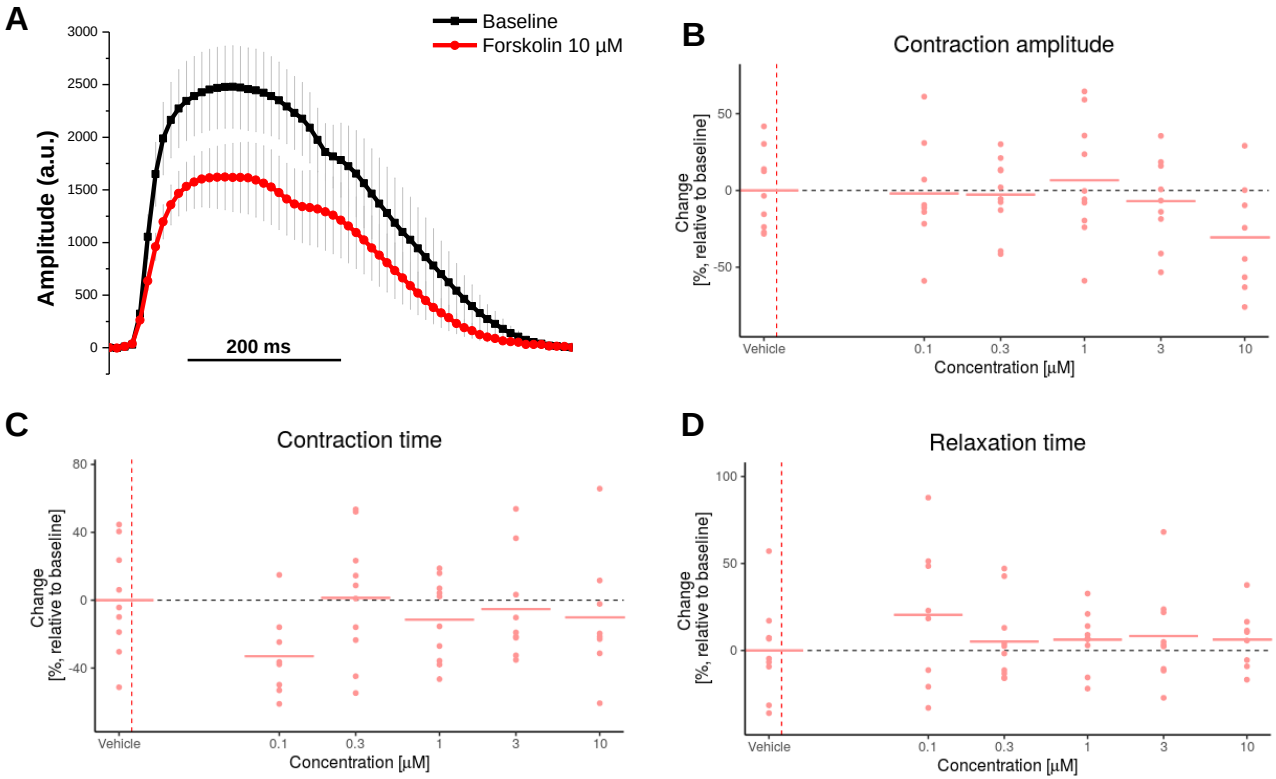

Figure 4-9. Contractility analysis of hiPSC-CMs on 2D monolayers treated with forskolin. (A) Representative contractility traces at highest concentration (10 µM). (B) Data in contraction amplitude showed no significant difference after treatment. (C) Data in contraction time showed no significant difference after treatment. (D) Data in relaxation time showed no significant difference after treatment. hiPSC-CMs were analysed using CellOPTIQ® as previously described. Baseline (black) and treatment (red). One data point per well was recorded (n=5 per concentration). Concentration range: 0.1-10 µM. Data are displayed as mean ± SEM. Red dotted line is free therapeutic plasma concentration (FTPC). One-way ANOVA followed by Dunnett's multiple comparisons test vs vehicle control (p ⩽: * 0.05, ** 0.01, *** 0.001, **** 0.0001).

4.3.1.3 Levosimendan treatment

Levosimendan is categorised a positive inotrope compound and its mechanism of action is indicated in **Table *4-1***. Readouts representing R-PAT-CMs in response to treatment were plotted as mean ± SEM. Traces for voltage showed prolonged APD after treatment (**Figure *4-10***A). The data were plotted as percentage of change from baseline. There was no significant different for voltage Triangulation, but significant increase was noted for APD_{30} and APD_{90} (both at concentration of 0.1 and 1 μM) compared to their respective vehicle control (**Figure *4-10***B-D).

Traces for contraction amplitude showed trend increase after treatment, with large variation of distributed data (**Figure *4-11***A). There was no significant difference noted for contraction amplitude, contraction time, and relaxation time in vehicle control vs baseline, as well as all levosimendan treated conditions (**Figure *4-11***B-D).

4.3.1.4 Pimobendan treatment

Pimobendan is categorised a positive inotrope compound and its mechanism of action is indicated in **Table *4-1***. Readouts representing R-PAT-CMs in response to treatment were plotted as mean ± SEM. Traces for voltage showed trend in prolonged APD after treatment (**Figure *4-12***A). The data were plotted as percentage of change from baseline. There was noted for trend concentration dependent increase for voltage Triangulation, APD_{30} and APD_{90} compared to their respective vehicle control (**Figure *4-12***B-D).

Traces for contraction amplitude showed trend increase after treatment, with large variation of distributed data (**Figure *4-13***A). There was no significant difference noted for contraction amplitude and contraction time, and there was noted for trend concentration dependent increase in relaxation time (**Figure *4-13***B-D).

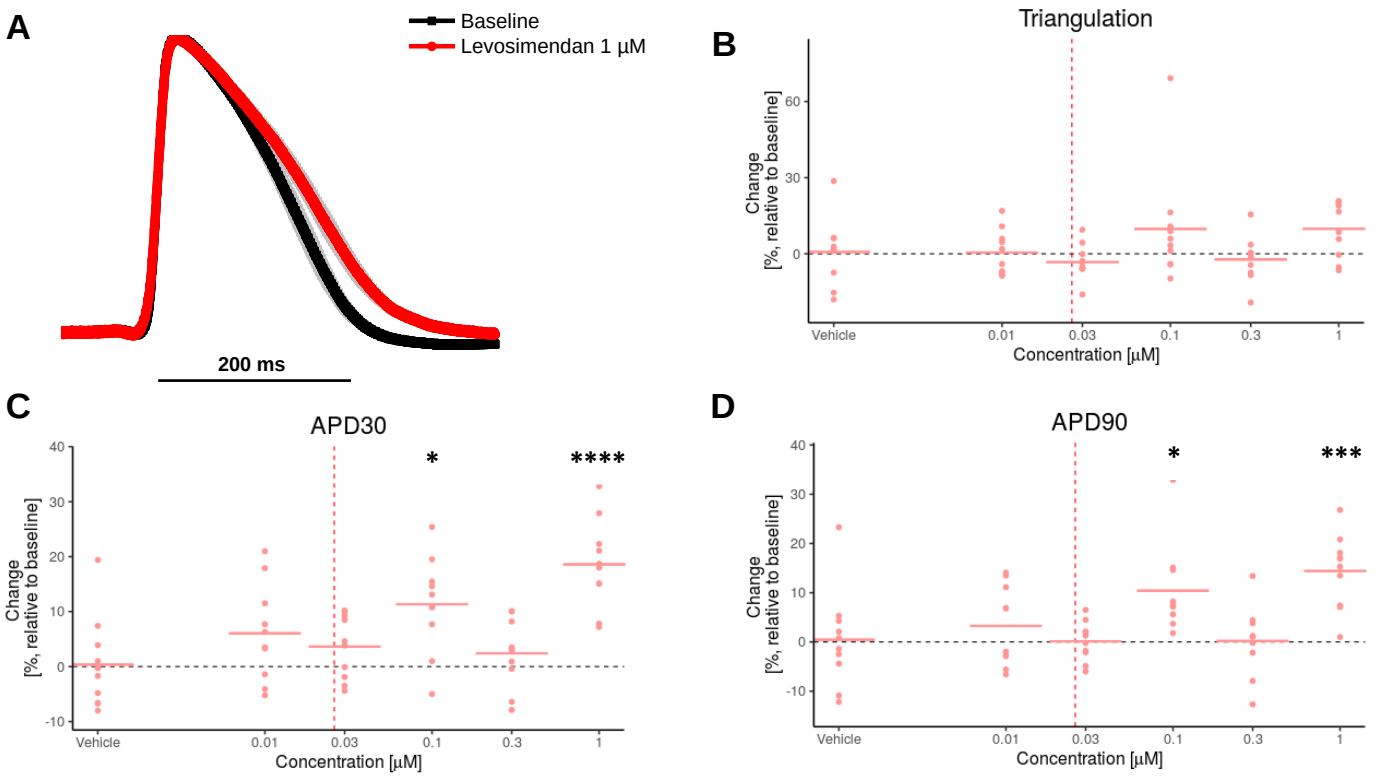

Figure 4-10. Electrophysiology analysis of hiPSC-CMs on 2D monolayers treated with levosimendan. (A) Representative voltage traces at highest concentration (1 µM). (B) Data in Triangulation (APD90-APD30) showed no significant difference after treatment. (C-D) Data in action potential duration at 30 and 90% of repolarisation showed significant increase at higher concentration (0.1 and 1 µM). hiPSC-CMs were analysed using CellOPTIQ® as previously described. Baseline (black) and treatment (red). One data point per well was recorded (n=5 per concentration). Concentration range: 0.01-1 µM. Data are displayed as mean ± SEM. Red dotted line is free therapeutic plasma concentration (FTPC). One-way ANOVA followed by Dunnett's multiple comparisons test vs vehicle control (p ⩽: * 0.05, ** 0.01, *** 0.001, **** 0.0001).

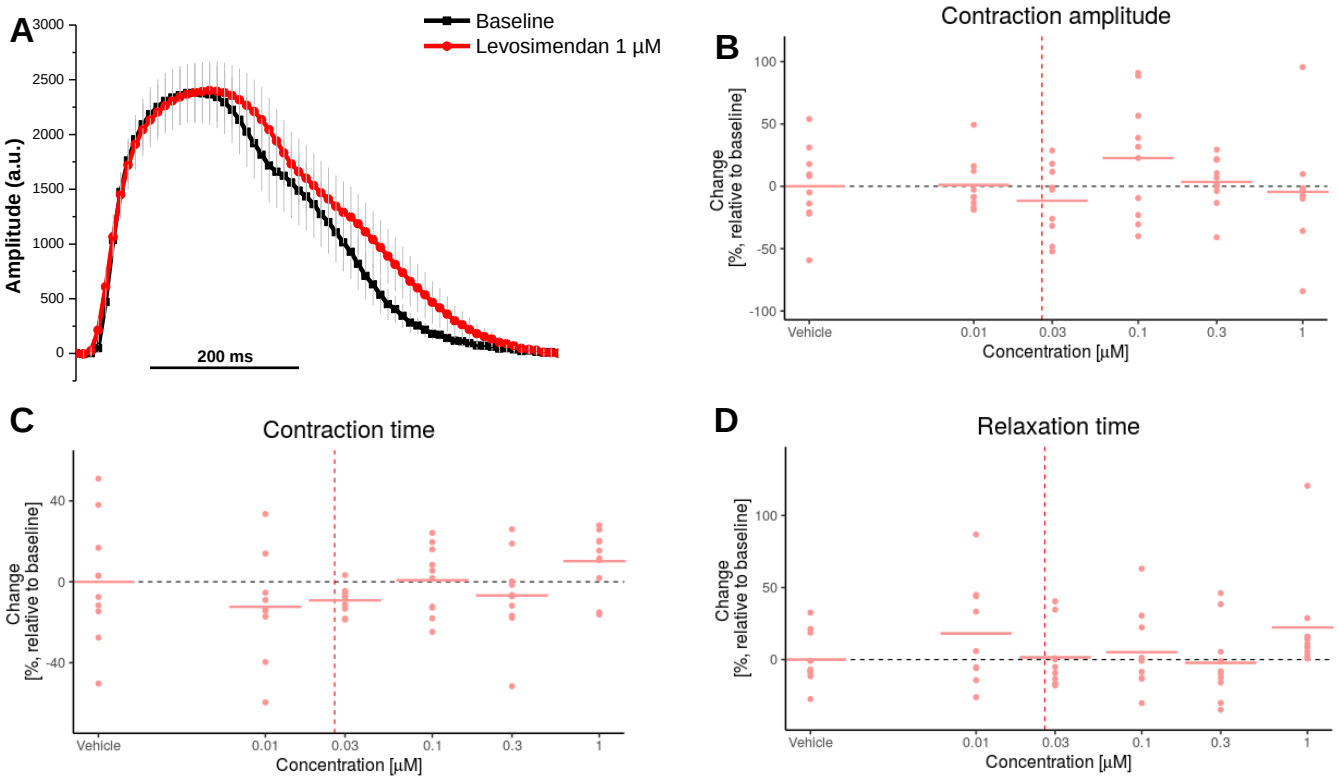

Figure 4-11. Contractility analysis of hiPSC-CMs on 2D monolayers treated with levosimendan. (A) Representative contractility traces at highest concentration (1 µM). (B) Data in contraction amplitude showed no significant difference after treatment. (C) Data in contraction time showed no significant difference after treatment. (D) Data in relaxation time showed no significant difference after treatment. hiPSC-CMs were analysed using CellOPTIQ® as previously described. Baseline (black) and treatment (red). One data point per well was recorded (n=5 per concentration). Concentration range: 0.01-1 µM. Data are displayed as mean ± SEM. Red dotted line is free therapeutic plasma concentration (FTPC). One-way ANOVA followed by Dunnett's multiple comparisons test vs vehicle control (p ⩽: * 0.05, ** 0.01, *** 0.001, **** 0.0001).

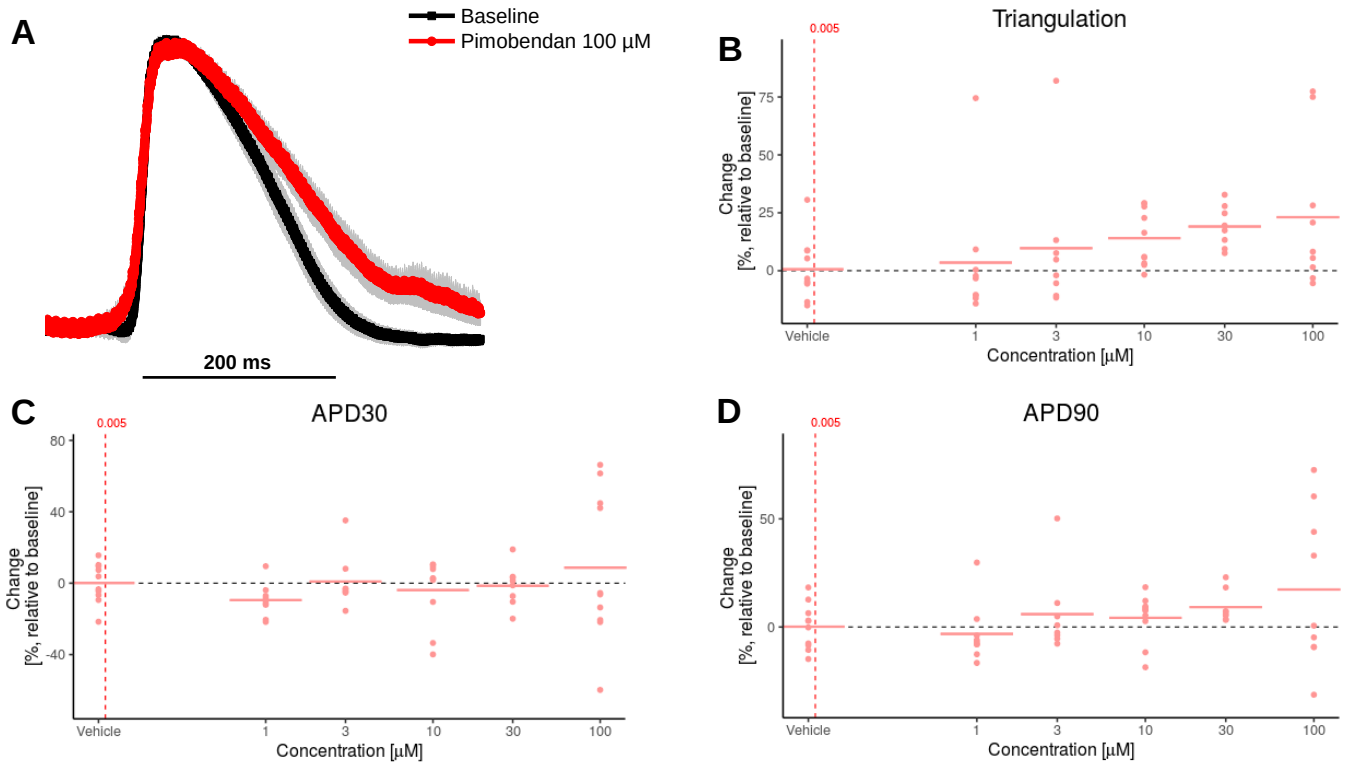

Figure 4-12. Electrophysiology analysis of hiPSC-CMs on 2D monolayers treated with pimobendan. (A) Representative voltage traces at highest concentration (100 µM). (B) Data in Triangulation (APD90-APD30) showed no significant difference after treatment. (C-D) Data in action potential duration at 30 and 90% of repolarisation showed no significant increase after treatment. hiPSC-CMs were analysed using CellOPTIQ® as previously described. Baseline (black) and treatment (red). One data point per well was recorded (n=5 per concentration). Concentration range: 1-100 µM. Data are displayed as mean ± SEM. Red dotted line is free therapeutic plasma concentration (FTPC). One-way ANOVA followed by Dunnett's multiple comparisons test vs vehicle control (p ⩽: * 0.05, ** 0.01, *** 0.001, **** 0.0001).

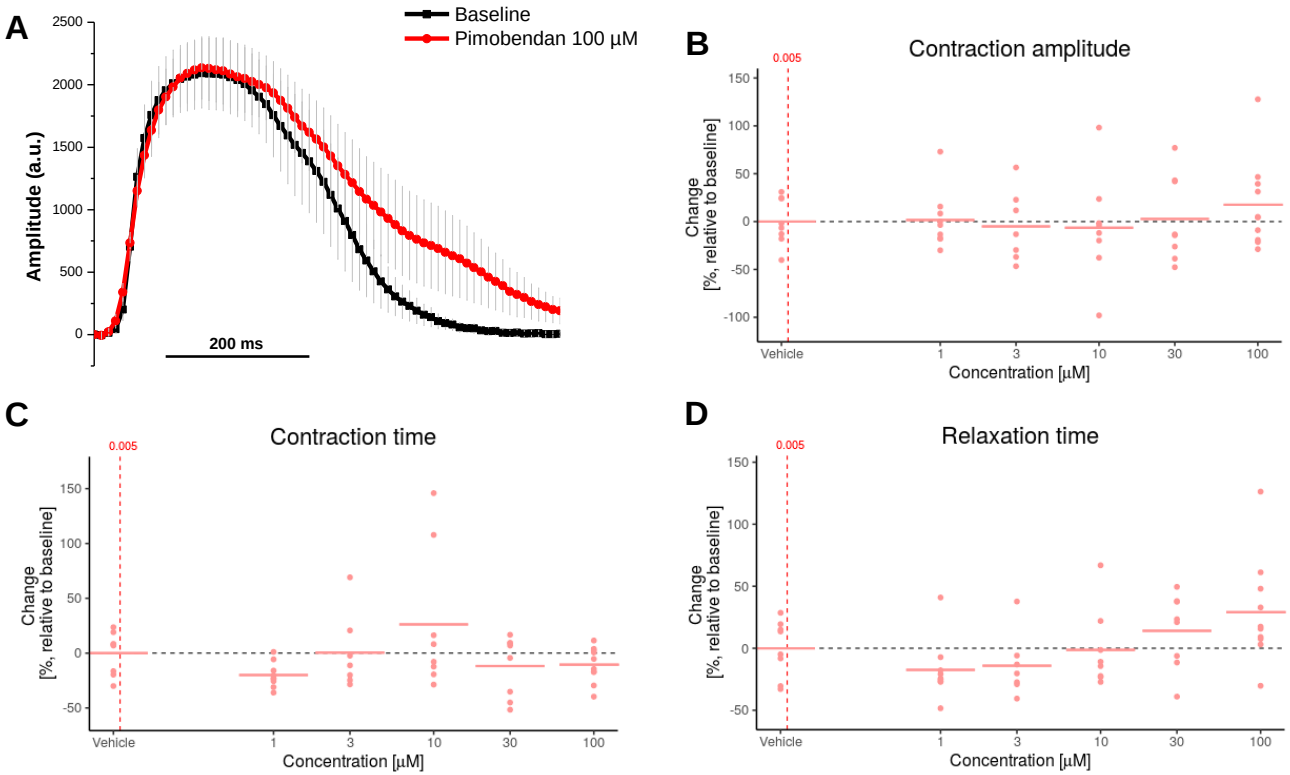

Figure 4-13. Contractility analysis of hiPSC-CMs on 2D monolayers treated with pimobendan. (A) Representative contractility traces at highest concentration (100 µM). (B) Data in contraction amplitude showed no significant difference after treatment. (C) Data in contraction time showed no significant difference after treatment. (D) Data in relaxation time showed trend in concentration dependent increase after treatment. hiPSC-CMs were analysed using CellOPTIQ® as previously described. Baseline (black) and treatment (red). One data point per well was recorded (n=5 per concentration). Concentration range: 1-100 µM. Data are displayed as mean ± SEM. Red dotted line is free therapeutic plasma concentration (FTPC). One-way ANOVA followed by Dunnett's multiple comparisons test vs vehicle control (p ⩽: * 0.05, ** 0.01, *** 0.001, **** 0.0001).

4.3.1.5 Verapamil treatment

Verapamil is categorised a negative inotrope compound and its mechanism of action is indicated in **Table *4-1***. Readouts representing R-PAT-CMs in response to treatment were plotted as mean ± SEM. Traces for voltage showed mainly (70%) quiescent after treatment (**Figure *4-14***A). The data were plotted as percentage of change from baseline. There was significant decrease for voltage Triangulation (at 0.3 and 1 μM), APD_{30} and APD_{90} (at 0.01, 0.3, and 1 μM) compared to their respective vehicle control (**Figure *4-14***B-D).

Traces for contraction amplitude showed significant decrease after treatment (**Figure *4-15***A). There was significant decrease noted for contraction amplitude (at 1 μM), contraction time (at 0.01, 0.3, and 1 μM), and relaxation time (at 1 μM) (**Figure *4-15***B-D).

4.3.1.6 Doxorubicin treatment

Doxorubicin is categorised a negative inotrope compound and its mechanism of action is indicated in **Table *4-1***. Readouts representing R-PAT-CMs in response to treatment were plotted as mean ± SEM. Traces for voltage showed 100% noisy data after treatment, due to media was overly red in compound's highest concentration, and therefore caused overexposure during voltage reading (**Figure *4-16***A). The data were plotted as percentage of change from baseline. There was significant decrease for voltage Triangulation, APD_{30} and APD_{90} (at 100 μM) compared to their respective vehicle control (**Figure *4-16***B-D).

Traces for contraction amplitude showed no effect after treatment, with large variation of distributed data (**Figure *4-17***A). There was no significant effect noted for contraction amplitude and relaxation time, and there was noted significant increase in contraction time (at 30 μM) (**Figure *4-17***B-D).

4.3.1.7 Sunitinib treatment

Sunitinib is categorised a negative inotrope compound and its mechanism of action is indicated in **Table *4-1***. Readouts representing R-PAT-CMs in response to treatment were plotted as mean ± SEM. Traces for voltage showed trend in prolonged APDs (**Figure *4-18***A). The data were

plotted as percentage of change from baseline. One well was found to have quiescent cells. There was no significant difference found for voltage Triangulation, APD_{30} and APD_{90} compared to their respective vehicle control (**Figure *4-18***B-D).

Traces for contraction amplitude showed trend decrease after treatment (**Figure *4-19***A). There was no significant effect noted for contraction amplitude, contraction time, and relaxation time (**Figure *4-19***B-D).

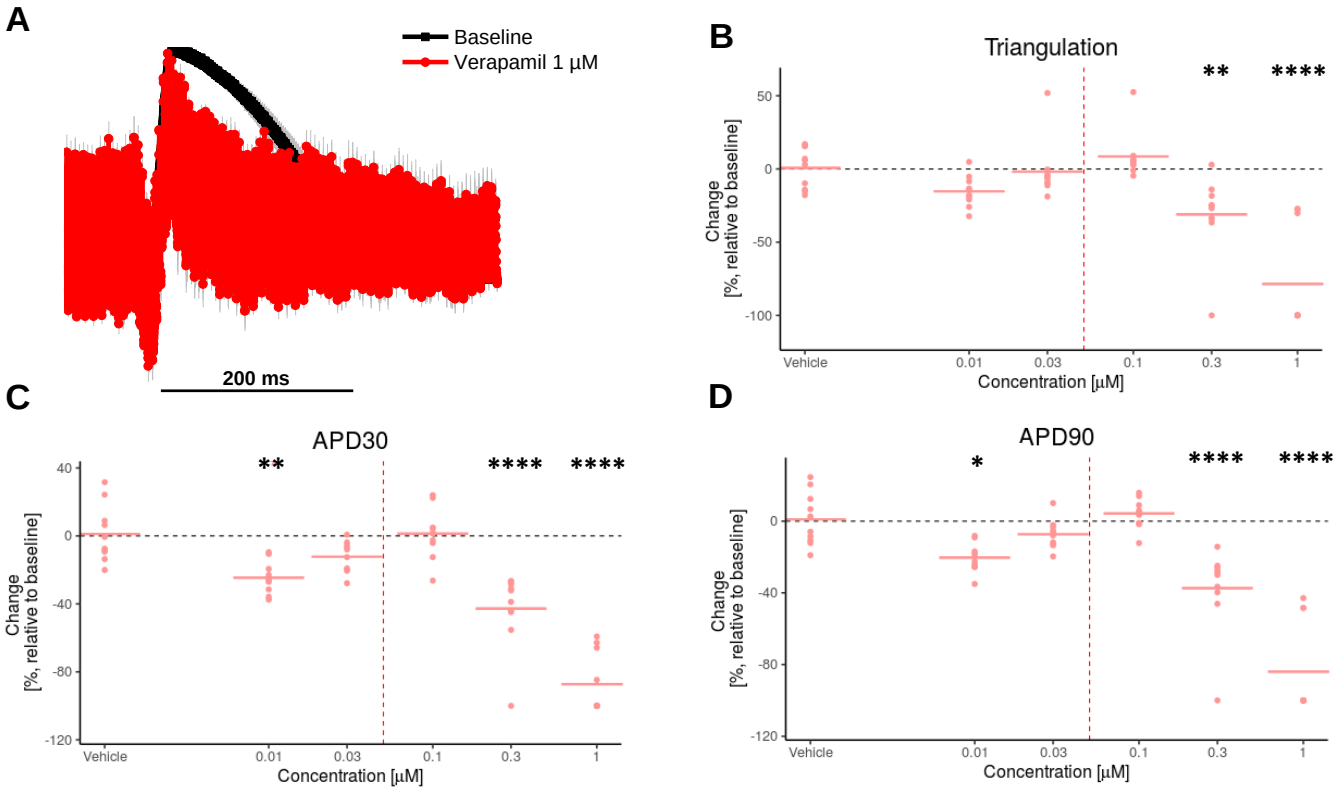

Figure 4-14. Electrophysiology analysis of hiPSC-CMs on 2D monolayers treated with verapamil. (A) Representative voltage traces at highest concentration (1 µM). (B) Data in Triangulation (APD90-APD30) showed significant decrease at higher concentrations (0.3 and 1 µM). (C-D) Data in action potential duration at 30 and 90% of repolarisation showed significant decrease at 0.01, 0.3, and 1 µM. 70% wells contained quiescent cells. hiPSC-CMs were analysed using CellOPTIQ® as previously described. Baseline (black) and treatment (red). One data point per well was recorded (n=5 per concentration). Concentration range: 0.01-1 µM. Data are displayed as mean ± SEM. Red dotted line is free therapeutic plasma concentration (FTPC). One-way ANOVA followed by Dunnett's multiple comparisons test vs vehicle control (p ⩽: * 0.05, ** 0.01, *** 0.001, **** 0.0001).

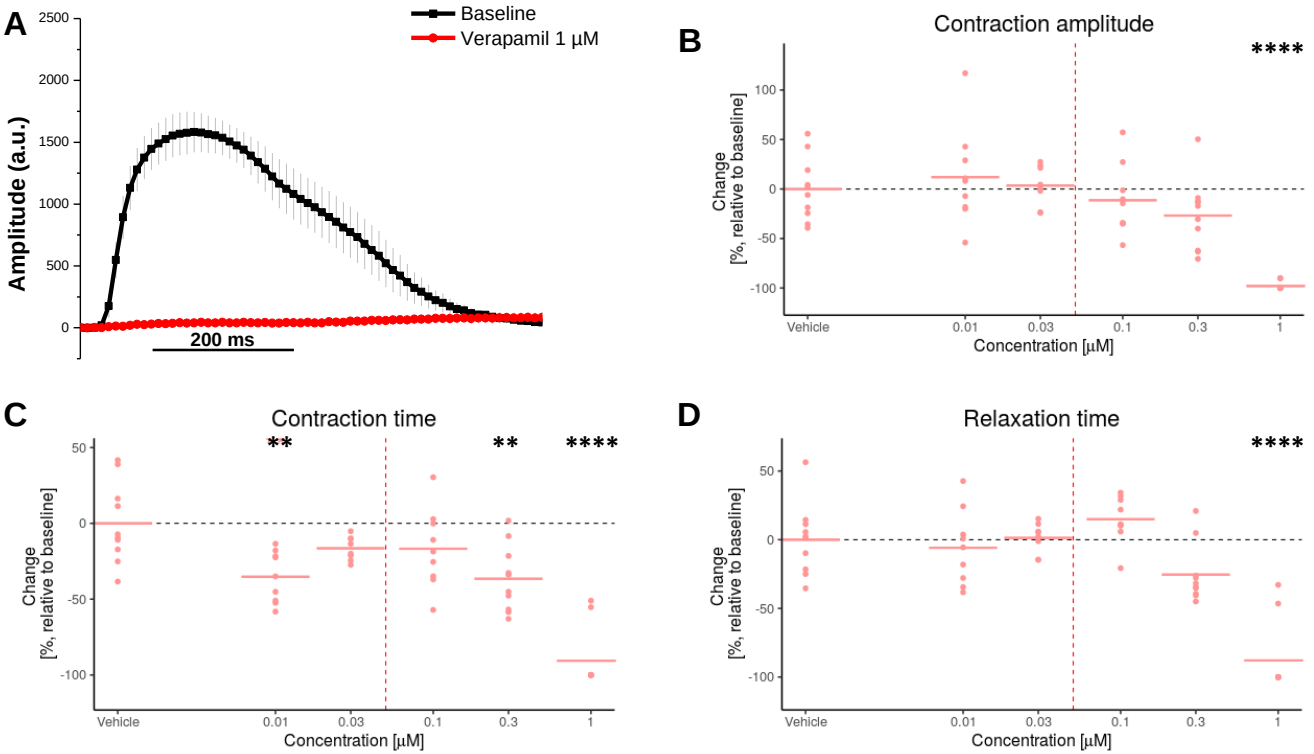

Figure 4-15. Contractility analysis of hiPSC-CMs on 2D monolayers treated with verapamil. (A) Representative contractility traces at highest concentration (1 µM). (B) Data in contraction amplitude showed significant decrease at highest concentration (1 µM). (C) Data in contraction time showed significant decrease at 0.01, 0.3, and 1 µM. (D) Data in relaxation time showed significant decrease at highest concentration (1 µM). 70% wells contained quiescent cells. hiPSC-CMs were analysed using CellOPTIQ® as previously described. Baseline (black) and treatment (red). One data point per well was recorded (n=5 per concentration). Concentration range: 0.01-1 µM. Data are displayed as mean ± SEM. Red dotted line is free therapeutic plasma concentration (FTPC). One-way ANOVA followed by Dunnett's multiple comparisons test vs vehicle control (p ⩽: * 0.05, ** 0.01, *** 0.001, **** 0.0001).

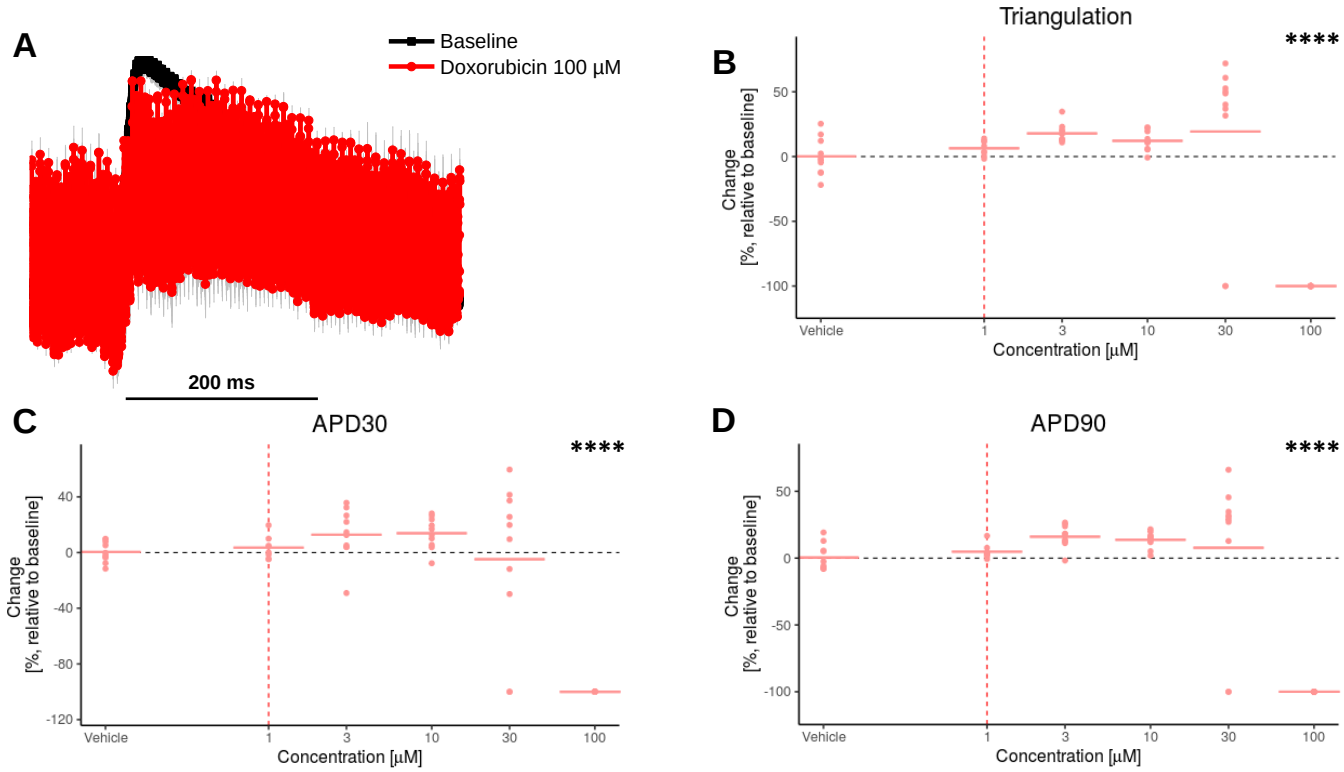

Figure 4-16. Electrophysiology analysis of hiPSC-CMs on 2D monolayers treated with doxorubicin. (A) Representative voltage traces at highest concentration (100 µM). (B) Data in Triangulation (APD90-APD30) showed significant decrease at highest concentration (100 µM). (C-D) Data in action potential duration at 30 and 90% of repolarisation showed significant decrease at highest concentration (100 µM). 100% of wells at highest concentration could not be read due to overexposure (very red media). hiPSC-CMs were analysed using CellOPTIQ® as previously described. Baseline (black) and treatment (red). One data point per well was recorded (n=5 per concentration). Concentration range: 1-100 µM. Data are displayed as mean ± SEM. Red dotted line is free therapeutic plasma concentration (FTPC). One-way ANOVA followed by Dunnett's multiple comparisons test vs vehicle control (p ⩽: * 0.05, ** 0.01, *** 0.001, **** 0.0001).

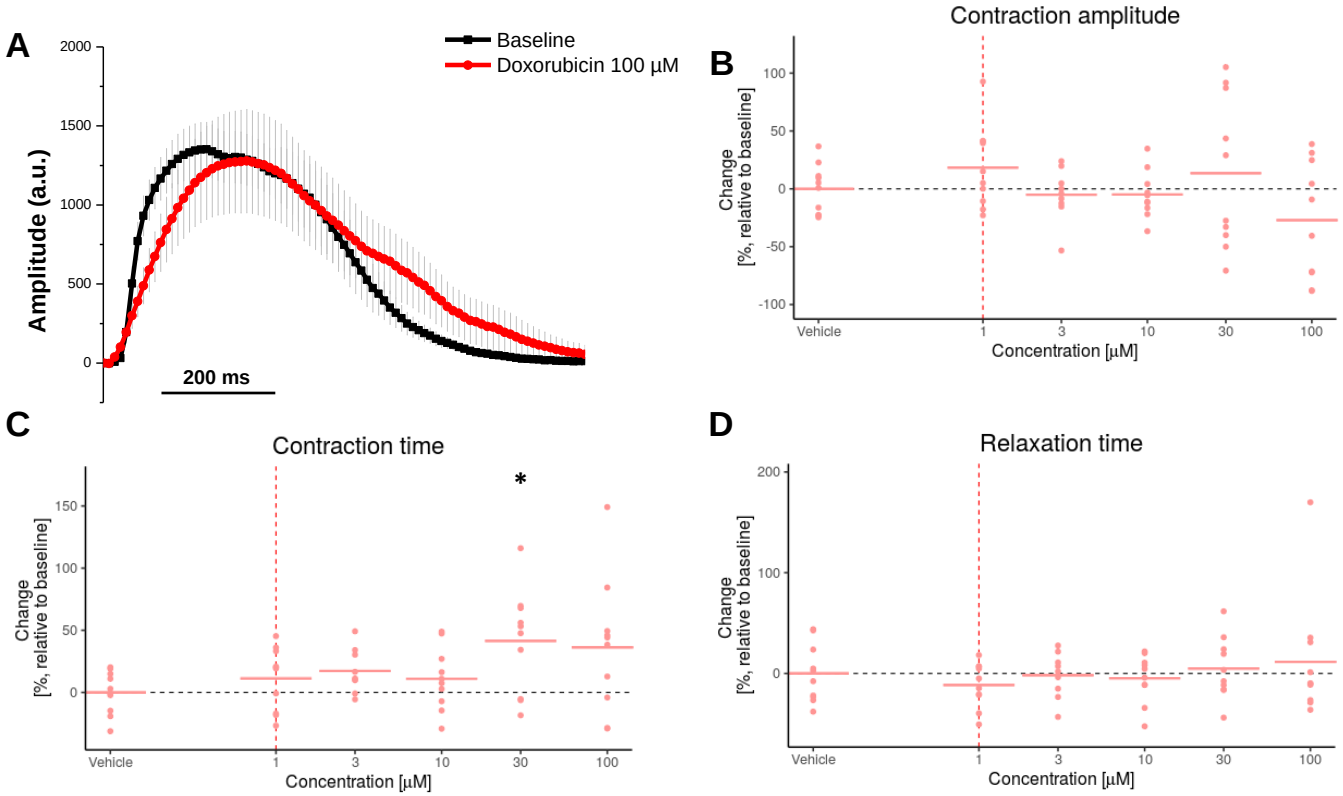

Figure 4-17. Contractility analysis of hiPSC-CMs on 2D monolayers treated with doxorubicin. (A) Representative contractility traces at highest concentration (100 µM). (B) Data in contraction amplitude showed no significant effect after treatment. (C) Data in contraction time showed significant increase at 30 µM. (D) Data in relaxation time showed no significant effect after treatment. hiPSC-CMs were analysed using CellOPTIQ® as previously described. Baseline (black) and treatment (red). One data point per well was recorded (n=5 per concentration). Concentration range: 1-100 µM. Data are displayed as mean ± SEM. Red dotted line is free therapeutic plasma concentration (FTPC). One-way ANOVA followed by Dunnett's multiple comparisons test vs vehicle control ($p \leqslant$: * 0.05, ** 0.01, *** 0.001, **** 0.0001).

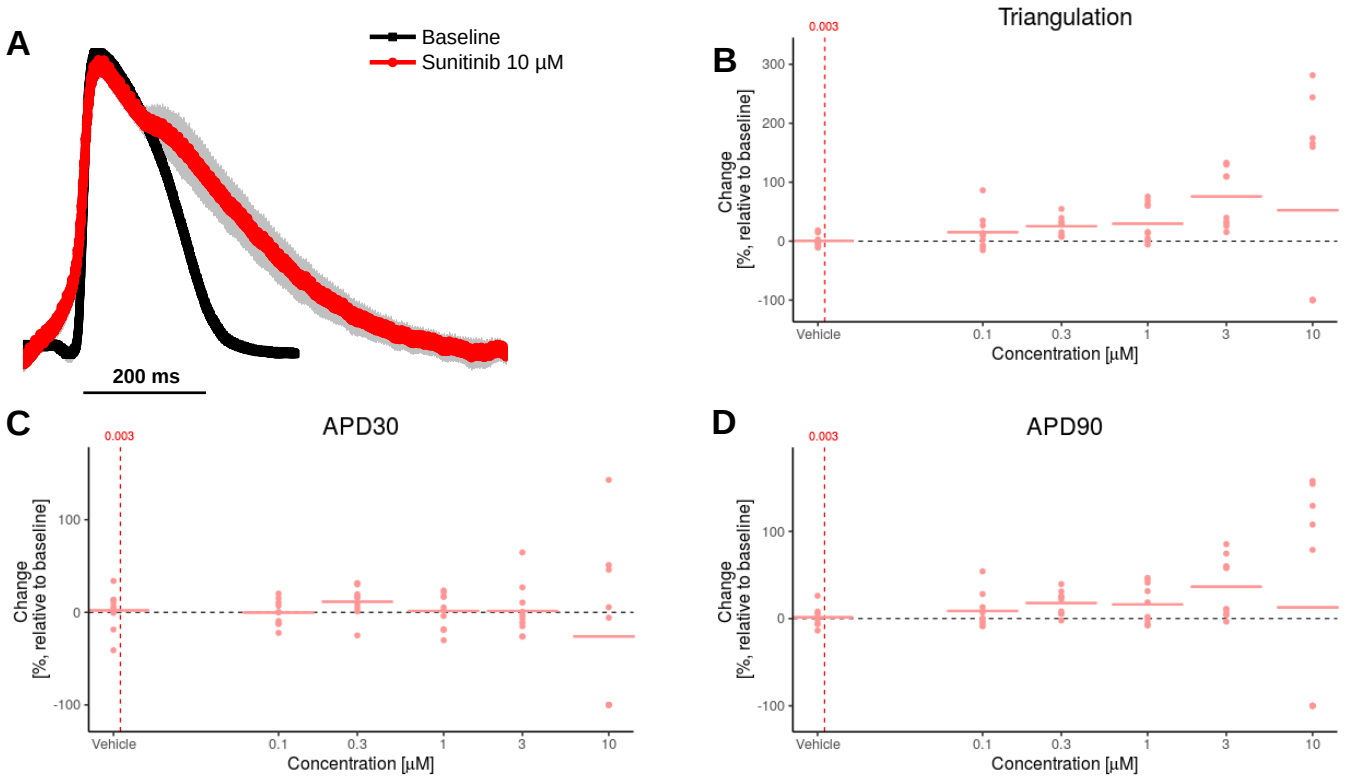

Figure 4-18. Electrophysiology analysis of hiPSC-CMs on 2D monolayers treated with sunitinib. (A) Representative voltage traces at highest concentration (10 µM). (B) Data in Triangulation (APD90-APD30) showed no significant effect after treatment. (C-D) Data in action potential duration at 30 and 90% of repolarisation showed no significant effect after treatment. hiPSC-CMs were analysed using CellOPTIQ® as previously described. Baseline (black) and treatment (red). One data point per well was recorded (n=5 per concentration). Concentration range: 0.1-10 µM. Data are displayed as mean ± SEM. Red dotted line is free therapeutic plasma concentration (FTPC). One-way ANOVA followed by Dunnett's multiple comparisons test vs vehicle control (p ⩽: * 0.05, ** 0.01, *** 0.001, **** 0.0001).

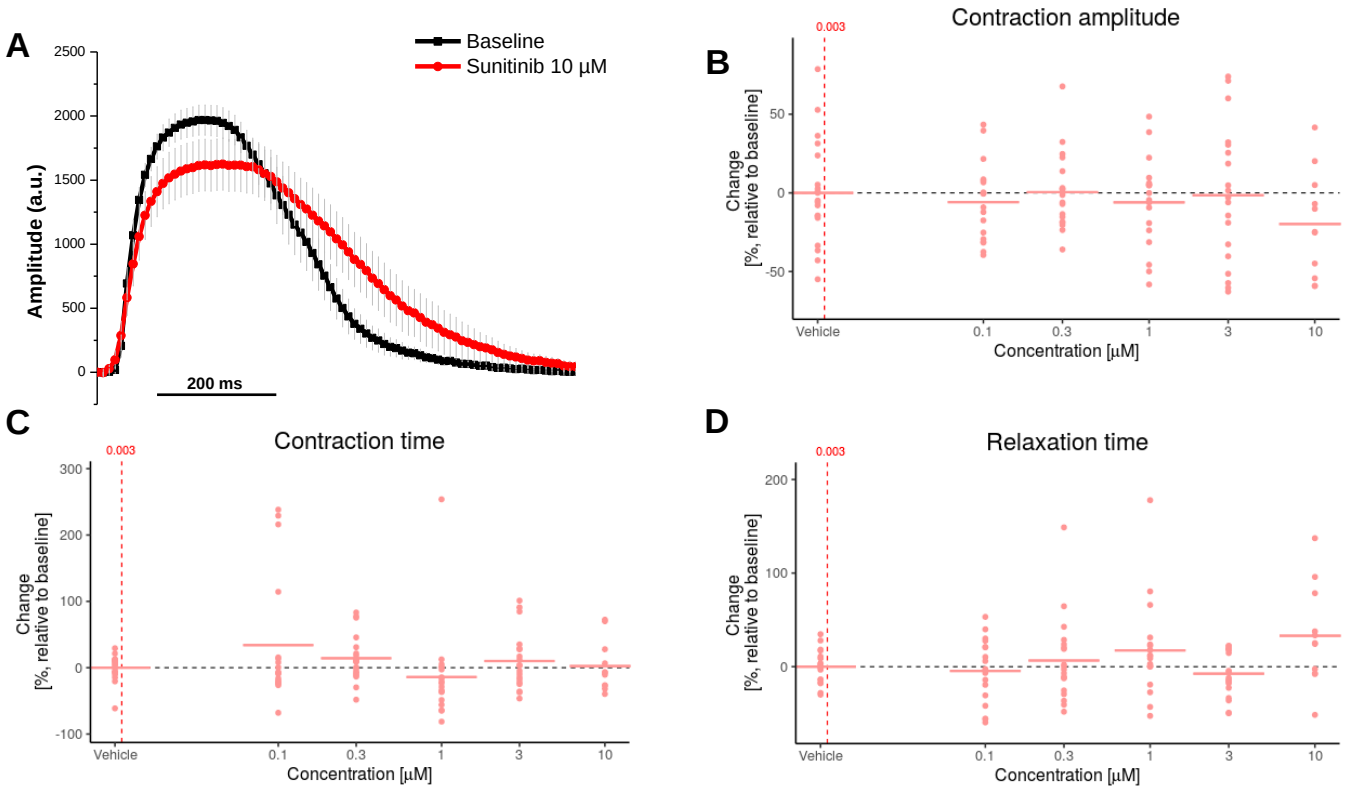

Figure 4-19. Contractility analysis of hiPSC-CMs on 2D monolayers treated with sunitinib. (A) Representative contractility traces at highest concentration (10 µM). (B) Data in contraction amplitude showed no significant effect after treatment. (C) Data in contraction time showed no significant effect after treatment. (D) Data in relaxation time showed no significant effect after treatment. hiPSC-CMs were analysed using CellOPTIQ® as previously described. Baseline (black) and treatment (red). One data point per well was recorded (n=5 per concentration). Concentration range: 0.1-10 µM. Data are displayed as mean ± SEM. Red dotted line is free therapeutic plasma concentration (FTPC). One-way ANOVA followed by Dunnett's multiple comparisons test vs vehicle control (p ⩽: * 0.05, ** 0.01, *** 0.001, **** 0.0001).

4.3.1.8 Acetylsalicylic acid treatment

Acetylsalicylic acid is categorised a no effect compound and its mechanism of action is indicated in **Table *4-1***. Readouts representing R-PAT-CMs in response to treatment were plotted as mean ± SEM. Traces for voltage showed no effect after treatment (**Figure *4-20***A). The data were plotted as percentage of change from baseline. There was significant increase found for voltage Triangulation and APD_{90} at highest concentration (1000 µM) compared to their respective vehicle control (**Figure *4-20***B-D).

Traces for contraction amplitude showed no effect after treatment (**Figure *4-21***A). There was no significant effect noted for contraction amplitude, contraction time, and relaxation time (**Figure *4-21***B-D).

4.3.1.9 Atenolol treatment

Atenolol is categorised a no effect compound and its mechanism of action is indicated in **Table *4-1***. Readouts representing R-PAT-CMs in response to treatment were plotted as mean ± SEM. Traces for voltage showed no effect after treatment (**Figure *4-22***A). The data were plotted as percentage of change from baseline. There was no significant difference found for voltage Triangulation, APD_{30}, and APD_{90} compared to their respective vehicle control (**Figure *4-22***B-D).

Traces for contraction amplitude showed no effect after treatment (**Figure *4-23***A). There was no significant effect noted for contraction amplitude, contraction time, and relaxation time (**Figure *4-23***B-D).

4.3.1.10 Captopril treatment

Captopril is categorised a no effect compound and its mechanism of action is indicated in **Table *4-1***. Readouts representing R-PAT-CMs in response to treatment were plotted as mean ± SEM. Traces for voltage showed no effect after treatment (**Figure *4-24***A). The data were plotted as percentage of change from baseline. There was no significant difference found for voltage Triangulation, APD_{30}, and APD_{90} compared to their respective vehicle control (**Figure *4-24***B-D).

Traces for contraction amplitude showed no effect after treatment (**Figure *4-25***A). There was no significant effect noted for contraction amplitude, contraction time, and relaxation time (**Figure *4-25***B-D).

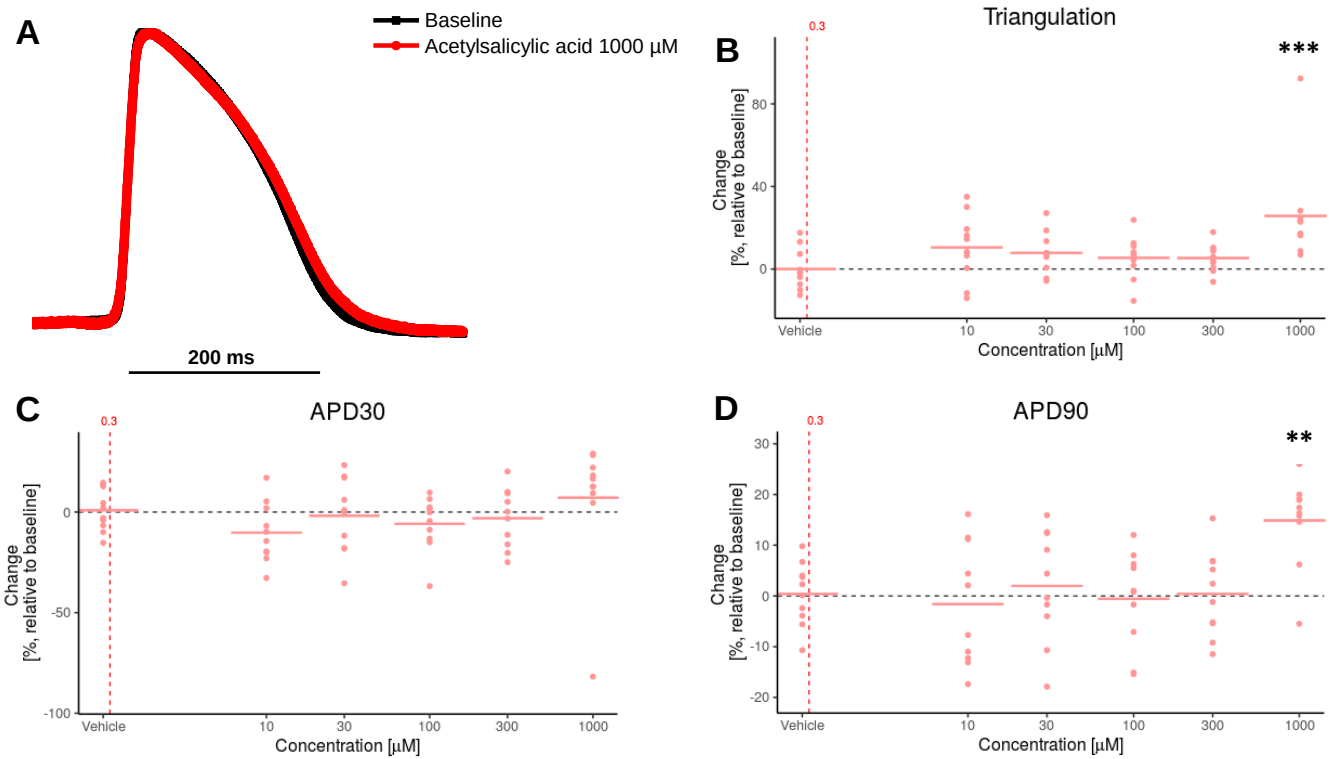

Figure 4-20. Electrophysiology analysis of hiPSC-CMs on 2D monolayers treated with acetylsalicylic acid. (A) Representative voltage traces at highest concentration (1000 µM). (B) Data in Triangulation (APD90-APD30) showed significant increase at highest concentration (1000 µM). (D) Data in action potential duration at 90% of repolarisation showed significant increase at highest concentration (1000 µM). hiPSC-CMs were analysed using CellOPTIQ® as previously described. Baseline (black) and treatment (red). One data point per well was recorded (n=5 per concentration). Concentration range: 10-1000 µM. Data are displayed as mean ± SEM. Red dotted line is free therapeutic plasma concentration (FTPC). One-way ANOVA followed by Dunnett's multiple comparisons test vs vehicle control (p ⩽: * 0.05, ** 0.01, *** 0.001, **** 0.0001).

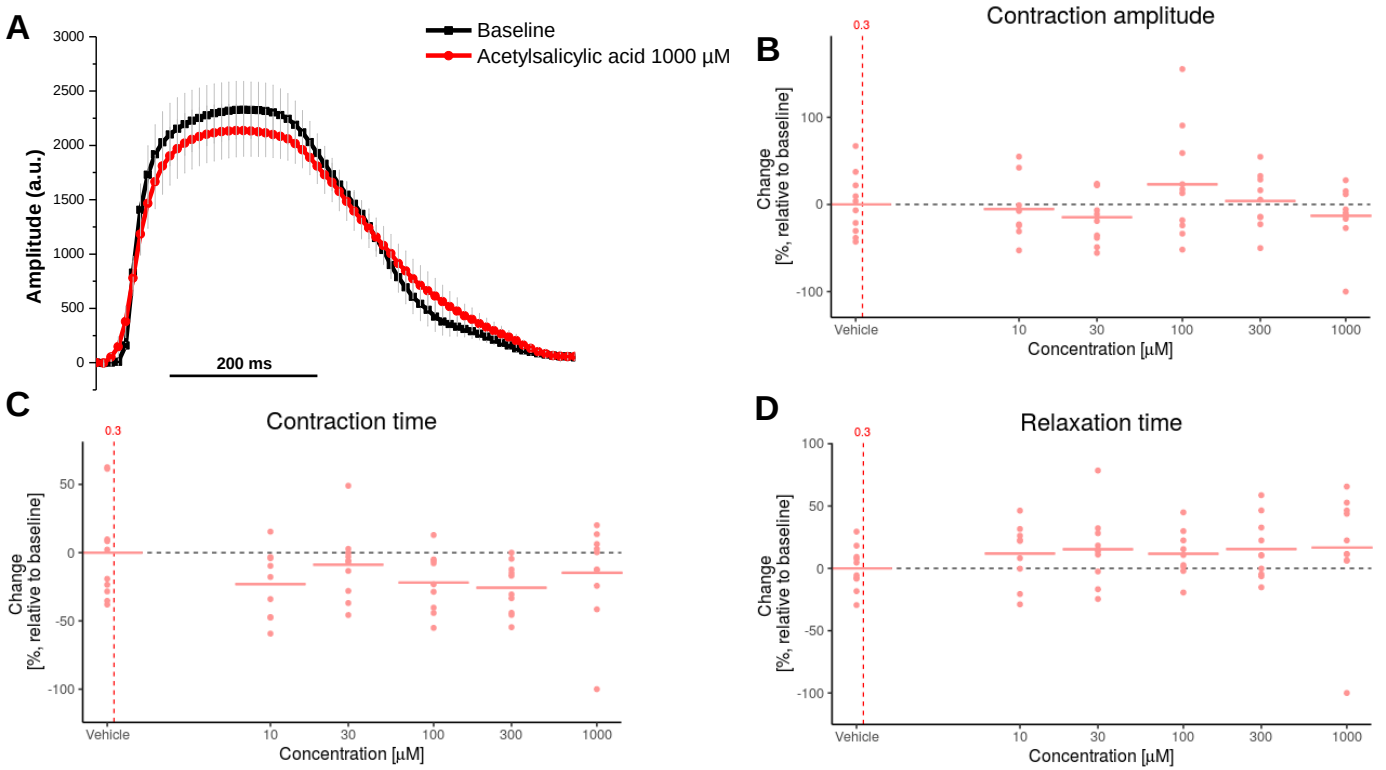

Figure 4-21. Contractility analysis of hiPSC-CMs on 2D monolayers treated with acetylsalicylic acid. (A) Representative contractility traces at highest concentration (1000 µM). (B) Data in contraction amplitude showed no significant effect after treatment. (C) Data in contraction time showed no significant effect after treatment. (D) Data in relaxation time showed no significant effect after treatment. hiPSC-CMs were analysed using CellOPTIQ® as previously described. Baseline (black) and treatment (red). One data point per well was recorded (n=5 per concentration). Concentration range: 10-1000 µM. Data are displayed as mean ± SEM. Red dotted line is free therapeutic plasma concentration (FTPC). One-way ANOVA followed by Dunnett's multiple comparisons test vs vehicle control (p ⩽: * 0.05, ** 0.01, *** 0.001, **** 0.0001).

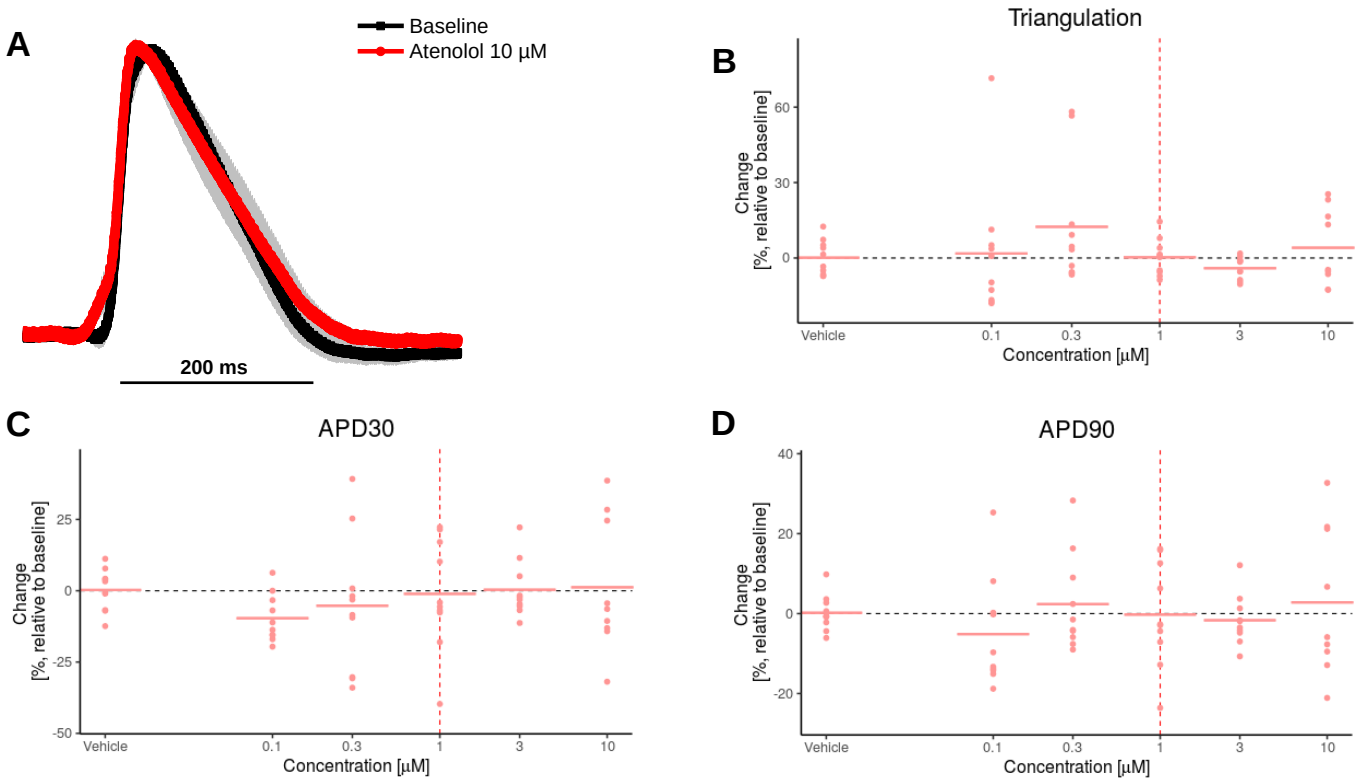

Figure 4-22. Electrophysiology analysis of hiPSC-CMs on 2D monolayers treated with atenolol. (A) Representative voltage traces at highest concentration (10 µM). (B) Data in Triangulation (APD90-APD30) showed no significant effect after treatment. (C-D) Data in action potential duration at 30 and 90% of repolarisation showed no significant effect after treatment. hiPSC-CMs were analysed using CellOPTIQ® as previously described. Baseline (black) and treatment (red). One data point per well was recorded (n=5 per concentration). Concentration range: 0.1-10 µM. Data are displayed as mean ± SEM. Red dotted line is free therapeutic plasma concentration (FTPC). One-way ANOVA followed by Dunnett's multiple comparisons test vs vehicle control (p ⩽: * 0.05, ** 0.01, *** 0.001, **** 0.0001).

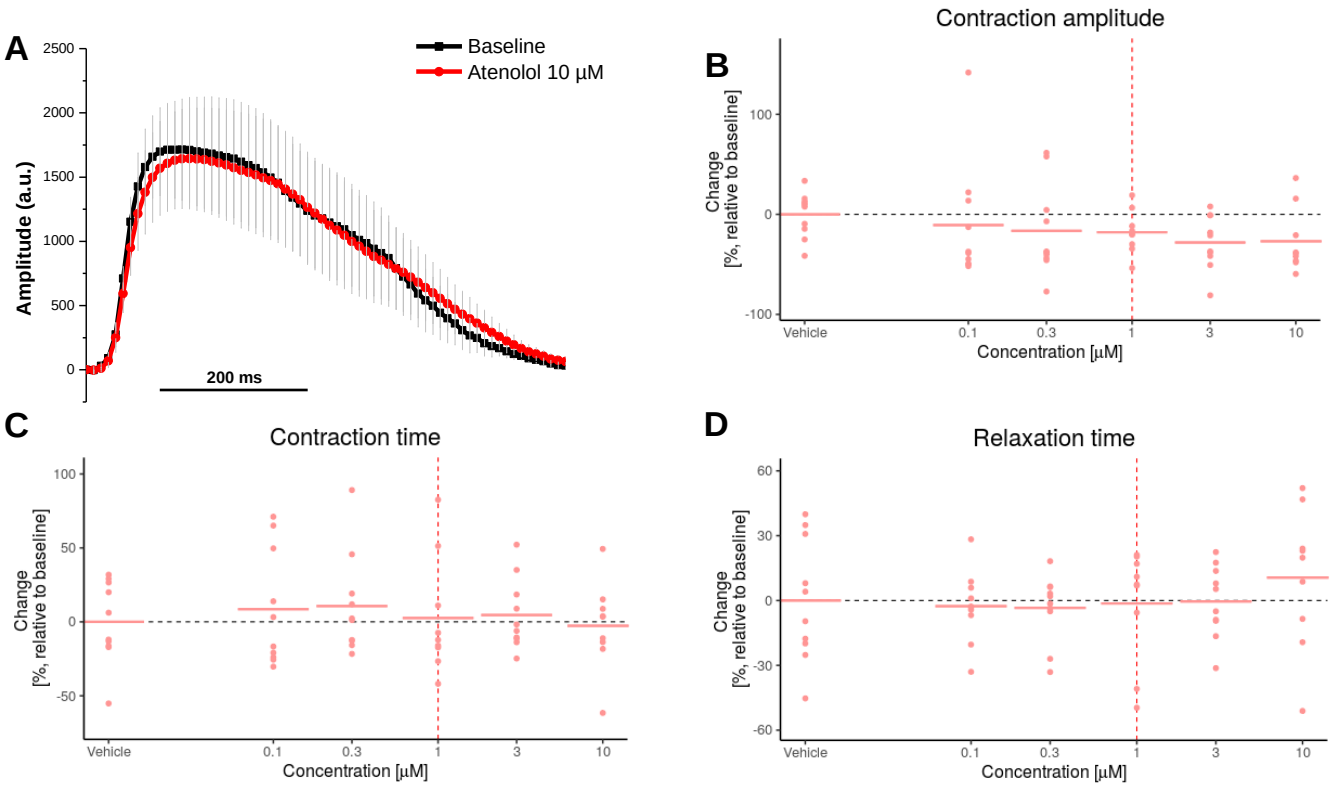

Figure 4-23. Contractility analysis of hiPSC-CMs on 2D monolayers treated with atenolol. (A) Representative contractility traces at highest concentration (10 µM). (B) Data in contraction amplitude showed no significant effect after treatment. (C) Data in contraction time showed no significant effect after treatment. (D) Data in relaxation time showed no significant effect after treatment. hiPSC-CMs were analysed using CellOPTIQ® as previously described. Baseline (black) and treatment (red). One data point per well was recorded (n=5 per concentration). Concentration range: 0.1-10 µM. Data are displayed as mean ± SEM. Red dotted line is free therapeutic plasma concentration (FTPC). One-way ANOVA followed by Dunnett's multiple comparisons test vs vehicle control (p ⩽: * 0.05, ** 0.01, *** 0.001, **** 0.0001).

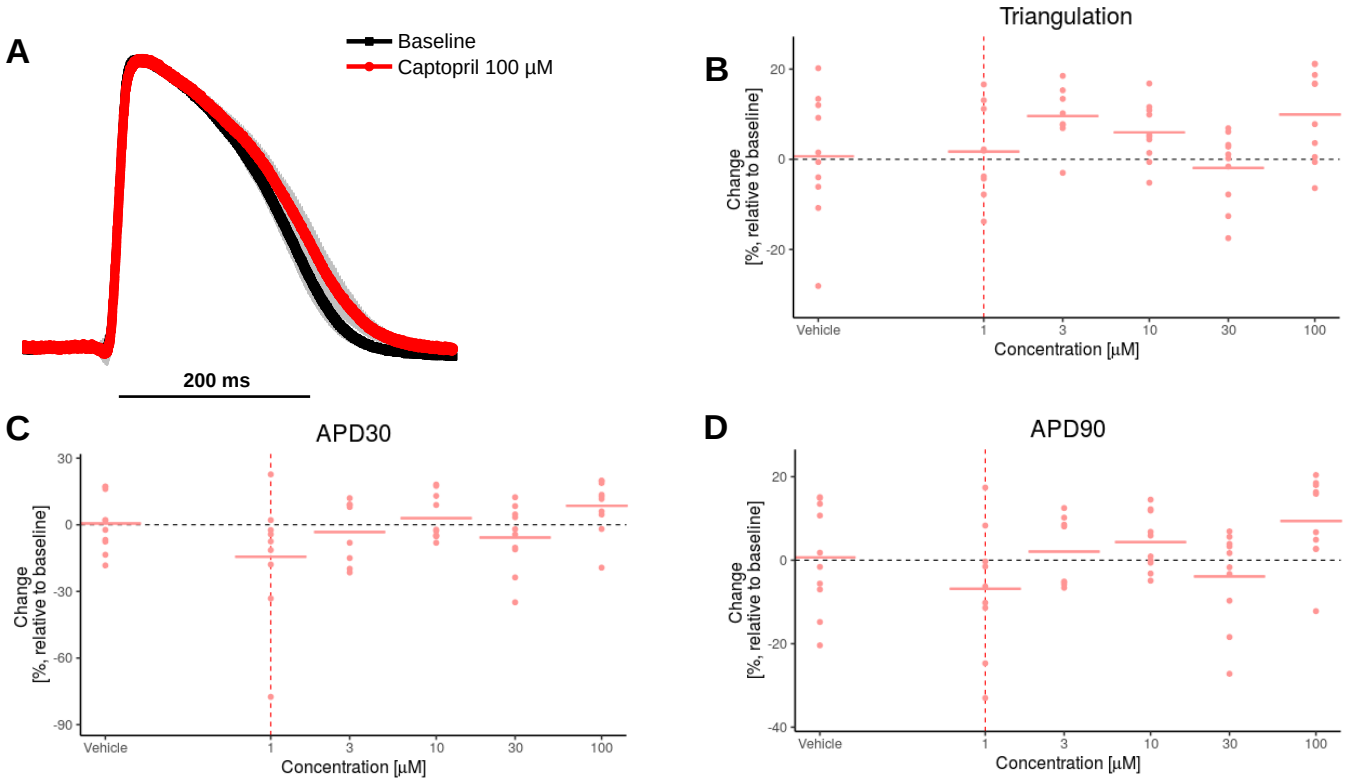

Figure 4-24. Electrophysiology analysis of hiPSC-CMs on 2D monolayers treated with captopril. (A) Representative voltage traces at highest concentration (100 µM). (B) Data in Triangulation (APD90-APD30) showed no significant effect after treatment. (C-D) Data in action potential duration at 30 and 90% of repolarisation showed no significant effect after treatment. hiPSC-CMs were analysed using CellOPTIQ® as previously described. Baseline (black) and treatment (red). One data point per well was recorded (n=5 per concentration). Concentration range: 1-100 µM. Data are displayed as mean ± SEM. Red dotted line is free therapeutic plasma concentration (FTPC). One-way ANOVA followed by Dunnett's multiple comparisons test vs vehicle control (p ⩽: * 0.05, ** 0.01, *** 0.001, **** 0.0001).

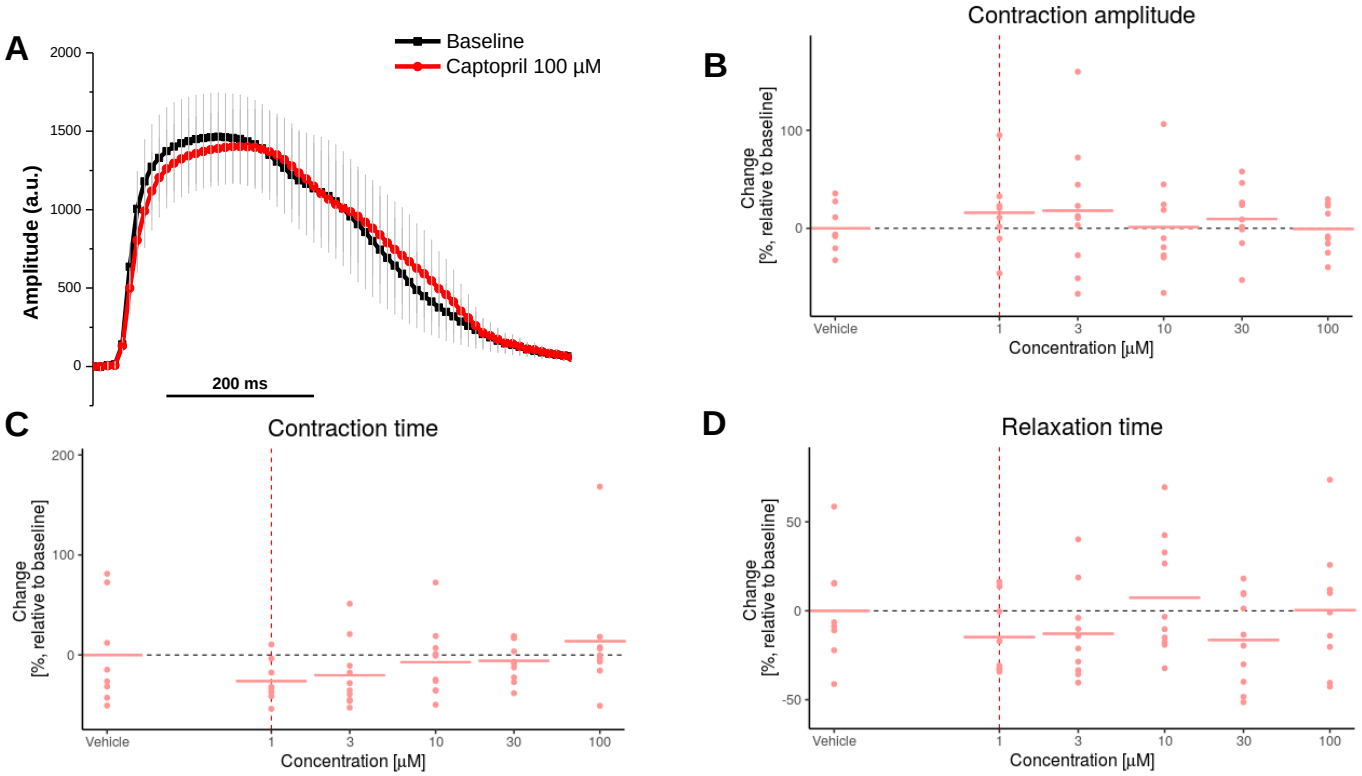

Figure 4-25. Contractility analysis of hiPSC-CMs on 2D monolayers treated with captopril. (A) Representative contractility traces at highest concentration (100 µM). (B) Data in contraction amplitude showed no significant effect after treatment. (C) Data in contraction time showed no significant effect after treatment. (D) Data in relaxation time showed no significant effect after treatment. hiPSC-CMs were analysed using CellOPTIQ® as previously described. Baseline (black) and treatment (red). One data point per well was recorded (n=5 per concentration). Concentration range: 1-100 µM. Data are displayed as mean ± SEM. Red dotted line is free therapeutic plasma concentration (FTPC). One-way ANOVA followed by Dunnett's multiple comparisons test vs vehicle control (p ⩽: * 0.05, ** 0.01, *** 0.001, **** 0.0001).

4.3.2 Predictivity and sensitivity of platform-cell combinations for all compounds evaluated

In order to investigate drug response prediction pattern, the maximum responses (both positive and negative value) were related to their corresponding drug concentration (**Table *4-3***). It is noted that the 2D monolayers platforms have wider response range compared to 3D EHTs. In this instance, the mean maximum measurable percentage changes in contraction amplitude for TTM and CO platforms ranged from -100% to +196%, it was -100% to +53% for the EHT platform (**Table *4-3***). Similar trend is the same for contraction time for TTM and CO platforms (-100% to +163%) versus EHT platform (-37% to +38%), as well as relaxation time for TTM and CO platforms (-100% to +300%) versus EHT platform (-35% to +43%). The tighter data spread in 3D EHTs were likely due to cumulative concentration response protocol as shown in previous chapter.

Table 4-3. Effects of compounds on cardiomyocyte contractility *in vitro*. For each platform-cell combination, data listed represent mean maximum measurable percentage change relative to baseline for CA, CT and RT. The concentration at which this effect occurred is listed, but when it was different for CA, CT and RT, the concentration is superscripted. Green indicates the predicted effect matched the known effect on inotropy. Abbreviations: CA, contraction amplitude; CT, contraction time; RT, relaxation time; SSR inhibitor, selective serotonin reuptake inhibitor; ACE, angiotensin converting enzyme; PDE, phosphodiesterase; FPTC, free plasma therapeutic concentration; PI, positive inotrope; NI, negative inotrope; NE, no effect. Analysis platforms were CO, CellOPTIQ; TTM, Triple Transient Measurement; EHT, Engineered Heart Tissue. Cardiomyocyte types were rabbit adult cardiomyocytes (as comparator) or hiPSC lines: P-Cyte, Pluricyte (Ncardia); iCell^2 (Cellular Dynamics International); R-PAT (University of Nottingham); ERC18 (University of Hamburg).

Compound	Rank	Mode of action	Platform	Cell	Contraction Amplitude	Contraction Time	Relaxation Time	Test range µM	Conc µM	FPTC µM	Known effect	Blinded assignment
Epinephrine	1	Non-selective α1-, β1- and β2-adrenoceptor agonist	CO	Rabbit	+196	-26	+6 $^{0.03\ \mu M}$	0.01-1	0.1	0.0002-0.05	PI	PI
			TTM	P-Cyte	+53 $^{0.03\ \mu M}$	-34 $^{1\ \mu M}$	-9		0.01			PI
			CO	P-Cyte	+18 $^{0.3\ \mu M}$	+67 $^{1\ \mu M}$	-36		0.1			NE
			CO	iCell2	-12 $^{0.3\ \mu M}$	-43	+39		0.03			PI
			CO	R-PAT	+27 $^{0.01\ \mu M}$	+16	-18		1			NE
			EHT	R-PAT	+22	-16 $^{1\ \mu M}$	-22 $^{0.3\ \mu M}$		0.1			PI
			EHT	ERC18	-8	-6 $^{1\ \mu M}$	-7		0.01			NE
Forskolin	2	Adenylyl cyclase stimulator	CO	Rabbit	-16	-34 $^{0.1\ \mu M}$	+45	0.1-10	3	0.012-0.024	PI	PI
			TTM	P-Cyte	+72 $^{10\ \mu M}$	-37 $^{3\ \mu M}$	-38		0.3			PI
			CO	P-Cyte	+31 $^{1\ \mu M}$	+55 $^{3\ \mu M}$	+47		0.3			NE
			CO	iCell2	-44	+64	+44		10			NI
			CO	R-PAT	-31 $^{10\ \mu M}$	-33	+20		0.1			NE
			EHT	R-PAT	+15 $^{10\ \mu M}$	-7	-22 $^{3\ \mu M}$		0.3			PI
			EHT	ERC18	+18 $^{3\ \mu M}$	-33	-23		10			PI
Levosimendan	3	Calcium sensitizer PDE3 inhibitor	CO	Rabbit	+16 $^{0.1\ \mu M}$	-33	-25	0.01-1	0.01	0.026-0.35	PI	NE
			TTM	P-Cyte	+42 $^{0.1\ \mu M}$	+11 $^{0.3\ \mu M}$	-12		0.03			NE

		K_{ATP} channel agonist	CO	P-Cyte	-54	+54	-40		0.03		NE
			CO	iCell2	+14 $^{0.3\ \mu M}$	+80	+54		0.1		NE
			CO	R-PAT	+23 $^{0.1\ \mu M}$	-12	22 $^{1\ \mu M}$		0.01		NE
			EHT	R-PAT	+6	-7	-14 $^{0.3\ \mu M}$		0.01		NE
			EHT	ERC18	+13 $^{1\ \mu M}$	-9 $^{0.1\ \mu M}$	-4		0.01		NE
Pimobendan	4	Calcium sensitizer PDE3 inhibitor	CO	Rabbit	+132 $^{1\ \mu M}$	+72	+42	1-100	3	0.005-0.01	NE
			TTM	P-Cyte	+55	-31 $^{10\ \mu M}$	+73		30		NE
			CO	P-Cyte	-23 $^{10\ \mu M}$	+69	-19		3		NE
			CO	iCell2	+65	+69	-13 $^{100\ \mu M}$		1		NE
			CO	R-PAT	+18	+26 $^{10\ \mu M}$	+29		100		NE
			EHT	R-PAT	+12	-3.5	+12 $^{100\ \mu M}$		1		NE
			EHT	ERC18	+13 $^{30\ \mu M}$	-13	+14 $^{100\ \mu M}$		3		PI
Dobutamine	11	α1-, β1- and β2 adrenoceptor agonist	CO	R-PAT	+39 $^{3\ \mu M}$	-16 $^{10\ \mu M}$	+29	0.1-10	0.3	0.07-1	NE
			EHT	R-PAT	+44 $^{3\ \mu M}$	-25	-22		10		PI
			EHT	ERC18	+18 $^{3\ \mu M}$	-37 $^{10\ \mu M}$	+7		0.3		PI
Milrinone	13	PDE3 inhibitor	CO	R-PAT	-17	+16 $^{3\ \mu M}$	+15 $^{100\ \mu M}$	1-100	1	0.1-0.15	NE
			EHT	R-PAT	+18	-11	-9		30		PI
			EHT	ERC18	+7	-18	-6 $^{30\ \mu M}$		100		PI
Omecamtiv mecarbil	14	Cardiac specific myosin activator	CO	R-PAT	-47	+117	-34 $^{0.01\ \mu M}$	0.01-1	1	0.05-4.2	NI
			EHT	R-PAT	+53	+37	-26		0.3		PI
			EHT	ERC18	+22	+38	-6 $^{0.3\ \mu M}$		1		PI
Terbutaline	21	β2-adrenoceptor agonist	CO	R-PAT	+28	-32 $^{3\ \mu M}$	-35 $^{10\ \mu M}$	0.1-10	0.3	1.3	NE
			EHT	R-PAT	+17	-24	-35 $^{0.3\ \mu M}$		3		PI
			EHT	ERC18	+29 $^{10\ \mu M}$	-30	-17		1		PI
Verapamil	7		CO	Rabbit	-82 $^{0.03\ \mu M}$	+24	+61	0.01-1	0.1	0.05	NI
			TTM	P-Cyte	-79	-68	-11		0.1		NI

		L-type calcium channel blocker, hERG blocker	CO	P-Cyte	(5/5)Q	(5/5)Q	(5/5)Q		1			NI
			CO	iCell2	(4/5)Q	+103 [0.1 µM]	(4/5)Q		1			NI
			CO	R-PAT	-98	-91	-88		1			NI
			EHT	R-PAT	(5/5)Q [0.1 µM]	-7	-6		0.03			NI
			EHT	ERC18	(3/5)Q [0.3 µM]	-25 [0.1 µM]	-17		0.1			NI
Doxorubicin	8	Impairs Ca^{2+} transport mechanisms in sarcoplasmic reticulum	TTM	P-Cyte	-47	-46	+51	0.1-10	100	1-2	NI	NE
			CO	P-Cyte	-15	+70	+72		100			NE
			CO	iCell2	+65	-39	+57 [30 µM]		1			NE
			CO	R-PAT	-27 [100 µM]	+41 [30 µM]	-12		1			NE
Sunitinib	9	Multi-targeted TK inhibitor	CO	Rabbit	-78	+46	+300	0.1-10	10	0.003	NI	NI
			TTM	P-Cyte	+42	-23 [10 µM]	+28		0.1			NI
			CO	P-Cyte	(5/5)Q	+163 [0.1 µM]	(5/5)Q		10			NI
			CO	iCell2	-25 [10 µM]	-43	+62		1			NI
			CO	R-PAT	-20	+34 [0.1 µM]	+33		10			NE
			EHT	R-PAT	+11	+6	+4 [0.1 µM]		0.3			NE
			EHT	ERC18	-8	+6	-8		3			NE
Citalopram	16	SSR inhibitor, hERG & L type calcium channel inhibitor	CO	R-PAT	(10/10)Q	(10/10)Q	(10/10)Q	1-100	30	0.05	NI	NI
			EHT	R-PAT	(4/4)Q [10 µM]	-6 [3 µM]	+5		1			NI
			EHT	ERC18	(5/5)Q [10 µM]	+2 [1 µM]	+7		3			NI
Itraconazole	18	Triazole antifungal, mechanism unclear	CO	R-PAT	(5/5)Q	(5/5)Q	(5/5)Q	0.1-10	10	0.00086	NI	NI
			EHT	R-PAT	-51	+14 [0.1 µM]	-33		3			NI
			EHT	ERC18	(5/5)Q [10 µM]	+11	-29 [3 µM]		1			NI
Sorafenib	19	Multi-targeted TK inhibitor	CO	R-PAT	(10/10)Q	(10/10)Q	(10/10)Q	0.1-10	10	0.03	NI	NI
			EHT	R-PAT	-50	+14	+6 [3 µM]		10			NI
			EHT	ERC18	-56	+6 [3 µM]	-24		10			NI
Ivabradine	20	I_f inhibitor	CO	R-PAT	+46	+22	+24 [0.3 µM]	0.1-10	0.1	0.01-0.1	NI	NE

			EHT	R-PAT	-16	-27	+3 [0.1 µM]		10			NI
			EHT	ERC18	-56	14	+45		10			NI
Flecainide	22	Sodium channel blocker, hERG blocker	CO	R-PAT	+31	+26 [10 µM]	+29 [1 µM]	0.1-10	0.1	0.2-0.4	NI	NE
			EHT	R-PAT	(6/6)Q [3 µM]	-16	-26 [1 µM]		0.3			NI
			EHT	ERC18	-74 [10 µM]	-21	+42		3			NI
Phentolamine	24	Non-selective α adrenoceptor antagonist	CO	R-PAT	(5/5)Q	(5/5)Q	(5/5)Q	1-100	30	2.25	NI	NI
			EHT	R-PAT	5/5)Q [10 µM]	-18	-28		3			NI
			EHT	ERC18	(5/5)Q	-30	+53		10			NI
Zimelidine	28	SSR inhibitor	EHT	R-PAT	18 [1 µM]	-15	-22	1-100	3	0.78	NI	NI
			EHT	ERC18	(5/5)Q [100 µM]	-25 [30 µM]	+43		3			NI
Acetylsalicylic acid	5	Cyclooxygenase inhibitor	CO	Rabbit	+26	-21	-13	10-1000	100	0.3-2	NE	NE
			TTM	P-Cyte	+34	-8 [1000 µM]	+24 [100 µM]		10			NE
			CO	P-Cyte	-21 [30 µM]	-35	+20		10			NE
			CO	iCell2	-58 [30 µM]	-44	+47 [1000 µM]		10			NE
			CO	R-PAT	+23	-26 [300 µM]	+17 [1000 µM]		100			NE
			EHT	R-PAT	-14	+8 [100 µM]	+15		1000			NE
			EHT	ERC18	+8 [300 µM]	-8	-15		1000			NE
Atenolol	6	β1>β2 adrenoceptor antagonist	CO	Rabbit	+16	-13	+968 [0.3 µM]	0.1-10	1	1	NE	NE
			TTM	P-Cyte	+54	+8	-19 [3 µM]		1			NE
			CO	P-Cyte	-29	-71 [10 µM]	+69 [3 µM]		1			NE
			CO	iCell2	-42 [0.1 µM]	+58	-52		0.3			NE
			CO	R-PAT	-28 [3 µM]	+11	+11 [10 µM]		0.3			NE
			EHT	R-PAT	-25	+7 [1 µM]	+14		10			NE
			EHT	ERC18	+3	-13	-9 [3 µM]		10			NE

Captopril	10	ACE inhibitor	CO	Rabbit	-91	+72	+212	1-100	100	1-2	NE	NI
			TTM	P-Cyte	+136	-5	-14 [10 µM]		1			NE
			CO	P-Cyte	+24 [30 µM]	+132	-38		100			NE
			CO	iCell2	-27	+15 [3 µM]	-20 [10 µM]		1			NE
			CO	R-PAT	+18 [3 µM]	-26	-16 [30 µM]		1			NE
			EHT	R-PAT	-18	-7 [100 µM]	-9 [10 µM]		3			NE
			EHT	ERC18	+7	-10	-6 [1 µM]		3			NE
Glibenclamide	12	K_{ATP} channel antagonist	CO	Rabbit	+66 [1 µM]	-27 [0.3 µM]	+61	0.1-10	0.1	0.02-0.06	NE	NE
			CO	R-PAT	+36	-26 [10 µM]	+31		0.1			NE
			EHT	R-PAT	+3	+6	-12		1			NE
			EHT	ERC18	+6	+10	-5 [3 µM]		10			NE
Enalapril	15	ACE inhibitor	CO	R-PAT	+54	+20 [10 µM]	+34	1-100	100	0.12	NE	NE
			EHT	R-PAT	+33	+5 [1 µM]	-14		30			PI
			EHT	ERC18	+2 [10 µM]	-3	-4		100			NE
Clonidine	17	α2-adrenoceptor agonist	CO	R-PAT	-24	+26	-27	0.01-1	0.3	0.002-0.004	NE	NE
			EHT	R-PAT	+10	+11 [0.1 µM]	-12		0.3			NE
			EHT	ERC18	+5 [0.3 µM]	+5	+4		0.1			NE
Paracetamol	23	Prostaglandin synthesis inhibitor	CO	R-PAT	+19 [100 µM]	+26	+13 [1000 µM]	10-1000	30	50	NE	NE
			EHT	R-PAT	-19	-20	-9 [100 µM]		1000			NE
			EHT	ERC18	+3 [100 µM]	-9	+10		1000			NE
Tolbutamide	25	K_{ATP} channel antagonist, Adenylyl cyclase stimulator	CO	R-PAT	+35	-16 [10 µM]	+45	1-100	100	20-30	NE	NE
			EHT	R-PAT	-12	+9	-8 [10 µM]		1			NE
			EHT	ERC18	+21	-3	-9		100			PI
Pravastatin	26	HMG CoA reductase inhibitor	CO	R-PAT	+53	+42	+12 [1 µM]	1-100	3	0.018	NE	NE
			EHT	R-PAT	-19	-15 [30 µM]	13 [100 µM]		3			NE
			EHT	ERC18	+19	+3 [30 µM]	-11 [100 µM]		10			PI

Sildenafil	27	PDE5 inhibitor	CO	R-PAT	+56	+39	+30 [3 µM]	0.3-30	10	0.02	NE	NE
			EHT	R-PAT	-10	-16	+13 [3 µM]		10			NE
			EHT	ERC18	+9	-4 [10 µM]	-6		1			NE

This is further validated in the wide data spread shown in **Figure *4-26*** to **Figure *4-30***. For positive inotrope compounds, some of the platform-cell combination (CO:Rb, EHT:R-PAT, TTM:Pluricyte, CO: iCell^2) were able to predict epinephrine response correctly, which is indicated by significant increase in contraction amplitude, and significant decrease in contraction time and relaxation time, while none of the platform were able to predict levosimendan response correctly (**Figure *4-26***). For negative inotrope compounds, all platform-cell combination were able to predict verapamil response correctly, which is indicated by significant decrease in contraction amplitude, while only some of the platform-cell combination were able to predict sunitinib response correctly (CO:Rb, TTM:Pluricyte, CO:iCell^2 and CO:Pluricyte) (**Figure *4-27***). For no effect compound, all platform-cell combination were able to predict acetylsalicylic acid response correctly, while only one of the platform-cell combination were not able to detect captopril correctly (CO:Rb) (**Figure *4-28***). Some of the positive and negative inotrope assignment were guided based on Ca^{2+} handling and/or voltage analysis for epinephrine (TTM:Pluricyte) and verapamil (EHT:ERC and TTM:Pluricyte) (**Figure *4-29*** and **Figure *4-30***).

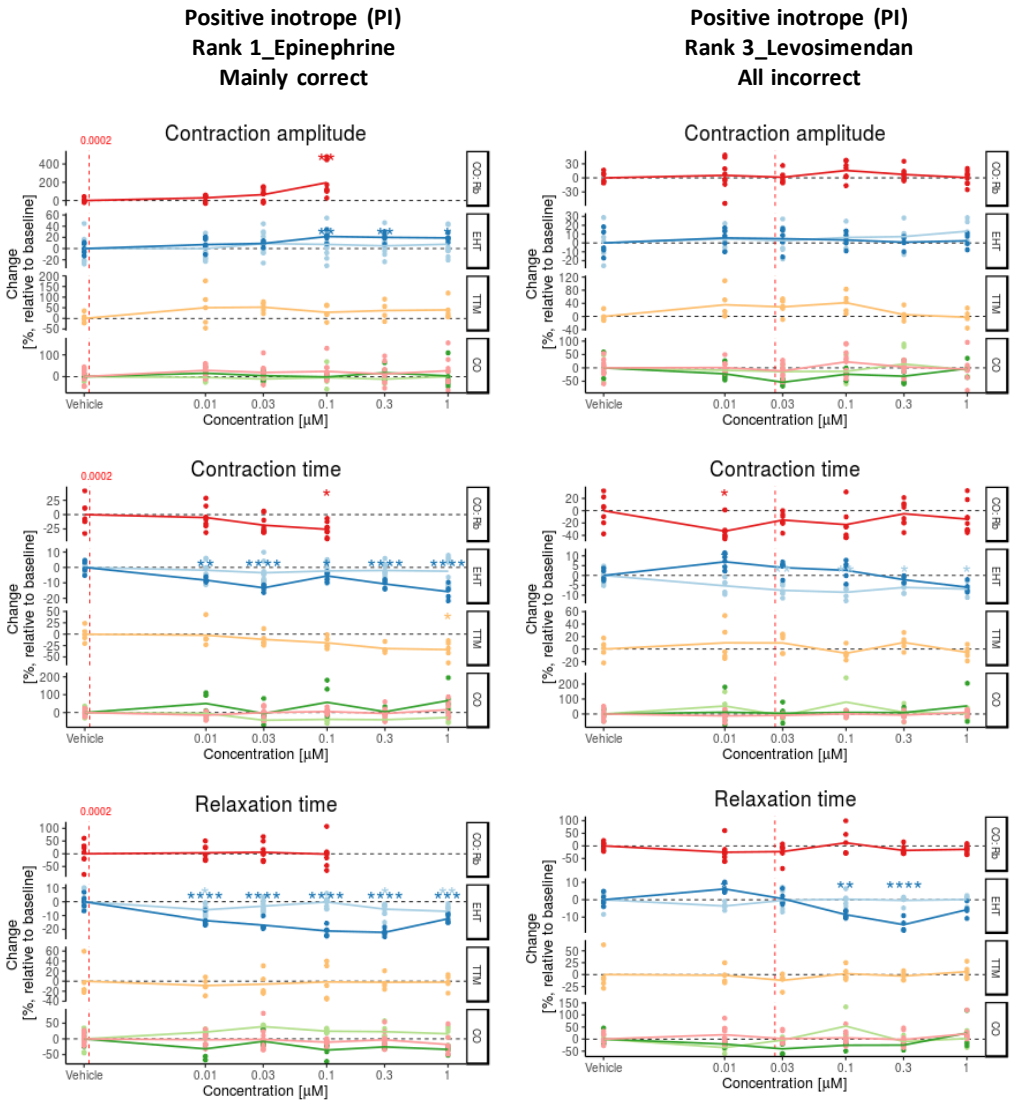

	Predicted correctly? Epinephrine	Predicted correctly? Levosimendan
CO: Rb: Rabbit CMs	Yes	No
EHT: R-PAT	Yes	No
EHT: ERC	No	No
TTM: Pluricyte	Yes (with Ca^{2+})	No
CO: R-PAT	No	No
CO: iCell2	Yes	No
CO: Pluricyte	No	No

Figure 4-26. Contraction analysis across the platform-cell combinations for PIs. Representative of cases in which platform-cell combinations enable correct or incorrect predictions of the PIs, epinephrine and levosimendan, respectively. The table indicates where drug assignment was assisted by data from Ca^{2+} transients and/or voltage, with example data provided for epinephrine and verapamil in **Figure 4-29** and . Red dotted line is free therapeutic plasma concentration (FTPC). One-way ANOVA followed by Dunnett's multiple comparisons test vs vehicle control (p ⩽: * 0.05, ** 0.01, *** 0.001, **** 0.0001).

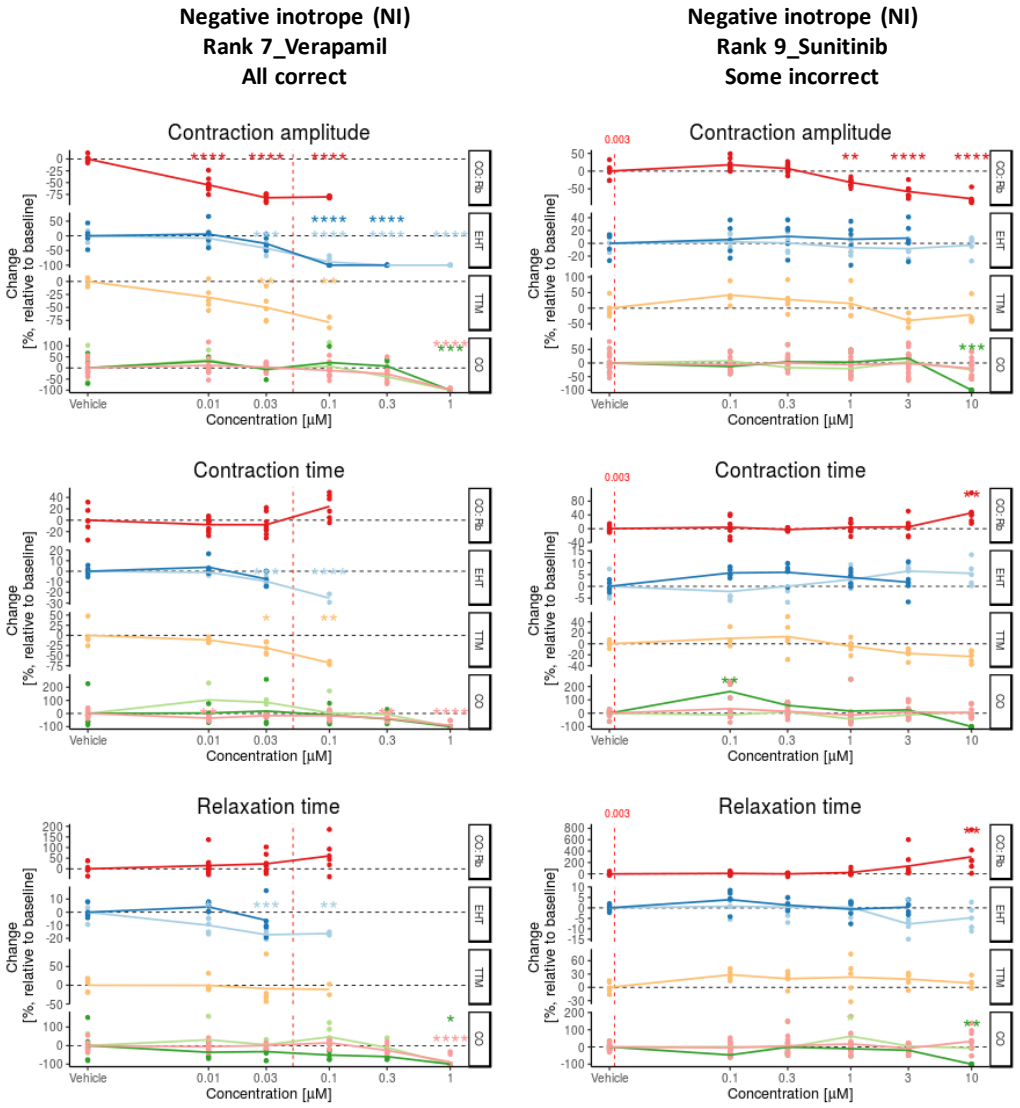

	Predicted correctly? Verapamil	Predicted correctly? Sunitinib
CO: Rb: Rabbit CMs	Yes	Yes
EHT: R-PAT	Yes	No
EHT: ERC	Yes (supported by Ca^{2+})	No
TTM: Pluricyte	Yes (supported by Ca^{2+})	Yes
CO: R-PAT	Yes	No
CO: iCell2	Yes	Yes
CO: Pluricyte	Yes	Yes

Figure 4-27. Contraction analysis across the platform-cell combinations for NIs. Representative of cases in which platform-cell combinations enable correct or incorrect predictions of the NIs, verapamil and sunitinib, respectively. The table indicates where drug assignment was assisted by data from Ca^{2+} transients and/or voltage, with example data provided for epinephrine and verapamil in **Figure 4-29** and **Figure 4-30**. Red dotted line is free therapeutic plasma concentration (FTPC). One-way ANOVA followed by Dunnett's multiple comparisons test vs vehicle control (p ⩽: * 0.05, ** 0.01, *** 0.001, **** 0.0001).

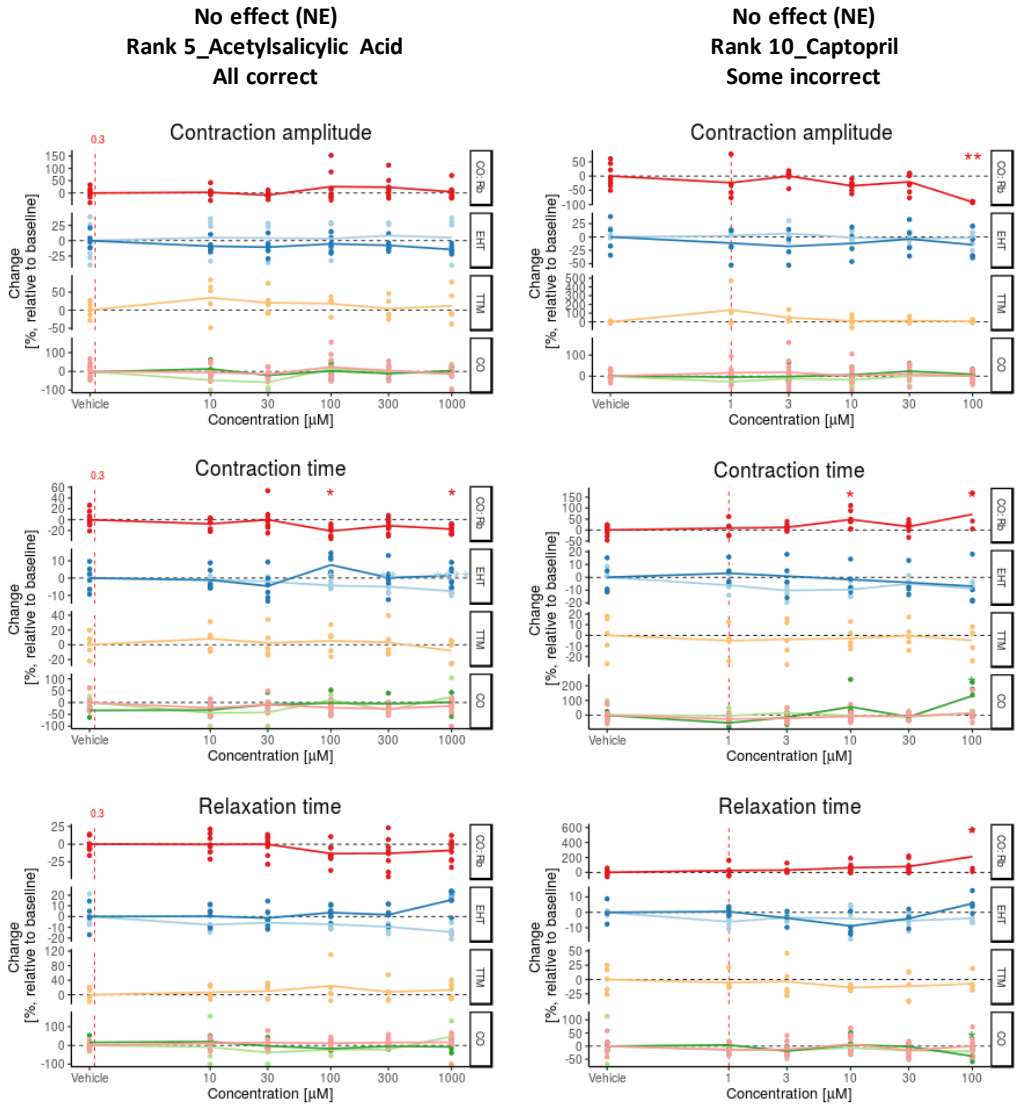

	Predicted correctly? Acetylsalicylic Acid	Predicted correctly? Captopril
CO: Rb: Rabbit CMs	Yes	No
EHT: R-PAT	Yes	Yes
EHT: ERC	Yes	Yes
TTM: Pluricyte	Yes	Yes
CO: R-PAT	Yes	Yes
CO: iCell2	Yes	Yes
CO: Pluricyte	Yes	Yes

Figure 4-28. Contraction analysis across the platform-cell combinations for NEs. Representative of cases in which platform-cell combinations enable correct or incorrect predictions of the NEs, acetylsalicylic acid and captopril, respectively. Red dotted line is free therapeutic plasma concentration (FTPC). One-way ANOVA followed by Dunnett's multiple comparisons test vs vehicle control ($p \leqslant$: * 0.05, ** 0.01, *** 0.001, **** 0.0001).

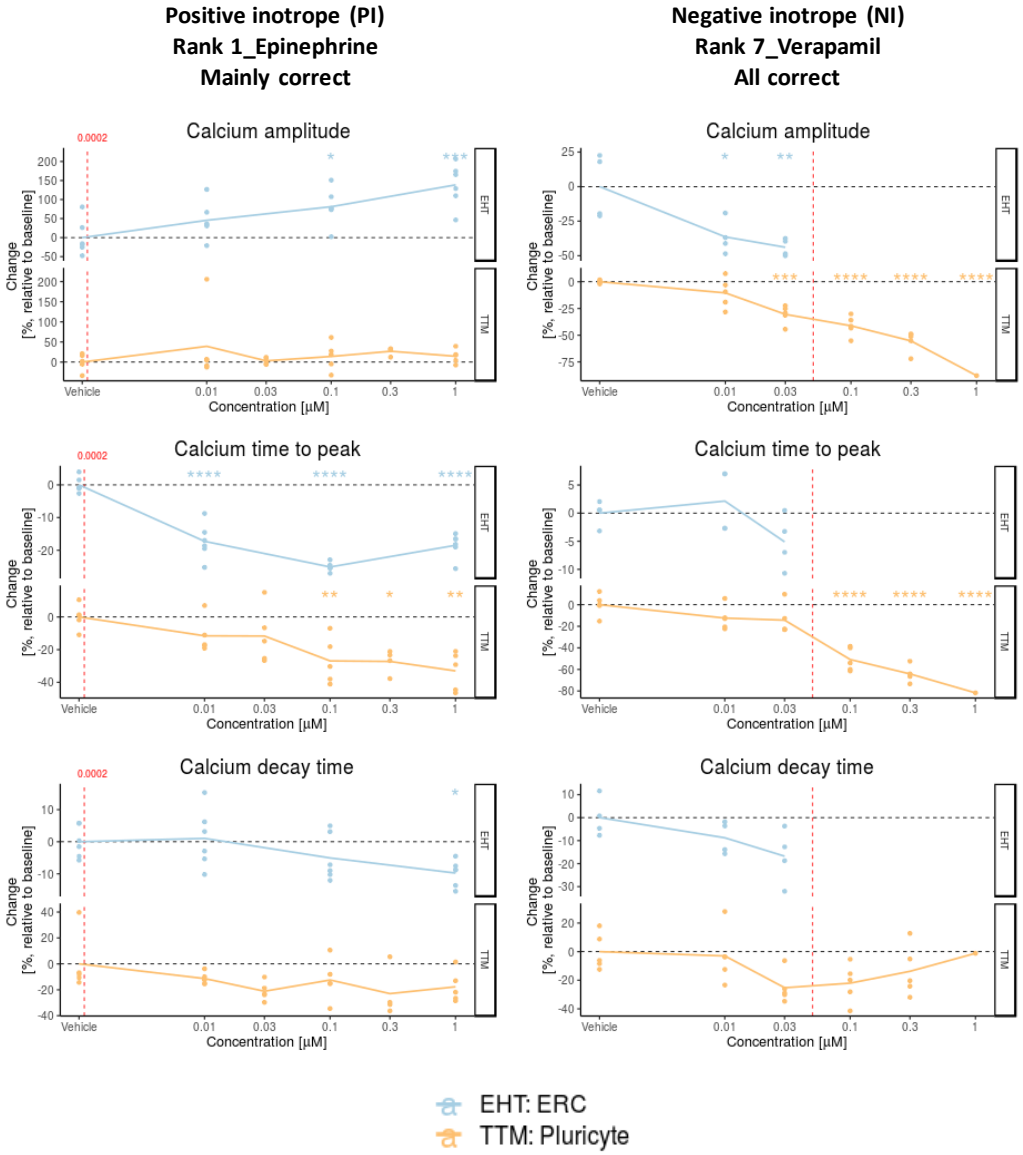

Figure 4-29. Role of Ca2+ analysis in prediction of inotropic response. In some instances, Ca^{2+} transient analysis was used to guide prediction of whether a compound had a positive or negative inotropic effect. Red dotted line is free therapeutic plasma concentration (FTPC). One-way ANOVA followed by Dunnett's multiple comparisons test vs vehicle control (p ⩽: * 0.05, ** 0.01, *** 0.001, **** 0.0001).

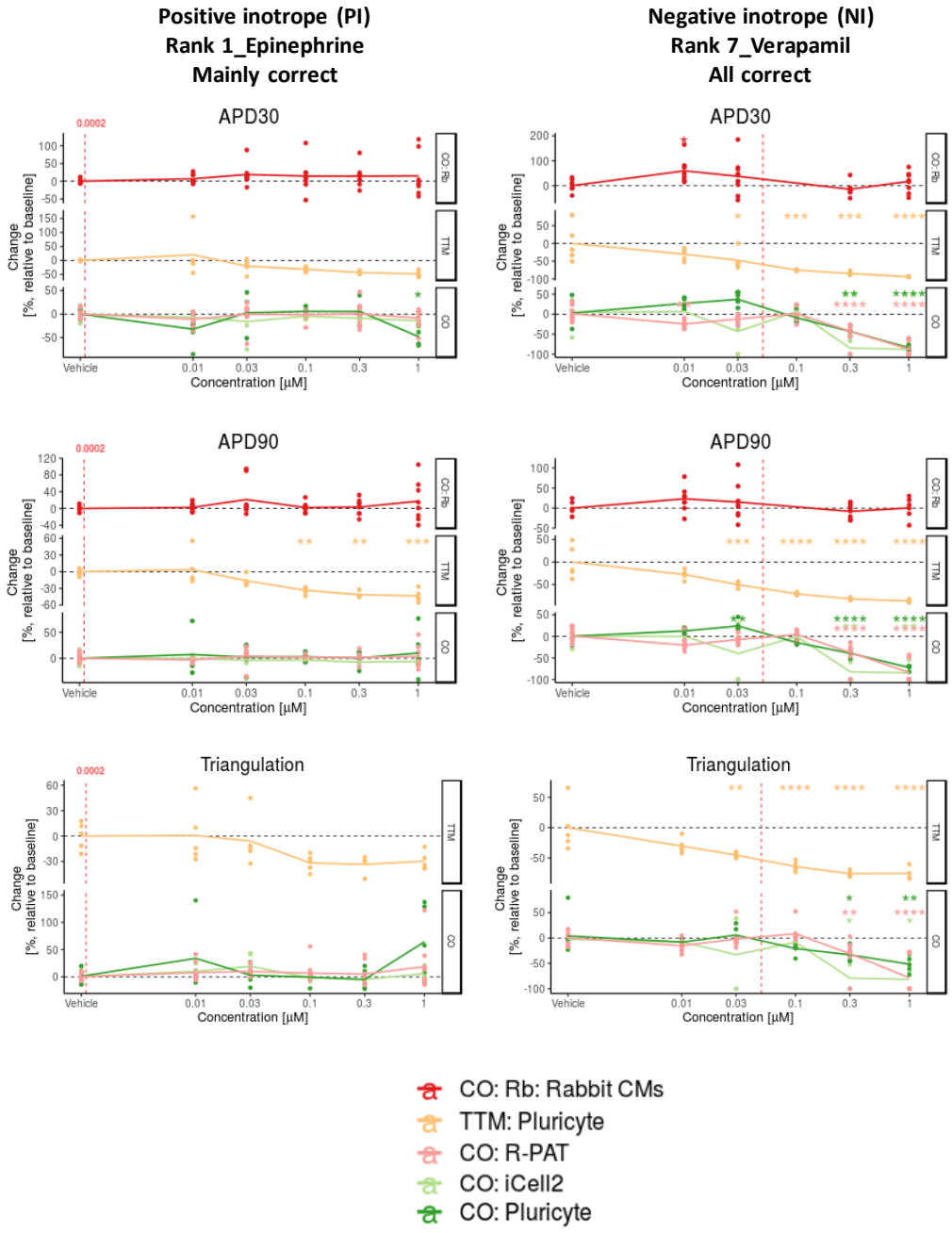

Figure 4-30. Role of voltage analysis in prediction of inotropic response. In some instances, voltage transient analysis was used to guide prediction of whether a compound had a positive or negative inotropic effect. Red dotted line is free therapeutic plasma concentration (FTPC). One-way ANOVA followed by Dunnett's multiple comparisons test vs vehicle control (p ⩽: * 0.05, ** 0.01, *** 0.001, **** 0.0001).

In order to investigate drug response sensitivity of the different platforms, the data were converted into a heat map, reflecting the percentage change of PI drugs (**Figure *4-31***) and NI drugs (**Figure *4-32***). 3D EHT platform showed to be more sensitive, as in 6/7 correctly predicted PI drugs, the contractile parameters in overall showed statistical significance within or in range of free plasma therapeutic concentration (FTPC) (**Figure *4-31***). However, this trend was not observed in NI drugs, likely due to higher concentration used compared to the FTPC, and longer incubation times needed.

Concentration (µM)

Drug	Rank	CellLine	parameter	0.01	0.03	0.1	0.3	1	3	10	30	100
Epinephrine	1		FTPC	0.0002 - 0.05 µM								
		CO:Rb	CA	30.07	65.04	**196.24**	NR	NR				
			CT	-5.19	-18.51	**-25.74**	NR	NR				
			RT	3.81	5.91	-1.28	NR	NR				
		EHT:R-PAT	CA	7.09	9.12	**21.56**	**20.03**	**19.01**				
			CT	**-8.25**	**-13.22**	**-5.5**	**-10.7**	**-15.73**				
			RT	**-13.66**	**-16.98**	**-21.16**	**-22.2**	**-12.31**				
		TTM:	CA	50.36	52.81	28.71	36.91	39.83				
			CT	-2.29	-11.44	-18.99	-31.56	**-33.84**	-	-	-	-
			RT	-8.72	-5.98	-1.49	-2.16	-1.96	-	-	-	-
		CO:iCell2	CA	-3.6	-10.7	-3.9	-11.66	0.88	-	-	-	-
			CT	-4.16	-42.92	-37.92	-39.86	-27.74	-	-	-	-
			RT	21.74	39.32	24.58	23.08	16.28	-	-	-	-
Forskolin	2		FTPC	0.012 - 0.024 µM								
		CO:Rb	CA	-	-	-12.35	13.09	-4.22	-15.54	7.04	-	-
			CT	-	-	-33.78	6.68	30.44	-5.28	8.26	-	-
			RT	-	-	7.1	9.92	36.35	45.43	34.6	-	-
		EHT:ERC	CA	-	-	-3.31	3.37	15.59	17.71	13.29	-	-
			CT	-	-	**-23.21**	**-30.5**	**-32.53**	**-30.3**	**-32.7**	-	-
			RT	-	-	**-11.15**	**-13**	**-18.03**	**-22.4**	**-23.2**	-	-
		EHT:R-PAT	CA	-	-	5.07	3.93	9.63	-0.39	-15.07	-	-
			CT	-	-	-2.05	**-7.33**	2.09	-0.56	-4.19	-	-
			RT	-	-	-3.69	**-17.1**	**-20.9**	**-21.8**	**-19**	-	-
		TTM:	CA	-	-	31.98	22.85	6.91	13.63	7.17	-	-
			CT	-	-	-26.83	-26.78	**-31.31**	**-37.4**	**-35.1**	-	-
			RT	-	-	11.15	-38.03	-37.12	-28.9	-33.23	-	-
Pimobendan	4		FTPC	0.005 - 0.01 µM								
		EHT:ERC	CA	-	-	-	-	-3.26	-7.67	5.58	13.42	13.29
			CT	-	-	-	-	-9.17	**-12.5**	**-11.2**	-8.21	**-11.4**
			RT	-	-	-	-	-3.72	3.43	5	13.03	13.55

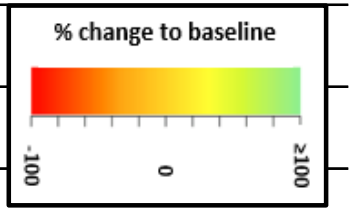

Dobutamine	11		FTPC			0.07 - 1 µM						
		EHT:ERC	CA	-	-	5.01	3.75	**17.2**	**18.07**	12.27	-	-
			CT	-	-	-2.43	**-11.5**	**-26.23**	**-31.7**	**-37.2**	-	-
			RT	-	-	1.97	7.23	-4.42	-6.38	1.23	-	-
		EHT:R-PAT	CA	-	-	**17**	**28.48**	**37.5**	**43.62**	**31.95**	-	-
			CT	-	-	**-9.74**	**-12.9**	**-11.53**	**-12.3**	**-25.2**	-	-
			RT	-	-	**-20**	**-20.3**	**-18.29**	**-17.9**	**-21.6**	-	-
Milrinone	13		FTPC			0.1 - 0.15 µM						
		EHT:ERC	CA	-	-	-	-	2.32	1.61	-0.59	7.51	7.64
			CT	-	-	-	-	**-7.84**	**-8.45**	**-12.9**	**-15.57**	**-17.6**
			RT	-	-	-	-	2.96	0.11	0.33	-6.06	-1.51
		EHT:R-PAT	CA	-	-	-	-	-1.98	-2.27	4.87	18.46	NR
			CT	-	-	-	-	0.4	-5.11	-1.59	-10.85	NR
			RT	-	-	-	-	-0.07	-2.91	-3.65	**-8.98**	NR
Omecamtiv mecarbil	14		FTPC		0.05 - 0.42 µM							
		EHT:ERC	CA	3.03	5.86	11.22	**20.63**	**21.75**	-	-	-	-
			CT	0.66	0.04	3.8	18.9	37.51	-	-	-	-
			RT	2.88	1.98	-1.06	-5.53	-1.94	-	-	-	-
		EHT:R-PAT	CA	-12.48	0.75	17.48	**53.19**	NR	-	-	-	-
			CT	-2.22	2.07	**19.04**	**36.85**	NR	-	-	-	-
			RT	1.43	1.17	-9.2	**-25.8**	NR	-	-	-	-
Terbutaline	21		FTPC					1.3 µM				
		EHT:ERC	CA	-	-	4.46	9.04	**16.84**	**23.59**	**29.18**	-	-
			CT	-	-	**-22.01**	**-28.4**	**-29.62**	**-23.9**	**-22.3**	-	-
			RT	-	-	-14.96	-16.51	-17.06	-16.25	-1.97	-	-
		EHT:R-PAT	CA	-	-	7.94	1.9	14.3	**17.48**	NR	-	-
			CT	-	-	**-14.82**	**-21.3**	**-16.82**	**-24.2**	NR	-	-
			RT	-	-	**-24.73**	**-35.2**	**-30.03**	**-32.8**	NR	-	-

Figure 4-31. Sensitivity of platform-cell combinations for predicting PIs. Where positive inotropes were correctly predicted, data are presented as percent change relative to baseline for any of the three contractility parameters (CA, contraction amplitude; CT, contraction time; RT, relaxation time). The bolded black text indicates where significance was reached using one-way ANOVA followed by Dunnett's multiple comparisons test vs vehicle control and $P<0.05$. FPTC, Free plasma therapeutic concentration. NR, not recorded.

Concentration

Drug	Rank	CellLine	parameter	0.01	0.03	0.1	0.3	1	3	10	30	100
Verapamil	7		FTPC		0.05 µM							
		CO: Rb	CA	**-54.95**	**-82.09**	**-80.27**	NR	NR				
			CT	-7.87	-7.92	24.26	NR	NR				
			RT	15.17	23.28	60.89	NR	NR				
		EHT: ERC	CA	-8.17	**-42.18**	**-89.19**	**-100**	**-100**				
			CT	-106	-9.48	-25.36	NR	NR				
			RT	-10.05	-17.26	-16.33	NR	NR				
		EHT: R-PAT	CA	5.93	-26.48	**-100**	**-100**	NR				
			CT	3.79	-7.32	NR	NR	NR	-	-	-	-
			RT	4.07	-6.23	NR	NR	NR	-	-	-	-
		TTM:	CA	-30.53	**-50.11**	**-78.76**	NR	NR	-	-	-	-
			CT	-1149	-3101	-68.09	NR	NR	-	-	-	-
			RT	-0.44	-8.95	-112	NR	NR	-	-	-	-
		CO: iCell2	CA	36.23	-7.03	8.1	-39.6	-100	-	-	-	-
			CT	103.13	84.97	4.58	-7.93	-100	-	-	-	-
			RT	313	4.47	47.12	-10.27	-100	-	-	-	-
		CO: Pluricyte	CA	30.6	-6	24.3	8.3	**-100**	-	-	-	-
			CT	3.43	18.5	-1154	-4148	-100	-	-	-	-
			RT	-35.77	-32.36	-50.72	-59.18	-100	-	-	-	-
		CO: R-PAT	CA	12.04	3.47	-1134	-26.84	**-98.03**	-	-	-	-
			CT	-35.26	-16.5	-16.76	-36.58	-90.63	-	-	-	-
			RT	-5.87	128	14.88	-25.46	-87.94	-	-	-	-
Sunitinib	9		FTPC	0.003 µM								
		CO: Rb	CA	-	-	17.79	7.28	**-3196**	**-57.64**	**-77.7**	-	-
			CT	-	-	4.17	-2.68	3.91	5.18	**45.93**	-	-
			RT	-	-	8.87	0.33	23.64	137.67	**300.4**	-	-
		TTM:	CA	-	-	42.31	27.58	15.24	-39.48	-20.73	-	-
			CT	-	-	9.95	13.19	-4.28	-17.53	-23.25	-	-
			RT	-	-	28.32	19.51	22.97	18.57	9.33	-	-
		CO: iCell2	CA	-	-	7.6	-16.86	-20.5	4.82	-24.76	-	-
			CT	-	-	-1192	117	-43.4	-1172	9.86	-	-
			RT	-	-	178	-2.26	**62.3**	5.38	-7.1	-	-
		CO: Pluricyte	CA	-	-	-13.02	4.46	3.08	17.57	**-100**	-	-
			CT	-	-	162.66	58.3	16.26	24.83	-100	-	-
			RT	-	-	-46.48	-1.14	-10.16	-19.22	-100	-	-

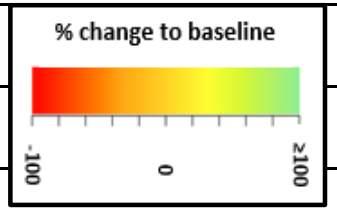

Citalopram	16		FTPC		0.05 µM							
		EHT:ERC	CA	-	-	-	-	-26.58	**-65.22**	**-100**	**-100**	**-100**
			CT	-	-	-	-	182	0.76	NR	NR	NR
			RT	-	-	-	-	5	7.72	NR	NR	NR
		EHT:R-PAT	CA	-	-	-	-	-152	**-30.72**	**-100**	NR	NR
			CT	-	-	-	-	6.49	-4.03	NR	NR	NR
			RT	-	-	-	-	4.96	-133	NR	NR	NR
		CO:R-PAT	CA	-	-	-	-	1174	-13.54	**-61.3**	**-100**	**-100**
			CT	-	-	-	-	-1144	-2.23	-19.46	-100	-100
			RT	-	-	-	-	6.18	-8.13	-30.71	-100	-100
Itraconazole	18		FTPC	0.00086 µM								
		EHT:ERC	CA	-	-	-9.9	-16.06	**-36.58**	**-51.18**	**-100**	-	-
			CT	-	-	6.88	6.19	**11.31**	8.49	NR	-	-
			RT	-	-	193	174	-10.18	-29.37	NR	-	-
		EHT:R-PAT	CA	-	-	5.93	-139	-15.86	**-51.14**	NR	-	-
			CT	-	-	**13.55**	4.63	4.61	12.2	NR	-	-
			RT	-	-	-2.65	-8.52	-19.46	-33.17	NR	-	-
		CO:R-PAT	CA	-	-	-32.83	-25.86	-16.36	**-48.12**	**-100**	-	-
			CT	-	-	8.5	25.46	6.66	-29.86	-100	-	-
			RT	-	-	-2.15	-2.14	-2.08	-62.62	-100	-	-
Sorafenib	19		FTPC		0.03 µM							
		EHT:ERC	CA	-	-	**-15.06**	**-16.8**	**-22.49**	**-37.56**	**-56.3**	-	-
			CT	-	-	-134	-2.42	3.62	6.27	4.68	-	-
			RT	-	-	3.4	2.78	-117	-14.39	-24.43	-	-
		EHT:R-PAT	CA	-	-	-168	-3.89	-1175	-25.63	**-50.4**	-	-
			CT	-	-	3.22	18	8.7	6.42	**13.89**	-	-
			RT	-	-	0.22	131	-198	-6.48	155	-	-
		CO:R-PAT	CA	-	-	-12.8	-2.87	-10.56	**-49.21**	**-100**	-	-
			CT	-	-	4.36	28.21	10.03	-48.43	-100	-	-
			RT	-	-	-3.54	23.61	-12.26	-55.68	-100	-	-
Ivabradine	20		FTPC	0.01 - 0.1 µM								
		EHT:ERC	CA	-	-	-5.9	-7.34	-9.23	**-19.14**	**-55.6**	-	-
			CT	-	-	0.77	-0.27	-3.68	-8.35	-13.62	-	-
			RT	-	-	-161	-3.04	4.08	**27.35**	**45.3**	-	-
		EHT:R-PAT	CA	-	-	-6.21	-7.39	-2.05	8.83	-15.68	-	-
			CT	-	-	0.17	-7.87	-6.8	-13.46	-26.88	-	-
			RT	-	-	3.15	0.06	-113	-0.25	-2.34	-	-

Flecainide	22		FTPC			0.2 - 0.4 µM						
		EHT:ERC	CA	-	-	-8.14	-9.09	**-24.62**	**-38.05**	**-74.5**	-	-
			CT	-	-	3.26	-0.71	-4.9	-21.24	NR	-	-
			RT	-	-	0.83	1.07	**18.08**	**42.22**	NR	-	-
		EHT:R-PAT	CA	-	-	-5.47	**-20**	-6.8	**-100**	NR	-	-
			CT	-	-	-4.73	-15.53	-6.29	NR	NR	-	-
			RT	-	-	-5.29	-17.79	-25.78	NR	NR	-	-
Phentolamine	24		FTPC						2.25 µM			
		EHT:ERC	CA	-	-	-	-	-1.62	**-23.21**	**-89.9**	**-100**	**-100**
			CT	-	-	-	-	-8.02	-16.4	-30.49	NR	NR
			RT	-	-	-	-	**25.36**	**39.86**	**52.53**	NR	NR
		EHT:R-PAT	CA	-	-	-	-	-3.14	**-28.82**	NR	NR	NR
			CT	-	-	-	-	-4.82	-17.74	NR	NR	NR
			RT	-	-	-	-	-12.69	-27.78	NR	NR	NR
		CO:R-PAT	CA	-	-	-	-	-20.04	-27.6	**-41.1**	**-100**	**-100**
			CT	-	-	-	-	-7.2	-7.9	-22.32	-100	-100
			RT	-	-	-	-	**41.8**	-2.7	-23.44	-100	-100
Zimelidine	28		FTPC					0.78 µM				
		EHT:ERC	CA	-	-	-	-	5.12	-6.91	**-37.4**	**-95.23**	**-100**
			CT	-	-	-	-	-3.17	-8.58	-13.03	-24.92	NR
			RT	-	-	-	-	**23.76**	**42.78**	**42.59**	**27.92**	NR
		EHT:R-PAT	CA	-	-	-	-	18.37	-1.27	NR	NR	NR
			CT	-	-	-	-	-2.11	-15	NR	NR	NR
			RT	-	-	-	-	-7.02	-22.03	NR	NR	NR

Figure 4-32. Sensitivity of platforms-cell combinations for predicting NIs. Where negative inotropes were correctly predicted, data are presented as percent change relative to baseline for any of the three contractility parameters (CA, contraction amplitude; CT, contraction time; RT, relaxation time). The bolded black text indicates where significance was reached using one-way ANOVA followed by Dunnett's multiple comparisons test vs vehicle control and $P<0.05$. FPTC, Free plasma therapeutic concentration. NR, not recorded.

In order to investigate the correlation of contractility parameter to drug response, the lowest drug concentration that gives statistical significance was noted. In general, all compounds showed no distinct pattern for contraction amplitude, contraction time, and relaxation time (**Figure *4-33***A). However, contraction time showed to be informative in positive inotrope compounds (**Figure *4-33***B), while contraction amplitude showed to be majorly affected in negative inotrope compounds (**Figure *4-33***C).

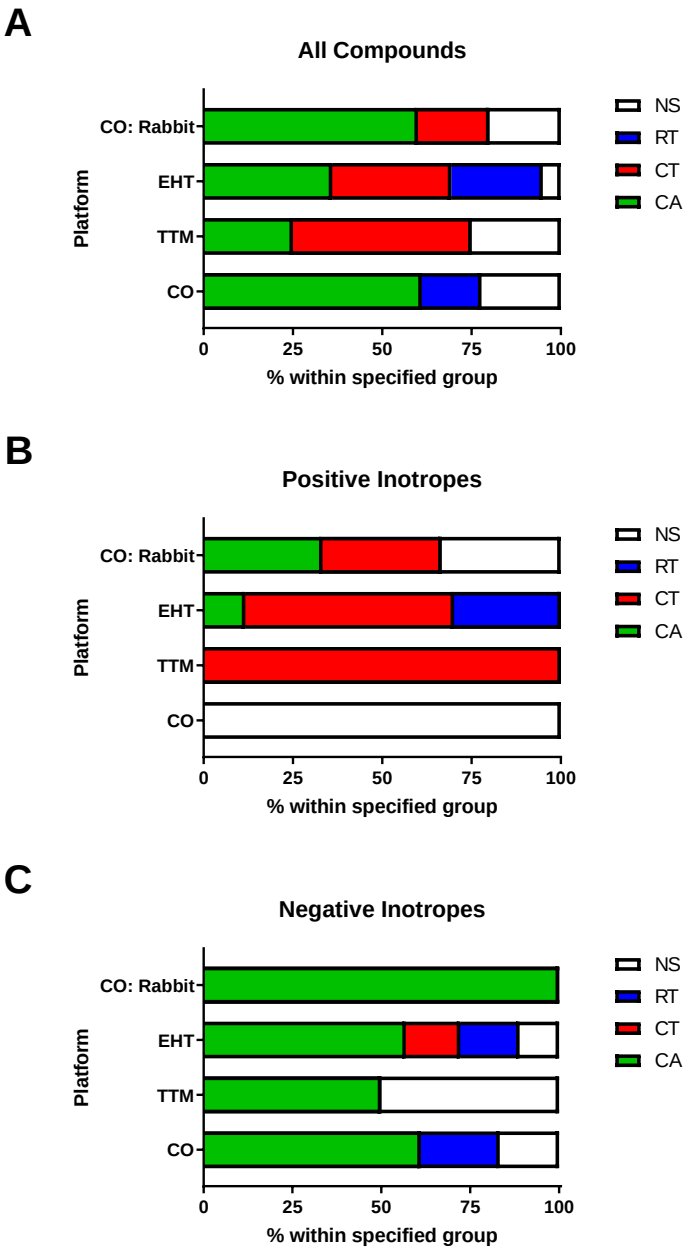

Figure 4-33. Most informative contractility marker. Parameters that led to the correct prediction of drug responses were assessed in all compounds, positive and negative inotropes (A-C). Data show the breakdown by percentage for the parameters (CA, contraction amplitude; CT, contraction time; RT, relaxation time) that reached significance at the lowest concentration (One-way ANOVA followed by Dunnett's multiple comparisons test vs vehicle control and $P<0.05$). White boxes (NS, not significant) indicate where predictions were made due to a trend rather than reaching significance, and/or by guidance from Ca^{2+} and/or voltage data.

4.4 Discussion

During Tier 2 phase of testing up to 28 blinded compounds, 7 different platform cell-combinations were evaluated to predict positive, negative, and neutral inotrope compounds. Key readouts for cardiomyocytes were performed: electrophysiology (voltage triangulation, APD_{30}, APD_{90}), Ca^{2+} handling (calcium amplitude, calcium time to peak, calcium decay time), and contractility (contraction amplitude, contraction time, relaxation time). All of experiments were done under pacing condition with range of 1-1.5 Hz.

Evaluating the effect of a candidate drug on cardiac inotropy is regarded as essential assessment in the pharmaceutical industry to determine whether the drug could proceed to the next development path. Stem cell-derived cardiomyocytes are capable of taking a role during early drug safety assignment by relying on the beating rate as a biomarker to predict the risk (Butler et al., 2015, Pointon et al., 2015, Sirenko et al., 2013, Huo et al., 2017). A previous study showed that pacing rate affects drug-induced changes in contractility (Butler et al., 2015). Verapamil, an L-type Ca^{2+} channel blocker, under spontaneous beating recording, had IC_{50} value of 0.1 μM for contractility measurement and 1.5 μM for Ca^{2+} transient measurement, while under pacing stimulation at 1 Hz, had IC_{50} value of 0.07 μM for contractility measurement and 0.5 μM for Ca^{2+} transient measurement (Pointon et al., 2015).

Standard drugs which are usually detected in hiPSC-CM-based assays will not be discussed further. PDE3-inhibitors levosimendan, pimobendan, and milrinone had no effect on the 2D systems, whilst based on literature, these drugs should bring positive inotropic effects by regulating cAMP levels (Abi-Gerges et al., 2013). This might be due to low cAMP levels in hiPSC-CMs (Scott et al., 2014) and the more dominant role of PDE4 over PDE3 in hiPSC-CMs (Mannhardt et al., 2017).

When the hPSC-CMs are spontaneously beating, the force generated is linked to the beating frequency. By setting a fixed pacing frequency, any changes to the force waveform can be only referred to the compound's inotropic and lusitropic effect (Lee et al., 2017a). Previous studies have stated that hPSC-CMs treated with nifedipine, a Ca^{2+} channel blocker, would have most likely demonstrate positive chronotropic effect in

nifedipine-treated strips under spontaneous beating (Guo et al., 2011, Harris et al., 2013, Pillekamp et al., 2012).

Studies have shown that hPSC-CMs extort from non-existent to minimal response to positive inotropic compounds, such as β-adrenergic agonists, due to immature intracellular structural features (Lundy et al., 2013, Pillekamp et al., 2012). This diminished response, combined with baseline reading in condition of increased contractility over time (i.e. increased pacing frequency), will result in positive inotropic effects of a compound to be masked and therefore harder to be detected (Lee et al., 2017a). Furthermore, studies in native heart muscle preparations showed that lower beating rate is associated with a positive force-frequency relationship (up to ~2 Hz), as well as stronger inotropic effects (contractility) on most positive inotrope drugs (Butler et al., 2015).

Therefore, it is crucial to have spontaneous beating rate <1 Hz, so that the cells could be paced up to 1 Hz in order to increase the platform's sensitivity to positive inotropic agents, and subsequently in better predictability in the drug safety assignment.

It is also need to be noted, that different cell lines have different baseline characteristics due to the production process of hiPSC-CMs, the differentiation stages, the impact of custom culture medium used by each manufacturer for commercial cell lines, the differences in the cardiomyocytes subtypes (nodal, atrial, ventricular), and also the differences in cardiac ion channel expression (Huo et al., 2017, Goineau and Castagne, 2018). However, result for 9 drugs tested in common have shown that same commercial cell line (Pluricyte) tested on different platform (CO vs TTM) resulted in different accuracy (56% vs 78%, respectively). This is the same case with in house cell line (R-PAT) tested on different platform (CO vs EHT) resulted in 44% vs 67% accuracy, respectively.

Between CO platform with other platform-cell combination (2D, TTM:Pluricyte and 3D, EHT:ERC), 3D platform has better predictability at detecting positive inotrope compounds. The TTM:Pluricyte platform was able to predict epinephrine and forskolin correctly, while could only elicit neutral response for levosimendan and pimobendan (**Figure *4-34***A-D). On the other hand, the EHT:ERC platform was able to predict forskolin and

pimobendan correctly, while could only elicit neutral response for epinephrine and levosimendan (**Figure *4-35***A-D). For negative inotrope compounds, these platforms were able to predict verapamil correctly, while the TTM:Pluricyte platform was able to predict sunitinib correctly but could only elicit neutral response for doxorubicin (**Figure *4-34***E-G). EHT site didn't get doxorubicin distribution, and the EHT:ERC platform could only elicit neutral response for sunitinib (**Figure *4-35***E-G). As for neutral inotrope compounds, all platforms were able to predict those compounds correctly (**Figure *4-34***H-J and **Figure *4-35***H-J).

These assays have limitation. In the 2D CO system, there are differences in field of view (FOV) size, in which the electrophysiology (voltage) measurements record a large area within the well that is tweaked with manual adjustments, whilst the contractility measurements have a specific, smaller FOV size that is consistent across wells. In the 2D TTM system, the high predictivity might be due to simultaneously quantifying multiple dynamic parameters in hiPSC-CMs (voltage, Ca^{2+} handling, and contractility), instead of sequentially as in the 2D CO platform. In the 3D EHT system, the high predictivity was likely facilitated by the ability to measure absolute force of contraction instead of cell movement, which is a surrogate of contractility, on the 2D platforms. Furthermore, during measurements, the 3D EHT system used cumulative concentrations on the same well instead of individual concentration per well as in the 2D platforms.

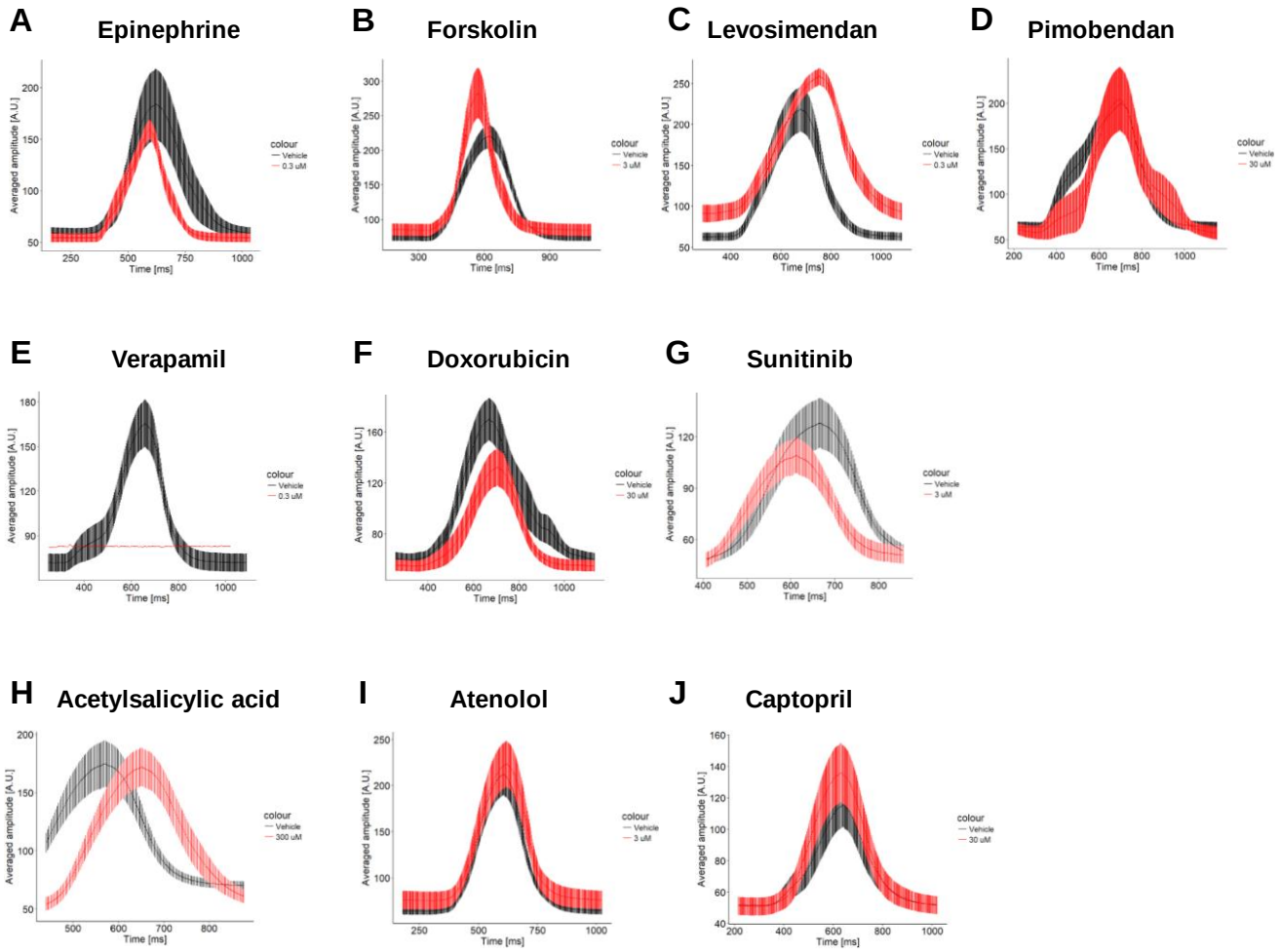

Figure 4-34. Representative contraction force traces of hiPSC-CMs on 2D TTM. (A-D) showed positive inotrope drugs whilst (E-G) showed negative inotrope drugs and (H-J) showed neutral inotrope drugs. Baseline (black) and treatment (red). Data were generated by Berend J van Meer, Ana Krotenberg Garcia, and Leon Tertoolen (Leiden University).

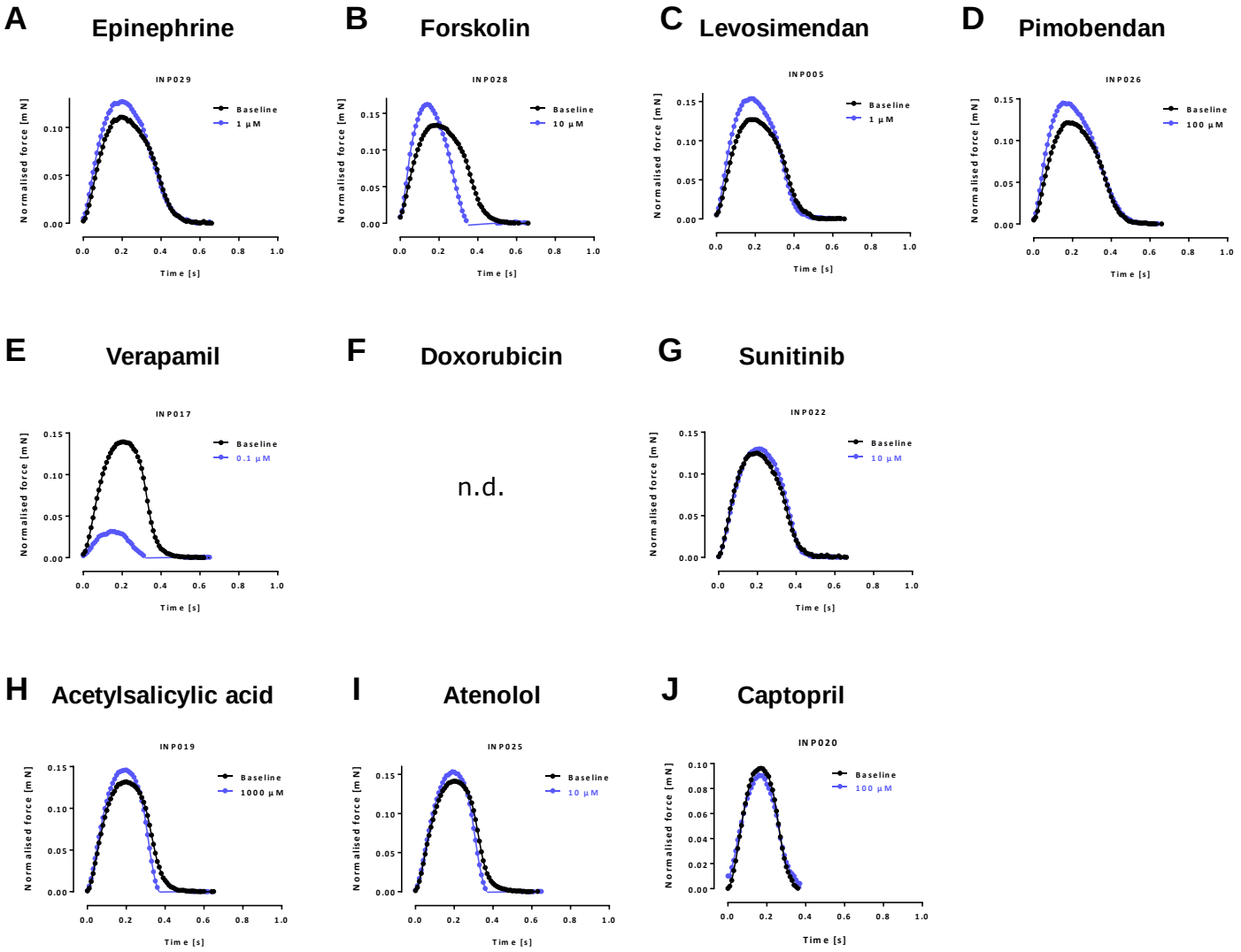

Figure 4-35. Representative contraction force traces of hiPSC-CMs on 3D EHTs. (A-D) showed positive inotrope drugs whilst (E-G) showed negative inotrope drugs and (H-J) showed neutral inotrope drugs. Baseline (black) and treatment (blue). Data were generated by Umber Saleem and Ingra Mannhardt (University of Hamburg).

4.5 Conclusion

In order to improve predictivity of test platforms against positive, negative, and neutral inotrope compounds, the hypothesis is suggested that actions are needed to reduce spontaneous beating rate of hiPSC-CMs to below 1 Hz. To this end, the next chapter will consider the role of culture medium composition and/or pharmacological inhibition of the I_f pacemaker current.

5 Cardiovascular Safety Liabilities Screening – Refinement

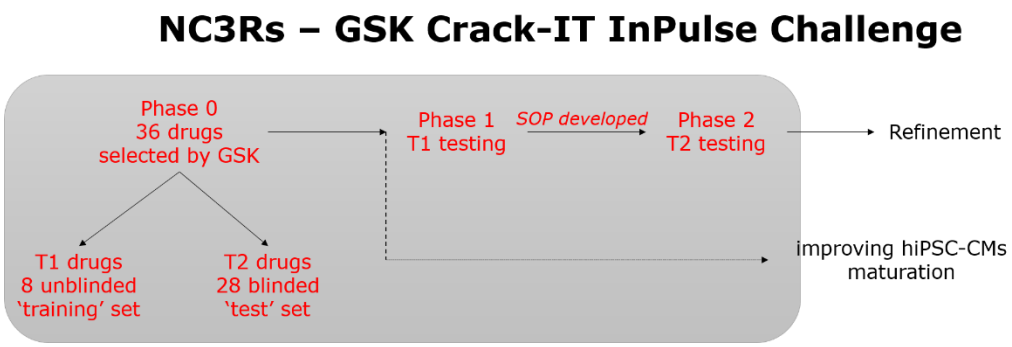

5.1 Introduction

Previous work in chapter 4 described the blinded test set of 'Tier 2' drugs, which demonstrated the predictability of platform-cell combinations across academic partners. It was noted that positive inotrope compounds were least well predicted by the platforms. During the process of recording contractility, 2D platforms used intermittent video measurements using a motion algorithm, which is different from 3D platform with continuous tension measurements. It was highlighted in previous work that same commercial cell line tested in different platforms resulted in different accuracy. Therefore, rather than cell line factor, methods of measuring contractility and 2D versus 3D platform were more important.

Furthermore, as implied in chapter 4, beating rate plays a role in detecting risk during early drug safety assignment. The force-frequency relationship (FFR) is a vital intrinsic regulatory mechanism in cardiac contractility (Endoh, 2004). Most mammalian ventricular myocardium have positive FFR; which is, an increase in contractile force in association with an increase in the Ca^{2+} transient amplitude is induced by increase in frequency stimulation. The cardiac contractile force correlates positively with heart rate or beating frequency (known as Bowditch effect) in human myocardium (Janssen, 2010).

It was also noted that chronic toxicants, such as doxorubicin, were poorly predicted after the acute (30 minute) treatment duration. Results showed that these compounds altered the electrophysiology of hiPSC-CMs,

however, it was noted that varied accuracy on contractility measurement were found across all platforms. This chapter will explore the effect of longer term exposures of chronic toxicants (doxorubicin and sunitinib) would affect contractility.

Finally, in order to address the limitation of 2D platform versus 3D platform, this chapter will explore attempts on improvement of maturation of hiPSC-CMs.

5.2 Chapter Aims

- To investigate the factors contributing to beating rate, in which will improve the prediction of positive inotrope compounds.
- To investigate the longer term exposure of chronic toxicants, in which will improve the prediction of negative inotrope
- To investigate the correlation of maturation level of hiPSC-CMs in order to have better accuracy and sensitivity in predicting outcome of drug effect.

5.3 Results

5.3.1 Medium composition and correlation with beat rate

One of the contributing factors affecting beating rate is medium composition. Serum-/protein-free medium contain sodium pyruvate, an intermediate in the glycolytic pathway, which improves the cardiomyocyte's ability to metabolise glucose in the medium to produce energy (Mallet et al., 2018). In addition to major change in medium composition (from protein to protein-free), it is hypothesised that these altogether contributes to higher spontaneous beat rates (1.5-1.7 Hz) and subsequently partial detachment of the hiPSC-CMs from the culture substrate. Previous work as described in chapter 3 was aimed to stabilise the beat rates after medium changing to serum-/protein-free medium, however, the mean baseline beat rate in SPF is still higher compared to the one in RPMI-B27 (**Figure *5-1***).

Blinded Tier 2 phase experimentation was done using serum-/protein-free (SPF) medium, in order to avoid protein-drug binding that might mask the effect of compounds. However, it was noted that after adding SPF medium, the mean baseline beat rate was increased from 0.7 Hz to ≥1.2

Hz (**Figure *5-1***). Furthermore, highly varied distribution of data was found in contraction amplitude (CA), contraction time (CT), and relaxation time (RT), with standard deviation of protein-containing (RPMI-B27) versus SPF medium were 12.1 versus 32.8, 14.5 versus 20.1, and 10.7 versus 26.9, respectively (**Figure *5-1***). Overall, SPF medium in the CO:R-PAT platform-cell combination leads to high spontaneous beat rates and poor signal-to-noise ratios.

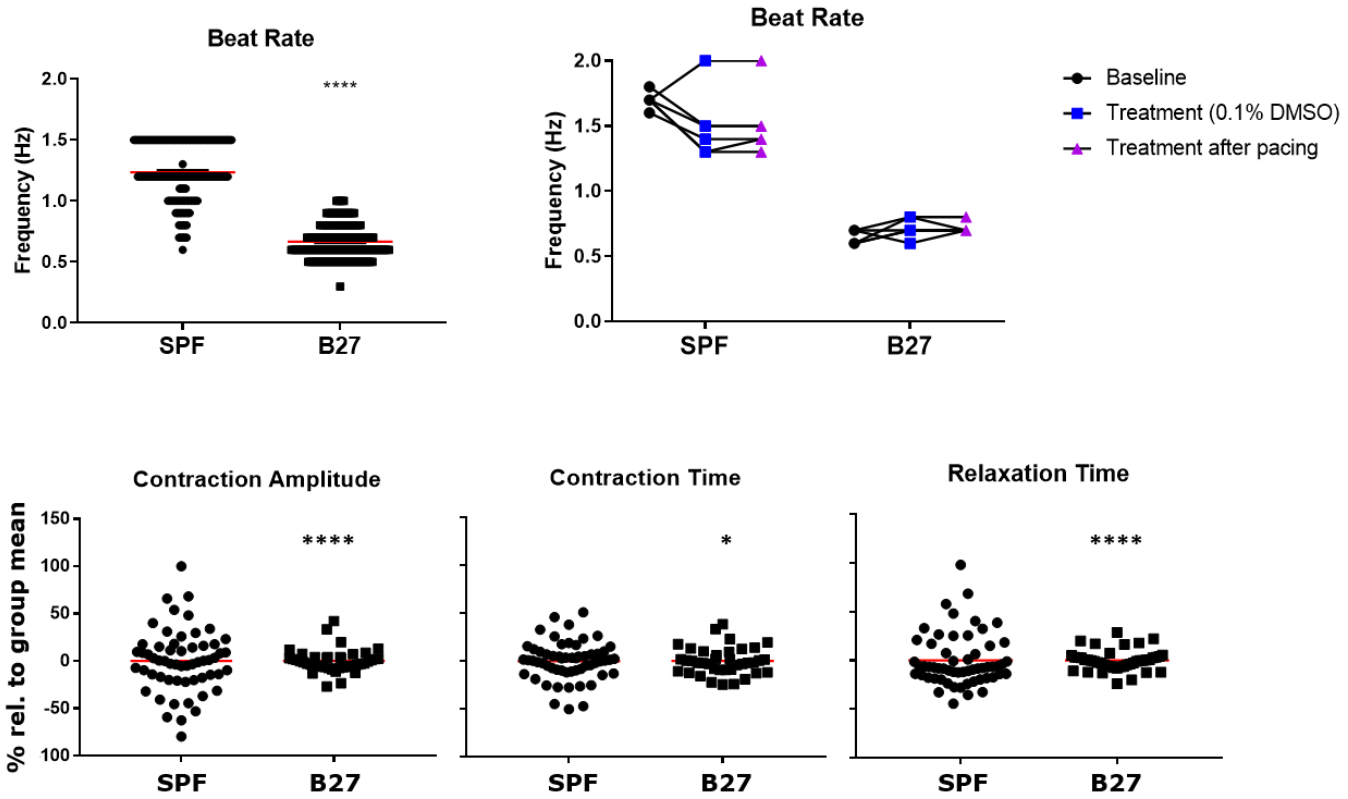

Figure 5-1. Serum-/protein-free medium increases spontaneous beating rates and data distribution. Using the CO:R-PAT platform-cell combination, recordings were evaluated in hiPSC-CMs cultured as 2D monolayers in serum-/protein-free medium (SPF) versus the protein-containing medium, RPMI-B27 (B27). Culture in SPF significantly increased spontaneous beating rates ($P \leq 0.0001$, Mann Whitney), and increased variance of data distribution for CA, CT and RT ($P \leq 0.0001$, 0.05 and 0.0001, respectively; F-test for variance). N=3 biological repeats.

However, switching to RPMI-B27 medium makes recording of voltage measurement to become off-limit. One of the possible explanations is, before entering depolarized cells, the voltage-sensitive dye (VSD) might bind to protein component in medium instead of binding to cell membranes before exhibiting enhanced fluorescence. Over time, this protein-VSD binding reduce the signal-to-noise ratio, which might result in weak detection of the voltage traces (**Figure *5-2***). Baseline recordings were done as negative control and to exclude possibility of unexpected noise (**Figure *5-2***A). FluoVolt™ preparation and addition into hiPSC-CMs were described in methodology chapter. After incubation of 20 minutes, each wells had it replaced with fresh medium before subsequent recordings.

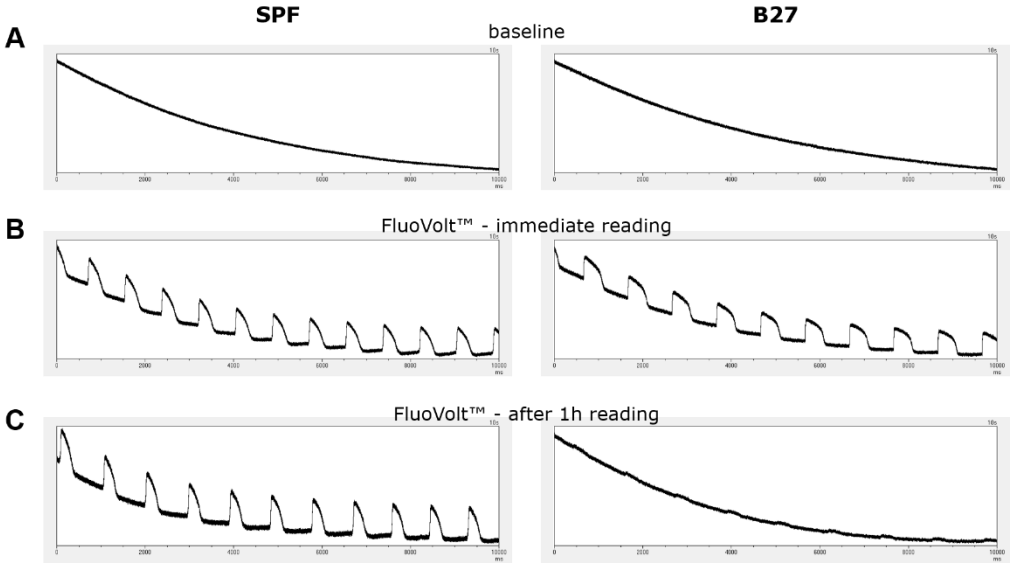

Figure 5-2. Representative voltage traces of hiPSC-CMs under different medium composition. Using the CO:R-PAT platform-cell combination, recordings were evaluated in hiPSC-CMs cultured as 2D monolayers in serum-/protein-free medium (SPF) versus the protein-containing medium, RPMI-B27 (B27). N=2 biological repeats.

Immediate recording after replacement with fresh medium showed that hiPSC-CMs both in SPF and in RPMI-B27 medium elicit adequate voltage traces with little/minimal noise (**Figure *5-2***B). However, it was noted that over time (i.e. after 1h period), weak to non-existent voltage traces were observed in hiPSC-CMs with RPMI-B27 medium (**Figure *5-2***C).

Due to this limitation, further experiments done in order to enhance the accuracy of predicting positive inotrope compounds on the CO:R-PAT

platform were only focusing on contractility, without taking any electrophysiology measurements.

5.3.2 *Ivabradine and its role in reducing beat rate*

Recent study in EHT showed that positive FFR had not been observed in spontaneously beating hiPSC-CM EHTs (Mannhardt et al., 2016). It was then reasoned that the positive FFR is masked by the high frequency of spontaneous beat rate ranging from 1-1.5 Hz. I_f current is responsible for spontaneous beat rate in hiPSC-CMs, therefore the study used ivabradine (0.3 µM), an I_f current blocker (Bois et al., 1996), which reduces spontaneous beat rate to <0.5 Hz. These enabled pacing rates in increments from 0.5 to 2.5 Hz (**Figure *5-3***), with positive FFR responses between 0.5 and 1.5 Hz, followed by negative FFR above 1.5 Hz. The positive FFR was shown by a 147% increase in force generation that is concurrent with significant shortening of contraction time and relaxation time.

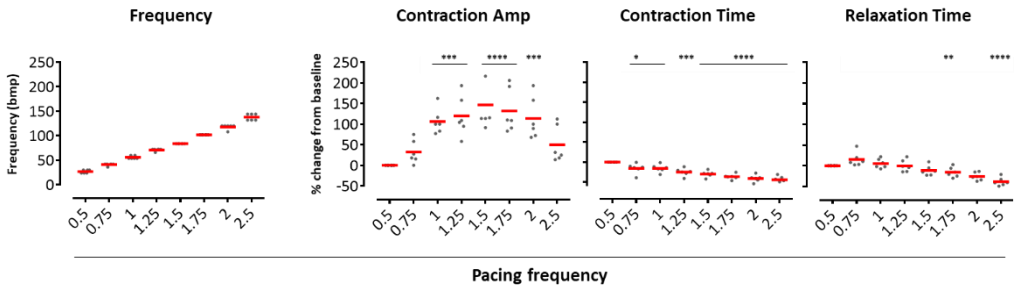

Figure 5-3. Positive force-frequency relationship in EHTs paced between 0.5 and 1.5 Hz. Spontaneous beat rate of EHTs was reduced by 2 hour pre-treatment with 0.3 µM ivabradine, an I_f current inhibitor. Subsequent electrical pacing showed beating frequencies that followed the frequency of the stimulus. Contraction amplitude increased from 0.5 to 1.5 Hz but plateaued and declined at higher frequencies. These changes were reflected in the contraction time and relaxation time data. One-way ANOVA followed by Dunnett's multiple comparisons test vs vehicle control (p ⩽: * 0.05, ** 0.01, *** 0.001, **** 0.0001). Data were generated by Umber Saleem and Ingra Mannhardt (University of Hamburg).

Therefore, 6 positive inotrope compounds were retested in EHT platform in the presence of 0.3 µM ivabradine with electrical pacing at 0.5, 0.7, 1.0, 1.5, and 2.0 Hz (**Figure *5-4***). This included epinephrine,

levosimendan, and pimobendan, which had been incorrectly predicted in EHT platform. It was noted that positive inotropic response was detected by increased contraction amplitude, although only at 0.5-1 Hz, and not apparent at 1.5-2 Hz. Furthermore, shortening of contraction time was observed in all compounds with mechanism of action increasing cAMP, which is more pronounced at lower pacing frequencies (**Figure *5-4***).

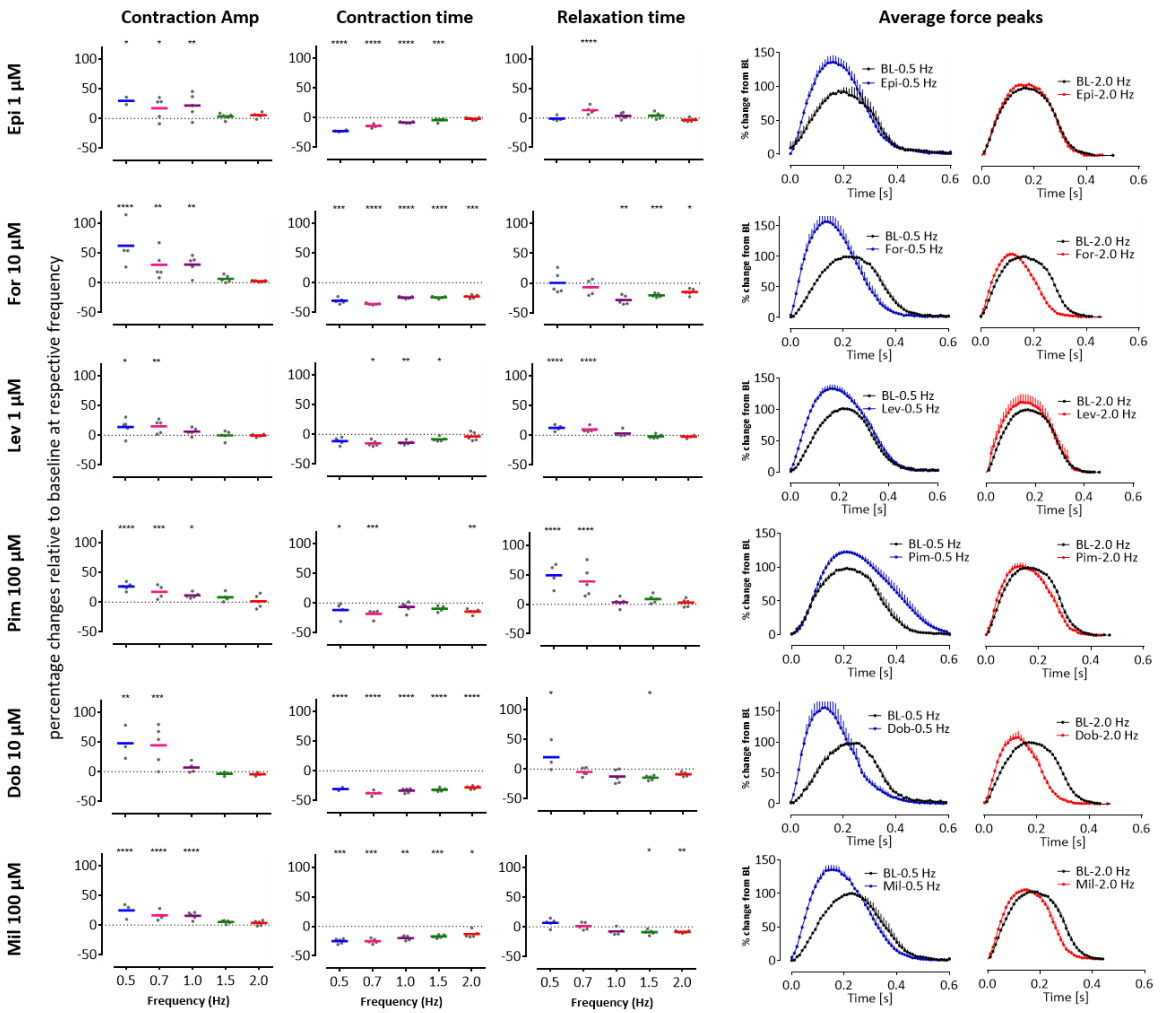

Figure 5-4. Slowed beat rate increases the predictivity of PIs in 3D EHTs. Contraction analysis was carried out using EHTs with 6 of the PIs from the drug test set: epinephrine (Epi), forskolin (For), levosimendan (Lev), pimobendan (Pim), dobutamine (Dob) and milrinone (Mil) which had been predicted with variable accuracy. Scatter plots show percentage changes relative to baseline at respective frequency. Averaged peaks for force are shown for baseline (BL, black peaks) versus after treatment in EHTs paced at 0.5 Hz (blue peaks) or 2.0 Hz (red peaks). One-way ANOVA followed by Dunnett's multiple comparisons test vs baseline at respective frequency ($p \leqslant$: * 0.05, ** 0.01, *** 0.001, **** 0.0001). Data were generated by Umber Saleem and Ingra Mannhardt (University of Hamburg).

Based on these findings, all positive inotropes that had been incorrectly predicted in CO:R-PAT platform-cell combination, were retested using protein-containing medium (RPMI-B27) and ivabradine, with the aim of hiPSC-CMs to be paced at maximum 1 Hz.

Since the concentration of ivabradine was used in EHT which is a 3D system, an optimisation using RPMI-B27 medium was performed in order to determine best concentration range for 2D system (**Figure *5-5***). hiPSC-CMs were incubated with ivabradine for 3h period prior to measurement to mimic drug testing by adding 0.1% DMSO for 30 minutes as 'treatment'. Notably, significant reduced beat rate to <1 Hz was observed in the presence of 0.3 μM of ivabradine (**Figure *5-5***A), which is the same concentration used in EHT platform. Contractility measurements were recorded in order to evaluate ivabradine's effect on contraction amplitude, contraction time, and relaxation time. No significant difference was observed for those parameters (**Figure *5-5***B).

Overall, concentration of ivabradine at 0.3 μM is significant enough to decrease the beat rate in 2D platform without causing undesirable effect on contractility parameters.

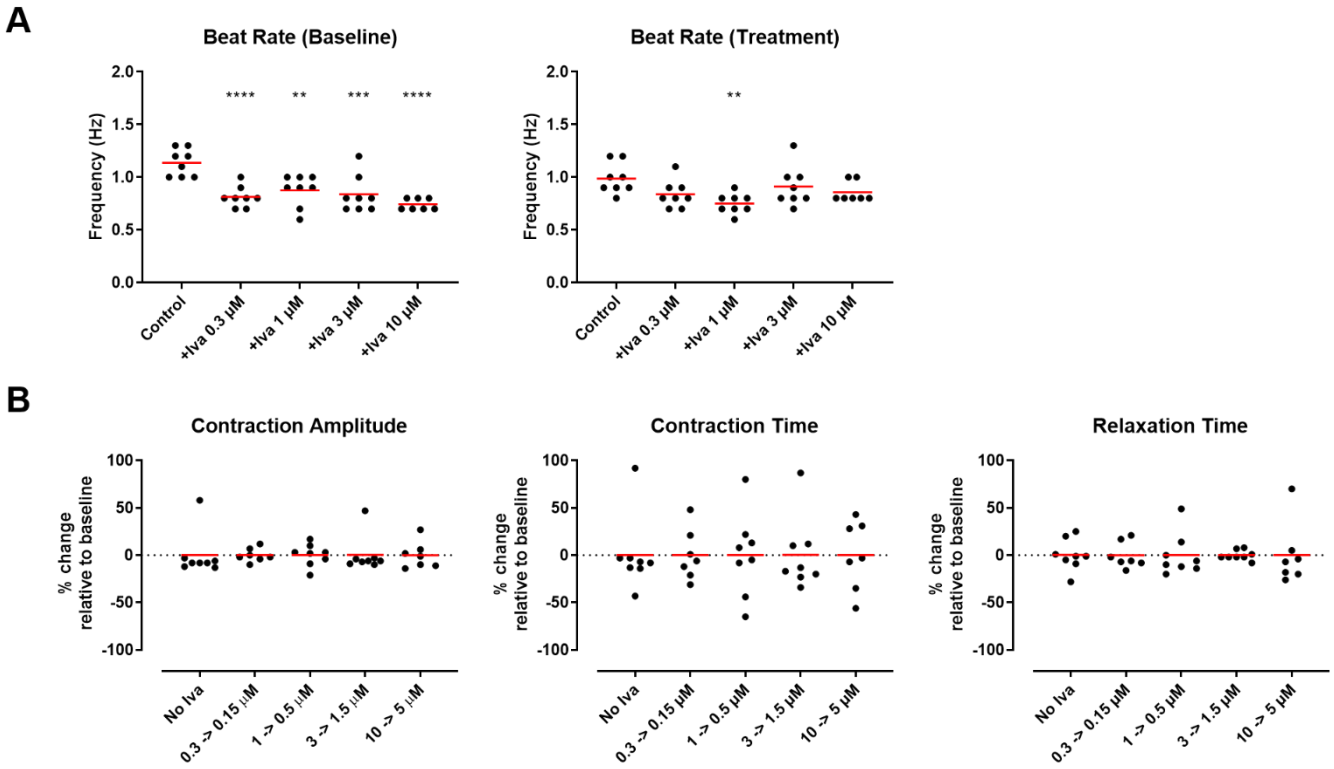

Figure 5-5. Optimisation of ivabradine concentration in hiPSC-CMs cultured as 2D monolayers. hiPSC-CMs were previously treated with ivabradine for 3h incubation period before addition of 0.1% DMSO for 30 minutes to reflect the condition during compound testing. (A) Significant reduced beat rate was found at 0.3 µM concentration. (B) No significant difference was found in contraction amplitude, contraction time, and relaxation time. One-way ANOVA followed by Dunnett's multiple comparisons test vs vehicle control ($p \leqslant$: * 0.05, ** 0.01, *** 0.001, **** 0.0001). N=3 biological repeats.

5.3.3 Refinement in Tier 2 drug testing

The combination of protein-containing medium (RPMI-B27) and 0.3 μM ivabradine is expected to bring greater consistency of baseline recordings, with spontaneous hiPSC-CMs beat rates of 0.5-0.7 Hz, which could be paced at 0.7 to 1 Hz. All positive inotropes (epinephrine, forskolin, levosimendan, pimobendan, dobutamine, milrinone, omecamtiv mecarbil, and terbutaline) were retested with contractility measurement only. Based on previous work in chapter 4, contraction time and relaxation time are more informative parameters for positive inotrope compounds compared to contraction amplitude, hence in this retesting, only contraction time and relaxation time data are shown. Previous work in chapter 4 was based on serum-/protein-free medium, which failed to identify positive inotrope compounds correctly.

After switching to protein-containing medium and using 0.3 μM ivabradine, the slowed beat rate and improved signal-to-noise ratio (as shown by tighter data distribution) allowed correct identification of 6/8 positive inotropes by significant decreases in contraction time and relaxation time (**Figure *5-6***). Prominently, the significant concentration dependent decrease in relaxation time was found in epinephrine, forskolin, and dobutamine. Significant decrease in relaxation time at highest concentration was found in pimobendan, milrinone, and terbutaline at 100 μM, 100 μM, and 10 μM, respectively. There was still no significant difference found in levosimendan, and omecamtiv mecarbil showed increased in contraction time and relaxation time as found in negative inotrope compounds (**Figure *5-6***).

Thus, in both 2D and 3D configurations, lower beating frequencies associated well with increased predictivity for positive inotropes.

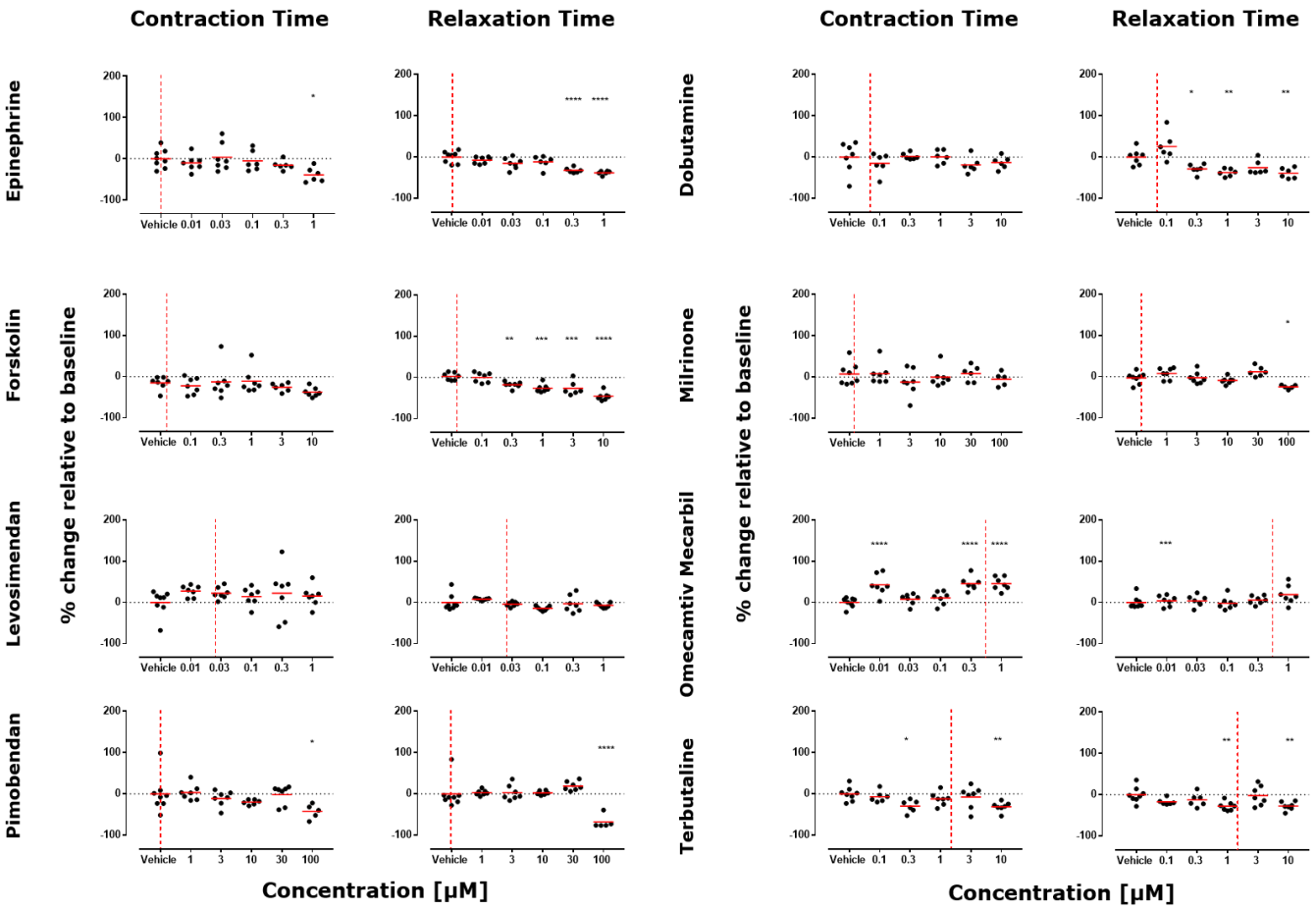

Figure 5-6. Refined culture conditions increase predictivity of positive inotropes in 2D monolayers of hiPSC-CMs. Contractility measurement was carried out on the 8 PIs from the drug test set using the CO:R-PAT platform-cell combination. Whereas testing in serum-/protein-free medium failed to identify any PIs correctly, the slowed beat rate and improved signal to noise ratio afforded by culture in RPMI-B27 and addition of ivabradine allowed correct identification of 6/8 PIs by significant decreases in contraction time and/or relaxation time. Red dotted line is free therapeutic plasma concentration (FTPC). One-way ANOVA followed by Dunnett's multiple comparisons test vs vehicle control (p ⩽: * 0.05, ** 0.01, *** 0.001, **** 0.0001).

5.3.4 Refinement in Tier 1 drug testing

This improved condition, after switching to RPMI-B27 medium and 0.3 μM ivabradine, led to retesting of Tier 1 compounds. Previous work in chapter 3 were done under spontaneous beating; therefore, this retesting was done with electrical stimulation. As previously mentioned, only contraction time and relaxation time data are shown for positive inotropes (isoprenaline, digoxin, Bay K 8644, and EMD 57033). Based on previous work in chapter 4, contraction amplitude is more informative parameters for negative inotrope compounds compared to contraction time and relaxation time, hence in this retesting, only contraction amplitude data are shown for negative inotropes (nifedipine, ryanodine, and thapsigargin). Direct comparison to Nottingham's previous work in chapter 3 is not feasible; due to limitation of data (i.e. only electrophysiology measurements were performed for Bay K 8644, EMD 57033, ryanodine, and thapsigargin).

Positive inotrope response was shown in isoprenaline with significant decrease in contraction time at 0.1 μM. Fibrillation event was observed on higher concentrations of digoxin at 0.3 μM and followed by quiescent at 1 μM, which was not found in previous work under spontaneous beating. Previous work done in 2D platform at University of Glasgow for Bay K 8644 demonstrated trend in increase of relaxation time, which is also found in this retesting. In addition, higher beat rate was found in 0.03 μM, and fibrillation event was noted from 0.1-1 μM. Retesting on EMD 57033 showed negative inotrope response with significant increase in relaxation time, which is consistent with previous work done in 2D platform at University of Glasgow (**Figure *5-7***).

Negative inotrope response was shown in nifedipine with significant decrease in contraction amplitude at 0.3 μM with quiescent event. No significant effect on contraction amplitude was found in ryanodine, which is consistent with previous work done in 2D platform at University of Glasgow. Negative inotrope response was shown in thapsigargin with significant decrease in contraction amplitude at 30 μM and 100 μM with quiescent event (**Figure *5-7***).

Overall, retesting of Tier 1 compounds has a purpose to complete the data set and confirmed some of the findings found on other academic partner’s previous work.

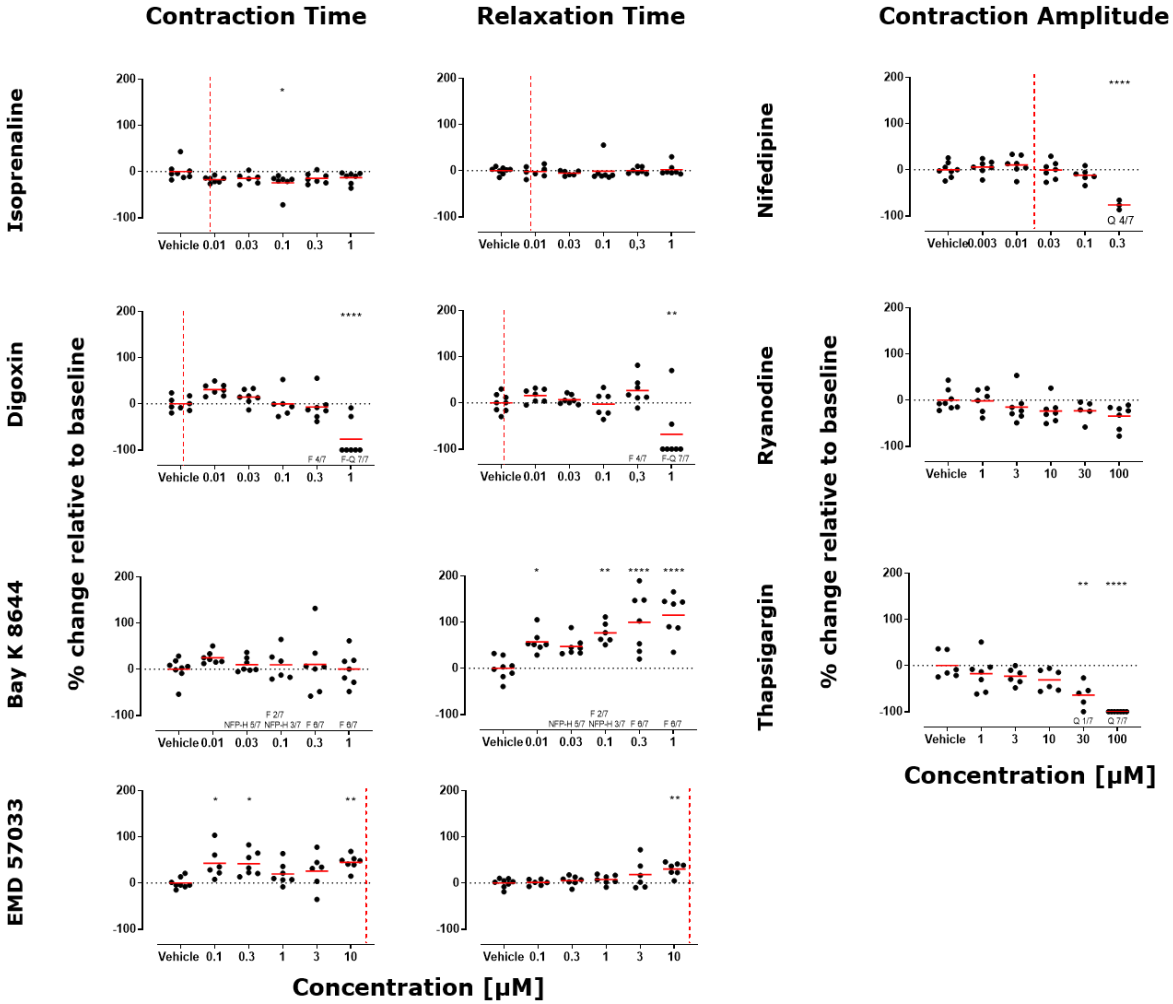

Figure 5-7. Tier 1 retesting under refined culture conditions in 2D monolayers of hiPSC-CMs. Contractility measurement was carried out on the 4 positive inotropes and 3 negative inotropes using the CO:R-PAT platform-cell combination. Red dotted line is free therapeutic plasma concentration (FTPC). Abbreviations: F, fibrillation; Q, quiescent; NFP-H, not following pacing (high). One-way ANOVA followed by Dunnett's multiple comparisons test vs vehicle control ($p \leqslant$: * 0.05, ** 0.01, *** 0.001, **** 0.0001).

5.3.5 Prolonged exposure of selected Tier 2 drug compounds

Tier 2 phase drug testing was done under acute (i.e. 30 min exposure) condition. In this section, longer exposure of hiPSC-CMs to positive inotrope compounds and negative compounds at highest concentration in the top 10 drug list up to 24 hours were conducted in order to investigate the effect in contractility parameters. Specifically, to focus on chronic toxicants such as doxorubicin and sunitinib, which had been incorrectly predicted (or not tested). Due to limitation of CellOPTIQ® ability in recording real-time of prolonged exposure of compound, doxorubicin and sunitinib incubation was done 24h before the recording.

To overcome the drawback, commercially available combination of impedance and multielectrode array (MEA) platform, xCELLigence® RTCA CardioECR (ACEA Biosciences, Inc.) was utilised (**Figure *5-8***). This platform allows real-time, simultaneous recording of electrophysiology (MEA based) and contractility (impedance based) (**Figure *5-8***A) (Mulder et al., 2018). Cell-induced electrical impedance depends on cell size/shape and the manner in which the cell interacts with the electrode located in plate bottom. The contraction-relaxation state of hiPSC-CMs gives rise to a rhythmic fluctuation in impedance that is captured on the millisecond time scale (**Figure *5-8***B).

hiPSC-CMs are seeded in a 48-well electronic microtiter plate (E-Plate® CardioECR 48) containing gold microelectrode arrays that are fused to the bottom of each well. Electric current between the electrodes are established by application of a low voltage (<20 mV), which is affected by cell confluency, morphology, and attachment strength. Changes of cell morphology and adhesion in hiPSC-CMs contraction-relaxation cycle can be dynamically monitored using impedance with rate of every 1 ms. Extracellular field potential (FP) measurements are done at 10 kHz (**Figure *5-8***A-B). Representative of simultaneous measurements is depicted in **Figure *5-8***C.

Since Tier 2 phase drug testing was evaluated mainly for contractility measurement, this section will focus on exploring the chronic exposure effects on contractility parameters (contraction amplitude, contraction time, and relaxation time) as depicted in **Figure *5-8***D. Amplitude in this platform is defined as the difference from baseline to peak. Contraction

time in this platform is defined as the time it takes to increase from 20% amplitude to 80% amplitude in the upstroke stage of each beating. Relaxation time in this platform is defined as the time it takes to decrease from 80% amplitude to 20% amplitude in the downstroke stage of each beating.

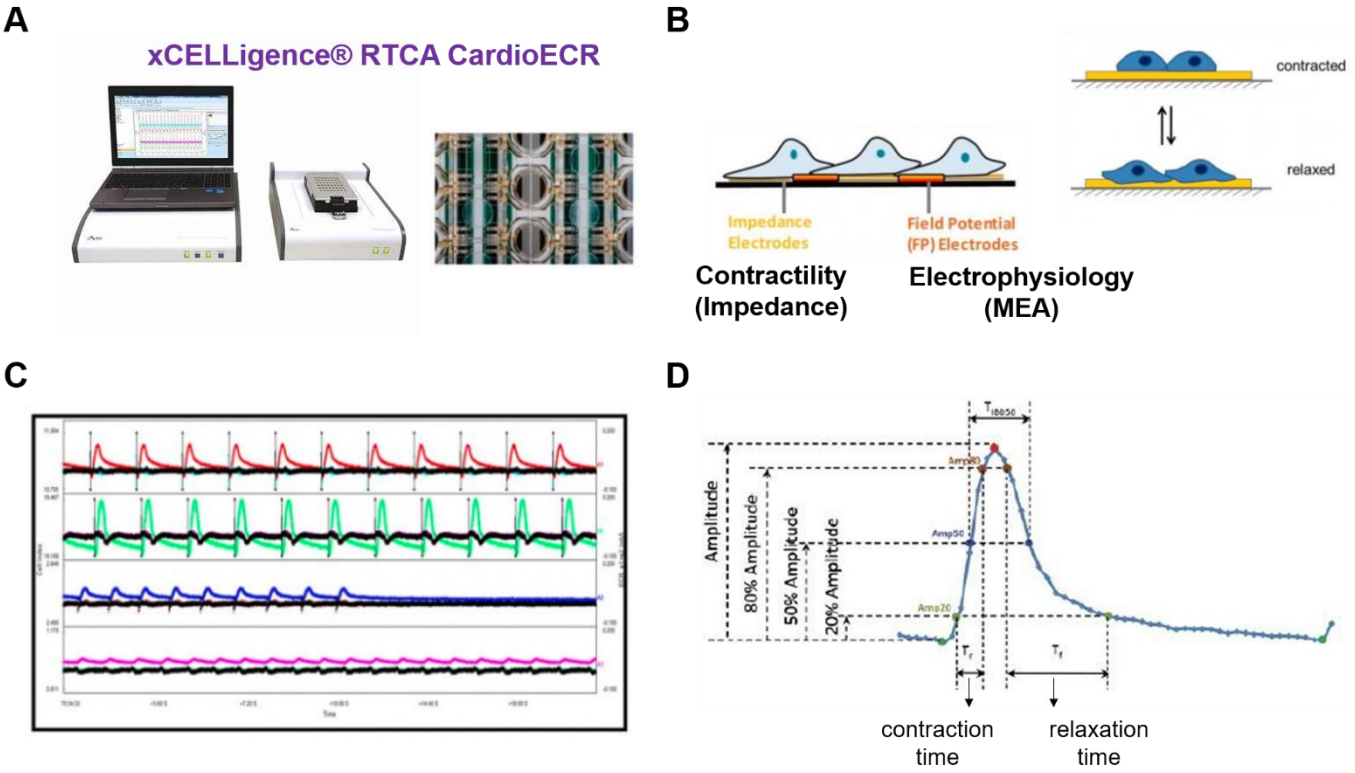

Figure 5-8. Schematic illustration of xCELLigence® RTCA CardioECR platform. (A) xCELLigence® RTCA CardioECR is a combination of impedance and multielectrode array platform with electrical stimulation feature, manufactured by ACEA Biosciences, Inc., for electrophysiology and contractility measurements in the 48-well electronic microtiter plate. (B) Graphic depiction of cardiomyocytes interacting with impedance and field potential electrodes. The differences in cell size/shape and the manner in which cells contact the electrode cause contracted vs. relaxed states of cardiomyocytes to impede the flow of electric current differently. (C) Real-time, simultaneous measurement of cardiomyocyte for contraction (red, green, blue, and pink traces) and field potential (integrated ion channel activity; black traces). Negative control (upper set of traces), tested compounds (bottom three sets of traces). (D) Schematic description of the parameters used to quantify drug effect in hiPSC-CMs, with focusing on contraction amplitude, contraction time, and relaxation time.

This study evaluated the predictive value of impedance measurements of hiPSC-CMs in acute and chronic compound exposure settings. Combination of cell line R-PAT-CMs in xCELLigence® RTCA CardioECR platform is hence referred as ECR:R-PAT. Baseline readings were recorded for 1h followed by incubation of 0.3 µM ivabradine. Following 1h of incubation, the cells underwent continuous pacing for 2h with frequency set at 0.7 Hz based on previous readings. Before experimentation, the compounds were prepared in RPMI-B27 at 2X final concentration with 0.1% DMSO. 100 µL of medium in the plate were aspirated before the addition of 100 µL of compound-containing medium, with total of 200 µL of medium per well. A series of sweeps steps were set with details as depicted in **Figure *5-9***. Contractility analysis was done with proprietary software RTCA CardioECR System Data Acquisition and Data Analysis via offline.

5.3.5.1 Evaluation of positive inotrope compounds on chronic exposure setting

As previously mentioned, the compounds were added after 3 hour incubation of 0.3 µM ivabradine. The DMSO control demonstrated that cellular impedance remained stable over the course of the experiment. Representative data collected with ECR:R-PAT platform-cell combination demonstrating the effect of positive inotrope compounds are shown in **Figure *5-10***. At the 0.5h time point a significant increase on contraction amplitude occurs at 1 µM epinephrine and 100 µM pimobendan, which was not observed on CO:R-PAT cell-platform combination. The first effect on increased beat rate occurs at 1 µM epinephrine and 10 µM forskolin. There was no significant effect observed in levosimendan, which is consistently found in previous work. After 2h time point, 100 µM pimobendan went into full arrest (cellular impedance reached a plateau), which was also found during recording on different plate under spontaneous beating, and yet could not be observed during acute exposure. By the 12h time point, a time dependent decrease in contraction time was observed in 10 µM forskolin. By the 24h time point, trend decrease in relaxation time was observed in 1 µM epinephrine (**Figure *5-10***).

Overall, while short-term exposure of positive inotrope compounds already exhibited inotropic effect, longer-term exposure revealed overt cytotoxicity and cell death.

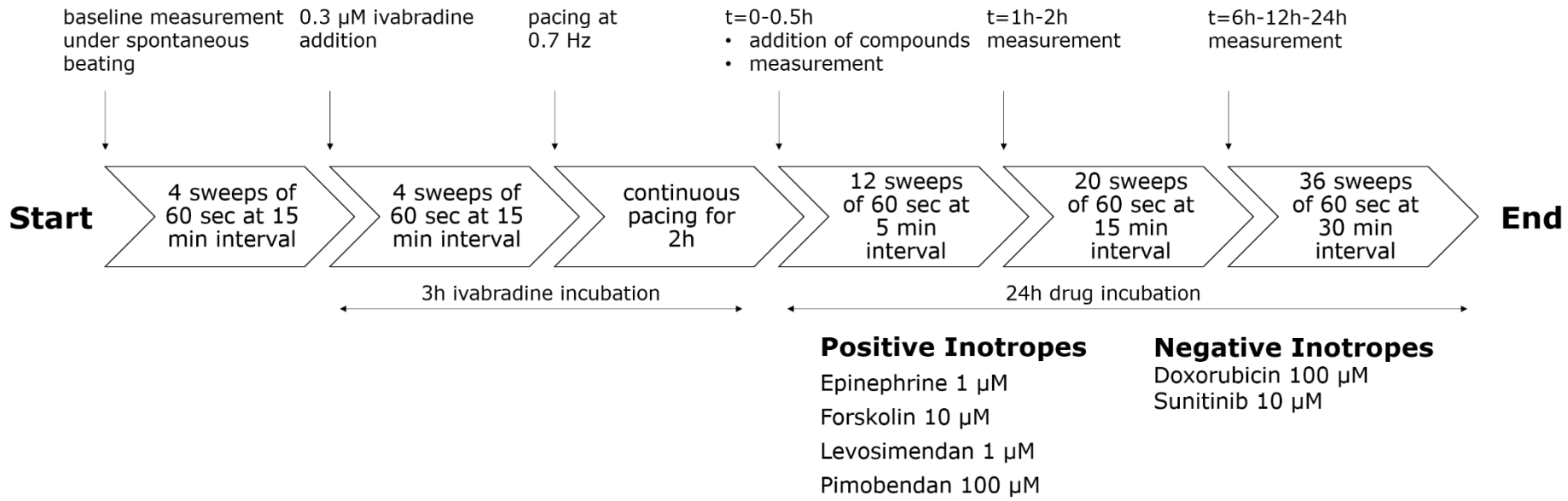

Figure 5-9. Experimental timeline for evaluating long term drug effects. hiPSC-CMs were seeded in a 48-well electronic microtiter plate, incubated with 0.3 μM ivabradine and paced continuously at 0.7 Hz based on the previous baseline readings. Compounds were added at 2X desired concentrations through half medium replacement. Negative control is 0.1% DMSO.

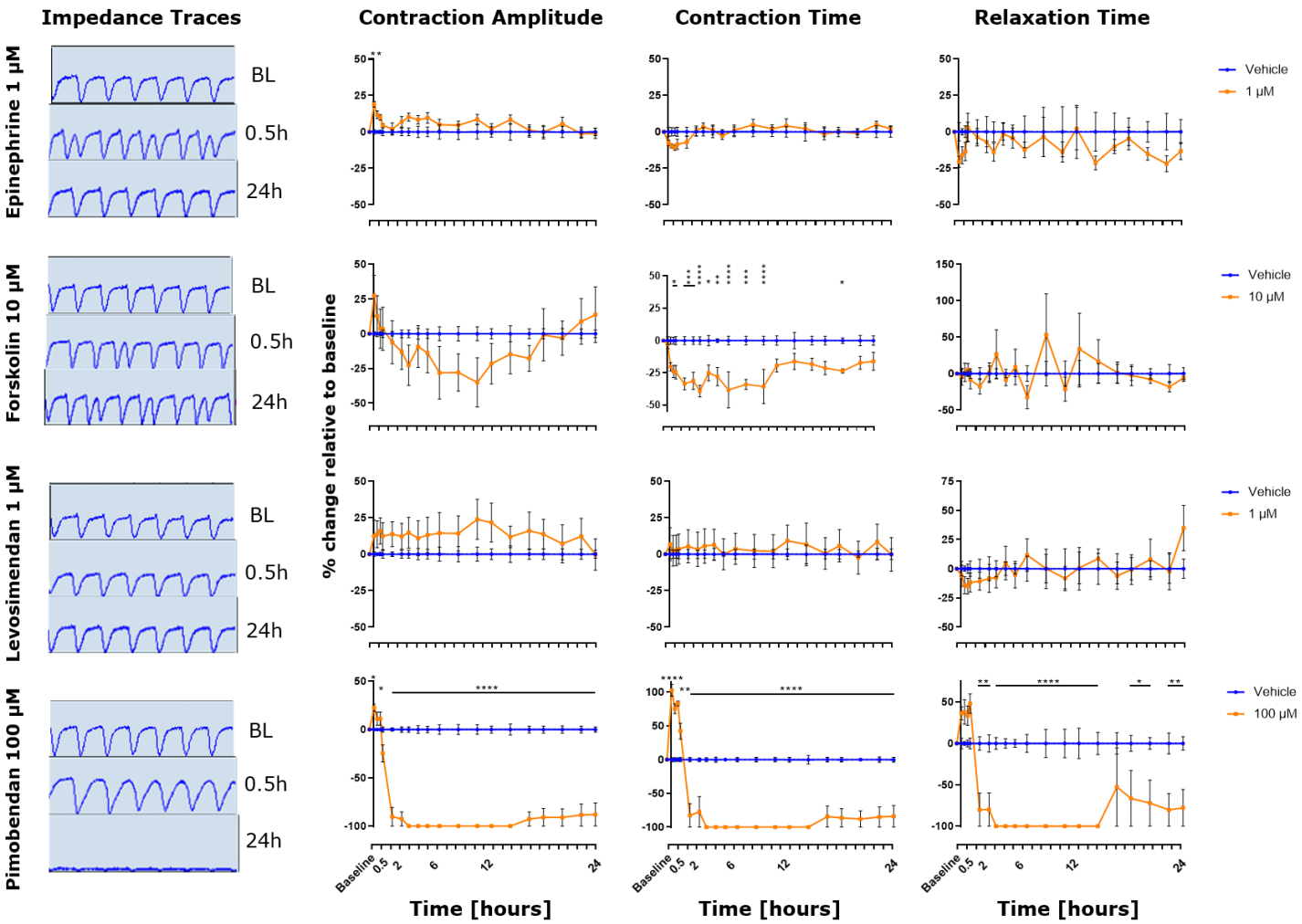

Figure 5-10. Prolonged exposure of positive inotrope compounds in 2D cultures of hiPSC-CMs. Representative impedance traces, contraction amplitude, contraction time, and relaxation time measurement in the ECR:R-PAT platform-cell combination for 24 hours. Data were shown as normalised to vehicle control. Abbreviation: BL, baseline. Two-way ANOVA followed by Sidak's multiple comparisons test vs vehicle control (p ⩽: * 0.05, ** 0.01, *** 0.001, **** 0.0001). Stars in forskolin are presented vertically.

5.3.5.2 Evaluation of negative inotrope compounds on chronic exposure setting

Acute exposure of hiPSC-CMs to doxorubicin and sunitinib altered electrophysiology properties, yet the accuracy on contractility response prediction was varied. In addition to evaluation of these anti-cancer drugs on ECR:R-PAT platform-cell combination, this section also explore the use of CO:R-PAT and EHT:ERC platform-cell combination (**Figure *5-11***). The CO:R-PAT platform-cell combination showed that exposure to doxorubicin or sunitinib at highest concentration for 24 hours led to cell death (**Figure *5-11***A-B). Representative data collected with ECR:R-PAT platform-cell combination demonstrating the effect of doxorubicin and sunitinib at highest concentration are shown in **Figure *5-11***C-D. From the 5.5h time point, a significant steady decrease in contraction amplitude was observed in 100 µM doxorubicin until the cellular impedance reached a plateau from the 9h time point. On the other hand, sunitinib already exhibited full arrest from the 0.5h time point. Similar trend was found on the EHT:ERC platform-cell combination, in which exposure to doxorubicin ceased EHT contraction after 17.5 hours, whilst exposure to 1 µM sunitinib (middle range from 5 x ½ log concentration) led to a time dependent decrease in contraction amplitude over a 7 day period (**Figure *5-11***E-F).

Overall, while short-term exposure of negative inotrope compounds already affect the electrophysiology of hiPSC-CMs, longer-term exposure revealed overt cytotoxicity and cell death.

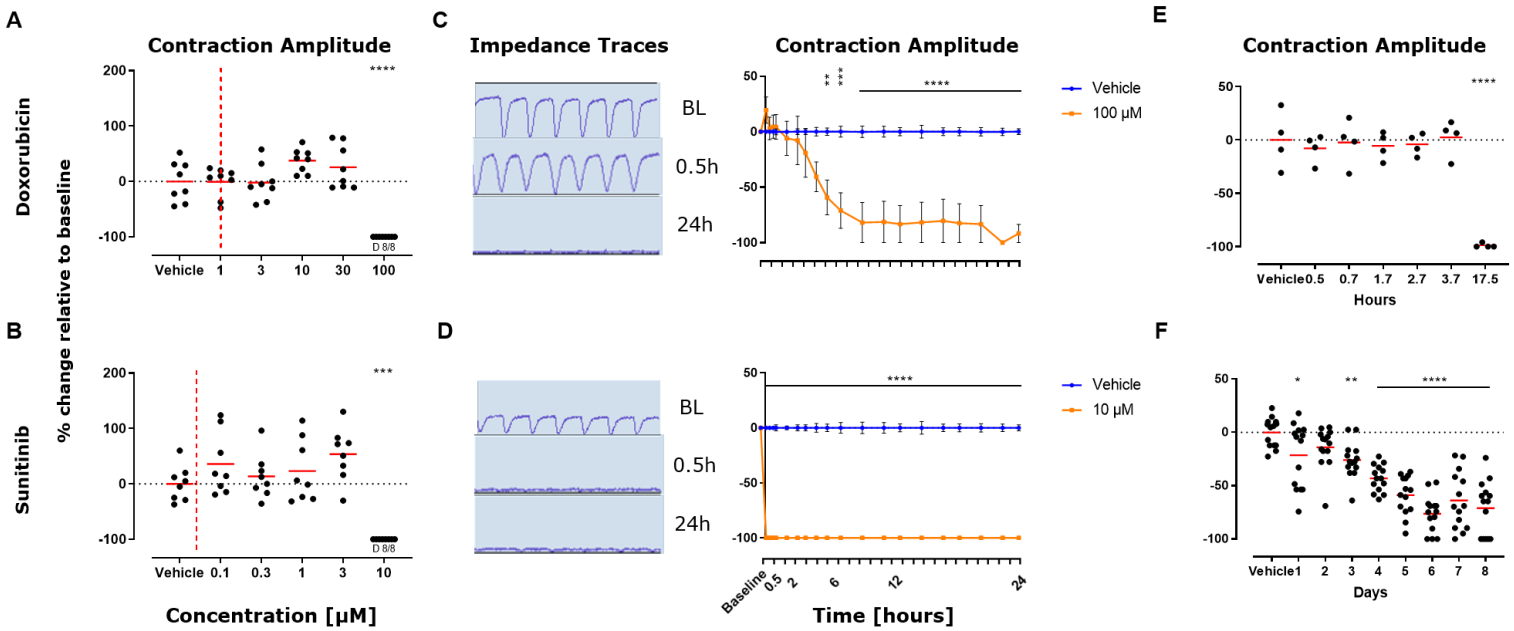

Figure 5-11. Prolonged exposure of negative inotrope compounds in 2D and 3D cultures of hiPSC-CMs. Contraction amplitude was measured in the CO:R-PAT platform-cell combination exposed to various concentrations of doxorubicin (A) or sunitinib (B) for 24 hours, with the highest test concentration causing cell death. Red dotted line is free therapeutic plasma concentration (FTPC). Representative impedance traces and contraction amplitude measurement of doxorubicin (C) and sunitinib (D) in various times exposure in the ECR:R-PAT platform-cell combination. The EHT:ERC platform-cell combination was exposed to 100 µM doxorubicin (E) or 1 µM sunitinib (F) for up to 17.5 hr (E) or up to 8 days (F). Data were shown as normalised to vehicle control. Abbreviation: BL, baseline. CO:R-PAT and EHT:ERC: One-way ANOVA followed by Dunnett's multiple comparisons test vs vehicle control. ECR:R-PAT: Two-way ANOVA followed by Sidak's multiple comparisons test vs vehicle control. p ⩽: * 0.05, ** 0.01, *** 0.001, **** 0.0001. For (F), data were generated by Umber Saleem and Ingra Mannhardt (University of Hamburg).

5.3.6 Structural features of hiPSC-CMs in Tier 2 phase

Previous sections have described the context of use, throughput, and which platform that can accurately detect/reproducibly inotropic response of the compounds. Another key point to consider for application of *in vitro* contractility assays for pharma industry use is the phenotypic characteristics of hiPSC-CMs to reflect their degree of maturation.

Recent studies have explored the approaches to specify atrial- and ventricular-like hiPSC-CM subtypes by modulating retinoic acid signaling (Devalla et al., 2015, Lee et al., 2017b, Lemme et al., 2018) as tools for the development of chamber-specific drugs. Adult cardiomyocytes have shown to have higher expression of MLC2v (myosin regulatory light chain 2, ventricular/cardiac muscle isoform; encoded by the *MYL2* gene) compared to MLC2a (myosin regulatory light chain 2, atrial isoform; encoded by the *MYL7* gene) (Denning et al., 2016). Ventricular cardiomyocytes are derived from either MLC2v+ population or MLC2a+ MLC2v+ dual positive population, while atrial cardiomyocytes are derived only from MLC2a+ population, which is pronounced during cardiac development process *in vivo* (Franco et al., 1998). Previous study revealed the presence of MLC2a+ MLC2v+ dual positive population is found in immature characteristics of hiPSC-CMs (Mummery et al., 2012).

Therefore, the ratio between MLC2a+ and MLC2v+ cells in the population was investigated by performing immunocytochemistry on R-PAT, iCell^2, and Pluricyte to provide an indicator of the level of maturity of hiPSC-CMs used in 2D platform during Tier 2 phase testing. Plates were scanned for imaging on the Operetta™ high content imaging system (PerkinElmer). Quantitative analysis were done using Harmony® high-content analysis software, with workflow as depicted in ***Figure 5-12***. Intensity of fluorescence level was used as gating to exclude negative population, which are derived from control well stained only with secondary antibody, as described in chapter 3.

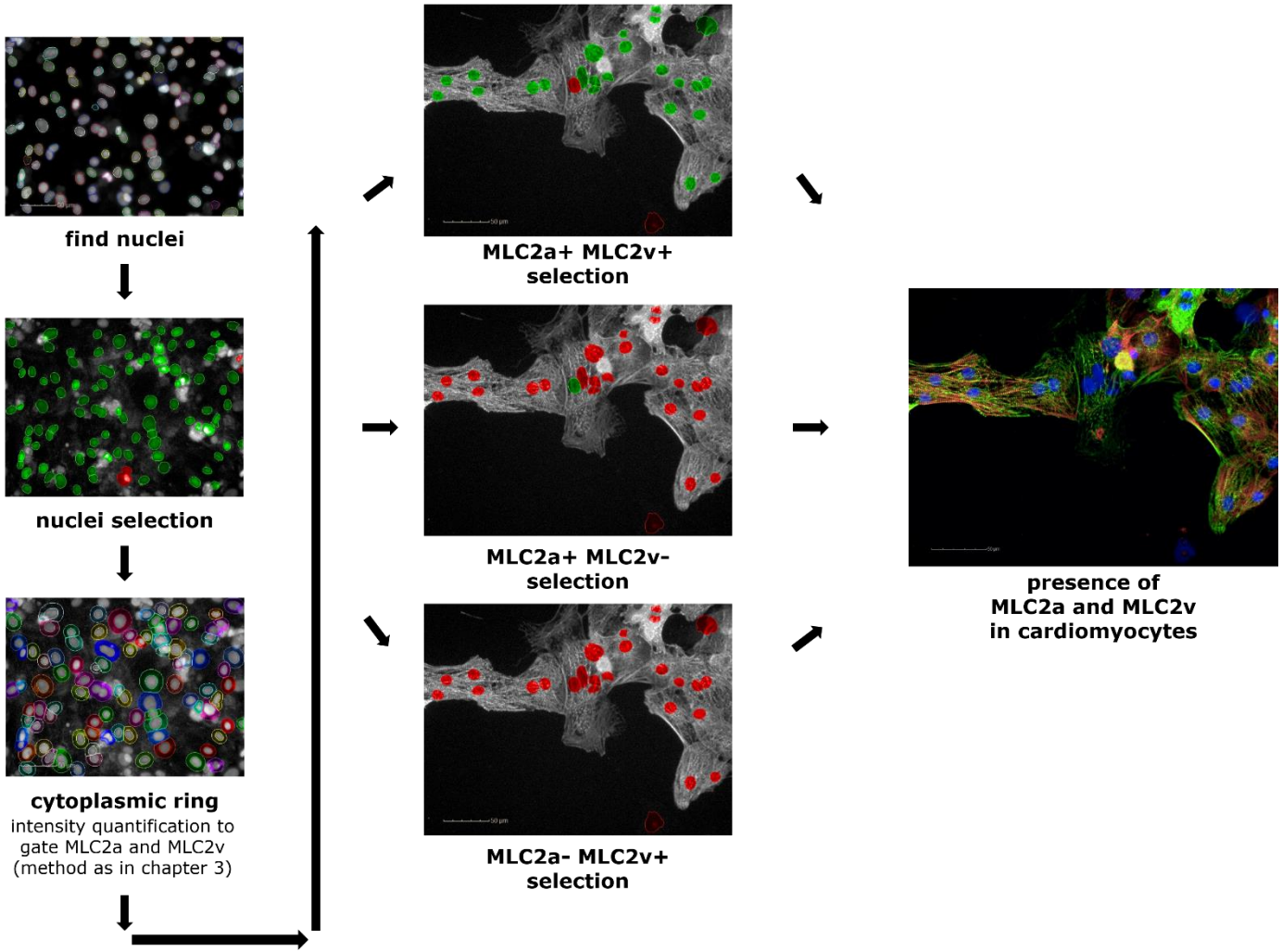

Figure 5-12. Workflow to quantify MLC2a and MLC2v as markers of cardiac subtype atrial and ventricular, respectively. Inclusion of positive (green round) population and exclusion of negative population (red round) led to quantitative measurement of MLC2a and MLC2v dual positive, MLC2a positive, and MLC2v positive population. Finding nuclei was derived from DAPI staining. Building blocks were made with Harmony® high-content analysis software.

Immunocytochemistry result of hiPSC-CMs stained with MLC2a and MLC2v antibodies is in ***Figure 5-13***. Representative images are in ***Figure 5-13***A, with MLC2a+ population stained as green and MLC2v+ population stained as red. MLC2a+ MLC2v+ dual positive population was majorly found in Pluricyte (97 ± 0.30%), and less found in iCell^2 (36.31 ± 6.13%) and R-PAT (17.07 ± 1.76%). MLC2a+ population with percentage more than half population was found in iCell^2 (63.69 ± 6.13%) and R-PAT (56.30 ± 4.29%), with least percentage in Pluricyte (1.12 ± 0.60%). Lastly, MLC2v+ population is significantly more prominent in R-PAT (26.63 ± 4.27%) compared to Pluricyte (1.87 ± 0.58%) and none are found in iCell^2 ($p<0.001$) (***Figure 5-13***B).

This result showed that major population of Pluricyte expressed heterogeneous population of both MLC2a and MLC2v, with minimal expression of MLC2a+ and MLC2v+. iCell^2 exhibited a mixture of population with more proportion of MLC2a+ compared to the rest. Despite earlier days of cardiac differentiation in R-PAT (20-25 days of differentiation) compared to iCell2 and Pluricyte (at least 30 days of differentiation according to manufacturer's datasheet), R-PAT showed to have expression of MLC2v+ positive population compared to rest cell lines.

Collectively, this result demonstrated that in MLC2a and MLC2v there was an early stage of expression shift from atrial towards ventricular specification, which is related to the maturation process stage in hiPSC-CMs.

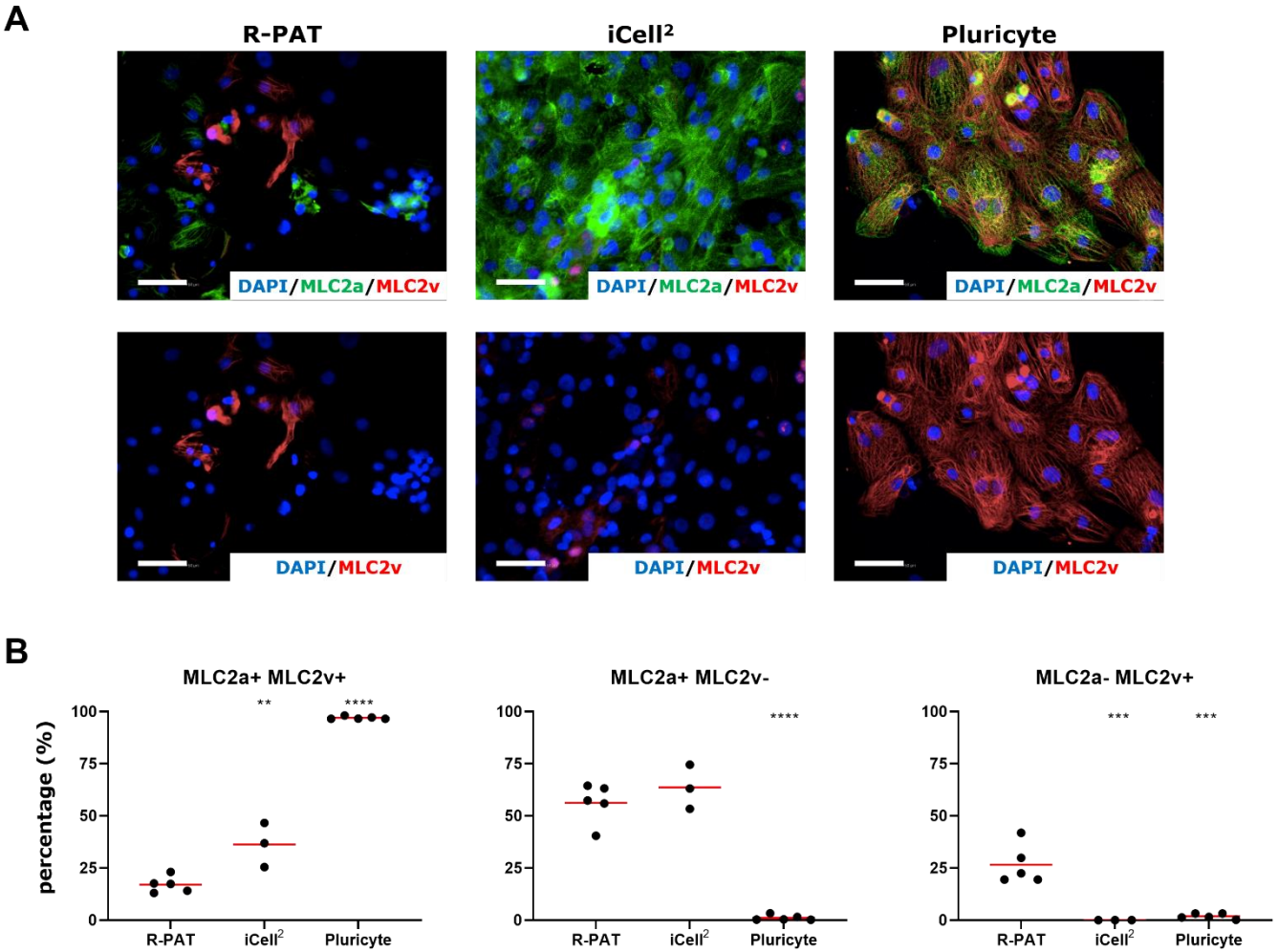

Figure 5-13. Representative of MLC2a and MLC2v presence in hiPSC-CMs. (A) Images of hiPSC-CMs immunostained for 3 distinct populations: MLC2a and MLC2v dual positive, MLC2a positive, and MLC2v positive population, with (B) displaying quantification. More than half population of R-PAT and iCell displayed atrial subtype, while majority of Pluricyte demonstrated heterogeneous population of both atrial and ventricular subtype. Scale bar: 50 μM. Data are presented as Mean ± SEM. One-way ANOVA followed by Dunnett's multiple comparisons test vs R-PAT as control (p ⩽: * 0.05, ** 0.01, *** 0.001, **** 0.0001).

Next, morphologic features related with maturation such as sarcomeric organisation and protein expression related with conduction velocity were evaluated. Connexin 43 (Cx43) is the predominant cardiac gap junction protein that contribute to cardiomyocyte's in action potential (Noorman et al., 2009). In fetal stage of development, Cx43 is circumferentially distributed, and as maturation progress *in vivo*, Cx43 become gradually more concentrated in intercalated disks at the ends of the cells, resulting in increasing conduction velocity (Angst et al., 1997). In hiPSC-CMs, Cx43 is shown in various studies to have circumferential distribution, indicating immature phenotype (Cyganek et al., 2018, Yang et al., 2014a).

Therefore, sarcomeric organisation and presence of Cx43 population were investigated by performing immunocytochemistry on R-PAT, iCell^2, and Pluricyte with similar purpose; to determine the level of maturity of hiPSC-CMs used in 2D platform during Tier 2 phase testing. As mentioned previously, plates were scanned for imaging on the Operetta™ high content imaging system (PerkinElmer). Quantitative analysis were done using Harmony® high-content analysis software, with workflow as depicted in ***Figure 5-14***. Intensity of fluorescence level was used as gating to exclude negative population, which are derived from control well stained only with secondary antibody, as described in chapter 3.

This workflow has similar feature with previous ones to select cardiomyocytes population by defining the "cytoplasmic ring" region to measure the intensity of fluorescence. In addition, since Cx43 expression is shown as "spots", this workflow also defined the spots region into two sections: within the cells and inside nuclei. Spots of Cx43 (outside nuclei) is then calculated by subtracting the number of spots inside nuclei from number of spots within the cells. The building blocks were not able to determine how many Cx43 spots per cell, therefore, the quantification was made based on its relative presence in cardiomyocytes (number of spots outside nuclei of cardiomyocytes divided to number of cardiomyocytes).

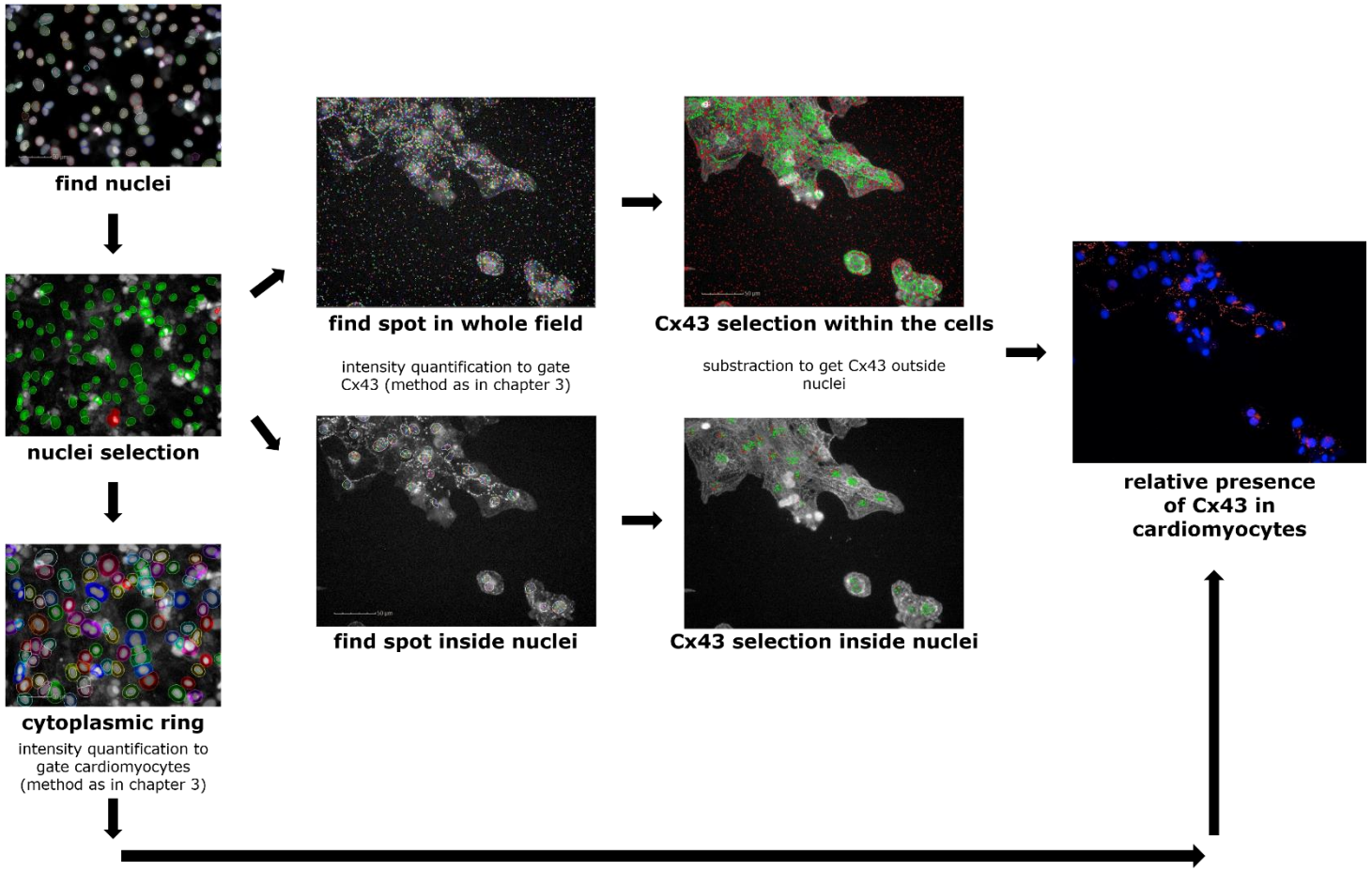

Figure 5-14. Workflow to quantify gap junction protein connexin 43 (Cx43) in hiPSC-CMs. Inclusion of positive (green round) population and exclusion of negative population (red round) led to quantitative measurement of Cx43 (spots outside nuclei) by substracting spots inside nuclei from all spots within the cells. Finding nuclei was derived from DAPI staining. Building blocks were made with Harmony® high-content analysis software.

Immunocytochemistry result of hiPSC-CMs stained with α-actinin (for sarcomeric organisation) and Cx43 antibodies is in ***Figure 5-15***. Representative images are in ***Figure 5-15***A, with α-actinin population stained as green and Cx43 population stained as red. In general, all cell lines displayed rather well organised striated patterns visualised by α-actinin. High cardiomyocytes purity are all shown in iCell^2 (99.09 ± 0.39%), Pluricyte (92.66 ± 1.27%), and R-PAT (77.01 ± 2.46%) (***Figure 5-15***B). Relative presence of Cx43 in cardiomyocytes was more pronounced in Pluricyte (32.17 ± 2.91) ($p<0.0001$) compared to iCell^2 (7.6 ± 0.74) and R-PAT (5.96 ± 0.97) (***Figure 5-15***C).

Although Pluricyte displayed the highest ratio of Cx43 in cardiomyocytes, its expression is still a mixture of circumferentially distributed and at the ends of the cells. Both iCell^2 and R-PAT had significantly lesser Cx43 spots, which might be explained since atrial subtype population also express Cx40 gap junction (Vozzi et al., 1999). A previous study using hiPSC-CMs showed that higher ratio of Cx43 concurrently have prolonged action potential duration (APD) (McSpadden et al., 2012).

Collectively, this result demonstrated that all cell lines still displayed rather immature phenotype characteristics of hiPSC-CMs.

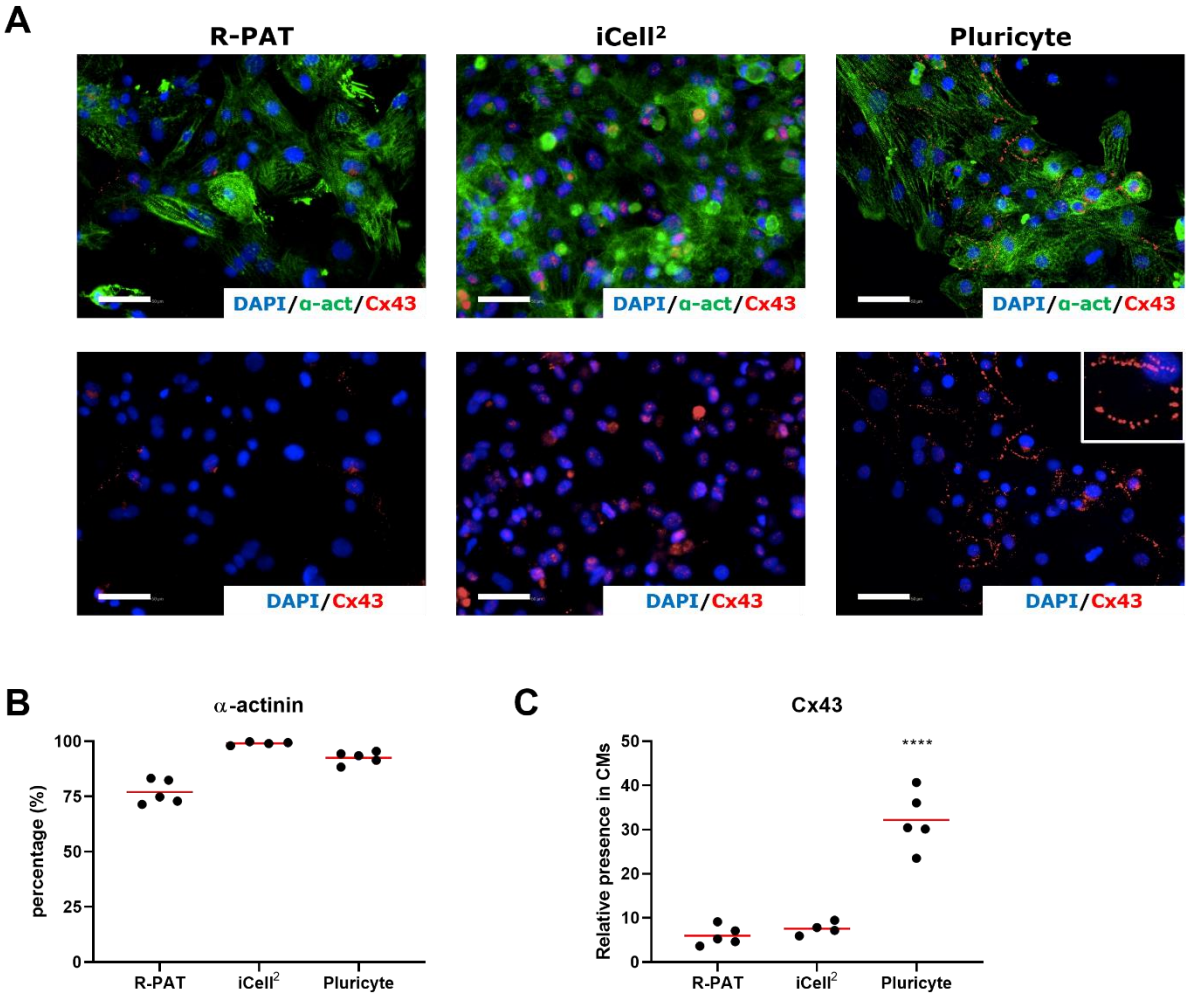

Figure 5-15. Representative of gap junction protein connexin 43 (Cx43) in hiPSC-CMs. (A) Images of hiPSC-CMs immunostained for spots defined as Cx43, with (B-C) displaying quantification. Cell population displayed more than 75% of cardiomyocytes as immunostained with α-actinin. Relative presence of Cx43 outside nuclei are significantly more prominent in Pluricyte compared to R-PAT and iCell^2. Scale bar: 50 μM. For (C), one-way ANOVA followed by Dunnett's multiple comparisons test vs R-PAT as control (p ⩽: * 0.05, ** 0.01, *** 0.001, **** 0.0001).

.

5.3.7 Retesting of Tier 2 compounds on Pluricyte

Due to limitated cell resources, Pluricyte were only tested on top 10 of Tier 2 compound list. After unblinding of Tier 2 phase, Ncardia was interested to evaluate the effect of remaining positive inotrope compounds (dobutamine, milrinone, omecamtiv mecarbil, terbutaline), as well as negative inotrope compound doxorubicin in chronic exposure, due to it failed to be detected during 30 minutes incubation. Concentration was selected to be only at the highest concentration due to limited vials sent by the company. Beat rate of Pluricyte range from 0.5-0.7 Hz, so the experiments were done in Pluricyte medium but without the presence of ivabradine.

Contractility analysis results are shown on ***Figure 5-16***. There was no significant difference found in contraction amplitude and contraction time at highest concentration of all positive inotropes, whereas terbutaline showed significant decrease in relaxation time (***Figure 5-16***A). After chronic exposure of doxorubicin for 24h, cell death were observed with increased events from 3 to 30 µM, with full events found at highest concentration (100 µM) (***Figure 5-16***B), which is similarly found with previous findings on CO:R-PAT and EHT:ERC platform-cell combination.

Despite the low beat rate, Pluricyte didn't exhibit the significant decrease in contraction time or relaxation time in most positive inotrope compounds as found in the Tier 2 retesting using CO:R-PAT platform-cell combination. Based on previous result in structural features of hiPSC-CMs used in Tier 2 phase, higher percentage of ventricular subtype found in R-PAT might be related to better predictivity in these compounds (3/4 showed reduced contraction time or relaxation time) versus in lower percentage of ventricular subtype in Pluricyte (1/4 showed reduced contraction time or relaxation time).

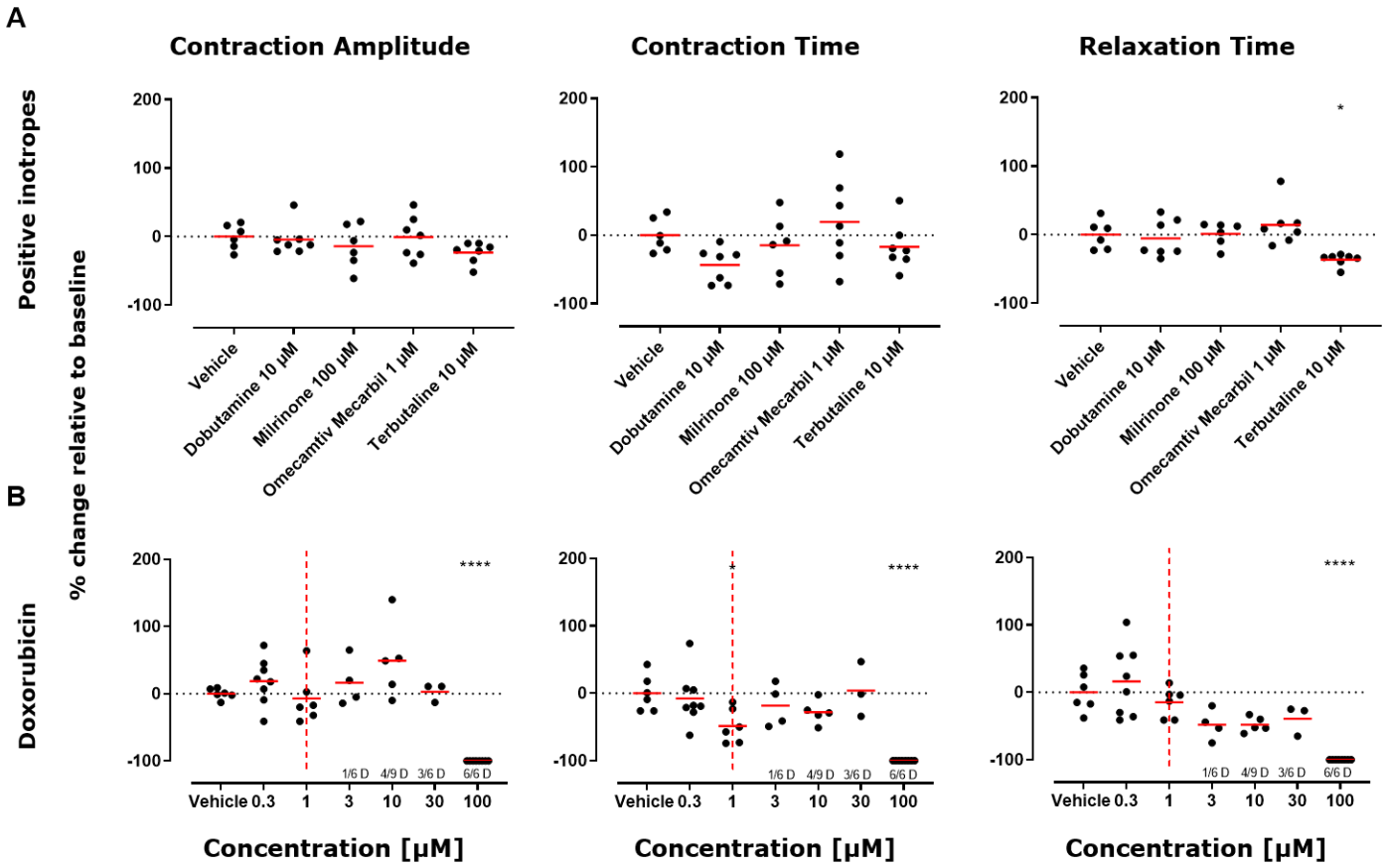

Figure 5-16. Tier 2 retesting of positive inotropes and doxorubicin on Pluricyte. Contractility measurement was carried out on the 4 positive inotropes in acute exposure and 1 negative inotrope (doxorubicin) using the CO:Pluricytes platform-cell combination. Red dotted line is free therapeutic plasma concentration (FTPC). Abbreviations: D, cell death. One-way ANOVA followed by Dunnett's multiple comparisons test vs vehicle control (p ⩽: * 0.05, ** 0.01, *** 0.001, **** 0.0001).

5.3.8 Exploring effects of selected positive inotropes outside of Tier 2 phase on Pluricyte

In addition to existing Tier 2 compounds, there was interest in exploring compounds with mechanism of actions not explored or not clear during the Tier 1 and Tier 2 phases. Two additional compounds were selected: CDN1163, which is a novel sarcoplasmic-endoplasmic reticulum Ca^{2+} -ATPase (SERCA) activator (Cornea et al., 2013, Gruber et al., 2014, Tadini-Buoninsegni et al., 2018, Singh et al., 2018), and ouabain, which is a Na^{+}/K^{+}-ATPase inhibitor (Torretti et al., 1972, Peng et al., 1996).

Contractility analysis results are shown in ***Figure 5-17***. There was no significant difference found in CDN1163-treated cells for contraction amplitude and contraction time, whilst there was significant decrease in relaxation time at highest concentration (30 μM) (***Figure 5-17***A). In ouabain-treated cells, there was no significant difference found for all contractility parameters (contraction amplitude, contraction time, and relaxation time), although there was a trend decrease noted for contraction time (***Figure 5-17***B). Fibrillation event was noted from concentration 0.1-3 μM, similarly found in digoxin, which is also a Na^{+}/K^{+}-ATPase inhibitor.

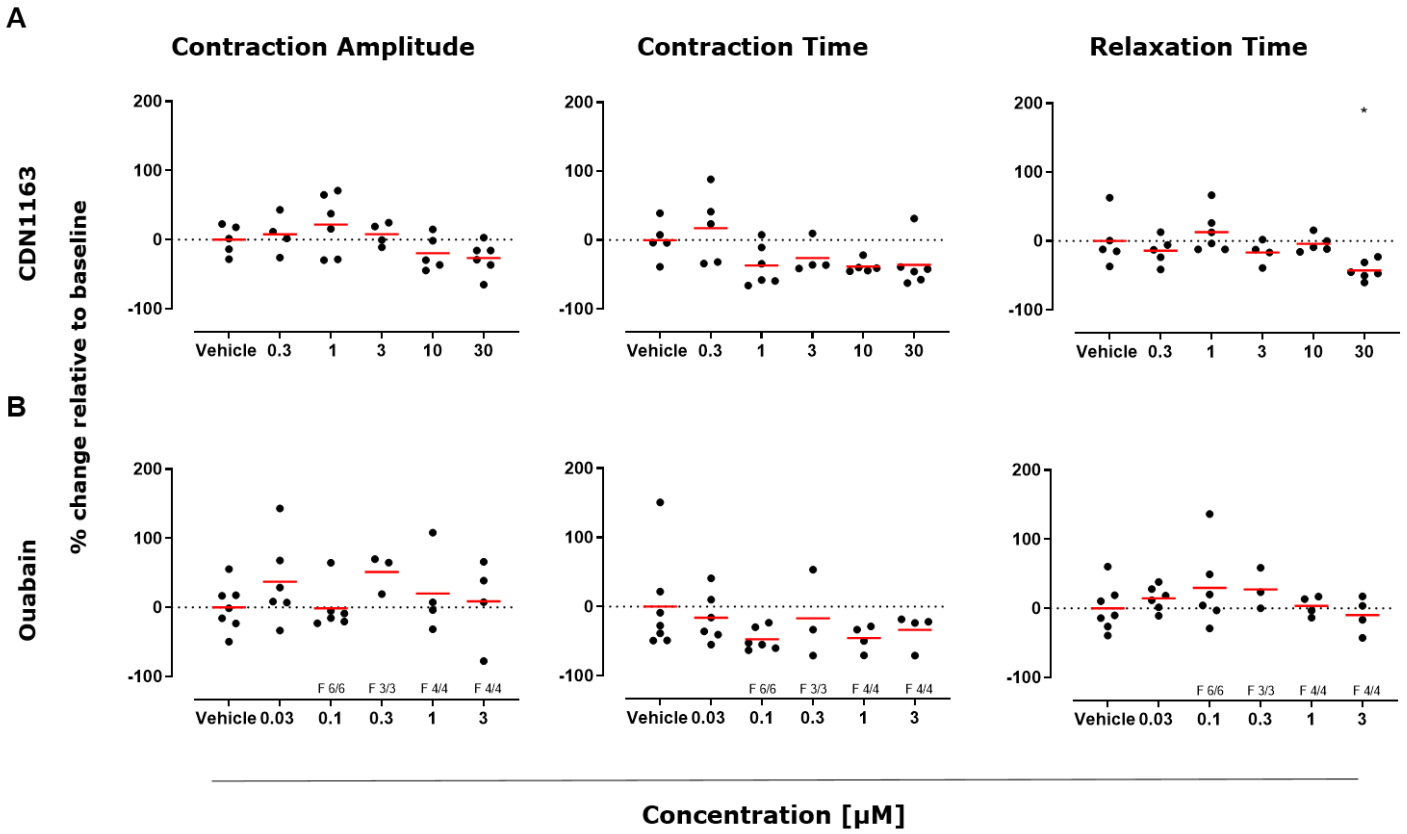

Figure 5-17. Contraction analysis of positive inotropes CDN1163 and ouabain on Pluricyte. Contractility measurement was carried out using the CO:Pluricytes platform-cell combination. CDN1163 displayed significant decrease in relaxation time at 30 μM, while there was no significant difference found in ouabain. Abbreviations: F, fibrillation. One-way ANOVA followed by Dunnett's multiple comparisons test vs vehicle control (p ⩽: * 0.05, ** 0.01, *** 0.001, **** 0.0001).

5.4 Discussion

After Tier 2 phase of testing up to 28 blinded compounds, efficient ways to improve the prediction of positive inotropic compounds were proposed. The first was to reduce spontaneous beating rates to <1 Hz, which can be achieved by modifying the culture medium and using pharmacological blockage with ivabradine. In previous study done on EHT (Mannhardt et al., 2016), this approach proved to unveil positive force-frequency relationship. The second is to increase the exposure time to ≥24h if no changes in inotropy are detected in the acute assay, in order to determine whether the drugs have a chronic effect. These approaches allowed a predictive accuracy of 85% in 2D monolayers and 93% in 3D EHTs.

During Crack-IT consortium meeting before unblinding process, analysis on EHT data during different stages of relaxation identified positive lusitropy for dobutamine (at 50% relaxation) and late relaxation deficit for ivabradine (at 80% relaxation). Furthermore, data on rank 14 were correctly predicted for omecamtiv mecarbil, due to the unusual response of increased contraction time (~40%) without prominent evidence for increased contraction amplitude (Malik et al., 2011). Therefore, applying pharmacological knowledge to drug responses in hiPSC-CMs is valuable to derive mechanistic information out of multi-parametric assessments.

Switching to protein-containing medium (RPMI-B27) enhanced the accuracy of predicting positive inotrope compounds on the CO:R-PAT platform from none to 75%. This indicates that the benefit outweigh the concerns of drug binding and batch-to-batch variations of protein ingredients. However, this approach could not be applied to electrophysiology measurement using voltage-sensitive dye (VSD), as experiment with FluoVolt™ in RPMI-B27 caused the dye to interact with protein on the medium, therefore reducing the signal-to-noise ratio. This means that recording of voltage and contraction traces could not be done sequentially on the same well.

Chronic exposure up to 1-7 days unveiled doxorubicin and sunitinib as negative inotrope compounds, which is consistent with clinical presence of cardiac toxicity over extended timescale and in line with previous study using tyrosine kinase inhibitors (Jacob et al., 2016). In experiment

performed on CO:R-PAT platform-cell combination during chronic exposure, the results demonstrated a trend of positive inotropy from 1-30 μM (increased contraction amplitude, decreased contraction time) but cell death at 10 μM. This is in line with previous study reporting the effects of doxorubicin, which is complex in that transient positive inotropy is followed by robust negative inotropy at higher concentrations (Wang and Korth, 1995, Vanboxtel et al., 1978, Kim et al., 1980). A study in isolated adult rat cardiomyocytes showed that reactive oxygen species (ROS) seem to be involved in doxorubicin cardiotoxicity by activating Ca/calmodulin dependent protein kinase II (CaMKII) through oxidation. CaMKII causes dysfunction in myocardium through the sarcoplasmic reticulum (SR) Ca^{2+} leakage. It was shown that inhibition on CaMKII partly reduced doxorubicin effects on diastolic SR Ca^{2+} leak (Sag et al., 2011). The mechanism of SR Ca^{2+} leak by doxorubicin is also shown on a study in guinea pig heart (Wang and Korth, 1995).

Based on the data derived from contractility measurements of hiPSC-CMs, it is suggested that contraction amplitude is informative for negative inotrope drugs in all cell-platforms combinations and for positive inotrope drugs in the 3D EHT platform. However, contraction time and relaxation time may be informative for positive inotrope drugs in the 2D systems. Possible explanations for this observation is the 2D systems are less adept at showing an increase in contraction amplitude (due to relying on cell movement instead of absolute contractile force), and a decrease in contraction time reflects an increase in rate of change of force (dF/dt), whilst a decrease in relaxation time also reflects an increase in -dF/dt. Another explanation is that, it may be a quirk of hiPSC-CMs as a model system whilst there are limitations and adaptations to be made.

Phenotypic characteristics/properties of the cells on the assay system need to be as translationally relevant as possible to mature cardiomyocytes. It was shown that in house cell line R-PAT and commercial cell lines iCell^2 and Pluricyte on 2D platform still exhibited rather immature phenotype as demonstrated by the ratio of atrial and ventricular subtype, as well as the distribution pattern of gap junction Cx43. The lack of maturation characteristics compared to EHT platform might explain the

better prediction of detecting positive inotrope compounds in the latter platform.

5.5 Conclusion

This study shows that hiPSC-CMs cultured in 2D and 3D still have considerable value in predictive safety pharmacology even with their current status of maturity below adult cardiomyocytes and technology evolution.

5.6 Maturating hiPSC-CMs in pseudo 3D microenvironment and/or chemical agents

In concurrent with Tier 1 phase, driving maturity of hiPSC-CMs is part of the Crack-IT InPulse Challenge. Attempts were made, including patterned substrates of synthetic polymers (polydimethylsiloxane; PDMS) from Nottingham site. However, the fabrication of patterned substrates in 96-well formats was challenging and time-limiting, therefore not accomplished in the timeframe of the InPulse Challenge. Furthermore, it was found that absorption of drugs into PDMS was variable and time dependent, and was not determined exclusively by hydrophobicity and therefore not easily predicted (van Meer et al., 2017). This was a concern when using a blinded drug panel.

In similar timeline with the fabrication of patterned substrates of PDMS, using aligned electrospun nanofiber scaffolds since the differentiation of hiPSC into cardiomyocytes were evaluated. Nanofiber scaffolds are composed of polymers that recapitulate the extracellular matrix (ECM) architecture, nanoscale topography, and bio-activity, allowing cellular integration and tissue formation. Electrospinning nanofiber scaffold is the most popular method for producing nanofiber scaffolds, which uses a high voltage to extrude polymer through an orifice that solidifies into nanofibers (Braghirolli et al., 2014). By this approach, scaffold characteristics such as fiber diameter, alignment, thickness, and porosity can be biomechanically tuned for specific tissue.

Aligned electrospun nanofiber scaffolds have been commonly used in studies for hPSC-CMs maturation, due to its capability of mimicking mechanical properties and anisotropy of the in vivo 3D microenvironment in heart (Lundy et al., 2014, Prabhakaran et al., 2014). Synthetic polymer widely used in electrospun nanofibers are poly(D,L-lactide-co-glycolide) (PLGA) that is nontoxic and biodegradable, yet have hydrophobic characteristic that have negative impact on cell adhesion (Prabhakaran et al., 2014). Therefore, a more hydrophilic, poly(ε-caprolactone) (PCL) nanofiber scaffolds has greater applications in hPSC-CMs (Kai et al., 2011, Han et al., 2016). This polymer has slow biodegradation rates.

Recent studies have shown that hPSC-CMs cultured on aligned nanofiber scaffolds had parallel alignment due to topographical guidance

(Han et al., 2016, Carson et al., 2016, Khan et al., 2015). Furthermore, hPSC-CMs on aligned nanofiber scaffolds had enhanced molecular maturation (shown by increased expression of *CASQ2* and *KCNJ2*), yet smaller amplitude and slower kinetics in intracellular calcium transient kinetics compared to standard 2D culture (Han et al., 2016). Therefore, maturation on hPSC-CMs on nanofiber scaffolds is currently still limited, and it is a long way to reach maturation level of adult cardiomyocytes *in vivo*.

Other approach on cardiomyocyte maturation strategy is by addition of chemical agents. Thyroid hormone, widely known to be involved in metabolism regulation, plays essential role during cardiac development (Forhead and Fowden, 2014). In human, triiodothyronine (T3) level only starts to increase after 30 weeks of gestation and by average of 40 weeks of gestation (at term) T3 level is more than three-fold compared to 30 weeks (Keung et al., 2014). In this study, T3 has been reported to upregulate numerous cardiac genes such as *SERCA*, *PLN*, *NCX* and potassium channels. *In vitro* studies have also demonstrated structural and functional maturation trends after T3 supplementation, with increased cell area, cell elongation, sarcomere length, Ca^{2+} handling and contractility (Keung et al., 2014, Yang et al., 2014b).

Glucocorticoid, a steroid hormone, is important for maturation of organs in postnatal life and its levels rise significantly shortly before birth (Rog-Zielinska et al., 2014). However, evidence of glucocorticoid involvement in heart maturation is less well known until study done on dexamethasone, a synthetic glucocorticoid, demonstrated to promote sarcomeric organisation and myofibril assembly in mouse; therefore, enhancing structural and functional maturation of foetal heart *in vivo* (Rog-Zielinska et al., 2014). Same author also revealed mechanism behind the glucocorticoid action in foetal heart maturation by identifying the role of PGC-1α, known to be regulator of cardiac mitochondrial capacity (Rog-Zielinska et al., 2015). Study using human embryonic stem cell derived cardiomyocytes (hESC-CMs) reported role of synthetic glucocorticoid (dexamethasone) in increasing contraction force, sarcomere length and calcium handling properties in respect of systolic Ca^{2+} transient decay,

however action potential and L-type calcium current properties were not affected (Kosmidis et al., 2015).

This study served the purpose by investigating the usage of aligned nanofiber scaffolds with combination of T3 or dexamethasone to enhance maturation of hPSC-CMs. During the CRACK-IT project meetings, it was decided that at least two hiPSC-CMs lines, the NCRM5 line (National Institutes of Health) and in-house ReBl-PAT (R-PAT; The University of Nottingham), would be used for drug testing. NCRM5 was chosen to provide a standardised cell line across the consortium and for easier comparison. R-PAT was chosen due to its routine use within the lab. For the reason of standardised cell line, NCRM5 was chosen in the study using aligned nanofiber scaffolds with addition of chemical agent. However, due to time limitation, only R-PAT to be taken forward for Tier 2 phase drug testing.

5.6.1 Structural features of hiPSC-CMs in aligned nanofiber scaffolds and chemical agent

To evaluate the role of aligned nanofiber scaffolds and chemical agent in inducing structural maturation of hiPSC-CMs, NCRM5 on both 2D platform and nanofiber were treated with dexamethasone as described in materials and method, before fixed and stained for sarcomeric protein α-actinin by immunocytochemistry and analysed for structural organisation of sarcomeres. NCRM5 on 2D platform and nanofiber without chemical treatment (untreated) served as control (***Figure 5-18***).

As shown in ***Figure 5-18***A, NCRM5 in 2D platform have characteristics of immature cardiomyocytes, with circular shape, random orientation, and disorganised sarcomere organisation and alignment. On the other hand, NCRM5 in nanofiber demonstrated a more mature cardiomyocyte phenotype, with elongated shape, anisotropic orientation parallel to the nanofiber. This is supported by the images derived from super resolution microscopy (***Figure 5-18***B), in which NCRM5 in 2D platform displayed chaotic organization compared to the one in nanofiber.

Furthermore, length-to-width ratio, or known as aspect ratio, was shown to be significantly higher compared to control ($p<0.0001$), reaching around 7:1 (6.56 ± 0.62 in untreated and 6.71 ± 0.35 in dexamethasone-

treated) which is similar to found in native adult cardiomyocytes (Gerdes, 2002). Treatment with dexamethasone on 2D platform seemed to enhance the sarcomeric organization, however it (2.76 ± 0.23) didn't give significant result in aspect ratio compared to control (2.07 ± 0.22) (***Figure 5-18***C).

Overall, results suggested that dexamethasone had no significant effect on increased aspect ratio, and nanofiber platform provide nanotopographical guidance for anisotropic orientation, rod shape, improved aspect ratio and sarcomere organisation, trending towards greater structural maturation compared to 2D culture. This is consistent with previous studies (Han et al., 2016, Khan et al., 2015), which investigated the effect of electrospun aligned nanofiber scaffolds on structural maturation of hPSC-CMs.

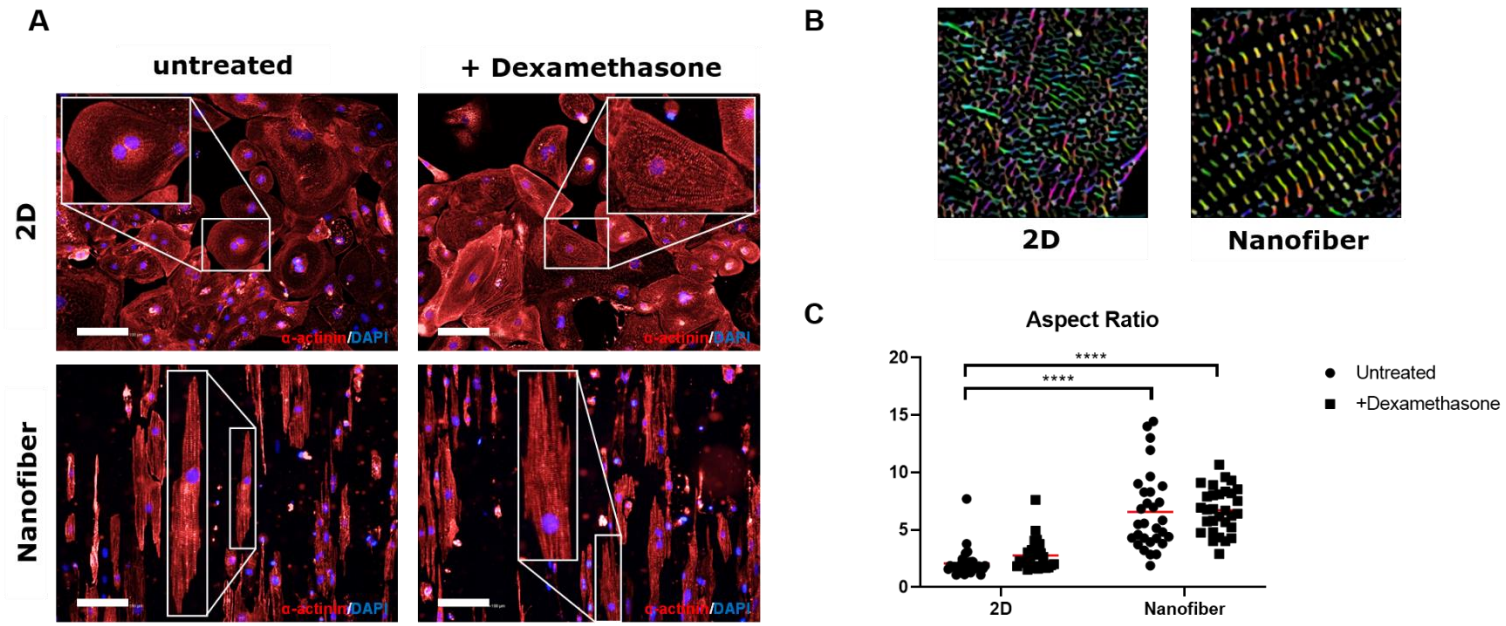

Figure 5-18. hiPSC-CMs on pseudo 3D nanofiber scaffolds displayed features of structural maturation. (A) hiPSC-CMs stained with α-actinin by immunocytochemistry on 2D platform showed immature phenotype, characterised by circular shape, random orientation and disorganised sarcomere structure. hiPSC-CMs on nanofiber displayed more mature phenotype by having rod-shape, anisotropic orientation parallel to the nanofiber, and highly organised sarcomere structure. Treatment with dexamethasone in 2D platform seemed to improve sarcomere organisation (upper right panel) but not so much in nanofiber with dexamethasone (bottom right panel). (B) Representative image of super resolution microscopy at 63x objective to demonstrate sarcomere organisation on 2D vs nanofiber platform. (C) hiPSC-CMs in nanofiber demonstrated significant higher aspect ratio compared to in 2D platform, with value reaching 7:1. Scale bar: 100 μm. Two-way ANOVA followed by Sidak's multiple comparisons test vs untreated ($p \leqslant$: * 0.05, ** 0.01, *** 0.001, **** 0.0001).

5.6.2 Ultrastructural features of hiPSC-CMs in aligned nanofiber scaffolds and chemical agent

Previous study on ultrastructural characteristics of hPSC-CMs have reported formation of M-band, indicative of structural maturation, after one year in 2D culture (Kamakura et al., 2013). In order to prepare the samples for assessing ultrastructural features, NCRM5 on 2D platform were harvested to be seeded in Thermanox™coverslips, while NCRM5 on nanofiber were seeded in nanofiber inserts (the equivalent shape coverslips but coated with nanofiber on top). This was followed by treatment with dexamethasone and T3 as described in materials and method, before NCRM5 were fixed and stained for transmission electron microscopy (TEM) imaging. NCRM5 on 2D platform and nanofiber without chemical treatment (untreated) served as control.

Results of NCRM5 (***Figure 5-19***) at 45-day differentiation on 2D platform on TEM imaging without chemical treatment demonstrated myofibrils, that lacked sufficient ultrastructural alignment (***Figure 5-19***A). In contrast, at 45 day NCRM5 on nanofiber without chemical treatment exhibited aligned myofibrils and highly organised sarcomeric pattern. Furthermore, distinct A- and I-bands were observed, with maturation representative H- bands being prevalent at ~45 days (***Figure 5-19***B). In addition, abundant mitochondria and lipid droplets were observed in ***Figure 5-19***C-D. Most strikingly, at ~120-day differentiation in NCRM5 on nanofiber without chemical treatment, in addition to prominent expression of A-, I-, and H- bands, M-bands started to be distinct ***Figure 5-19***E. There is no distinct feature found in NCRM5 treated with dexamethasone and T3, so results were not shown.

Therefore, in combination, results suggest that cardiomyocytes on 3D aligned nanofiber scaffolds were approaching maturation faster than those in 2D platform, as indicated by presence of M-bands, without the need of chemical agent addition.

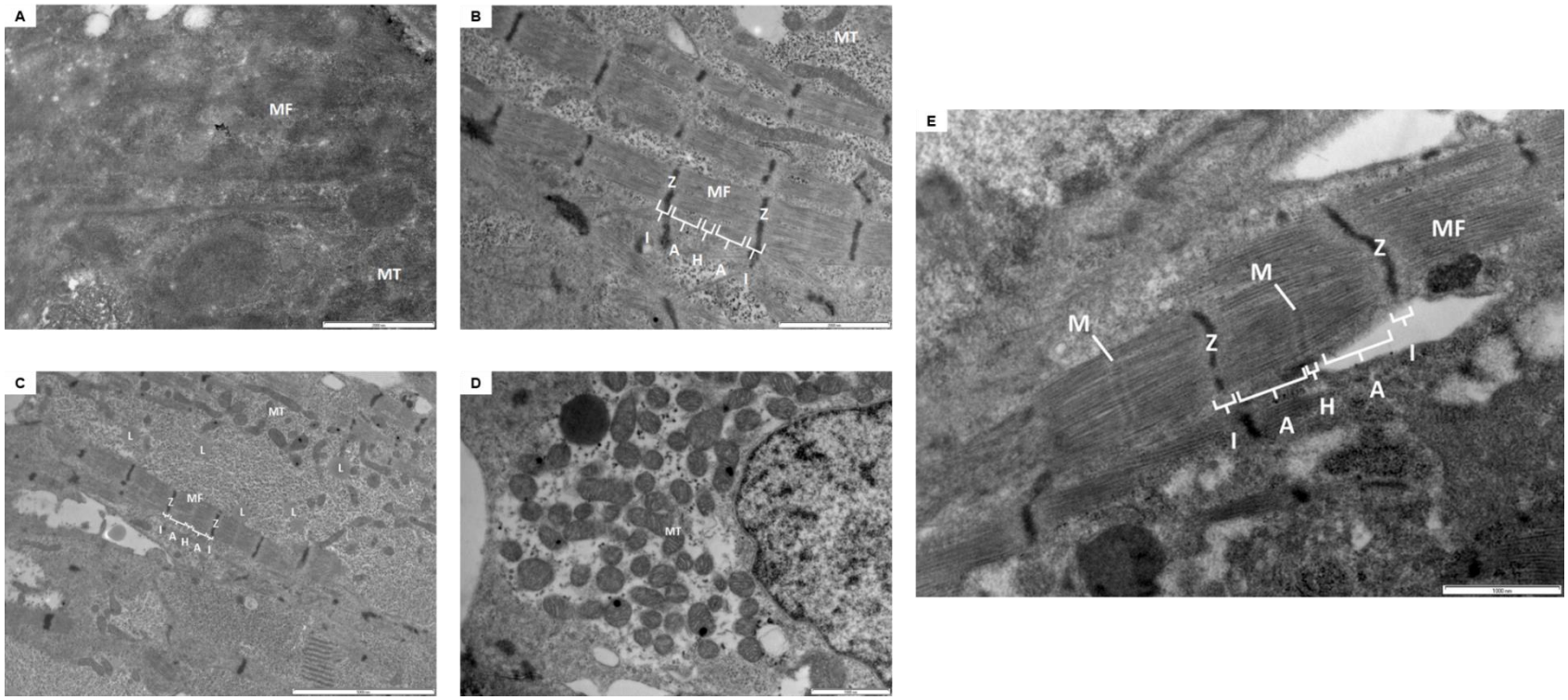

Figure 5-19. hiPSC-CMs on pseudo 3D nanofiber scaffolds displayed features of ultrastructural maturation. Transmission electron microscopy (TEM) imaging of hiPSC-CMs at 45 days (A-D) and ~ 4 months (E) after cardiac differentiation. (A) At 45 days NCRM5 on 2D platform showed disorganised sarcomeric pattern in myofibrils (MF) and few mitochondria (MT). (B) Instead, hiPSC-CMs on nanofiber showed discrete A-, I-, and H- bands between Z-bands in all myofibrils (MF). (C-D) Indication of higher metabolic activity in hiPSC-CMs on nanofiber at 45 days posti differentiation were represented by presence of lipid droplet (L) and abundant presence of mitochondria (MT). (E) At ~120 days hiPSC-CMs on nanofiber showed discrete A-, H-, I-, Z- and also M-bands, characteristic of maturation. Scale bar: (A-B) 2000 nm, (C) 5000 nm, (D-E) 1000 nm.

5.6.3 Electrophysiology analysis of hiPSC-CMs in aligned nanofiber scaffolds with chemical agent

To evaluate the role of pseudo 3D nanofiber scaffolds in improving functional maturation of hiPSC-CMs, NCRM5 on 2D platform and on nanofiber were treated with dexamethasone or T3 as described in materials and method, before subsequently analysed in CellOPTIQ® platform using voltage-sensitive dyes as detailed in materials and methods. NCRM5 on 2D platform and nanofiber without chemical treatment (untreated) served as control. Measurement to mimic drug testing was done by adding 0.1% DMSO for 30 minutes as 'treatment'. In order to distinguish the action potential (AP) phenotypes: atrial-like APs with a ratio (APD_{30-40}/APD_{70-80}) <1.5 (minimal plateau phase) and ventricular-like APs with a ratio >1.5 (distinct plateau phase) (Ma et al., 2011) were analysed in this study.

As shown in ***Figure 5-20***, electrophysiology analysis demonstrated the effect of chemical agent on hiPSC-CMs. Representative traces of NCRM5 on 2D platforms showed prolonged APD on cells treated with T3, whilst on nanofiber there was a shift in TRise to the right on cells treated with dexamethasone or T3 (***Figure 5-20***A). Interestingly, treatment with dexamethasone in NCRM5 on both 2D and nanofiber platform showed atrial subtype properties, as shown with RO index of <1.5 ($p<0.0001$) (***Figure 5-20***B).

Quantitative analysis showed significant increase in rise time (TRise) in NCRM5 treated with dexamethasone on 2D platform, and there was a trend decrease with T3 but it was shown to be not significant. There was significant increase in TRise in NCRM5 treated with dexamethasone or T3 on nanofiber (***Figure 5-20***C). Analysis on triangulation, APD_{30}, and APD_{90} all demonstrated significant increase on NCRM5 treated with T3 on 2D platform, while no significant difference found on nanofiber (***Figure 5-20***D-F).

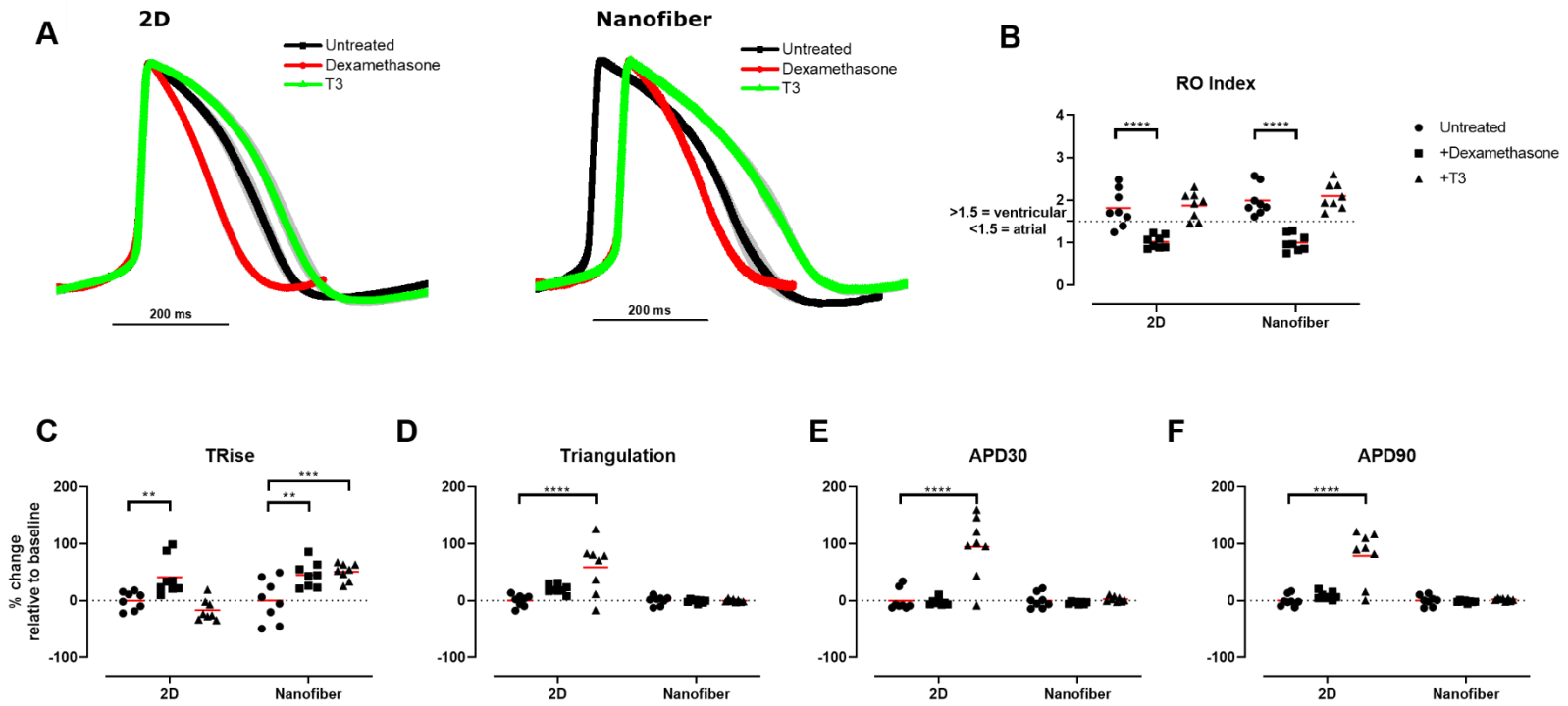

Figure 5-20. Electrophysiology analysis of hiPSC-CMs on 2D monolayers vs pseudo 3D platform with chemical agents. hiPSC-CMs were previously treated with dexamethasone or T3 before addition of 0.1% DMSO for 30 minutes to reflect the condition during compound testing. (A) Representative voltage traces after addition of 0.1% DMSO. (B) RO index showed atrial subtype for hiPSC-CMs treated with dexamethasone. (C) There was significant increase in TRise in hiPSC-CMs treated with dexamethasone on 2D platform, and significant increase in hiPSC-CMs treated with dexamethasone or T3 on nanofiber. (D-F) There was significant increase in triangulation, APD_{30} and APD_{90} in cells treated with T3 on 2D platform, but none on nanofiber. Two-way ANOVA followed by Dunnett's multiple comparisons test vs untreated ($p \leqslant$: * 0.05, ** 0.01, *** 0.001, **** 0.0001).

5.7 Discussion

This study proved the effect of pseudo 3D cell culture microenvironment using aligned nanofiber scaffolds in inducing structural maturation of hiPSC-CMs. As predicted, NCRM5 cardiomyocytes on pseudo 3D aligned nanofiber scaffolds had improved structural maturation by exhibiting anisotropic orientation, highly organised sarcomeric alignment, and high aspect ratio (~7:1) that is similar to adult cardiomyocytes (Gerdes, 2002), regardless of chemical agent treatment.

The presence of M-bands had only been detected in hPSC-CMs after prolonged time culture in 2D culture (Kamakura et al., 2013). Presence of M-bands was detected in NCRM5 cardiomyocytes on pseudo 3D aligned nanofiber scaffolds insert. To our knowledge, this is the first study using pseudo 3D aligned nanofiber scaffolds to report the presence of H-bands in hiPSC-CMs without external stimulation after just 45 days post differentiation induction. Kamakura et al., 2013 showed H-bands in cardiomyocytes over 90 days post differentiation. This is also the first study to demonstrate the presence of M-band at mere ~120 days old culture, far earlier than 360 days to develop M-bands as described in a previous study done by Kamakura et al., 2013. Furthermore, abundant mitochondria and lipid droplets are indication of increased mitochondrial oxidative capacity and fatty acid β-oxidation as main energy source found in adult cardiomyocytes (Robertson et al., 2013, Yang et al., 2014a). Recent study demonstrated presence of M-bands in hiPSC-CMs after 4 weeks of culture since spontaneous beating was observed; however, this was done under mechanical and electrical stimulation (Ronaldson-Bouchard et al., 2018).

However, electrophysiology analysis in this study showed the limitation of nanofiber platform. It was noted that during the experiment, NCRM5 on 2D platforms were as monolayer, whilst NCRM5 on nanofiber were more as patches. This is due to cells tend to form patches on nanofiber instead of forming monolayer despite higher seeding density compared to 2D platform.

Significant increase of APD in hiPSC-CMs treated with T3 and yet no effect with dexamethasone is consistent with data from previous study (Birket et al., 2015). Effect of dexamethasone on APD in previous study showed trend decrease but not significant, but it was after exposure of 72h

(Kosmidis et al., 2015) instead of in this study which had prolonged exposure of chemical agent. In summary, treatment of T3 is more effective to help induce maturation compared to with dexamethasone.

5.8 Conclusion

Although pseudo 3D cell culture microenvironment using aligned nanofiber scaffolds has proven to induce structural maturation of hiPSC-CMs, limitation in forming a monolayer which is crucial for functional (i.e. electrophysiology) analysis creates a hindrance in detecting the effect of compounds during drug testing.

6 General Discussion and Future Work

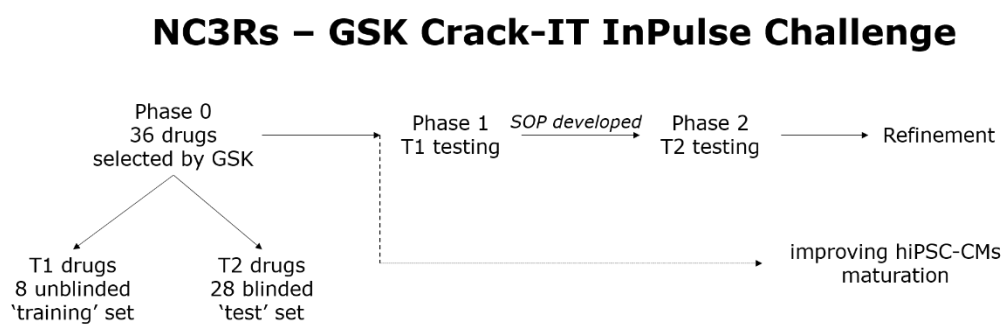

6.1 Synopsis

This study illustrated the ability of 3 technology platforms (TTM, CellOPTIQ®, and EHT) in evaluating responses of up to 36 drugs provided by GSK, which is divided into up to 8 Tier 1 unblinded 'training' drugs and up to 28 Tier 2 blinded 'test' drugs, in 2 configurations on hiPSC-CMs (2D monolayers and 3D EHTs). Initially, it was proposed that GSK would provide drugs that had made it part way through the pipeline or that were proprietary; however, this proved to be challenging through the GSK internal mechanism and/or not enough drugs were available. Therefore, the compounds were chosen on a rational way basis as described in the introduction of chapter 3.

The Tier 1 phase testing was used to: (1) unify standard operating procedures (SOP) including pacing regimes, drug incubation times, DMSO concentrations in vehicle controls and tests, and drug concentration test ranges; (2) establish data analysis using simplified contractility software (Sala et al., 2018) to unify the methods used in each platforms across academic partners; (3) set terminology to define the nature of the metrics calculated from electrophysiology, Ca^{2+} handling and contractility traces; and (4) act as the driver in choosing which functional parameters to be tested (i.e. contractility, Ca^{2+} handling and electrophysiology for the TTM system; contractility and electrophysiology for the CellOPTIQ®; contraction force and Ca^{2+} handling for the EHT platform).

The Tier 2 phase testing allowed an evaluation of the predictivity of the platforms based on compound's inotropic effect for *in vitro* setting. It

was shown that the 3D EHT system provided the highest level of reproducibility between data points and greatest accuracy in predicting outcome of drug effect (up to 85%), as well as greatest sensitivity.

Evaluation of the results from the Tier 2 phase testing showed that positive inotropes (PIs) were least well predicted by the hiPSC-CM model. Incorrect predictions were also noted for negative inotropes (Nis). Slowing beat rates using 0.3 μM ivabradine (I_f current blocker) showed to improve predictivity of previously incorrectly assigned PIs on both 2D platform CellOPTIQ® and EHT system. In particularly, on 2D platform CellOPTIQ®, switching from serum-free medium to protein-containing medium (RPMI-B27) combined with ivabradine had been demonstrated to reduce the level of 'noise' in the contractility data set, and therefore created greater consistency of baseline recordings, with spontaneous hiPSC-CM beat rates of 0.5-0.7 Hz, which could be paced at 0.7-1 Hz.

Chronic toxicity could not previously be detected due to the assay window, which was 30 minutes post compound addition. Prolonged exposure from 24 hours up to 8 days revealed detection of chronic toxicity. Optimisation showed that ivabradine didn't have impact on no effect drugs or negative inotropes; hence it could be included in all assays.

As the aim of CRACK-IT InPulse Challenge was "to generate a physiologically-relevant contractility platform with cells that are phenotypically 'mature', possess a robust contractile apparatus, move calcium between intracellular and extracellular spaces and metabolically generate substantive amounts of energy" (https://crackit.org.uk/challenge-13-inpulse), methods were evaluated, including on Nottingham site, to improve maturation of hiPSC-CMs. This ran concurrently with the Tier 1 phase testing. However, routine integration of maturation into the Crack-IT InPulse challenge was difficult. Use of patterned substrates of synthetic polymers were not ready by the time of standard operating procedure (SOP) for the Tier 2 phase testing was established. Meanwhile, use of pseudo 3D nanofiber scaffolds were proved to have limitation in reaching the monolayer state of hiSPC-CMs, which is crucial for the reading of CellOPTIQ® platform during drug testing. Overall, maturation project is an area that still requires work across the field.

6.1.1 Potential of 2D vs 3D platform for drug testing

Generally, there are two areas in which hiPSC-CMs could serve as a tool in preclinical drug development for therapeutic applications: (1) prediction of proarrhythmic adverse effect of compounds and (2) prediction of positive and negative inotropic compounds (del Alamo et al., 2016).

Advantages of using 2D platform for drug screening are: (1) simplicity, (2) lower cost, and (3) commercially available setups for analysis. However, there are several limitations in using 2D platform. In evaluating electrophysiology and Ca^{2+}-handling properties, previous studies revealed low sensitivity and specificity in predicting human QT effects (Abi-Gerges et al., 2017, Blinova et al., 2017), particularly on iCell cardiomyocytes, which led to development of iCell^2 cardiomyocytes. This cell line was included in recent study involving international blinded multisite comparison, revealing specificity of 0.89 and a sensitivity of 0.63 (Blinova et al., 2018).

Evaluating contractility function and inotropic responses on 2D platform is even more challenging. Measurement of contractile force on 2D platform is surrogated by using cell motion in video-optic-edge detection. A study revealed the limitation of screening on 2D platform by incorrectly predicted response of positive inotropic compounds, with the exception of the β-adrenergic agonists isoprenaline and epinephrine (Pointon et al., 2015). This was reasoned due to the immature phenotype of hiPSC-CMs. Approach on enhancing maturation such improvement of matrix, as found in Matrigel mattress (Feaster et al., 2015), had the contractile kinetics (i.e. time to peak and time to baseline) that were comparable to adult rabbit cardiomyocytes. Adult rabbit cardiomyocytes are a closer model of human cardiomyocytes as a representative example of positive force-frequency relationship (FFR), compared to mouse cardiomyocytes, which exhibit negative force-frequency relationship (Endoh, 2004, Bers, 2002). This Matrigel mattress approach demonstrated the expected positive and negative inotropic effects in a concentration-dependent manner as observed on EMD 570533 and verapamil, respectively (Feaster et al., 2015).

The advantages of using 3D platform for drug screening, in this case Engineered Heart Tissue (EHT), are: (1) providing a more physiological

environment, (2) allowing subjected to an increase in afterload, and (3) integrating the heterogeneous cells with low variability, thus being robust compared to single cells. Evaluation of several positive and negative inotropic compounds showed good reproducibility of concentration-dependent responses of peak force, contraction time, and relaxation time as described in previous study (Mannhardt et al., 2016). However, the 3D EHT system has several disadvantages: (1) larger costs by higher input of cells (1.0×10^6 human cells/EHT), (2) more challenging to generate hiPSC-CMs compared to 2D platforms due to differentiation efficiency which is hiPSC line-dependent, (3) needs to be kept in culture for minimum of 2 weeks before the first measurement, (4) only suitable for low to medium throughput, and (5) evaluating electrophysiology properties by action potential recording using sharp microelectrodes are technically demanding and require harsh conditions (Eder et al., 2016, Schaaf et al., 2011).

6.1.2 Impact of CRACK-IT InPulse Challenge on the 3Rs

The CRACK-IT InPulse Challenge brought reliability hiPSC-CMs as a tool. This study showed that the 2D system provided accuracy in prediction up to 70% and the 3D EHT system up to 85% during Tier 2 phase testing. However, with switching medium composition and/or the usage of ivabradine to improve positive force-frequency analysis, accuracy of the 2D system increased up to 85% and the 3D EHT system up to 93%.

This is a substantial improvement that compared favourably with *in vivo* animal model with accuracy of 78% (Bailey et al., 2014, Valentin et al., 2009). The increased accuracy after refined conditions in predicting drug-induced changes in contractility in this study are also comparable to non-blinded compound study using 3D cardiac microtissues consisting of hiPSC-CMs, cardiac endothelial cells, and cardiac fibroblasts, which provided 85% correctly predicted inotropes (Pointon et al., 2017).

The study also highlighted points on strengths and weaknesses of hiPSC-CMs as a model system. The refinements will improve future studies. Collectively, this study has led to greater validation of the hiPSC-CM model in cardiovascular safety testing.

6.2 Limitations and improvements

In this study, the isolated single rabbit cardiomyocytes used near-physiological rates of stimulation (2 Hz) and sub-physiological rates (1Hz and lower), that may have improved scope to detect PIs. Spontaneous diastolic sarcoplasmic reticulum (SR) Ca^{2+} release, which raise intracellular Ca^{2+}, was observed in adult rabbit cardiomyocytes in response to β-adrenoreceptor stimulation and drugs that raise cAMP directly. This is not reported in any of the hiPSC-CMs platform, due to minimal SR involvement in excitation-contraction coupling and instead is mainly mediated by L-type Ca^{2+} current, as seen in both hESC-CMs and hiPSC-CMs (Li et al., 2013).

Due to positive inotropic compounds being cardio-active drugs, the free therapeutic plasma concentrations (FTPC) might align with responses from hiPSC-CMs. This was clearly seen on the 3D EHT platform, where significant responses were within or in close range to the FTPC. However, the sensitivity of hiPSC-CMs on 2D platform and isolated single rabbit cardiomyocytes was considerably lower. It was reasoned that 2D monolayers were evaluated in unloaded conditions, whereas the 3D EHT platform had it under loaded conditions (Eder et al., 2016). This afterload condition facilitates maturation (Leonard et al., 2018) and the following Frank-Starling mechanism for force generation lead to higher basal tone and cAMP signaling (Uzun et al., 2016). Increased cAMP is an inotropic effect found in isoprenaline, epinephrine, forskolin, levosimendan, pimobendan, dobutamine, milrinone, and terbutaline; which most of all were able to be detected correctly in the 3D EHT system even before refined condition with the addition of ivabradine during contractility measurement.

Screening for drug-induced changes in contractility is useful to minimize the chances of a drug with liability to advance further into the later stages of drug discovery. The primary aim of using cardiomyocytes in contractility assay is for hazard detection (i.e. having contractility liability) and raising flags for follow-up studies to further explore potential liabilities, rather than cardiac risk evaluation (i.e. having an effect in human). In addition, *in vitro* contractility parameters (contraction amplitude, contraction time, and relaxation time) are not straightforwardly translated to predict clinical effects in patients.

It needs to be noted that the *in vitro* test system could not predict indirect mechanism as the cause of *in vivo* contractility effects. For example, a compound may affect cardiac contractility by also affecting the autonomic nervous system or antagonizing the endogenous hormone, neither of which is available in the *in vitro* contractility assay. For example, atenolol requires intact sympathetic innervation and is detected as a no effect drug in hiPSC-CMs instead of a negative inotrope in clinical setting (Lemoine et al., 1988, Kaumann and Blinks, 1980). Another example involving sympathetic neurons is clonidine, which is also detected as a no effect drug in hiSPC-CMs instead of a negative inotrope (Jarrott et al., 1979, Kleiber et al., 2017). Furthermore, a compound may have a metabolite, in which case both the parent and the metabolite need to be tested *in vitro*. In addition, compounds affecting cardiovascular haemodynamics, such as: (1) increasing vascular resistance and blood pressure may result in a compensatory decrease in contractility (Levine and Leenen, 1992), and (2) altering the preload or afterload of the heart will affect cardiac contractility via Frank-Starling mechanism.

Therefore, data from both *in vitro* and *in vivo* assay— in particular pharmacological profiling (e.g. L-type Ca^{2+} channel, β-adrenergic receptor), isolated heart, echocardiography, and left ventricular ejection fraction; are needed for integrated assessment of a compound's inotropic effects (Harmer et al., 2012, Guth et al., 2015). Wider range of drugs with more varied mechanism of action also need to be investigated for relevancy to *in vivo* cardiac physiology. Inclusion of auxiliary cell types, such as neural lineages to enable evaluation of drugs with mechanism of action involving neuro-hormonal system, will also benefit from predictive screening.

Integration of different cell types into the 2D and 3D cell configurations, including cardiomyocytes, fibroblasts, endothelial cells, and/or smooth muscle cells were initially planned in this study; however, it was proved to be too ambitious and complex and were instead continued outside of CRACK-IT (mixed cell architectures; presented by Christine Mummery at ISSCR 2018, Australia). Other issues that need to be considered are throughput, user variability, cell availability, cost and batch to batch variability.

6.3 Future perspectives

Over the past few year, hiPSC-CMs as a novel *in vitro* platform are becoming valuable for potential high-throughput screening and drug safety testing. They have been involved in advancing drugs into Phase I clinical testing (Reynolds et al., 2012) and in developing suitable treatment regimens for patients with complex LQTS (Terrenoire et al., 2013). Recently, hiPSC-CMs have been used in functional assessment of cardiotoxicity screening of cosmetic compounds (Chaudhari et al., 2018), showing the utility of hiPSC-CMs for safety evaluation in pharmaceutical-cosmetic industry.

Recently, a new technology was developed that enables quantification of cardiovascular waveform data by replotting into a 3-dimensional cube followed by rotation to extract triangle form, which is called an 'attractor' or 'cardiomorph' (Nandi et al., 2018, Aston et al., 2018). This method was made in mind for arterial blood pressure waveform data, but it can also be applied to ECG, pulse oximetry, respiratory impedance, and other waveforms that are approximately periodic (Charlton et al., 2015, Aston et al., 2018, Lyle et al., 2017). This includes contractility data in this study.

Preliminary results using sorafenib, a negative inotropic compound in Tier 2 phase testing which is an anti-cancer tyrosine kinase inhibitors (Henderson et al., 2013, Duran et al., 2014, Kim et al., 2013), showed a distinct shape of the triangle form compared to vehicle control (***Figure 6-1***). As explained by Dr. Manasi Nandi, "there is a one-to-one relationship between the waveform shape and the cardiomorph shape. Tiny changes in the shape of the waveform appear as much bigger changes on the cardiomorph."

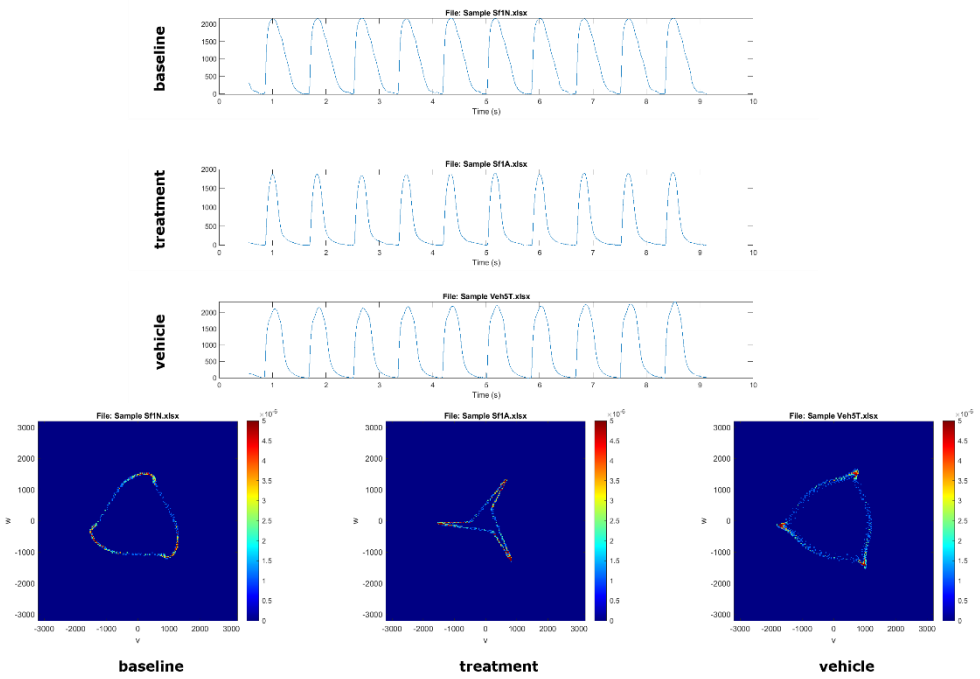

Figure 6-1. Preliminary result of cardiomorph analysis on sorafenib at 1 µM. The waveform extracted from contractility traces of hiPSC-CMs treated with sorafenib showed minimal change compared to its baseline and vehicle control, yet the cardiomorph shape of said condition showed the distinct shape of a "star", whilst the baseline and vehicle control showed a rounder shape.

Collectively, this new technology can help visualize and quantify the inotropic effect of the compounds and therefore could uncover its potential utility in predicting a clinically-relevant detrimental effect on the heart.

6.4 Final remarks

Drug development involves high burden on resource and cost so that even modest improvements in the drug development pipeline could have large socioeconomic and 3R benefits. An annual total cost of $11.3Bn is due for more than 6000 putative medicines in preclinical development using millions of animals, and so reducing drug attrition in Phase 1 clinical trials by 5% could reduce costs by 5.5-7.1%, with each percentile reduction equates to ~$100M.

This study shows that hiPSC-CMs both in 2D and 3D platform can be used in up to high throughput primary screens and discovery work, even with current limitations. A perfect hiPSC-CMs system is unrealistic and it is important to play to the strength and adapt to the limitations, in particular of immature phenotypes. Further improvements and validation studies in a blinded manner will facilitate uptake of hiPSC-CMs as a routine tool in safety pharmacology.

References

AASS, H., SKOMEDAL, T. & OSNES, J. B. 1988. INCREASE OF CYCLIC-AMP IN SUBCELLULAR-FRACTIONS OF RAT-HEART MUSCLE AFTER BETA-ADRENERGIC STIMULATION - PRENALTEROL AND ISOPRENALINE CAUSED DIFFERENT DISTRIBUTION OF BOUND CYCLIC-AMP. *Journal of Molecular and Cellular Cardiology,* 20**,** 847-860.

ABI-GERGES, N., POINTON, A., OLDMAN, K. L., BROWN, M. R., PILLING, M. A., SEFTON, C. E., GARSIDE, H. & POLLARD, C. E. 2017. Assessment of extracellular field potential and Ca2+ transient signals for early QT/pro arrhythmia detection using human induced pluripotent stem cell-derived cardiomyocytes. *Journal of Pharmacological and Toxicological Methods,* 83**,** 1-15.

ABI-GERGES, N., POINTON, A., PULLEN, G. F., MORTON, M. J., OLDMAN, K. L., ARMSTRONG, D., VALENTIN, J. P. & POLLARD, C. E. 2013. Preservation of cardiomyocytes from the adult heart. *Journal of Molecular and Cellular Cardiology,* 64**,** 108-119.

ALLINGHAM, J. S., SMITH, R. & RAYMENT, I. 2005. The structural basis of blebbistatin inhibition and specificity for myosin II. *Nature Structural & Molecular Biology,* 12**,** 378-379.

ANGST, B. D., KHAN, L. U. R., SEVERS, N. J., WHITELY, K., ROTHERY, S., THOMPSON, R. P., MAGEE, A. I. & GOURDIE, R. G. 1997. Dissociated spatial patterning of gap junctions and cell adhesion junctions during postnatal differentiation of ventricular myocardium. *Circulation Research,* 80**,** 88-94.

ANGUS, J., SARSERO, D., FUJIWARA, T., MOLENAAR, P. & XI, Q. 2000. Quantitative analysis of vascular to cardiac selectivity of L- and T-type voltage-operated calcium channel antagonists in human tissues. *Clinical and Experimental Pharmacology and Physiology,* 27**,** 1019-1021.

APRIGLIANO, O., RYBIN, V. O., PAK, E., ROBINSON, R. B. & STEINBERG, S. F. 1997. beta 1-and beta 2-adrenergic receptors exhibit differing susceptibility to muscarinic accentuated antagonism. *The American journal of physiology,* 272**,** H2726-35.

ARCHER, C. R., SARGEANT, R., BASAK, J., PILLING, J., BARNES, J. R. & POINTON, A. 2018. Characterization and Validation of a Human 3D Cardiac Microtissue for the Assessment of Changes in Cardiac Pathology. *Scientific reports,* 8**,** 10160.

ASAKURA, K., HAYASHI, S., OJIMA, A., TANIGUCHI, T., MIYAMOTO, N., NAKAMORI, C., NAGASAWA, C., KITAMURA, T., OSADA, T., HONDA, Y., KASAI, C., ANDO, H., KANDA, Y., SEKINO, Y. & SAWADA, K. 2015. Improvement of acquisition and analysis methods in multi-electrode array experiments with iPS cell-derived cardiomyocytes. *Journal of Pharmacological and Toxicological Methods,* 75**,** 17-26.

ASTON, P. J., CHRISTIE, M. I., HUANG, Y. H. & NANDI, M. 2018. Beyond HRV: attractor reconstruction using the entire cardiovascular waveform data for novel feature extraction. *Physiological Measurement,* 39**,** 32.

AURSNES, I., OSNES, J.-B., TVETE, I., GÅSEMYR, J. & NATVIG, B. 2007. Does atenolol differ from other β-adrenergic blockers? 7**,** 4.

BAILEY, J., THEW, M. & BALLS, M. 2014. An Analysis of the Use of Animal Models in Predicting Human Toxicology and Drug Safety. *Atla-Alternatives to Laboratory Animals,* 42**,** 181-199.

BAILEY, J. M., LEVY, J. H., KIKURA, M., SZLAM, F. & HUG, C. C. 1994. PHARMACOKINETICS OF INTRAVENOUS MILRINONE IN PATIENTS UNDERGOING CARDIAC-SURGERY. *Anesthesiology,* 81**,** 616-622.

BAKER, L. C. 2004. Effects of mechanical uncouplers, diacetyl monoxime, and cytochalasin-D on the electrophysiology of perfused mouse hearts. 287**,** H1771-H1779.

BARSTOW, C. & MCDIVITT, J. D. 2017. Cardiovascular Disease Update: Bradyarrhythmias. *FP essentials,* 454**,** 18-23.

BAUDET, S., SHAOULIAN, R. & BERS, D. M. 1993. EFFECTS OF THAPSIGARGIN AND CYCLOPIAZONIC ACID ON TWITCH FORCE AND SARCOPLASMIC-RETICULUM CA-2+ CONTENT OF RABBIT VENTRICULAR MUSCLE. *Circulation Research,* 73**,** 813-819.

BEDUT, S., SEMINATORE-NOLE, C., LAMAMY, V., CAIGNARD, S., BOUTIN, J. A., NOSJEAN, O., STEPHAN, J. P. & COGE, F. 2016. High-throughput drug profiling with voltage- and calcium-sensitive fluorescent probes in human iPSC-derived cardiomyocytes. *American Journal of Physiology-Heart and Circulatory Physiology,* 311**,** H44-H53.

BELLMANN, R. 2007. Clinical pharmacokinetics of systemically administered antimycotics. *Current clinical pharmacology,* 2**,** 37-58.
BELLO, C. L., SHERMAN, L., ZHOU, J. H., VERKH, L., SMERAGLIA, J., MOUNT, J. & KLAMERUS, K. J. 2006. Effect of food on the pharmacokinetics of sunitinib malate (SU11248), a multi-targeted receptor tyrosine kinase inhibitor: results from a phase I study in healthy subjects. *Anti-Cancer Drugs,* 17**,** 353-358.
BERGER, C., MEYER, W., SCHOLZ, H. & STARBATTY, J. 1985. EFFECTS OF THE BENZIMIDAZOLE DERIVATIVES PIMOBENDAN AND 2-(4-HYDROXY-PHENYL)-5-(5-METHYL-3-OXO-4,5-DIHYDRO-2H-6-PYRIDAZINYL) BENZIMIDAZOLE . HCL ON PHOSPHODIESTERASE ACTIVITY AND FORCE OF CONTRACTION IN GUINEA-PIG HEARTS. *Arzneimittel-Forschung/Drug Research,* 35-2**,** 1668-&.
BERGMANN, O., BHARDWAJ, R. D., BERNARD, S., ZDUNEK, S., BARNABE-HEIDER, F., WALSH, S., ZUPICICH, J., ALKASS, K., BUCHHOLZ, B. A., DRUID, H., JOVINGE, S. & FRISEN, J. 2009. Evidence for Cardiomyocyte Renewal in Humans. *Science,* 324**,** 98-102.
BERS, D. M. 2002. Cardiac excitation-contraction coupling. *Nature,* 415**,** 198-205.
BERS, D. M. 2006. Altered Cardiac Myocyte Ca Regulation In Heart Failure. *Physiology,* 21**,** 380-387.
BERS, D. M. 2008. Calcium Cycling and Signaling in Cardiac Myocytes. *Annual Review of Physiology,* 70**,** 23-49.
BERS, D. M., POGWIZD, S. M. & SCHLOTTHAUER, K. 2002. Upregulated Na/Ca exchange is involved in both contractile dysfunction and arrhythmogenesis in heart failure. *Basic Research in Cardiology,* 97**,** 1-1.
BIEL, M., WAHL-SCHOTT, C., MICHALAKIS, S. & ZONG, X. 2009. Hyperpolarization-activated cation channels: from genes to function. *Physiological reviews,* 89**,** 847-85.
BIRKET, M. J., RIBEIRO, M. C., KOSMIDIS, G., WARD, D., LEITOGUINHO, A. R., VAN DE POL, V., DAMBROT, C., DEVALLA, H. D., DAVIS, R. P., MASTROBERARDINO, P. G., ATSMA, D. E., PASSIER, R. & MUMMERY, C. L. 2015. Contractile Defect Caused by Mutation in MYBPC3 Revealed under Conditions Optimized for Human PSC-Cardiomyocyte Function. *Cell Reports,* 13**,** 733-745.
BLABER, M. 2001. *Skeletal Muscle Myosin and Muscle Contraction* [Online]. Available: http://www.mikeblaber.org/oldwine/BCH4053/Lecture31/Lecture31.htm [Accessed].
BLINOVA, K., DANG, Q. Y., MILLARD, D., SMITH, G., PIERSON, J., GUO, L., BROCK, M., LU, H. R., KRAUSHAAR, U., ZENG, H. Y., SHI, H., ZHANG, X. Y., SAWADA, K., OSADA, T., KANDA, Y., SEKINO, Y., PANG, L., FEASTER, T. K., KETTENHOFEN, R., STOCKBRIDGE, N., STRAUSS, D. G. & GINTANT, G. 2018. International Multisite Study of Human-Induced Pluripotent Stem Cell-Derived Cardiomyocytes for Drug Proarrhythmic Potential Assessment. *Cell Reports,* 24**,** 3582-3592.
BLINOVA, K., STOHLMAN, J., VICENTE, J., CHAN, D., JOHANNESEN, L., HORTIGON-VINAGRE, M. P., ZAMORA, V., SMITH, G., CRUMB, W. J., PANG, L., LYN-COOK, B., ROSS, J., BROCK, M., CHVATAL, S., MILLARD, D., GALEOTTI, L., STOCKBRIDGE, N. & STRAUSS, D. G. 2017. Comprehensive Translational Assessment of Human-Induced Pluripotent Stem Cell Derived Cardiomyocytes for Evaluating Drug-Induced Arrhythmias. *Toxicological Sciences,* 155**,** 234-247.
BOIS, P., BESCOND, J., RENAUDON, B. & LENFANT, J. 1996. Mode of action of bradycardic agent, S 16257, on ionic currents of rabbit sinoatrial node cells. *British Journal of Pharmacology,* 118**,** 1051-1057.
BOKNIK, P., NEUMANN, J., KASPAREIT, G., SCHMITZ, W., SCHOLZ, H., VAHLENSIECK, U. & ZIMMERMANN, N. 1997. Mechanisms of the contractile effects of levosimendan in the mammalian heart. *Journal of Pharmacology and Experimental Therapeutics,* 280**,** 277-283.
BOLDT, A., GERGS, U., PONICKE, K., SIMM, A., SILBER, R. E. & NEUMANN, J. 2010. Inotropic Effects of Ivabradine in the Mammalian Heart. *Pharmacology,* 86**,** 249-258.
BOT, C. T., JUHASZ, K., HAEUSERMANN, F., POLONCHUK, L., TRAEBERT, M. & STOELZLE-FEIX, S. 2018. Cross - site comparison of excitation-contraction coupling using impedance and field potential recordings in hiPSC cardiomyocytes. *Journal of pharmacological and toxicological methods,* 93**,** 46-58.
BOUDOU, T., LEGANT, W. R., MU, A. B., BOROCHIN, M. A., THAVANDIRAN, N., RADISIC, M., ZANDSTRA, P. W., EPSTEIN, J. A., MARGULIES, K. B. & CHEN, C. S. 2012. A Microfabricated Platform to Measure and Manipulate the Mechanics of Engineered Cardiac Microtissues. *Tissue Engineering Part A,* 18**,** 910-919.

BOWERS, S. L. K., BANERJEE, I. & BAUDINO, T. A. 2010. The extracellular matrix: At the center of it all. *Journal of Molecular and Cellular Cardiology,* 48**,** 474-482.
BOYLE, K. L. & LEECH, E. 2012. A review of the pharmacology and clinical uses of pimobendan. *Journal of veterinary emergency and critical care (San Antonio, Tex. : 2001),* 22**,** 398-408.
BRAAM, S. R., TERTOOLEN, L., VAN DE STOLPE, A., MEYER, T., PASSIER, R. & MUMMERY, C. L. 2010. Prediction of drug-induced cardiotoxicity using human embryonic stem cell-derived cardiomyocytes. *Stem Cell Research,* 4**,** 107-116.
BRACK, K. E., NARANG, R., WINTER, J. & NG, G. A. 2013. The mechanical uncoupler blebbistatin is associated with significant electrophysiological effects in the isolated rabbit heart. *Experimental Physiology,* 98**,** 1009-1027.
BRAGHIROLLI, D. I., STEFFENS, D. & PRANKE, P. 2014. Electrospinning for regenerative medicine: a review of the main topics. *Drug Discovery Today,* 19**,** 743-753.
BRECKWOLDT, K., LETUFFE-BRENIERE, D., MANNHARDT, I., SCHULZE, T., ULMER, B., WERNER, T., BENZIN, A., KLAMPE, B., REINSCH, M. C., LAUFER, S., SHIBAMIYA, A., PRONDZYNSKI, M., MEARINI, G., SCHADE, D., FUCHS, S., NEUBER, C., KRAMER, E., SALEEM, U., SCHULZE, M. L., RODRIGUEZ, M. L., ESCHENHAGEN, T. & HANSEN, A. 2017. Differentiation of cardiomyocytes and generation of human engineered heart tissue. *Nature Protocols,* 12**,** 1177-1197.
BRETTE, F. & ORCHARD, C. 2003. T-tubule function in mammalian cardiac myocytes. *Circulation Research,* 92**,** 1182-1192.
BRISTOW, M. R. 1993. Pathophysiologic and pharmacologic rationales for clinical management of chronic heart failure with beta-blocking agents. *The American journal of cardiology,* 71**,** 12C-22C.
BRISTOW, M. R., GINSBURG, R., STROSBERG, A., MONTGOMERY, W. & MINOBE, W. 1984. PHARMACOLOGY AND INOTROPIC POTENTIAL OF FORSKOLIN IN THE HUMAN-HEART. *Journal of Clinical Investigation,* 74**,** 212-223.
BRISTOW, M. R., MINOBE, W., RASMUSSEN, R., HERSHBERGER, R. E. & HOFFMAN, B. B. 1988. ALPHA-1 ADRENERGIC-RECEPTORS IN THE NONFAILING AND FAILING HUMAN-HEART. *Journal of Pharmacology and Experimental Therapeutics,* 247**,** 1039-1045.
BRIXIUS, K., REICKE, S., REUTER, H. & SCHWINGER, R. H. G. 2002. Effects of the Ca2+ sensitizers EMD 57033 and CGP 48506 on myocardial contractility and Ca2+ transients in human ventricular and atrial myocardium. *Zeitschrift für Kardiologie,* 91**,** 312-318.
BRODDE, O. E. 1993. Beta-adrenoceptors in cardiac disease. *Pharmacology & therapeutics,* 60**,** 405-30.
BRODDE, O. E., BROEDE, A., DAUL, A., KUNDE, K. & MICHEL, M. C. 1992. Receptor systems in the non-failing human heart. *Basic research in cardiology,* 87 Suppl 1**,** 1-14.
BROWN, L., NABAUER, M. & ERDMANN, E. 1986. THE POSITIVE INOTROPIC RESPONSE TO MILRINONE IN ISOLATED HUMAN AND GUINEA-PIG MYOCARDIUM. *Naunyn-Schmiedebergs Archives of Pharmacology,* 334**,** 196-201.
BROWN, L., NABAUER, M. & ERDMANN, E. 1987. DOBUTAMINE - POSITIVE INOTROPY BY NONSELECTIVE ADRENOCEPTOR AGONISM IN ISOLATED GUINEA-PIG AND HUMAN MYOCARDIUM. *Naunyn-Schmiedebergs Archives of Pharmacology,* 335**,** 385-390.
BROWN, R. D., WILSON, J. T., KEARNS, G. L., EICHLER, V. F., JOHNSON, V. A. & BERTRAND, K. M. 1992. SINGLE-DOSE PHARMACOKINETICS OF IBUPROFEN AND ACETAMINOPHEN IN FEBRILE CHILDREN. *Journal of Clinical Pharmacology,* 32**,** 231-241.
BUTLER, L., CROS, C., OLDMAN, K. L., HARMER, A. R., POINTON, A., POLLARD, C. E. & ABI-GERGES, N. 2015. Enhanced Characterization of Contractility in Cardiomyocytes During Early Drug Safety Assessment. *Toxicological Sciences,* 145**,** 396-406.
CAPULLI, A. K., MACQUEEN, L. A., SHEEHY, S. P. & PARKER, K. K. 2016. Fibrous scaffolds for building hearts and heart parts. *Advanced drug delivery reviews,* 96**,** 83-102.
CARDIAC ARRHYTHMIA SUPPR TIAL, I. 1989. PRELIMINARY REPORT EFFECT OF ENCAINIDE AND FLECAINIDE ON MORTALITY IN A RANDOMIZED TRIAL OF ARRHYTHMIA SUPPRESSION AFTER MYOCARDIAL INFARCTION. *New England Journal of Medicine,* 321**,** 406-412.
CARSON, D., HNILOVA, M., YANG, X., NEMETH, C. L., TSUI, J. H., SMITH, A. S. T., JIAO, A., REGNIER, M., MURRY, C. E., TAMERLER, C. & KIM, D.-H. 2016. Nanotopography-Induced Structural Anisotropy and Sarcomere Development in Human Cardiomyocytes Derived from Induced Pluripotent Stem Cells. *ACS Appl Mater Interfaces,* 8**,** 21923-32.

CATAPULT. 2018. *State of the Discovery Nation 2018 and the role of the Medicines Discovery Catapult* [Online]. BioIndustry Association and Medicines Discovery Catapult. Available: https://s3-eu-west-1.amazonaws.com/media.newmd.catapult/wp-content/uploads/2018/01/16220811/MDC10529-Thought-Leader_v10_Interactive_v1.pdf [Accessed 2019].

CHABAN, R., KORNBERGER, A., BRANSKI, N., BUSCHMANN, K., STUMPF, N., BEIRAS-FERNANDEZ, A. & VAHL, C. F. 2017. In-vitro examination of the positive inotropic effect of caffeine and taurine, the two most frequent active ingredients of energy drinks. *Bmc Cardiovascular Disorders,* 17**,** 8.

CHARLTON, P. H., CAMPOROTA, L., SMITH, J., NANDI, M., CHRISTIE, M., ASTON, P. J., BEALE, R. & IEEE. 2015. MEASUREMENT OF CARDIOVASCULAR STATE USING ATTRACTOR RECONSTRUCTION ANALYSIS. 23rd European Signal Processing Conference (EUSIPCO), 2015

Aug 31-Sep 04 2015 Nice, FRANCE. 444-448.

CHAUDHARI, U., NEMADE, H., SURESHKUMAR, P., VINKEN, M., ATES, G., ROGIERS, V., HESCHELER, J., HENGSTLER, J. G. & SACHINIDIS, A. 2018. Functional cardiotoxicity assessment of cosmetic compounds using human-induced pluripotent stem cell-derived cardiomyocytes. *Archives of Toxicology,* 92**,** 371-381.

CHEEK, T. R., MORETON, R. B., BERRIDGE, M. J., STAUDERMAN, K. A., MURAWSKY, M. M. & BOOTMAN, M. D. 1993. QUANTAL CA2+ RELEASE FROM CAFFEINE-SENSITIVE STORES IN ADRENAL CHROMAFFIN CELLS. *Journal of Biological Chemistry,* 268**,** 27076-27083.

CHEN, L., EL-SHERIF, N. & BOUTJDIR, M. 1999. Unitary current analysis of L-type Ca2+ channels in human fetal ventricular myocytes. *Journal of Cardiovascular Electrophysiology,* 10**,** 692-700.

CHEN, V. C., YE, J. J., SHUKLA, P., HUA, G., CHEN, D. L., LIN, Z. G., LIU, J. C., CHAI, J., GOLD, J., WU, J., HSU, D. & COUTURE, L. A. 2015. Development of a scalable suspension culture for cardiac differentiation from human pluripotent stem cells. *Stem Cell Research,* 15**,** 365-375.

CHOI, H. Y., BAE, K. S., CHO, S. H., GHIM, J. L., CHOE, S., JUNG, J. A. & LIM, H. S. 2016. Population plasma and urine pharmacokinetics of ivabradine and its active metabolite S18982 in healthy Korean volunteers. *Journal of Clinical Pharmacology,* 56**,** 439-449.

CHONG, J. J. H. & MURRY, C. E. 2014. Cardiac regeneration using pluripotent stem cells-Progression to large animal models. *Stem Cell Research,* 13**,** 654-665.

CHONG, J. J. H., YANG, X. L., DON, C. W., MINAMI, E., LIU, Y. W., WEYERS, J. J., MAHONEY, W. M., VAN BIBER, B., COOK, S. M., PALPANT, N. J., GANTZ, J. A., FUGATE, J. A., MUSKHELI, V., GOUGH, G. M., VOGEL, K. W., ASTLEY, C. A., HOTCHKISS, C. E., BALDESSARI, A., PABON, L., REINECKE, H., GILL, E. A., NELSON, V., KIEM, H. P., LAFLAMME, M. A. & MURRY, C. E. 2014. Human embryonic-stem-cell-derived cardiomyocytesregenerate non-humanprimate hearts. *Nature,* 510**,** 273-+.

CHU, K. M., SHIEH, S. M. & HU, O. Y. P. 1995. PHARMACOKINETICS AND PHARMACODYNAMICS OF ENANTIOMERS OF PIMOBENDAN IN PATIENTS WITH DILATED CARDIOMYOPATHY AND CONGESTIVE-HEART-FAILURE AFTER SINGLE AND REPEATED ORAL DOSING. *Clinical Pharmacology & Therapeutics,* 57**,** 610-621.

CLELAND, J. G. F., TEERLINK, J. R., SENIOR, R., NIFONTOV, E. M., MC MURRAY, J. J. V., LANG, C. C., TSYRLIN, V. A., GREENBERG, B. H., MAYET, J., FRANCIS, D. P., SHABURISHVILI, T., MONAGHAN, M., SALTZBERG, M., NEYSES, L., WASSERMAN, S. M., LEE, J. H., SAIKALI, K. G., CLARKE, C. P., GOLDMAN, J. H., WOLFF, A. A. & MALIK, F. I. 2011. The effects of the cardiac myosin activator, omecamtiv mecarbil, on cardiac function in systolic heart failure: a double-blind, placebo-controlled, crossover, dose-ranging phase 2 trial. *Lancet,* 378**,** 676-683.

CORDA, S., SAMUEL, J. L. & RAPPAPORT, L. 2000. Extracellular matrix and growth factors during heart growth. *Heart failure reviews,* 5**,** 119-30.

CORNEA, R. L., GRUBER, S. J., LOCKAMY, E. L., MURETTA, J. M., JIN, D. Z., CHEN, J. Q., DAHL, R., BARTFAI, T., ZSEBO, K. M., GILLISPIE, G. D. & THOMAS, D. D. 2013. High-Throughput FRET Assay Yields Allosteric SERCA Activators. *Journal of Biomolecular Screening,* 18**,** 97-107.

COSTANTINE, M. M., CLEARY, K., HEBERT, M. F., AHMED, M. S., BROWN, L. M., REN, Z. X., EASTERLING, T. R., HAAS, D. M., HANELINE, L. S., CARITIS, S. N., VENKATARAMANAN, R., WEST, H., D'ALTON, M., HANKINS, G. & EUNICE KENNEDY SHRIVER NATL INST, C. 2016. Safety and pharmacokinetics of pravastatin used for

the prevention of preeclampsia in high-risk pregnant women: a pilot randomized controlled trial. *American Journal of Obstetrics and Gynecology,* 214**,** 17.
CUFFE, M. S., CALIFF, R. M., ADAMS, K. F., JR., BENZA, R., BOURGE, R., COLUCCI, W. S., MASSIE, B. M., O'CONNOR, C. M., PINA, I., QUIGG, R., SILVER, M. A., GHEORGHIADE, M. & OUTCOMES OF A PROSPECTIVE TRIAL OF INTRAVENOUS MILRINONE FOR EXACERBATIONS OF CHRONIC HEART FAILURE, I. 2002. Short-term intravenous milrinone for acute exacerbation of chronic heart failure: a randomized controlled trial. *Jama,* 287**,** 1541-7.
CYGANEK, L., TIBURCY, M., SEKERES, K., GERSTENBERG, K., BOHNENBERGER, H., LENZ, C., HENZE, S., STAUSKE, M., SALINAS, G., ZIMMERMANN, W. H., HASENFUSS, G. & GUAN, K. M. 2018. Deep phenotyping of human induced pluripotent stem cell-derived atrial and ventricular cardiomyocytes. *Jci Insight,* 3**,** 17.
DANESI, R., CONTE, P. F. & DEL TACCA, M. 1999. Pharmacokinetic optimisation of treatment schedules for anthracyclines and paclitaxel in patients with cancer. *Clinical Pharmacokinetics,* 37**,** 195-211.
DAVIS, R. P., VAN DEN BERG, C. W., CASINI, S., BRAAM, S. R. & MUMMERY, C. L. 2011. Pluripotent stem cell models of cardiac disease and their implication for drug discovery and development. *Trends in Molecular Medicine,* 17**,** 475-484.
DE ZEEUW, S., TRINES, S., KRAMS, R., DUNCKER, D. J. & VERDOUW, P. D. 2000. In vivo evidence that EMD 57033 restores myocardial responsiveness to intracoronary Ca2+ in stunned myocardium. *European Journal of Pharmacology,* 403**,** 99-109.
DEL ALAMO, J. C., LEMONS, D., SERRANO, R., SAVCHENKO, A., CERIGNOLI, F., BODMER, R. & MERCOLA, M. 2016. High throughput physiological screening of iPSC-derived cardiomyocytes for drug development. *Biochimica Et Biophysica Acta-Molecular Cell Research,* 1863**,** 1717-1727.
DEL ROSARIO, M. E., WEACHTER, R. & FLAKER, G. C. 2010. Drug-induced QT prolongation and sudden death. *Missouri medicine,* 107**,** 53-8.
DELANEY, A., BRADFORD, C., MCCAFFREY, J., BAGSHAW, S. M. & LEE, R. 2010. Levosimendan for the treatment of acute severe heart failure: a meta-analysis of randomised controlled trials. *International journal of cardiology,* 138**,** 281-9.
DEMASI, M. 2018. Statin wars: have we been misled about the evidence? A narrative review. *British journal of sports medicine,* 52**,** 905-909.
DEMIDOVA, M. M., SMITH, J. G., HOIJER, C. J., HOLMQVIST, F., ERLINGE, D. & PLATONOV, P. G. 2012. Prognostic impact of early ventricular fibrillation in patients with ST-elevation myocardial infarction treated with primary PCI. 1**,** 302-311.
DEMPSEY, G. T., CHAUDHARY, K. W., ATWATER, N., NGUYEN, C., BROWN, B. S., MCNEISH, J. D., COHEN, A. E. & KRALJ, J. M. 2016. Cardiotoxicity screening with simultaneous optogenetic pacing, voltage imaging and calcium imaging. *Journal of pharmacological and toxicological methods,* 81**,** 240-50.
DENNING, C., BORGDORFF, V., CRUTCHLEY, J., FIRTH, K. S. A., GEORGE, V., KALRA, S., KONDRASHOV, A., HOANG, M. D., MOSQUEIRA, D., PATEL, A., PRODANOV, L., RAJAMOHAN, D., SKARNES, W. C., SMITH, J. G. W. & YOUNG, L. E. 2016. Cardiomyocytes from human pluripotent stem cells: From laboratory curiosity to industrial biomedical platform. *Biochimica Et Biophysica Acta-Molecular Cell Research,* 1863**,** 1728-1748.
DEVALLA, H. D., SCHWACH, V., FORD, J. W., MILNES, J. T., EL-HAOU, S., JACKSON, C., GKATZIS, K., ELLIOTT, D. A., LOPES, S., MUMMERY, C. L., VERKERK, A. O. & PASSIER, R. 2015. Atrial-like cardiomyocytes from human pluripotent stem cells are a robust preclinical model for assessing atrial-selective pharmacology. *Embo Molecular Medicine,* 7**,** 394-410.
DIFRANCESCO, D. 2006. Funny channels in the control of cardiac rhythm and mode of action of selective blockers. *Pharmacological Research,* 53**,** 399-406.
DIGITALIS INVESTIGATION, G. 1997. The effect of digoxin on mortality and morbidity in patients with heart failure. *The New England journal of medicine,* 336**,** 525-33.
DOEVENDANS, P. A., DAEMEN, M. J., DE MUINCK, E. D. & SMITS, J. F. 1998. Cardiovascular phenotyping in mice. *Cardiovascular Research,* 39**,** 34-49.
DOLNIKOV, K., SHILKRUT, M., ZEEVI-LEVIN, N., GERECHT-NIR, S., AMIT, M., DANON, A., ITSKOVITZ-ELDOR, J. & BINAH, O. 2006. Functional properties of human embryonic stem cell-derived cardiomyocytes: Intracellular Ca2+ handling and the role of sarcoplasmic reticulum in the contraction. *Stem Cells,* 24**,** 236-245.
DOU, Y., ARLOCK, P. & ARNER, A. 2007. Blebbistatin specifically inhibits actin-myosin interaction in mouse cardiac muscle. *American Journal of Physiology-Cell Physiology,* 293**,** C1148-C1153.

DURAN, J. M., MAKAREWICH, C. A., TRAPPANESE, D., GROSS, P., HUSAIN, S., DUNN, J., LAL, H., SHARP, T. E., STAROSTA, T., VAGNOZZI, R. J., BERRETTA, R. M., BARBE, M., YU, D. H., GAO, E., KUBO, H., FORCE, T. & HOUSER, S. R. 2014. Sorafenib Cardiotoxicity Increases Mortality After Myocardial Infarction. *Circulation Research,* 114**,** 1700-+.

DYREBORG, A., KROGH, N., BACKER, V., RZEPPA, S., HEMMERSBACH, P. & HOSTRUP, M. 2016. Pharmacokinetics of Oral and Inhaled Terbutaline after Exercise in Trained Men. *Frontiers in Pharmacology,* 7**,** 10.

EDER, A., VOLLERT, I., HANSEN, A. & ESCHENHAGEN, T. 2016. Human engineered heart tissue as a model system for drug testing. *Advanced Drug Delivery Reviews,* 96**,** 214-224.

ENDOH, M. 2004. Force-frequency relationship in intact mammalian ventricular myocardium: physiological and pathophysiological relevance. *European Journal of Pharmacology,* 500**,** 73-86.

ERDINE, S. & ARI, O. 2006. ESH-ESC Guidelines for the Management of Hypertension. 31**,** 331-338.

ESCHENHAGEN, T. 2013. PDE4 in the human heart - major player or little helper? *British journal of pharmacology,* 169**,** 524-7.

ESCHENHAGEN, T., MUMMERY, C. & KNOLLMANN, B. C. 2015. Modelling sarcomeric cardiomyopathies in the dish: from human heart samples to iPSC cardiomyocytes. *Cardiovascular Research,* 105**,** 424-438.

FABIATO, A. 1983. CALCIUM-INDUCED RELEASE OF CALCIUM FROM THE CARDIAC SARCOPLASMIC-RETICULUM. *American Journal of Physiology,* 245**,** C1-C14.

FARMAN, G. P., TACHAMPA, K., MATEJA, R., CAZORLA, O., LACAMPAGNE, A. & DE TOMBE, P. P. 2008. Blebbistatin: use as inhibitor of muscle contraction. 455**,** 995-1005.

FEASTER, T. K., CADAR, A. G., WANG, L. L., WILLIAMS, C. H., CHUN, Y. W., HEMPEL, J. E., BLOODWORTH, N., MERRYMAN, W. D., LIM, C. C., WU, J. C., KNOLLMANN, B. C. & HONG, C. C. 2015. Matrigel Mattress A Method for the Generation of Single Contracting Human-Induced Pluripotent Stem Cell-Derived Cardiomyocytes. *Circulation Research,* 117**,** 995-+.

FEDOROV, V. V., LOZINSKY, I. T., SOSUNOV, E. A., ANYUKHOVSKY, E. P., ROSEN, M. R., BALKE, C. W. & EFIMOV, I. R. 2007. Application of blebbistatin as an excitation–contraction uncoupler for electrophysiologic study of rat and rabbit hearts. *Heart Rhythm,* 4**,** 619-626.

FEDOROV, V. V., SHARIFOV, O. F., PYATAKOVA, O. P., BELOSHAPKO, G. G., YUSHMANOVA, A. V. & ROSENSHTRAUKH, L. V. 2002. Effects of ryanodine receptors block on spontaneous initiation of atrial fibrillation in the intact canine heart. *Kardiologiya,* 42**,** 59-71.

FELDMAN, A. M. 1993. Modulation of adrenergic receptors and G-transduction proteins in failing human ventricular myocardium. *Circulation,* 87**,** IV27-34.

FERMINI, B., HANCOX, J. C., ABI-GERGES, N., BRIDGLAND-TAYLOR, M., CHAUDHARY, K. W., COLATSKY, T., CORRELL, K., CRUMB, W., DAMIANO, B., ERDEMLI, G., GINTANT, G., IMREDY, J., KOERNER, J., KRAMER, J., LEVESQUE, P., LI, Z., LINDQVIST, A., OBEJERO-PAZ, C. A., RAMPE, D., SAWADA, K., STRAUSS, D. G. & VANDENBERG, J. I. 2016. A New Perspective in the Field of Cardiac Safety Testing through the Comprehensive In Vitro Proarrhythmia Assay Paradigm. *Journal of biomolecular screening,* 21**,** 1-11.

FLEISCHER, S. & DVIR, T. 2013. Tissue engineering on the nanoscale: lessons from the heart. *Current Opinion in Biotechnology,* 24**,** 664-671.

FLUCHER, B. E., TAKEKURA, H. & FRANZINIARMSTRONG, C. 1993. DEVELOPMENT OF THE EXCITATION-CONTRACTION COUPLING APPARATUS IN SKELETAL-MUSCLE - ASSOCIATION OF SARCOPLASMIC-RETICULUM AND TRANSVERSE TUBULES WITH MYOFIBRILS. *Developmental Biology,* 160**,** 135-147.

FOOD AND DRUG ADMINISTRATION, H. H. S. 2001. International Conference on Harmonisation; guidance on S7A safety pharmacology studies for human pharmaceuticals; availability. Notice. *Federal register,* 66**,** 36791-2.

FOOD AND DRUG ADMINISTRATION, H. H. S. 2005a. International Conference on Harmonisation; guidance on E14 Clinical Evaluation of QT/QTc Interval Prolongation and Proarrhythmic Potential for Non-Antiarrhythmic Drugs; availability. Notice. *Federal register,* 70**,** 61134-5.

FOOD AND DRUG ADMINISTRATION, H. H. S. 2005b. International Conference on Harmonisation; guidance on S7B Nonclinical Evaluation of the Potential for Delayed Ventricular Repolarization (QT Interval Prolongation) by Human Pharmaceuticals; availability. Notice. *Federal register,* 70**,** 61133-4.

FORHEAD, A. J. & FOWDEN, A. L. 2014. Thyroid hormones in fetal growth and prepartum maturation. *Journal of Endocrinology,* 221**,** R87-R103.
FORSBERG, T. & LINDBOM, L. O. 1983. CARDIOVASCULAR EFFECTS OF ZIMELIDINE AND TRICYCLIC ANTI-DEPRESSANTS IN CONSCIOUS RATS. *Acta Pharmacologica Et Toxicologica,* 53**,** 223-229.
FRANCIS, G. S., BARTOS, J. A. & ADATYA, S. 2014. Inotropes. *Journal of the American College of Cardiology,* 63**,** 2069-2078.
FRANCO, D., LAMERS, W. H. & MOORMAN, A. F. M. 1998. Patterns of expression in the developing myocardium: towards a morphologically integrated transcriptional model. *Cardiovascular Research,* 38**,** 25-53.
FUENTES, A. V., PINEDA, M. D. & VENKATA, K. C. N. 2018. Comprehension of Top 200 Prescribed Drugs in the US as a Resource for Pharmacy Teaching, Training and Practice. *Pharmacy,* 6**,** 10.
FUJINO, K., SPERELAKIS, N. & SOLARO, R. J. 1988. Sensitization of dog and guinea pig heart myofilaments to Ca2+ activation and the inotropic effect of pimobendan: comparison with milrinone. 63**,** 911-922.
FULLER, B. J. 2004. Cryoprotectants: The essential antifreezes to protect life in the frozen state. *Cryoletters,* 25**,** 375-388.
GARG, P., GARG, V., SHRESTHA, R., SANGUINETTI, M. C., KAMP, T. J. & WU, J. C. 2018. Human Induced Pluripotent Stem Cell-Derived Cardiomyocytes as Models for Cardiac Channelopathies: A Primer for Non-Electrophysiologists. *Circulation research,* 123**,** 224-243.
GERDES, A. M. 2002. Cardiac myocyte remodeling in hypertrophy and progression to failure. *Journal of Cardiac Failure,* 8**,** S264-S268.
GERDES, A. M. & CAPASSO, J. M. 1995. STRUCTURAL REMODELING AND MECHANICAL DYSFUNCTION OF CARDIAC MYOCYTES IN HEART-FAILURE. *Journal of Molecular and Cellular Cardiology,* 27**,** 849-856.
GERDES, A. M., KELLERMAN, S. E., MOORE, J. A., MUFFLY, K. E., CLARK, L. C., REAVES, P. Y., MALEC, K. B., MCKEOWN, P. P. & SCHOCKEN, D. D. 1992. STRUCTURAL REMODELING OF CARDIAC MYOCYTES IN PATIENTS WITH ISCHEMIC CARDIOMYOPATHY. *Circulation,* 86**,** 426-430.
GERDES, A. M., ONODERA, T., TAMURA, T., SAID, S., BOHLMEYER, T. J., ABRAHAM, W. T. & BRISTOW, M. R. 1998. New method to evaluate myocyte remodeling from formalin-fixed biopsy and autopsy material. *Journal of cardiac failure,* 4**,** 343-8.
GERMANGUZ, I., SEDAN, O., ZEEVI-LEVIN, N., SHTRICHMAN, R., BARAK, E., ZISKIND, A., ELIYAHU, S., MEIRY, G., AMIT, M., ITSKOVITZ-ELDOR, J. & BINAH, O. 2011. Molecular characterization and functional properties of cardiomyocytes derived from human inducible pluripotent stem cells. *Journal of Cellular and Molecular Medicine,* 15**,** 38-51.
GHEORGHIADE, M., ST. CLAIR, J., ST. CLAIR, C. & BELLER, G. A. 1987. Hemodynamic effects of intravenous digoxin in patients with severe heart failure initially treated with diuretics and vasodilators. 9**,** 849-857.
GHERGHICEANU, M., BARAD, L., NOVAK, A., REITER, I., ITSKOVITZ-ELDOR, J., BINAH, O. & POPESCU, L. M. 2011. Cardiomyocytes derived from human embryonic and induced pluripotent stem cells: comparative ultrastructure. *Journal of Cellular and Molecular Medicine,* 15**,** 2539-2551.
GIACOMINI, K. M., MASSOUD, N., WONG, F. M. & GIACOMINI, J. C. 1984. DECREASED BINDING OF VERAPAMIL TO PLASMA-PROTEINS IN PATIENTS WITH LIVER-DISEASE. *Journal of Cardiovascular Pharmacology,* 6**,** 924-928.
GILBERT, E. M., OLSEN, S. L., RENLUND, D. G. & BRISTOW, M. R. 1993. beta-adrenergic receptor regulation and left ventricular function in idiopathic dilated cardiomyopathy. *The American journal of cardiology,* 71**,** 23C-29C.
GINTANT, G. 2011. An evaluation of hERG current assay performance: Translating preclinical safety studies to clinical QT prolongation. *Pharmacology & therapeutics,* 129**,** 109-19.
GINTANT, G., BURRIDGE, P., GEPSTEIN, L., HARDING, S., HERRON, T., HONG, C., JALIFE, J. & WU, J. C. 2019. Use of Human Induced Pluripotent Stem Cell-Derived Cardiomyocytes in Preclinical Cancer Drug Cardiotoxicity Testing: A Scientific Statement From the American Heart Association. *Circulation research,* 125**,** e75-e92.
GIOVANNITTI, J. A., THOMS, S. M. & CRAWFORD, J. J. 2015. Alpha-2 Adrenergic Receptor Agonists: A Review of Current Clinical Applications. *Anesthesia Progress,* 62**,** 31-38.

GIUDICELLI, J. F., RICHER, C. & MATTEI, A. 1987. PHARMACOKINETICS AND BIOLOGICAL EFFECTS OF CAPTOPRIL AND HYDROCHLOROTHIAZIDE AFTER ACUTE AND CHRONIC ADMINISTRATION EITHER ALONE OR IN COMBINATION IN HYPERTENSIVE PATIENTS. *British Journal of Clinical Pharmacology,* 23**,** S51-S61.

GIVERTZ, M. M., ANDREOU, C., CONRAD, C. H. & COLUCCI, W. S. 2007. Direct Myocardial Effects of Levosimendan in Humans With Left Ventricular Dysfunction. *Circulation,* 115**,** 1218-1224.

GOINEAU, S. & CASTAGNE, V. 2018. Electrophysiological characteristics and pharmacological sensitivity of two lines of human induced pluripotent stem cell derived cardiomyocytes coming from two different suppliers. *Journal of Pharmacological and Toxicological Methods,* 90**,** 58-66.

GORDON, A. C., PERKINS, G. D., SINGER, M., MCAULEY, D. F., ORME, R. M. L., SANTHAKUMARAN, S., MASON, A. J., CROSS, M., AL-BEIDH, F., BEST-LANE, J., BREALEY, D., NUTT, C. L., MCNAMEE, J. J., RESCHREITER, H., BREEN, A., LIU, K. D. & ASHBY, D. 2016. Levosimendan for the Prevention of Acute Organ Dysfunction in Sepsis. *New England Journal of Medicine,* 375**,** 1638-1648.

GORDON, A. M., HOMSHER, E. & REGNIER, M. 2000. Regulation of contraction in striated muscle. *Physiological Reviews,* 80**,** 853-924.

GROSBERG, A., NESMITH, A. P., GOSS, J. A., BRIGHAM, M. D., MCCAIN, M. L. & PARKER, K. K. 2012. Muscle on a chip: In vitro contractility assays for smooth and striated muscle. *Journal of Pharmacological and Toxicological Methods,* 65**,** 126-135.

GRUBER, S. J., CORNEA, R. L., LI, J., PETERSON, K. C., SCHAAF, T. M., GILLISPIE, G. D., DAHL, R., ZSEBO, K. M., ROBIA, S. L. & THOMAS, D. D. 2014. Discovery of Enzyme Modulators via High-Throughput Time-Resolved FRET in Living Cells. *Journal of Biomolecular Screening,* 19**,** 215-222.

GUELLICH, A., MEHEL, H. & FISCHMEISTER, R. 2014. Cyclic AMP synthesis and hydrolysis in the normal and failing heart. *Pflugers Archiv : European journal of physiology,* 466**,** 1163-75.

GUHA, K., ALLEN, C. J., HARTLEY, A. & SHARMA, R. 2016. Ivabradine: A Current Overview. *Current clinical pharmacology,* 11**,** 241-249.

GUI, P. C., CHAO, J. T., WU, X., YANG, Y., DAVIS, G. E. & DAVIS, M. J. 2010. Coordinated Regulation of Vascular Ca2+ and K+ Channels by Integrin Signaling. *In:* BECCHETTI, A. & ARCANGELI, A. (eds.) *Integrins and Ion Channels: Molecular Complexes and Signaling.* Berlin: Springer-Verlag Berlin.

GUO, L., DONG, Z. & GUTHRIE, H. 2009. Validation of a guinea pig Langendorff heart model for assessing potential cardiovascular liability of drug candidates. *Journal of Pharmacological and Toxicological Methods,* 60**,** 130-151.

GUO, L., QIAN, J. Y., ABRAMS, R., TANG, H. M., WEISER, T., SANDERS, M. J. & KOLAJA, K. L. 2011. The Electrophysiological Effects of Cardiac Glycosides in Human iPSC-derived Cardiomyocytes and in Guinea Pig Isolated Hearts. *Cellular Physiology and Biochemistry,* 27**,** 453-462.

GUTH, B. D., CHIANG, A. Y., DOYLE, J., ENGWALL, M. J., GUILLON, J. M., HOFFMANN, P., KOERNER, J., MITTELSTADT, S., OTTINGER, S., PIERSON, J. B., PUGSLEY, M. K., ROSSMAN, E. I., WALISSER, J. & SARAZAN, D. 2015. The evaluation of drug-induced changes in cardiac inotropy in dogs: Results from a HESI-sponsored consortium. *Journal of Pharmacological and Toxicological Methods,* 75**,** 70-90.

GYORKE, S., STEVENS, S. C. W. & TERENTYEV, D. 2009. Cardiac calsequestrin: quest inside the SR. *Journal of Physiology-London,* 587**,** 3091-3094.

HAJJAR, R. J., DISALVO, T. G., SCHMIDT, U., THAIYANANTHAN, G., SEMIGRAN, M. J., DEC, G. W. & GWATHMEY, J. K. 1997. Clinical correlates of the myocardial force-frequency relationship in patients with end-stage heart failure. *Journal of Heart and Lung Transplantation,* 16**,** 1157-1167.

HAN, J. J., WU, Q. L., XIA, Y. N., WAGNER, M. B. & XU, C. H. 2016. Cell alignment induced by anisotropic electrospun fibrous scaffolds alone has limited effect on cardiomyocyte maturation. *Stem Cell Research,* 16**,** 735-745.

HANDORF, A. M., ZHOU, Y., HALANSKI, M. A. & LI, W.-J. 2015. Tissue Stiffness Dictates Development, Homeostasis, and Disease Progression. *Organogenesis,* 11**,** 1-15.

HANSEN, A., EDER, A., BONSTRUP, M., FLATO, M., MEWE, M., SCHAAF, S., AKSEHIRLIOGLU, B., SCHWORER, A., UEBELER, J. & ESCHENHAGEN, T. 2010. Development of a Drug Screening Platform Based on Engineered Heart Tissue. *Circulation Research,* 107**,** 35-U70.

HARMER, A. R., ABI-GERGES, N., MORTON, M. J., PULLEN, G. F., VALENTIN, J. P. & POLLARD, C. E. 2012. Validation of an in vitro contractility assay using canine ventricular myocytes. *Toxicology and Applied Pharmacology,* 260**,** 162-172.

HARRIS, K., AYLOTT, M., CUI, Y., LOUTTIT, J. B., MCMAHON, N. C. & SRIDHAR, A. 2013. Comparison of Electrophysiological Data From Human-Induced Pluripotent Stem CellDerived Cardiomyocytes to Functional Preclinical Safety Assays. *Toxicological Sciences,* 134**,** 412-426.

HARTMAN, M. E., DAI, D.-F. & LAFLAMME, M. A. 2016. Human pluripotent stem cells: Prospects and challenges as a source of cardiomyocytes for in vitro modeling and cell-based cardiac repair. *Advanced drug delivery reviews,* 96**,** 3-17.

HARVEY, R. D. & HELL, J. W. 2013. Ca(V)1.2 signaling complexes in the heart. *Journal of Molecular and Cellular Cardiology,* 58**,** 143-152.

HASENFUSS, G., HOLUBARSCH, C., HERMANN, H. P., ASTHEIMER, K., PIESKE, B. & JUST, H. 1994. Influence of the force-frequency relationship on haemodynamics and left ventricular function in patients with non-failing hearts and in patients with dilated cardiomyopathy. *European heart journal,* 15**,** 164-70.

HASENFUSS, G. & PIESKE, B. 2002. Calcium cycling in congestive heart failure. *Journal of molecular and cellular cardiology,* 34**,** 951-69.

HASENFUSS, G., PIESKE, B., CASTELL, M., KRETSCHMANN, B., MAIER, L. S. & JUST, H. 1998. Influence of the novel inotropic agent levosimendan on isometric tension and calcium cycling in failing human myocardium. *Circulation,* 98**,** 2141-2147.

HASENFUSS, G. & TEERLINK, J. R. 2011. Cardiac inotropes: current agents and future directions. *European Heart Journal,* 32**,** 1838-1845.

HEAD, S. A., SHI, W., ZHAO, L., GORSHKOV, K., PASUNOOTI, K., CHEN, Y., DENG, Z. Y., LI, R. J., SHIM, J. S., TANG, W. Z., HARTUNG, T., ZHANG, J., ZHAO, Y. M., COLOMBINI, M. & LIU, J. O. 2015. Antifungal drug itraconazole targets VDAC1 to modulate the AMPK/mTOR signaling axis in endothelial cells. *Proceedings of the National Academy of Sciences of the United States of America,* 112**,** E7276-E7285.

HENDERSON, K. A., BORDERS, R. B., ROSS, J. B., HUWAR, T. B., TRAVIS, C. O., WOOD, B. J., MA, Z. X. J., HONG, S. P., VINCI, T. M. & ROCHE, B. M. 2013. Effects of tyrosine kinase inhibitors on rat isolated heart function and protein biomarkers indicative of toxicity. *Journal of Pharmacological and Toxicological Methods,* 68**,** 150-159.

HERRON, T. J., DA ROCHA, A. M., CAMPBELL, K. F., PONCE-BALBUENA, D., WILLIS, B. C., GUERRERO-SERNA, G., LIU, Q. H., KLOS, M., MUSA, H., ZARZOSO, M., BIZY, A., FURNESS, J., ANUMONWO, J., MIRONOV, S. & JALIFE, J. 2016. Extracellular Matrix-Mediated Maturation of Human Pluripotent Stem Cell-Derived Cardiac Monolayer Structure and Electrophysiological Function. *Circulation-Arrhythmia and Electrophysiology,* 9**,** 12.

HERRON, T. J., LEE, P. & JALIFE, J. 2012. Optical Imaging of Voltage and Calcium in Cardiac Cells & Tissues. *Circulation Research,* 110**,** 609-623.

HIRT, M. N., BOEDDINGHAUS, J., MITCHELL, A., SCHAAF, S., BOERNCHEN, C., MUELLER, C., SCHULZ, H., HUBNER, N., STENZIG, J., STOEHR, A., NEUBER, C., EDER, A., LUTHER, P. K., HANSEN, A. & ESCHENHAGEN, T. 2014. Functional improvement and maturation of rat and human engineered heart tissue by chronic electrical stimulation. *Journal of Molecular and Cellular Cardiology,* 74**,** 151-161.

HOFLING, B. & BOLTE, H. D. 1981. ACUTE NEGATIVE INOTROPIC EFFECT OF ADRIAMYCIN (DOXORUBICIN). *Naunyn-Schmiedebergs Archives of Pharmacology,* 317**,** 252-256.

HONERJAGER, P., HEISS, A., SCHAFERKORTING, M., SCHONSTEINER, G. & REITER, M. 1984. UD-CG 115 - A CARDIOTONIC PYRIDAZINONE WHICH ELEVATES CYCLIC-AMP AND PROLONGS THE ACTION-POTENTIAL IN GUINEA-PIG PAPILLARY-MUSCLE. *Naunyn-Schmiedebergs Archives of Pharmacology,* 325**,** 259-269.

HORVATH, B., SZENTANDRASSY, N., VERESS, R., ALMASSY, J., MAGYAR, J., BANYASZ, T., TOTH, A., PAPP, Z. & NANASI, P. P. 2017. Frequency-dependent effects of omecamtiv mecarbil on cell shortening of isolated canine ventricular cardiomyocytes. *Naunyn-Schmiedebergs Archives of Pharmacology,* 390**,** 1239-1246.

HUEBSCH, N., LOSKILL, P., DEVESHWAR, N., SPENCER, C. I., JUDGE, L. M., MANDEGAR, M. A., FOX, C. B., MOHAMED, T. M. A., MA, Z., MATHUR, A., SHEEHAN, A. M., TRUONG, A., SAXTON, M., YOO, J., SRIVASTAVA, D., DESAI, T. A., SO, P. L., HEALY, K. E. & CONKLIN, B. R. 2016. Miniaturized iPS-Cell-Derived Cardiac Muscles for Physiologically Relevant Drug Response Analyses. *Scientific Reports,* 6**,** 12.

HUGHES, C. S., POSTOVIT, L. M. & LAJOIE, G. A. 2010. Matrigel: A complex protein mixture required for optimal growth of cell culture. *Proteomics,* 10**,** 1886-1890.

HUO, J. H., KAMALAKAR, A., YANG, X., WORD, B., STOCKBRIDGE, N., LYN-COOK, B. & PANG, L. 2017. Evaluation of Batch Variations in Induced Pluripotent Stem Cell-

Derived Human Cardiomyocytes from 2 Major Suppliers. *Toxicological Sciences,* 156**,** 25-38.
HUTTER, O. F. 1956. VAGAL AND SYMPATHETIC EFFECTS ON THE PACEMAKER FIBERS IN THE SINUS VENOSUS OF THE HEART. 39**,** 715-733.
HWANG, H. S., KRYSHTAL, D. O., FEASTER, T. K., SANCHEZ-FREIRE, V., ZHANG, J., KAMP, T. J., HONG, C. C., WU, J. C. & KNOLLMANN, B. C. 2015. Comparable calcium handling of human iPSC-derived cardiomyocytes generated by multiple laboratories. *Journal of Molecular and Cellular Cardiology,* 85**,** 79-88.
ICHIKAWA, H., NAKATA, N., ABO, Y., SHIRASAWA, S., YOKOYAMA, T., YOSHIE, S., YUE, F. M., TOMOTSUNE, D. & SASAKI, K. 2012. Gene pathway analysis of the mechanism by which the Rho-associated kinase inhibitor Y-27632 inhibits apoptosis in isolated thawed human embryonic stem cells. *Cryobiology,* 64**,** 12-22.
IFPMA. 2017. *The Pharmaceutical Industry and Global Health Facts and Figures 2017* [Online]. International Federation of Pharmaceutical Manufacturers & Associations. Available: https://www.ifpma.org/wp-content/uploads/2017/02/IFPMA-Facts-And-Figures-2017.pdf [Accessed 2019].
IOSHII, S. O., IMANAKAYOSHIDA, K. & YOSHIDA, T. 1994. ORGANIZATION OF CALSEQUESTRIN-POSITIVE SARCOPLASMIC-RETICULUM IN RAT CARDIOMYOCYTES IN CULTURE. *Journal of Cellular Physiology,* 158**,** 87-96.
ISHIHATA, A., KUSHIDA, H. & ENDOH, M. 1988. ENANTIOMERS OF DOBUTAMINE INCREASE THE FORCE OF CONTRACTION VIA BETA-ADRENOCEPTORS, BUT ANTAGONIZE COMPETITIVELY THE POSITIVE INOTROPIC EFFECT MEDIATED BY ALPHA-1 ADRENOCEPTORS IN THE RABBIT VENTRICULAR MYOCARDIUM. *Journal of Pharmacology and Experimental Therapeutics,* 246**,** 1080-1087.
ISRAELI-ROSENBERG, S., MANSO, A. M., OKADA, H. & ROSS, R. S. 2014. Integrins and Integrin-Associated Proteins in the Cardiac Myocyte. *Circulation Research,* 114**,** 572-586.
ITZHAKI, I., RAPOPORT, S., HUBER, I., MIZRAHI, I., ZWI-DANTSIS, L., ARBEL, G., SCHILLER, J. & GEPSTEIN, L. 2011. Calcium Handling in Human Induced Pluripotent Stem Cell Derived Cardiomyocytes. *Plos One,* 6.
JACKSON, L., ELDAHSHAN, W., FAGAN, S. C. & ERGUL, A. 2018. Within the Brain: The Renin Angiotensin System. *International journal of molecular sciences,* 19.
JACOB, F., YONIS, A. Y., CUELLO, F., LUTHER, P., SCHULZE, T., EDER, A., STREICHERT, T., MANNHARDT, I., HIRT, M. N., SCHAAF, S., STENZIG, J., FORCE, T., ESCHENHAGEN, T. & HANSEN, A. 2016. Analysis of Tyrosine Kinase Inhibitor-Mediated Decline in Contractile Force in Rat Engineered Heart Tissue. *Plos One,* 11**,** 18.
JALIFE, J. 2016. Dynamics and Molecular Mechanisms of Ventricular Fibrillation in Structurally Normal Hearts. *Cardiac electrophysiology clinics,* 8**,** 601-12.
JANSSEN, P. M. L. 2010. Myocardial contraction-relaxation coupling. *American Journal of Physiology-Heart and Circulatory Physiology,* 299**,** H1741-H1749.
JARROTT, B., LOUIS, W. J. & SUMMERS, R. J. 1979. CHARACTERISTICS OF CLONIDINE-H-3 BINDING TO AN ALPHA-ADRENOCEPTOR IN MEMBRANES FROM GUINEA-PIG KIDNEY. *British Journal of Pharmacology,* 65**,** 663-670.
JOHNSON, W. B., KATUGAMPOLA, S., ABLE, S., NAPIER, C. & HARDING, S. E. 2012. Profiling of cAMP and cGMP phosphodiesterases in isolated ventricular cardiomyocytes from human hearts: comparison with rat and guinea pig. *Life sciences,* 90**,** 328-36.
JOU, C., SPITZER, K. & TRISTANI-FIROUZI, M. 2010. Blebbistatin Effectively Uncouples the Excitation-Contraction Process in Zebrafish Embryonic Heart. *Cellular Physiology and Biochemistry,* 25**,** 419-424.
JURKAT-ROTT, K. & LEHMANN-HORN, F. 2005. Muscle channelopathies and critical points in functional and genetic studies. *Journal of Clinical Investigation,* 115**,** 2000-2009.
KAI, D., PRABHAKARAN, M. P., JIN, G. & RAMAKRISHNA, S. 2011. Guided orientation of cardiomyocytes on electrospun aligned nanofibers for cardiac tissue engineering. *Journal of Biomedical Materials Research Part B-Applied Biomaterials,* 98B**,** 379-386.
KAMAKURA, T., MAKIYAMA, T., SASAKI, K., YOSHIDA, Y., WURIYANGHAI, Y., CHEN, J., HATTORI, T., OHNO, S., KITA, T., HORIE, M., YAMANAKA, S. & KIMURA, T. 2013. Ultrastructural Maturation of Human-Induced Pluripotent Stem Cell-Derived Cardiomyocytes in a Long-Term Culture. *Circulation Journal,* 77**,** 1307-1314.
KAMALI, F., THOMAS, S. H. L. & FERNER, R. E. 1993. PARACETAMOL ELIMINATION IN PATIENTS WITH NONINSULIN DEPENDENT DIABETES-MELLITUS. *British Journal of Clinical Pharmacology,* 35**,** 58-61.

KANDA, Y., YAMAZAKI, D., OSADA, T., YOSHINAGA, T. & SAWADA, K. 2018. Development of torsadogenic risk assessment using human induced pluripotent stem cell-derived cardiomyocytes: Japan iPS Cardiac Safety Assessment (JiCSA) update. *Journal of pharmacological sciences,* 138**,** 233-239.

KANE, C., COUCH, L. & TERRACCIANO, C. M. N. 2015. Excitation-contraction coupling of human induced pluripotent stem cell-derived cardiomyocytes. *Frontiers in cell and developmental biology,* 3**,** 59-59.

KAUMANN, A. J. & BLINKS, J. R. 1980. STIMULANT AND DEPRESSANT EFFECTS OF BETA-ADRENOCEPTOR BLOCKING-AGENTS ON ISOLATED HEART-MUSCLE - A POSITIVE INOTROPIC EFFECT NOT MEDIATED THROUGH ADRENOCEPTORS. *Naunyn-Schmiedebergs Archives of Pharmacology,* 311**,** 205-218.

KAWANO, H., ARAKAWA, S., SATOH, O., MATSUMOTO, Y., HAYANO, M., NAKATOMI, D., YAMASA, T. & MAEMURA, K. 2014. Effect of pimobendan in addition to standard therapy for heart failure on prevention of readmission in elderly patients with severe chronic heart failure. *Geriatrics & gerontology international,* 14**,** 109-14.

KETTLEWELL, S., WALKER, N. L., COBBE, S. M., BURTON, F. L. & SMITH, G. L. 2004. The electrophysiological and mechanical effects of 2,3-butane-dione monoxime and cytochalasin-D in the Langendorff perfused rabbit heart. *Experimental Physiology,* 89**,** 163-172.

KEUNG, W., BOHELER, K. R. & LI, R. A. 2014. Developmental cues for the maturation of metabolic, electrophysiological and calcium handling properties of human pluripotent stem cell-derived cardiomyocytes. *Stem Cell Research & Therapy,* 5.

KHAN, M., XU, Y., HUA, S., JOHNSON, J., BELEVYCH, A., JANSSEN, P. M. L., GYORKE, S., GUAN, J. & ANGELOS, M. G. 2015. Evaluation of Changes in Morphology and Function of Human Induced Pluripotent Stem Cell Derived Cardiomyocytes (HiPSC-CMs) Cultured on an Aligned-Nanofiber Cardiac Patch. *Plos One,* 10.

KIKURA, M., TAKADA, T. & SATO, S. 2004. Age- and sex-specific incidence, risk, and latency period of a perioperative acute thromboembolism syndrome (PATS). *Thrombosis and Haemostasis,* 91**,** 725-732.

KIM, A., DOMBI, E., TEPAS, K., FOX, E., MARTIN, S., WOLTERS, P., BALIS, F. M., JAYAPRAKASH, N., TURKBEY, B., MURADYAN, N., CHOYKE, P. L., REDDY, A., KORF, B. & WIDEMANN, B. C. 2013. Phase I trial and pharmacokinetic study of sorafenib in children with neurofibromatosis type I and plexiform neurofibromas. *Pediatric Blood & Cancer,* 60**,** 396-401.

KIM, C., MAJDI, M., XIA, P., WEI, K. A., TALANTOVA, M., SPIERING, S., NELSON, B., MERCOLA, M. & CHEN, H. S. V. 2010. Non-Cardiomyocytes Influence the Electrophysiological Maturation of Human Embryonic Stem Cell-Derived Cardiomyocytes During Differentiation. *Stem Cells and Development,* 19**,** 783-795.

KIM, D. H., AKERA, T. & BRODY, T. M. 1980. INOTROPIC ACTIONS OF DOXORUBICIN IN ISOLATED GUINEA-PIG ATRIA - EVIDENCE FOR LACK OF INVOLVEMENT OF NA+,K+-ADENOSINE TRIPHOSPHATASE. *Journal of Pharmacology and Experimental Therapeutics,* 214**,** 368-374.

KIM, Y. Y., KU, S. Y., LIU, H. C., CHO, H. J., OH, S. K., MOON, S. Y. & CHOI, Y. M. 2011. Cryopreservation of Human Embryonic Stem Cells Derived-Cardiomyocytes Induced by BMP2 in Serum-Free Condition. *Reproductive Sciences,* 18**,** 252-260.

KIRBY, M. S., SAGARA, Y., GAA, S., INESI, G., LEDERER, W. J. & ROGERS, T. B. 1992. THAPSIGARGIN INHIBITS CONTRACTION AND CA2+ TRANSIENT IN CARDIAC-CELLS BY SPECIFIC-INHIBITION OF THE SARCOPLASMIC-RETICULUM CA2+ PUMP. *Journal of Biological Chemistry,* 267**,** 12545-12551.

KIUCHI, K., SHANNON, R. P., KOMAMURA, K., COHEN, D. J., BIANCHI, C., HOMCY, C. J., VATNER, S. F. & VATNER, D. E. 1993. Myocardial beta-adrenergic receptor function during the development of pacing-induced heart failure. *The Journal of clinical investigation,* 91**,** 907-14.

KIVIKKO, M., POLLESELLO, P., TARVASMÄKI, T., SARAPOHJA, T., NIEMINEN, M. S. & HARJOLA, V.-P. 2016. Effect of baseline characteristics on mortality in the SURVIVE trial on the effect of levosimendan vs dobutamine in acute heart failure: Sub-analysis of the Finnish patients. *International Journal of Cardiology,* 215**,** 26-31.

KLEIBER, N., MATHOT, R. A. A., AHSMAN, M. J., WILDSCHUT, E. D., TIBBOEL, D. & DE WILDT, S. N. 2017. Population pharmacokinetics of intravenous clonidine for sedation during paediatric extracorporeal membrane oxygenation and continuous venovenous hemofiltration. *British Journal of Clinical Pharmacology,* 83**,** 1227-1239.

KLEINMAN, H. K., MCGARVEY, M. L., LIOTTA, L. A., ROBEY, P. G., TRYGGVASON, K. & MARTIN, G. R. 1982. ISOLATION AND CHARACTERIZATION OF TYPE-IV

PROCOLLAGEN, LAMININ, AND HEPARAN-SULFATE PROTEOGLYCAN FROM THE EHS SARCOMA. *Biochemistry,* 21**,** 6188-6193.
KLINGBEIL, A. U., SCHNEIDER, M., MARTUS, P., MESSERLI, F. H. & SCHMIEDER, R. E. 2003. A meta-analysis of the effects of treatment on left ventricular mass in essential hypertension. *The American journal of medicine,* 115**,** 41-6.
KNOLLMANN, B. C. 2013. Induced Pluripotent Stem Cell–Derived Cardiomyocytes. *Circulation Research,* 112**,** 969-976.
KOIZUMI, T. & TAGUCHI, S. 2016. Low-dose oral pimobendan emancipates patients with severe ischemic pump failure from intravenous catecholamine infusion for cardiogenic shock. *International journal of cardiology,* 202**,** 829-30.
KOMAJDA, M. 2017. Ivabradine. *Handbook of experimental pharmacology,* 243**,** 167-175.
KONG, H., JONES, P. P., KOOP, A., ZHANG, L., DUFF, H. J. & CHEN, S. R. W. 2008. Caffeine induces Ca2+ release by reducing the threshold for luminal Ca2+ activation of the ryanodine receptor. *Biochemical Journal,* 414**,** 441-452.
KONHILAS, J., IRVING, T. & DE TOMBE, P. 2002. Frank-Starling law of the heart and the cellular mechanisms of length-dependent activation. *Pfl**gers Archiv European Journal of Physiology,* 445**,** 305-310.
KORUTH, J. S., LALA, A., PINNEY, S., REDDY, V. Y. & DUKKIPATI, S. R. 2017. The Clinical Use of Ivabradine. *Journal of the American College of Cardiology,* 70**,** 1777-1784.
KOSMIDIS, G., BELLIN, M., RIBEIRO, M. C., VAN MEER, B., WARD-VAN OOSTWAARD, D., PASSIER, R., TERTOOLEN, L. G. J., MUMMERY, C. L. & CASINI, S. 2015. Altered calcium handling and increased contraction force in human embryonic stem cell derived cardiomyocytes following short term dexamethasone exposure. *Biochemical and Biophysical Research Communications,* 467**,** 998-1005.
KOWEY, P. R., MARINCHAK, R. A., RIALS, S. J. & BHARUCHA, D. B. 2000. Classification and pharmacology of antiarrhythmic drugs. *American Heart Journal,* 140**,** 12-20.
KRAWETZ, R. J., LI, X. Y. & RANCOURT, D. E. 2009. Human embryonic stem cells: caught between a ROCK inhibitor and a hard place. *Bioessays,* 31**,** 336-343.
KUMAR, K. & ZIMETBAUM, P. J. 2013. Antiarrhythmic Drugs 2013: State of the Art. *Current Cardiology Reports,* 15.
KUO, P.-L., LEE, H., BRAY, M.-A., GEISSE, N. A., HUANG, Y.-T., ADAMS, W. J., SHEEHY, S. P. & PARKER, K. K. 2012. Myocyte Shape Regulates Lateral Registry of Sarcomeres and Contractility. *American Journal of Pathology,* 181**,** 2030-2037.
KUROKAWA, Y. K. & GEORGE, S. C. 2016. Tissue engineering the cardiac microenvironment: Multicellular microphysiological systems for drug screening. *Advanced drug delivery reviews,* 96**,** 225-33.
KUSCHEL, M., ZHOU, Y. Y., SPURGEON, H. A., BARTEL, S., KARCZEWSKI, P., ZHANG, S. J., KRAUSE, E. G., LAKATTA, E. G. & XIAO, R. P. 1999. beta(2)-adrenergic cAMP signaling is uncoupled from phosphorylation of cytoplasmic proteins in canine heart. *Circulation,* 99**,** 2458-2465.
LAFUENTE-LAFUENTE, C., VALEMBOIS, L., BERGMANN, J.-F. & BELMIN, J. 2015. Antiarrhythmics for maintaining sinus rhythm after cardioversion of atrial fibrillation. *The Cochrane database of systematic reviews***,** CD005049.
LAI, F. A., ANDERSON, K., ROUSSEAU, E., LIU, Q. Y. & MEISSNER, G. 1988. EVIDENCE FOR A CA-2+ CHANNEL WITHIN THE RYANODINE RECEPTOR COMPLEX FROM CARDIAC SARCOPLASMIC-RETICULUM. *Biochemical and Biophysical Research Communications,* 151**,** 441-449.
LAKATTA, E. G., MALTSEV, V. A. & VINOGRADOVA, T. M. 2010. A Coupled SYSTEM of Intracellular Ca 2+ Clocks and Surface Membrane Voltage Clocks Controls the Timekeeping Mechanism of the Heart's Pacemaker. *Circulation Research,* 106**,** 659-673.
LAKATTA, E. G., VINOGRADOVA, T., LYASHKOV, A., SIRENKO, S., ZHU, W., RUKNUDIN, A. & MALTSEV, V. A. 2006. The integration of spontaneous intracellular Ca2+ cycling and surface membrane ion channel activation entrains normal automaticity in cells of the heart's pacemaker. *Annals of the New York Academy of Sciences,* 1080**,** 178-206.
LAKHE, M., FURUKAWA, Y., YONEZAWA, T., HIROSE, M., NAGASHIMA, Y., MIYASHITA, Y. & CHIBA, S. 1998. Different Chronotropic and Inotropic Effects of EMD 57033 and EMD 53998, Ca2+ Sensitizers, on Isolated, Blood-Perfused Dog Heart Preparations. *The Japanese Journal of Pharmacology,* 76**,** 435-439.
LAMBERT, D. G. 1993. SIGNAL TRANSDUCTION: G PROTEINS AND SECOND MESSENGERS. 71**,** 86-95.
LASSETER, K. C., LEVEY, G. S., MCCARTHY, J. S. & PALMER, R. F. 1972. EFFECT OF SULFONYLUREA DRUGS ON RABBIT MYOCARDIAL CONTRACTILITY, CANINE

PURKINJE FIBER AUTOMATICITY, AND ADENYL-CYCLASE ACTIVITY FROM RABBIT AND HUMAN HEARTS. *Journal of Clinical Investigation,* 51**,** 2429-&.
LAURENT, S. 2017. Antihypertensive drugs. *Pharmacological Research,* 124**,** 116-125.
LAVERTY, H. G., BENSON, C., CARTWRIGHT, E. J., CROSS, M. J., GARLAND, C., HAMMOND, T., HOLLOWAY, C., MCMAHON, N., MILLIGAN, J., PARK, B. K., PIRMOHAMED, M., POLLARD, C., RADFORD, J., ROOME, N., SAGER, P., SINGH, S., SUTER, T., SUTER, W., TRAFFORD, A., VOLDERS, P. G. A., WALLIS, R., WEAVER, R., YORK, M. & VALENTIN, J. P. 2011. How can we improve our understanding of cardiovascular safety liabilities to develop safer medicines? *British Journal of Pharmacology,* 163**,** 675-693.
LEE, E. K., TRAN, D. D., KEUNG, W., CHAN, P., WONG, G., CHAN, C. W., COSTA, K. D., LI, R. A. & KHINE, M. 2017a. Machine Learning of Human Pluripotent Stem Cell-Derived Engineered Cardiac Tissue Contractility for Automated Drug Classification. *Stem Cell Reports,* 9**,** 1560-1572.
LEE, J. H., PROTZE, S. I., LAKSMAN, Z., BACKX, P. H. & KELLER, G. M. 2017b. Human Pluripotent Stem Cell-Derived Atrial and Ventricular Cardiomyocytes Develop from Distinct Mesoderm Populations. *Cell Stem Cell,* 21**,** 179-+.
LEE, P., KLOS, M., BOLLENSDORFF, C., HOU, L., EWART, P., KAMP, T. J., ZHANG, J., BIZY, A., GUERRERO-SERNA, G., KOHL, P., JALIFE, J. & HERRON, T. J. 2012. Simultaneous Voltage and Calcium Mapping of Genetically Purified Human Induced Pluripotent Stem Cell-Derived Cardiac Myocyte Monolayers. *Circulation Research,* 110**,** 1556-1563.
LEE, Y.-K., NG, K.-M., LAI, W.-H., CHAN, Y.-C., LAU, Y.-M., LIAN, Q., TSE, H.-F. & SIU, C.-W. 2011. Calcium Homeostasis in Human Induced Pluripotent Stem Cell-Derived Cardiomyocytes. *Stem Cell Reviews and Reports,* 7**,** 976-986.
LEGANT, W. R., PATHAK, A., YANG, M. T., DESHPANDE, V. S., MCMEEKING, R. M. & CHEN, C. S. 2009. Microfabricated tissue gauges to measure and manipulate forces from 3D microtissues. *Proceedings of the National Academy of Sciences of the United States of America,* 106**,** 10097-10102.
LEHTONEN, L. & PODER, P. 2007. The utility of levosimendan in the treatment of heart failure. *Annals of medicine,* 39**,** 2-17.
LEI, M., WU, L., TERRAR, D. A. & HUANG, C. L. H. 2018. Modernized Classification of Cardiac Antiarrhythmic Drugs. *Circulation,* 138**,** 1879-1896.
LEMME, M., ULMER, B. M., LEMOINE, M. D., ZECH, A. T. L., FLENNER, F., RAVENS, U., REICHENSPURNER, H., ROL-GARCIA, M., SMITH, G., HANSEN, A., CHRIST, T. & ESCHENHAGEN, T. 2018. Atrial-like Engineered Heart Tissue: An In Vitro Model of the Human Atrium. *Stem Cell Reports,* 11**,** 1378-1390.
LEMOINE, H., SCHONELL, H. & KAUMANN, A. J. 1988. CONTRIBUTION OF BETA-1-ADRENOCEPTORS AND BETA-2-ADRENOCEPTORS OF HUMAN ATRIUM AND VENTRICLE TO THE EFFECTS OF NORADRENALINE AND ADRENALINE AS ASSESSED WITH (-)-ATENOLOL. *British Journal of Pharmacology,* 95**,** 55-66.
LEONARD, A., BERTERO, A., POWERS, J. D., BEUSSMAN, K. M., BHANDARI, S., REGNIER, M., MURRY, C. E. & SNIADECKI, N. J. 2018. Afterload promotes maturation of human induced pluripotent stem cell derived cardiomyocytes in engineered heart tissues. *Journal of Molecular and Cellular Cardiology,* 118**,** 147-158.
LEVEY, G. S., PALMER, R. F., LASSETER, K. C. & MCCARTHY, J. 1971. EFFECT OF TOLBUTAMIDE ON ADENYL CYCLASE IN RABBIT AND HUMAN HEART AND CONTRACTILITY OF ISOLATED RABBIT ATRIA. *Journal of Clinical Endocrinology & Metabolism,* 33**,** 371-+.
LEVINE, M. A. H. & LEENEN, F. H. H. 1992. ROLE OF VAGAL ACTIVITY IN THE CARDIOVASCULAR-RESPONSES TO PHENYLEPHRINE IN MAN. *British Journal of Clinical Pharmacology,* 33**,** 333-336.
LEVY, B., CLERE-JEHL, R., LEGRAS, A., MORICHAU-BEAUCHANT, T., LEONE, M., FREDERIQUE, G., QUENOT, J.-P., KIMMOUN, A., CARIOU, A., LASSUS, J., HARJOLA, V.-P., MEZIANI, F., LOUIS, G., ROSSIGNOL, P., DUARTE, K., GIRERD, N., MEBAZAA, A., VIGNON, P., MATTEI, M., THIVILIER, C., PEREZ, P., AUCHET, T., FRITZ, C., BOISRAME-HELME, J., MERCIER, E., GAROT, D., PERNY, J., GETTE, S., HAMMAD, E., VIGNE, C., DARGENT, A., ANDREU, P. & GUIOT, P. 2018. Epinephrine Versus Norepinephrine for Cardiogenic Shock After Acute Myocardial Infarction. *Journal of the American College of Cardiology,* 72**,** 173-182.
LEYTON-MANGE, J. S., MILLS, R. W., MACRI, V. S., JANG, M. Y., BUTTE, F. N., ELLINOR, P. T. & MILAN, D. J. 2014. Rapid Cellular Phenotyping of Human Pluripotent Stem Cell-Derived Cardiomyocytes using a Genetically Encoded Fluorescent Voltage Sensor. *Stem Cell Reports,* 2**,** 163-170.

LI, D. & NATTEL, S. 2007. Pharmacological elimination of motion artifacts during optical imaging of cardiac tissues: Is blebbistatin the answer? *Heart Rhythm,* 4**,** 627-628.
LI, R. A., KEUNG, W., CASHMAN, T. J., BACKERIS, P. C., JOHNSON, B. V., BARDOT, E. S., WONG, A. O. T., CHAN, P. K. W., CHAN, C. W. Y. & COSTA, K. D. 2018. Bioengineering an electro-mechanically functional miniature ventricular heart chamber from human pluripotent stem cells. *Biomaterials,* 163**,** 116-127.
LI, S., CHEN, G. & LI, R. A. 2013. Calcium signalling of human pluripotent stem cell-derived cardiomyocytes. *Journal of Physiology-London,* 591**,** 5279-5290.
LI, Y., LI, L., CHEN, Z. N., GAO, G., YAO, R. & SUN, W. 2017. Engineering-derived approaches for iPSC preparation, expansion, differentiation and applications. *Biofabrication,* 9**,** 19.
LI, Y. & MA, T. 2012. Bioprocessing of cryopreservation for large-scale banking of human pluripotent stem cells. *BioResearch open access,* 1**,** 205-14.
LIEU, D. K., LIU, J., SIU, C.-W., MCNERNEY, G. P., TSE, H.-F., ABU-KHALIL, A., HUSER, T. & LI, R. A. 2009. Absence of Transverse Tubules Contributes to Non-Uniform Ca2+ Wavefronts in Mouse and Human Embryonic Stem Cell-Derived Cardiomyocytes. *Stem Cells and Development,* 18**,** 1493-1500.
LIMOUZE, J., STRAIGHT, A. F., MITCHISON, T. & SELLERS, J. R. 2004. Specificity of blebbistatin, an inhibitor of myosin II. *Journal of Muscle Research and Cell Motility,* 25**,** 337-341.
LINDBOM, L. O. & FORSBERG, T. 1981. CARDIOVASCULAR EFFECTS OF ZIMELIDINE AND OTHER ANTI-DEPRESSANTS IN CONSCIOUS RATS. *Acta Psychiatrica Scandinavica,* 63**,** 380-384.
LIU, J., LAKSMAN, Z. & BACKX, P. H. 2016a. The electrophysiological development of cardiomyocytes. *Advanced Drug Delivery Reviews,* 96**,** 253-273.
LIU, L. C. Y., DORHOUT, B., VAN DER MEER, P., TEERLINK, J. R. & VOORS, A. A. 2016b. Omecamtiv mecarbil: a new cardiac myosin activator for the treatment of heart failure. *Expert Opinion on Investigational Drugs,* 25**,** 117-127.
LIU, T., BROWN, D. A. & O'ROURKE, B. 2010. Role of mitochondrial dysfunction in cardiac glycoside toxicity. *Journal of molecular and cellular cardiology,* 49**,** 728-36.
LOHSE, M. J., ENGELHARDT, S. & ESCHENHAGEN, T. 2003. What Is the Role of β-Adrenergic Signaling in Heart Failure? *Circulation Research,* 93**,** 896-906.
LOUCH, W. E., KOIVUMAKI, J. T. & TAVI, P. 2015. Calcium signalling in developing cardiomyocytes: implications for model systems and disease. *Journal of Physiology-London,* 593**,** 1047-1063.
LULLMANN, H. & RAVENS, U. 1973. TIME COURSES OF CHANGES IN CONTRACTILE-FORCE AND IN TRANSMEMBRANE POTENTIALS INDUCED BY CARDIAC-GLYCOSIDES IN GUINEA-PIG PAPILLARY-MUSCLE. *British Journal of Pharmacology,* 49**,** 377-390.
LUNDY, S. D., GANTZ, J. A., PAGAN, C. M., FILICE, D. & LAFLAMME, M. A. 2014. Pluripotent stem cell derived cardiomyocytes for cardiac repair. *Current treatment options in cardiovascular medicine,* 16**,** 319-319.
LUNDY, S. D., ZHU, W.-Z., REGNIER, M. & LAFLAMME, M. A. 2013. Structural and Functional Maturation of Cardiomyocytes Derived from Human Pluripotent Stem Cells. *Stem Cells and Development,* 22**,** 1991-2002.
LYLE, J. V., CHARLTON, P. H., BONET-LUZ, E., CHAFFEY, G., CHRISTIE, M., NANDI, M., ASTON, P. J. & IEEE 2017. Beyond HRV: Analysis of ECG Signals Using Attractor Reconstruction. *2017 Computing in Cardiology (Cinc)*.
MA, J. Y., GUO, L., FIENE, S. J., ANSON, B. D., THOMSON, J. A., KAMP, T. J., KOLAJA, K. L., SWANSON, B. J. & JANUARY, C. T. 2011. High purity human-induced pluripotent stem cell-derived cardiomyocytes: electrophysiological properties of action potentials and ionic currents. *American Journal of Physiology-Heart and Circulatory Physiology,* 301**,** H2006-H2017.
MAACK, C., ESCHENHAGEN, T., HAMDANI, N., HEINZEL, F. R., LYON, A. R., MANSTEIN, D. J., METZGER, J., PAPP, Z., TOCCHETTI, C. G., YILMAZ, M. B., ANKER, S. D., BALLIGAND, J.-L., BAUERSACHS, J., BRUTSAERT, D., CARRIER, L., CHLOPICKI, S., CLELAND, J. G., DE BOER, R. A., DIETL, A., FISCHMEISTER, R., HARJOLA, V.-P., HEYMANS, S., HILFIKER-KLEINER, D., HOLZMEISTER, J., DE KEULENAER, G., LIMONGELLI, G., LINKE, W. A., LUND, L. H., MASIP, J., METRA, M., MUELLER, C., PIESKE, B., PONIKOWSKI, P., RISTIĆ, A., RUSCHITZKA, F., SEFEROVIĆ, P. M., SKOURI, H., ZIMMERMANN, W. H. & MEBAZAA, A. 2019. Treatments targeting inotropy. *European Heart Journal,* 40**,** 3626-3644.
MACQUEEN, L. A., SHEEHY, S. P., CHANTRE, C. O., ZIMMERMAN, J. F., PASQUALINI, F. S., LIU, X. J., GOSS, J. A., CAMPBELL, P. H., GONZALEZ, G. M., PARK, S. J., CAPULLI, A. K., FERRIER, J. P., KOSARL, T. F., MAHADEVAN, L., PU, W. T. & PARKER, K. K.

2018. A tissue-engineered scale model of the heart ventricle. *Nature Biomedical Engineering,* 2**,** 930-941.
MAGYAR, J., IOST, N., KORTVELY, A., BANYASZ, T., VIRAG, L., SZIGLIGETI, P., VARRO, A., OPINCARIU, M., SZECSI, J., PAPP, J. G. & NANASI, P. P. 2000. Effects of endothelin-1 on calcium and potassium currents in undiseased human ventricular myocytes. *Pflugers Archiv-European Journal of Physiology,* 441**,** 144-149.
MAHONEY, L., SHAH, G., CROOK, D., ROJAS-ANAYA, H. & RABE, H. 2016. A Literature Review of the Pharmacokinetics and Pharmacodynamics of Dobutamine in Neonates. *Pediatric Cardiology,* 37**,** 14-23.
MALIK, F. I., HARTMAN, J. J., ELIAS, K. A., MORGAN, B. P., RODRIGUEZ, H., BREJC, K., ANDERSON, R. L., SUEOKA, S. H., LEE, K. H., FINER, J. T., SAKOWICZ, R., BALIGA, R., COX, D. R., GARARD, M., GODINEZ, G., KAWAS, R., KRAYNACK, E., LENZI, D., LU, P. P., MUCI, A., NIU, C. R., QIAN, X. P., PIERCE, D. W., POKROVSKII, M., SUEHIRO, I., SYLVESTER, S., TOCHIMOTO, T., VALDEZ, C., WANG, W. Y., KATORI, T., KASS, D. A., SHEN, Y. T., VATNER, S. F. & MORGANS, D. J. 2011. Cardiac Myosin Activation: A Potential Therapeutic Approach for Systolic Heart Failure. *Science,* 331**,** 1439-1443.
MALLET, R. T., OLIVENCIA-YURVATI, A. H. & BUNGER, R. 2018. Pyruvate enhancement of cardiac performance: Cellular mechanisms and clinical application. *Experimental Biology and Medicine,* 243**,** 198-210.
MALTSEV, V. A., VINOGRADOVA, T. M. & LAKATTA, E. G. 2006. The Emergence of a General Theory of the Initiation and Strength of the Heartbeat. *Journal of Pharmacological Sciences,* 100**,** 338-369.
MANFRA, O., FRISK, M. & LOUCH, W. E. 2017. Regulation of Cardiomyocyte T-Tubular Structure: Opportunities for Therapy. *Current Heart Failure Reports,* 14**,** 167-178.
MANKAD, P. & KALAHASTY, G. 2019. Antiarrhythmic Drugs: Risks and Benefits. *The Medical clinics of North America,* 103**,** 821-834.
MANNHARDT, I., BRECKWOLDT, K., LETUFFE-BRENIERE, D., SCHAAF, S., SCHULZ, H., NEUBER, C., BENZIN, A., WERNER, T., EDER, A., SCHULZE, T., KLAMPE, B., CHRIST, T., HIRT, M. N., HUEBNER, N., MORETTI, A., ESCHENHAGEN, T. & HANSEN, A. 2016. Human Engineered Heart Tissue: Analysis of Contractile Force. *Stem Cell Reports,* 7**,** 29-42.
MANNHARDT, I., EDER, A., DUMOTIER, B., PRONDZYNSKI, M., KRAMER, E., TRAEBERT, M., SOHREN, K. D., FLENNER, F., STATHOPOULOU, K., LEMOINE, M. D., CARRIER, L., CHRIST, T., ESCHENHAGEN, T. & HANSEN, A. 2017. Blinded Contractility Analysis in hiPSC-Cardiomyocytes in Engineered Heart Tissue Format: Comparison With Human Atrial Trabeculae. *Toxicological Sciences,* 158**,** 164-175.
MARKS, L., BORLAND, S., PHILP, K., EWART, L., LAINEE, P., SKINNER, M., KIRK, S. & VALENTIN, J. P. 2012. The role of the anaesthetised guinea-pig in the preclinical cardiac safety evaluation of drug candidate compounds. *Toxicology and Applied Pharmacology,* 263**,** 171-183.
MARWICK, T. H. 2018. Ejection Fraction Pros and Cons JACC State-of-the-Art Review. *Journal of the American College of Cardiology,* 72**,** 2360-2379.
MATSA, E., BURRIDGE, P. W., YU, K. H., AHRENS, J. H., TERMGLINCHAN, V., WU, H. D., LIU, C., SHUKLA, P., SAYED, N., CHURKO, J. M., SHAO, N., WOO, N. A., CHAO, A. S., GOLD, J. D., KARAKIKES, I., SNYDER, M. P. & WU, J. C. 2016. Transcriptome Profiling of Patient-Specific Human iPSC-Cardiomyocytes Predicts Individual Drug Safety and Efficacy Responses In Vitro. *Cell Stem Cell,* 19**,** 311-325.
MATSUSHITA, T., OKAMATO, M., TOYAMA, J., KODAMA, I., ITO, S., FUKUTOMI, T., SUZUKI, S. & ITOH, M. 2000. Adriamycin causes dual inotropic effects through complex modulation of myocardial Ca2+ handling. *Japanese Circulation Journal-English Edition,* 64**,** 65-71.
MCMURRAY, J. J. V., ADAMOPOULOS, S., ANKER, S. D., AURICCHIO, A., BOHM, M., DICKSTEIN, K., FALK, V., FILIPPATOS, G., FONSECA, C., GOMEZ-SANCHEZ, M. A., JAARSMA, T., KOBER, L., LIP, G. Y. H., MAGGIONI, A. P., PARKHOMENKO, A., PIESKE, B. M., POPESCU, B. A., RONNEVIK, P. K., RUTTEN, F. H., SCHWITTER, J., SEFEROVIC, P., STEPINSKA, J., TRINDADE, P. T., VOORS, A. A., ZANNAD, F., ZEIHER, A. & GUIDELINES, E. S. C. C. F. P. 2012. ESC Guidelines for the diagnosis and treatment of acute and chronic heart failure 2012: The Task Force for the Diagnosis and Treatment of Acute and Chronic Heart Failure 2012 of the European Society of Cardiology. Developed in collaboration with the Heart Failure Association (HFA) of the ESC. *European heart journal,* 33**,** 1787-847.

MCQUINN, R. L., PENTIKAINEN, P. J., CHANG, S. F. & CONARD, G. J. 1988. PHARMACOKINETICS OF FLECAINIDE IN PATIENTS WITH CIRRHOSIS OF THE LIVER. *Clinical Pharmacology & Therapeutics,* 44**,** 566-572.

MCSPADDEN, L. C., NGUYEN, H. & BURSAC, N. 2012. Size and Ionic Currents of Unexcitable Cells Coupled to Cardiomyocytes Distinctly Modulate Cardiac Action Potential Shape and Pacemaking Activity in Micropatterned Cell Pairs. *Circulation-Arrhythmia and Electrophysiology,* 5**,** 821-830.

MEBAZAA, A., NIEMINEN, M. S., FILIPPATOS, G. S., CLELAND, J. G., SALON, J. E., THAKKAR, R., PADLEY, R. J., HUANG, B. & COHEN-SOLAL, A. 2009. Levosimendan vs. dobutamine: outcomes for acute heart failure patients on β-blockers in SURVIVE†. *European Journal of Heart Failure,* 11**,** 304-311.

MEBAZAA, A., NIEMINEN, M. S., PACKER, M., COHEN-SOLAL, A., KLEBER, F. X., POCOCK, S. J., THAKKAR, R., PADLEY, R. J., PODER, P., KIVIKKO, M. & INVESTIGATORS, S. 2007. Levosimendan vs dobutamine for patients with acute decompensated heart failure - The SURVIVE randomized trial. *Jama-Journal of the American Medical Association,* 297**,** 1883-1891.

MESAELI, N., NAKAMURA, K., ZVARITCH, E., DICKIE, P., DZIAK, E., KRAUSE, K. H., OPAS, M., MACLENNAN, D. H. & MICHALAK, M. 1999. Calreticulin is essential for cardiac development. *Journal of Cell Biology,* 144**,** 857-868.

MESIRCA, P., ALIG, J., TORRENTE, A. G., MULLER, J. C., MARGER, L., ROLLIN, A., MARQUILLY, C., VINCENT, A., DUBEL, S., BIDAUD, I., FERNANDEZ, A., SENIUK, A., ENGELAND, B., SINGH, J., MIQUEROL, L., EHMKE, H., ESCHENHAGEN, T., NARGEOT, J., WICKMAN, K., ISBRANDT, D. & MANGONI, M. E. 2014. Cardiac arrhythmia induced by genetic silencing of 'funny' (f) channels is rescued by GIRK4 inactivation. *Nature Communications,* 5**,** 15.

MESSERLI, F. H., BANGALORE, S., BAVISHI, C. & RIMOLDI, S. F. 2018. Angiotensin-Converting Enzyme Inhibitors in Hypertension. *Journal of the American College of Cardiology,* 71**,** 1474-1482.

MILLS, R. J., PARKER, B. L., MONNOT, P., NEEDHAM, E. J., VIVIEN, C. J., FERGUSON, C., PARTON, R. G., JAMES, D. E., PORRELLO, E. R. & HUDSON, J. E. 2019. Development of a human skeletal micro muscle platform with pacing capabilities. *Biomaterials,* 198**,** 217-227.

MOFFAT, J. G., VINCENT, F., LEE, J. A., EDER, J. & PRUNOTTO, M. 2017. Opportunities and challenges in phenotypic drug discovery: an industry perspective. *Nature Reviews Drug Discovery,* 16**,** 531-543.

MOLENAAR, P., CHRIST, T., HUSSAIN, R. I., ENGEL, A., BERK, E., GILLETTE, K. T., CHEN, L., GALINDO-TOVAR, A., KROBERT, K. A., RAVENS, U., LEVY, F. O. & KAUMANN, A. J. 2013. PDE3, but not PDE4, reduces β1- and β2-adrenoceptor-mediated inotropic and lusitropic effects in failing ventricle from metoprolol-treated patients. *British Journal of Pharmacology,* 169**,** 528-538.

MOLENAAR, P., SAVARIMUTHU, S. M., SARSERO, D., CHEN, L., SEMMLER, A. B. T., CARLE, A., YANG, I., BARTEL, S., VETTER, D., BEYERDORFER, I., KRAUSE, E. G. & KAUMANN, A. J. 2007. (-)-Adrenaline elicits positive inotropic, lusitropic, and biochemical effects through beta(2)-adrenoceptors in human atrial myocardium from nonfailing and failing hearts, consistent with Gs coupling but not with Gi coupling. *Naunyn-Schmiedebergs Archives of Pharmacology,* 375**,** 11-28.

MOLINA, C. E., LEROY, J., RICHTER, W., XIE, M., SCHEITRUM, C., LEE, I.-O., MAACK, C., RUCKER-MARTIN, C., DONZEAU-GOUGE, P., VERDE, I., LLACH, A., HOVE-MADSEN, L., CONTI, M., VANDECASTEELE, G. & FISCHMEISTER, R. 2012. Cyclic Adenosine Monophosphate Phosphodiesterase Type 4 Protects Against Atrial Arrhythmias. 59**,** 2182-2190.

MOONEY, L., SKINNER, M., COKER, S. J. & CURRIE, S. 2015. Effects of acute and chronic sunitinib treatment on cardiac function and calcium/calmodulin-dependent protein kinase II. *British Journal of Pharmacology,* 172**,** 4342-4354.

MORETTI, A., BELLIN, M., WELLING, A., JUNG, C. B., LAM, J. T., BOTT-FLUGEL, L., DORN, T., GOEDEL, A., HOHNKE, C., HOFMANN, F., SEYFARTH, M., SINNECKER, D., SCHOMIG, A. & LAUGWITZ, K.-L. 2010. Patient-specific induced pluripotent stem-cell models for long-QT syndrome. *The New England journal of medicine,* 363**,** 1397-409.

MORGANROTH, J. 1986. Intravenous atenolol for ventricular arrhythmias. *The American journal of cardiology,* 58**,** 499-502.

MOSQUEIRA, D., MANNHARDT, I., BHAGWAN, J. R., LIS-SLIMAK, K., KATILI, P., SCOTT, E., HASSAN, M., PRONDZYNSKI, M., HARMER, S. C., TINKER, A., SMITH, J. G. W., CARRIER, L., WILLIAMS, P. M., GAFFNEY, D., ESCHENHAGEN, T., HANSEN, A. &

DENNING, C. 2018. CRISPR/Cas9 editing in human pluripotent stemcell-cardiomyocytes highlights arrhythmias, hypocontractility, and energy depletion as potential therapeutic targets for hypertrophic cardiomyopathy. *European Heart Journal,* 39**,** 3879-+.

MOTOMURA, S., REINHARD-ZERKOWSKI, H., DAUL, A. & BRODDE, O. E. 1990. On the physiologic role of beta-2 adrenoceptors in the human heart: in vitro and in vivo studies. *American heart journal,* 119**,** 608-19.

MULDER, P., DE KORTE, T., DRAGICEVIC, E., KRAUSHAAR, U., PRINTEMPS, R., VLAMING, M. L. H., BRAAM, S. R. & VALENTIN, J.-P. 2018. Predicting cardiac safety using human induced pluripotent stem cell-derived cardiomyocytes combined with multi-electrode array (MEA) technology: A conference report. *Journal of Pharmacological and Toxicological Methods,* 91**,** 36-42.

MULIERI, L. A., HASENFUSS, G., LEAVITT, B., ALLEN, P. D. & ALPERT, N. R. 1992. Altered myocardial force-frequency relation in human heart failure. 85**,** 1743-1750.

MUMMERY, C. L., ZHANG, J. H., NG, E. S., ELLIOTT, D. A., ELEFANTY, A. G. & KAMP, T. J. 2012. Differentiation of Human Embryonic Stem Cells and Induced Pluripotent Stem Cells to Cardiomyocytes A Methods Overview. *Circulation Research,* 111**,** 344-358.

MURAKAMI, M., FURUKAWA, Y., KARASAWA, Y., REN, L. M., TAKAYAMA, S. & CHIBA, S. 1992. INHIBITION BY GLIBENCLAMIDE OF NEGATIVE CHRONOTROPIC AND INOTROPIC RESPONSES TO PINACIDIL, ACETYLCHOLINE, AND ADENOSINE IN THE ISOLATED DOG HEART. *Journal of Cardiovascular Pharmacology,* 19**,** 618-624.

NACCARELLI, G. V., DORIAN, P., HOHNLOSER, S. H. & COUMEL, P. 1996. Prospective comparison of flecainide versus quinidine for the treatment of paroxysmal atrial fibrillation/flutter. 77**,** 53A-59A.

NANDI, M., VENTON, J. & ASTON, P. J. 2018. A novel method to quantify arterial pulse waveform morphology: attractor reconstruction for physiologists and clinicians. *Physiological Measurement,* 39**,** 18.

NARANJO, C. A., SELLERS, E. M., KAPLAN, H. L., HAMILTON, C. & KHOUW, V. 1984. ACUTE KINETIC AND DYNAMIC INTERACTIONS OF ZIMELIDINE WITH ETHANOL. *Clinical Pharmacology & Therapeutics,* 36**,** 654-660.

NARAYAN, S. M. & ZAMAN, J. A. B. 2016. Mechanistically based mapping of human cardiac fibrillation. *The Journal of Physiology,* 594**,** 2399-2415.

NAVARRETE, E. G., LIANG, P., LAN, F., SANCHEZ-FREIRE, V., SIMMONS, C., GONG, T. Y., SHARMA, A., BURRIDGE, P. W., PATLOLLA, B., LEE, A. S., WU, H. D., BEYGUI, R. E., WU, S. M., ROBBINS, R. C., BERS, D. M. & WU, J. C. 2013. Screening Drug-Induced Arrhythmia Events Using Human Induced Pluripotent Stem Cell-Derived Cardiomyocytes and Low-Impedance Microelectrode Arrays. *Circulation,* 128**,** S3-U51.

NERBONNE, J. M. 2004. Studying cardiac arrhythmias in the mouse--a reasonable model for probing mechanisms? *Trends in cardiovascular medicine,* 14**,** 83-93.

NOORMAN, M., VAN DER HEYDEN, M. A. G., VAN VEEN, T. A. B., COX, M. G. P. J., HAUER, R. N. W., DE BAKKER, J. M. T. & VAN RIJEN, H. V. M. 2009. Cardiac cell-cell junctions in health and disease: Electrical versus mechanical coupling. *Journal of Molecular and Cellular Cardiology,* 47**,** 23-31.

NOZAKI, Y., HONDA, Y., WATANABE, H., SAIKI, S., KOYABU, K., ITOH, T., NAGASAWA, C., NAKAMORI, C., NAKAYAMA, C., IWASAKI, H., SUZUKI, S., TANAKA, K., TAKAHASHI, E., MIYAMOTO, K., MORIMURA, K., YAMANISHI, A., ENDO, H., SHINOZAKI, J., NOGAWA, H., SHINOZAWA, T., SAITO, F. & KUNIMATSU, T. 2017. CSAHi study-2: Validation of multi-electrode array systems (MEA60/2100) for prediction of drug-induced proarrhythmia using human iPS cell-derived cardiomyocytes: Assessment of reference compounds and comparison with non-clinical studies and clinical information. *Regulatory Toxicology and Pharmacology,* 88**,** 238-251.

OBERWALLNER, B., BRODARAC, A., CHOI, Y. H., SARIC, T., ANIC, P., MORAWIETZ, L. & STAMM, C. 2014. Preparation of cardiac extracellular matrix scaffolds by decellularization of human myocardium. *Journal of Biomedical Materials Research Part A,* 102**,** 3263-3272.

ONAKPOYA, I. J., HENEGHAN, C. J. & ARONSON, J. K. 2016. Post-marketing withdrawal of 462 medicinal products because of adverse drug reactions: a systematic review of the world literature. *Bmc Medicine,* 14**,** 11.

ORCHARD, C. H., PASEK, M. & BRETTE, F. 2009. The role of mammalian cardiac t-tubules in excitation-contraction coupling: experimental and computational approaches. *Experimental Physiology,* 94**,** 509-519.

ORSTAVIK, O., ATA, S. H., RIISE, J., DAHL, C. P., ANDERSEN, G. O., LEVY, F. O., SKOMEDAL, T., OSNES, J. B. & QVIGSTAD, E. 2014. Inhibition of phosphodiesterase-3 by levosimendan is sufficient to account for its inotropic effect in failing human heart. *British Journal of Pharmacology,* 171**,** 5169-5181.

OTSUJI, T. G., MINAMI, I., KUROSE, Y., YAMAUCHI, K., TADA, M. & NAKATSUJI, N. 2010. Progressive maturation in contracting cardiomyocytes derived from human embryonic stem cells: Qualitative effects on electrophysiological responses to drugs. *Stem Cell Research,* 4**,** 201-213.

OVERGAARD, C. B. & DŽAVÍK, V. R. 2008. Inotropes and Vasopressors. *Circulation,* 118**,** 1047-1056.

PALCHESKO, R. N., ZHANG, L., SUN, Y. & FEINBERG, A. W. 2012. Development of Polydimethylsiloxane Substrates with Tunable Elastic Modulus to Study Cell Mechanobiology in Muscle and Nerve. *Plos One,* 7**,** 13.

PAPP, Z., EDES, I., FRUHWALD, S., DE HERT, S. G., SALMENPERA, M., LEPPIKANGAS, H., MEBAZAA, A., LANDONI, G., GROSSINI, E., CAIMMI, P., MORELLI, A., GUARRACINO, F., SCHWINGER, R. H. G., MEYER, S., ALGOTSSON, L., WIKSTROM, B. G., JORGENSEN, K., FILIPPATOS, G., PARISSIS, J. T., GONZALEZ, M. J. G., PARKHOMENKO, A., YILMAZ, M. B., KIVIKKO, M., POLLESELLO, P. & FOLLATH, F. 2012. Levosimendan: Molecular mechanisms and clinical implications Consensus of experts on the mechanisms of action of levosimendan. *International Journal of Cardiology,* 159**,** 82-87.

PARIKH, S. S., BLACKWELL, D. J., GOMEZ-HURTADO, N., FRISK, M., WANG, L., KIM, K., DAHL, C. P., FIANE, A., TØNNESSEN, T., KRYSHTAL, D. O., LOUCH, W. E. & KNOLLMANN, B. C. 2017. Thyroid and Glucocorticoid Hormones Promote Functional T-Tubule Development in Human-Induced Pluripotent Stem Cell–Derived Cardiomyocytes. *Circulation Research,* 121**,** 1323-1330.

PENG, M., HUANG, L., XIE, Z., HUANG, W. H. & ASKARI, A. 1996. Partial inhibition of Na+/K+-ATPase by ouabain induces the Ca2+-dependent expressions of early-response genes in cardiac myocytes. *Journal of Biological Chemistry,* 271**,** 10372-10378.

PENG, S., LACERDA, A. E., KIRSCH, G. E., BROWN, A. M. & BRUENING-WRIGHT, A. 2010. The action potential and comparative pharmacology of stem cell-derived human cardiomyocytes. *Journal of pharmacological and toxicological methods,* 61**,** 277-86.

PEREZ, O., GAY, P., FRANQUEZA, L., CARRON, R., VALENZUELA, C., DELPON, E. & TAMARGO, J. 1995. EFFECTS OF THE 2 ENANTIOMERS, S-16257-2 AND S-16260-2, OF A NEW BRADYCARDIAC AGENT ON GUINEA-PIG ISOLATED CARDIAC PREPARATIONS. *British Journal of Pharmacology,* 115**,** 787-794.

PHOON, WU & PARMLEY 1997. Digoxin's Minimal Inotropic Effect Is Not Limited by Sodium-Calcium Exchange in the Intact Immature Rabbit Heart. *Journal of cardiovascular pharmacology and therapeutics,* 2**,** 97-105.

PILLEKAMP, F., HAUSTEIN, M., KHALIL, M., EMMELHEINZ, M., NAZZAL, R., ADELMANN, R., NGUEMO, F., RUBENCHYK, O., PFANNKUCHE, K., MATZKIES, M., REPPEL, M., BLOCH, W., BROCKMEIER, K. & HESCHELER, J. 2012. Contractile Properties of Early Human Embryonic Stem Cell-Derived Cardiomyocytes: Beta-Adrenergic Stimulation Induces Positive Chronotropy and Lusitropy but Not Inotropy. *Stem Cells and Development,* 21**,** 2111-2121.

PLANELLES-HERRERO, V. J., HARTMAN, J. J., ROBERT-PAGANIN, J., MALIK, F. I. & HOUDUSSE, A. 2017. Mechanistic and structural basis for activation of cardiac myosin force production by omecamtiv mecarbil. *Nature Communications,* 8**,** 10.

POGATSA, G. & DUBECZ, E. 1977. DIRECT EFFECT OF HYPOGLYCEMIC SULFONYLUREAS ON MYOCARDIAL CONTRACTILE-FORCE AND ARTERIAL BLOOD-PRESSURE. *Diabetologia,* 13**,** 515-519.

POGWIZD, S. M., SCHLOTTHAUER, K., LI, L., YUAN, W. & BERS, D. M. 2001. Arrhythmogenesis and Contractile Dysfunction in Heart Failure. *Circulation Research,* 88**,** 1159-1167.

POINTON, A., HARMER, A. R., DALE, I. L., ABI-GERGES, N., BOWES, J., POLLARD, C. & GARSIDE, H. 2015. Assessment of Cardiomyocyte Contraction in Human-Induced Pluripotent Stem Cell-Derived Cardiomyocytes. *Toxicological Sciences,* 144**,** 227-237.

POINTON, A., PILLING, J., DORVAL, T., WANG, Y. H., ARCHER, C. & POLLARD, C. 2017. High-Throughput Imaging of Cardiac Microtissues for the Assessment of Cardiac Contraction during Drug. *Toxicological Sciences,* 155**,** 444-457.

POLLESELLO, P., OVASKA, M., KAIVOLA, J., TILGMANN, C., LUNDSTROM, K., KALKKINEN, N., ULMANEN, I., NISSINEN, E. & TASKINEN, J. 1994. Binding of a new Ca2+

sensitizer, levosimendan, to recombinant human cardiac troponin C. A molecular modelling, fluorescence probe, and proton nuclear magnetic resonance study. *The Journal of biological chemistry,* 269**,** 28584-90.

PONIKOWSKI, P., VOORS, A. A., ANKER, S. D., BUENO, H., CLELAND, J. G. F., COATS, A. J. S., FALK, V., RAMON GONZALEZ-JUANATEY, J., HARJOLA, V.-P., JANKOWSKA, E. A., JESSUP, M., LINDE, C., NIHOYANNOPOULOS, P., PARISSIS, J. T., PIESKE, B., RILEY, J. P., ROSANO, G. M. C., RUILOPE, L. M., RUSCHITZKA, F., RUTTEN, F. H. & VAN DER MEER, P. 2016. 2016 ESC Guidelines for the diagnosis and treatment of acute and chronic heart failure. *European Heart Journal,* 37**,** 2129-U130.

PRABHAKARAN, M. P., MOBARAKEH, L. G., KAI, D., KARBALAIE, K., NASR-ESFAHANI, M. H. & RAMAKRISHNA, S. 2014. Differentiation of embryonic stem cells to cardiomyocytes on electrospun nanofibrous substrates. *Journal of Biomedical Materials Research Part B-Applied Biomaterials,* 102**,** 447-454.

PREININGER, M. K., SINGH, M. & XU, C. H. 2016. Cryopreservation of Human Pluripotent Stem Cell-Derived Cardiomyocytes: Strategies, Challenges, and Future Directions. *In:* KARIMIBUSHERI, F. & WEINFELD, M. (eds.) *Biobanking and Cryopreservation of Stem Cells.* Cham: Springer Int Publishing Ag.

PRICE, P. S., KEENAN, R. E. & SWARTOUT, J. C. 2008. Characterizing interspecies uncertainty using data from studies of anti-neoplastic agents in animals and humans. *Toxicology and Applied Pharmacology,* 233**,** 64-70.

PUTTONEN, J., KANTELE, S., RUCK, A., RAMELA, M., HAKKINEN, S., KIVIKKO, M. & PENTIKAINEN, P. J. 2008. Pharmacokinetics of intravenous levosimendan and its metabolites in subjects with hepatic impairment. *Journal of Clinical Pharmacology,* 48**,** 445-454.

QU, Y. S., FANG, M., GAO, B. X., AMOUZADEH, H. R., LI, N. Y., NARAYANAN, P., ACTON, P., LAWRENCE, J. & VARGAS, H. M. 2013. Itraconazole decreases left ventricular contractility in isolated rabbit heart: Mechanism of action. *Toxicology and Applied Pharmacology,* 268**,** 113-122.

QU, Y. X. & BOUTJDIR, M. 2001. Gene expression of SERCA2a and L- and T-type Ca channels during human heart development. *Pediatric Research,* 50**,** 569-574.

RAAB, S., KLINGENSTEIN, M., LIEBAU, S. & LINTA, L. 2014. A Comparative View on Human Somatic Cell Sources for iPSC Generation. *Stem Cells International***,** 12.

RADKE, M. B., TAFT, M. H., STAPEL, B., HILFIKER-KLEINER, D., PRELLER, M. & MANSTEIN, D. J. 2014. Small molecule-mediated refolding and activation of myosin motor function. 3.

RAJAMOHAN, D., KALRA, S., HOANG, M. D., GEORGE, V., STANIFORTH, A., RUSSELL, H., YANG, X. B. & DENNING, C. 2016. Automated Electrophysiological and Pharmacological Evaluation of Human Pluripotent Stem Cell-Derived Cardiomyocytes. *Stem Cells and Development,* 25**,** 439-452.

RAO, N. 2007. The clinical pharmacokinetics of escitalopram. *Clinical Pharmacokinetics,* 46**,** 281-290.

REDFERN, W. S., CARLSSON, L., DAVIS, A. S., LYNCH, W. G., MACKENZIE, I., PALETHORPE, S., SIEGL, P. K. S., STRANG, I., SULLIVAN, A. T., WALLIS, R., CAMM, A. J. & HAMMOND, T. G. 2003. Relationships between preclinical cardiac electrophysiology, clinical QT interval prolongation and torsade de pointes for a broad range of drugs: evidence for a provisional safety margin in drug development. *Cardiovascular research,* 58**,** 32-45.

REYES, G., SCHWARTZ, P. H., NEWTH, C. J. L. & ELDADAH, M. K. 1993. THE PHARMACOKINETICS OF ISOPROTERENOL IN CRITICALLY ILL PEDIATRIC-PATIENTS. *Journal of Clinical Pharmacology,* 33**,** 29-34.

REYNOLDS, J. G., GERETTI, E., HENDRIKS, B. S., LEE, H., LEONARD, S. C., KLINZ, S. G., NOBLE, C. O., LUCKER, P. B., ZANDSTRA, P. W., DRUMMOND, D. C., OLIVIER, K. J., NIELSEN, U. B., NIYIKIZA, C., AGRESTA, S. V. & WICKHAM, T. J. 2012. HER2-targeted liposomal doxorubicin displays enhanced anti-tumorigenic effects without associated cardiotoxicity. *Toxicology and Applied Pharmacology,* 262**,** 1-10.

RIBEIRO, M. C., TERTOOLEN, L. G., GUADIX, J. A., BELLIN, M., KOSMIDIS, G., D'ANIELLO, C., MONSHOUWER-KLOOTS, J., GOUMANS, M.-J., WANG, Y.-L., FEINBERG, A. W., MUMMERY, C. L. & PASSIER, R. 2015. Functional maturation of human pluripotent stem cell derived cardiomyocytes in vitro - Correlation between contraction force and electrophysiology. *Biomaterials,* 51**,** 138-150.

RICHTER, W., XIE, M., SCHEITRUM, C., KRALL, J., MOVSESIAN, M. A. & CONTI, M. 2011. Conserved expression and functions of PDE4 in rodent and human heart. *Basic research in cardiology,* 106**,** 249-62.

ROBERTSON, C., TRAN, D. D. & GEORGE, S. C. 2013. Concise Review: Maturation Phases of Human Pluripotent Stem Cell-Derived Cardiomyocytes. *Stem Cells,* 31**,** 829-837.
ROCKMAN, H. A., KOCH, W. J. & LEFKOWITZ, R. J. 2002. Seven-transmembrane-spanning receptors and heart function. *Nature,* 415**,** 206-12.
RODRIGUEZ, A. G., RODRIGUEZ, M. L., HAN, S. J., SNIADECKI, N. J. & REGNIER, M. 2013. Enhanced contractility with 2-deoxy-ATP and EMD 57033 is correlated with reduced myofibril structure and twitch power in neonatal cardiomyocytes. *Integrative Biology,* 5**,** 1366.
ROG-ZIELINSKA, E. A., CRAIG, M. A., MANNING, J. R., RICHARDSON, R. V., GOWANS, G. J., DUNBAR, D. R., GHARBI, K., KENYON, C. J., HOLMES, M. C., HARDIE, D. G., SMITH, G. L. & CHAPMAN, K. E. 2015. Glucocorticoids promote structural and functional maturation of foetal cardiomyocytes: a role for PGC-1 alpha. *Cell Death and Differentiation,* 22**,** 1106-1116.
ROG-ZIELINSKA, E. A., RICHARDSON, R. V., DENVIR, M. A. & CHAPMAN, K. E. 2014. Glucocorticoids and foetal heart maturation; implications for prematurity and foetal programming. *Journal of Molecular Endocrinology,* 52**,** R125-R135.
RONALDSON-BOUCHARD, K., MA, S. P., YEAGER, K., CHEN, T., SONG, L. J., SIRABELLA, D., MORIKAWA, K., TELES, D., YAZAWA, M. & VUNJAK-NOVAKOVIC, G. 2018. Advanced maturation of human cardiac tissue grown from pluripotent stem cells. *Nature,* 556**,** 239-+.
ROSEN, M. R., GELBAND, H. & HOFFMAN, B. F. 1971. EFFECTS OF PHENTOLAMINE ON ELECTROPHYSIOLOGIC PROPERTIES OF ISOLATED CANINE PURKINJE FIBERS. *Journal of Pharmacology and Experimental Therapeutics,* 179**,** 586-&.
ROSS, R. S. & BORG, T. K. 2001. Integrins and the myocardium. *Circulation Research,* 88**,** 1112-1119.
ROSS, R. S., PHAM, C., SHAI, S. Y., GOLDHABER, J. I., FENCZIK, C., GLEMBOTSKI, C. C., GINSBERG, M. H. & LOFTUS, J. C. 1998. beta(1) integrins participate in the hypertrophic response of rat ventricular myocytes. *Circulation Research,* 82**,** 1160-1172.
RUFFOLO, R. R. 1985. Distribution and function of peripheral α-adrenoceptors in the cardiovascular system. *Pharmacology Biochemistry and Behavior,* 22**,** 827-833.
RUFFOLO, R. R., JR. 1987. The pharmacology of dobutamine. *The American journal of the medical sciences,* 294**,** 244-8.
RYBIN, V. O., XU, X. H. & STEINBERG, S. F. 1999. Activated protein kinase C isoforms target to cardiomyocyte caveolae - Stimulation of local protein phosphorylation. *Circulation Research,* 84**,** 980-988.
RYDBERG, T., JONSSON, A., KARLSSON, M. O. & MELANDER, A. 1997. Concentration-effect relations of glibenclamide and its active metabolites in man: Modelling of pharmacokinetics and pharmacodynamics. *British Journal of Clinical Pharmacology,* 43**,** 373-381.
SADA, H. 1978. EFFECT OF PHENTOLAMINE, ALPRENOLOL AND PRENYLAMINE ON MAXIMUM RATE OF RISE OF ACTION POTENTIAL IN GUINEA-PIG PAPILLARY-MUSCLES. *Naunyn-Schmiedebergs Archives of Pharmacology,* 304**,** 191-201.
SAG, C. M., KÖHLER, A. C., ANDERSON, M. E., BACKS, J. & MAIER, L. S. 2011. CaMKII-dependent SR Ca leak contributes to doxorubicin-induced impaired Ca handling in isolated cardiac myocytes. *Journal of Molecular and Cellular Cardiology,* 51**,** 749-759.
SAGER, P. T., GINTANT, G., TURNER, J. R., PETTIT, S. & STOCKBRIDGE, N. 2014. Rechanneling the cardiac proarrhythmia safety paradigm: A meeting report from the Cardiac Safety Research Consortium. *American Heart Journal,* 167**,** 292-300.
SALA, L., VAN MEER, B. J., TERTOOLEN, L. G. J., BAKKERS, J., BELLIN, M., DAVIS, R. P., DENNING, C., DIEBEN, M. A. E., ESCHENHAGEN, T., GIACOMELLI, E., GRANDELA, C., HANSEN, A., HOLMAN, E. R., JONGBLOED, M. R. M., KAMEL, S. M., KOOPMAN, C. D., LACHAUD, Q., MANNHARDT, I., MOL, M. P. H., MOSQUEIRA, D., ORLOVA, V. V., PASSIER, R., RIBEIRO, M. C., SALEEM, U., SMITH, G. L., BURTON, F. L. & MUMMERY, C. L. 2018. MUSCLEMOTION: A Versatile Open Software Tool to Quantify Cardiomyocyte and Cardiac Muscle Contraction In Vitro and In Vivo. *Circulation Research,* 122**,** e5-e16.
SALAMA, G. & LONDON, B. 2007. Mouse models of long QT syndrome. *Journal of Physiology-London,* 578**,** 43-53.
SALAMEH, A., WUSTMANN, A., KARL, S., BLANKE, K., APEL, D., ROJAS-GOMEZ, D., FRANKE, H., MOHR, F. W., JANOUSEK, J. & DHEIN, S. 2010. Cyclic Mechanical Stretch Induces Cardiomyocyte Orientation and Polarization of the Gap Junction Protein Connexin43. *Circulation Research,* 106**,** 1592-1602.

SAMAREL, A. M. 2005. Costameres, focal adhesions, and cardiomyocyte mechanotransduction. *American Journal of Physiology-Heart and Circulatory Physiology,* 289**,** H2291-H2301.
SATIN, J., ITZHAKI, I., RAPOPORT, S., SCHRODER, E. A., IZU, L., ARBEL, G., BEYAR, R., BALKE, C. W., SCHILLER, J. & GEPSTEIN, L. 2008. Calcium handling in human embryonic stem cell-derived cardiomyocytes. *Stem Cells,* 26**,** 1961-1972.
SATOH, E., YANAGISAWA, T. & TAIRA, N. 1990. SPECIFIC ANTAGONISM BY GLIBENCLAMIDE OF NEGATIVE INOTROPIC EFFECTS OF POTASSIUM CHANNEL OPENERS IN CANINE ATRIAL MUSCLE. *Japanese Journal of Pharmacology,* 54**,** 133-141.
SCHAAF, S., SHIBAMIYA, A., MEWE, M., EDER, A., STOHR, A., HIRT, M. N., RAU, T., ZIMMERMANN, W. H., CONRADI, L., ESCHENHAGEN, T. & HANSEN, A. 2011. Human Engineered Heart Tissue as a Versatile Tool in Basic Research and Preclinical Toxicology. *Plos One,* 6**,** 11.
SCHACHTER, A. D. & RAMONI, M. F. 2007. From the analyst's couch - Clinical forecasting in drug development. *Nature Reviews Drug Discovery,* 6**,** 107-108.
SCHAFERS, R. F., ADLER, S., DAUL, A., ZEITLER, G., VOGELSANG, M., ZERKOWSKI, H. R. & BRODDE, O. E. 1994. POSITIVE INOTROPIC EFFECTS OF THE BETA(2)-ADRENOCEPTOR AGONIST TERBUTALINE IN THE HUMAN HEART - EFFECTS OF LONG-TERM BETA(1)-ADRENOCEPTOR ANTAGONIST TREATMENT. *Journal of the American College of Cardiology,* 23**,** 1224-1233.
SCHLECHT, W., LI, K.-L., HU, D. & DONG, W. 2016. Fluorescence Based Characterization of Calcium Sensitizer Action on the Troponin Complex. *Chemical Biology & Drug Design,* 87**,** 171-181.
SCHWINGER, R. H., BOHM, M. & ERDMANN, E. 1990. Negative inotropic properties of isradipine, nifedipine, diltiazem, and verapamil in diseased human myocardial tissue. *Journal of cardiovascular pharmacology,* 15**,** 892-9.
SCOTT, C. W., ZHANG, X., ABI-GERGES, N., LAMORE, S. D., ABASSI, Y. A. & PETERS, M. F. 2014. An impedance-based cellular assay using human iPSC-derived cardiomyocytes to quantify modulators of cardiac contractility. *Toxicological sciences : an official journal of the Society of Toxicology,* 142**,** 331-8.
SEQUEIRA, V. & VAN DER VELDEN, J. 2015. Historical perspective on heart function: the Frank–Starling Law. *Biophysical Reviews,* 7**,** 421-447.
SHAH, R. R. 2006. Can pharmacogenetics help rescue drugs withdrawn from the market? *Pharmacogenomics,* 7**,** 889-908.
SHIBATA, E. F., DRURY, T., REFSUM, H., ALDRETE, V. & GILES, W. 1989. Contributions of a transient outward current to repolarization in human atrium. *The American journal of physiology,* 257**,** H1773-81.
SINGH, K., XIAO, L., REMONDINO, A., SAWYER, D. B. & COLUCCI, W. S. 2001. Adrenergic regulation of cardiac myocyte apoptosis. *Journal of Cellular Physiology,* 189**,** 257-265.
SINGH, R., MORENO, P., HAJJAR, R. J. & LEBECHE, D. 2018. A role for calcium in resistin transcriptional activation in diabetic hearts. *Scientific Reports,* 8**,** 14.
SIRENKO, O., CROMWELL, E. F., CRITTENDEN, C., WIGNALL, J. A., WRIGHT, F. A. & RUSYN, I. 2013. Assessment of beating parameters in human induced pluripotent stem cells enables quantitative in vitro screening for cardiotoxicity. *Toxicology and Applied Pharmacology,* 273**,** 500-507.
SIRTORI, C. R. 2014. The pharmacology of statins. *Pharmacological research,* 88**,** 3-11.
SLAWSKY, M. T., COLUCCI, W. S., GOTTLIEB, S. S., GREENBERG, B. H., HAEUSSLEIN, E., HARE, J., HUTCHINS, S., LEIER, C. V., LEJEMTEL, T. H., LOH, E., NICKLAS, J., OGILBY, D., SINGH, B. N. & SMITH, W. 2000. Acute Hemodynamic and Clinical Effects of Levosimendan in Patients With Severe Heart Failure. 102**,** 2222-2227.
SMITH, J. G. W., OWEN, T., BHAGWAN, J. R., MOSQUEIRA, D., SCOTT, E., MANNHARDT, I., PATEL, A., BARRIALES-VILLA, R., MONSERRAT, L., HANSEN, A., ESCHENHAGEN, T., HARDING, S. E., MARSTON, S. & DENNING, C. 2018. Isogenic Pairs of hiPSC-CMs with Hypertrophic Cardiomyopathy/LVNC-Associated ACTCI E99K Mutation Unveil Differential Functional Deficits. *Stem Cell Reports,* 11**,** 1226-1243.
SOMMER, G., SCHRIEFL, A. J., ANDRÄ, M., SACHERER, M., VIERTLER, C., WOLINSKI, H. & HOLZAPFEL, G. A. 2015. Biomechanical properties and microstructure of human ventricular myocardium. *Acta Biomaterialia,* 24**,** 172-192.
SPACH, M. S., HEIDLAGE, I. F., BARR, R. C. & DOLBER, P. C. 2004. Cell size and communication: Role in structural and electrical development and remodeling of the heart. *Heart Rhythm,* 1**,** 500-515.

STAGE, C., JURGENS, G., GUSKI, L. S., THOMSEN, R., BJERRE, D., FERRERO-MILIANI, L., LYAUK, Y. K., RASMUSSEN, H. B., DALHOFF, K. & CONSORTIUM, I. 2017. The Pharmacokinetics of Enalapril in Relation to CES1 Genotype in Healthy Danish Volunteers. *Basic & Clinical Pharmacology & Toxicology,* 121**,** 487-492.

STOPPEL, W. L., KAPLAN, D. L. & BLACK, L. D., 3RD 2016. Electrical and mechanical stimulation of cardiac cells and tissue constructs. *Advanced drug delivery reviews,* 96**,** 135-55.

SUGIYAMA, A., SATOH, Y., SHIINA, H., TAKAHARA, A., YONEYAMA, M. & HASHIMOTO, K. 2001. Cardiac electrophysiologic and hemodynamic effects of sildenafil, a PDE5 inhibitor, in anesthetized dogs. *Journal of Cardiovascular Pharmacology,* 38**,** 940-946.

SUTKO, J. L. & WILLERSON, J. T. 1980. RYANODINE ALTERATION OF THE CONTRACTILE STATE OF RAT VENTRICULAR MYOCARDIUM - COMPARISON WITH DOG, CAT, AND RABBIT VENTRICULAR TISSUES. *Circulation Research,* 46**,** 332-343.

SZILAGYI, S., POLLESELLO, P., LEVIJOKI, J., KAHEINEN, P., HAIKALA, H., EDES, I. & PAPP, Z. 2004. The effects of levosimendan and OR-1896 on isolated hearts, myocyte-sized preparations and phosphodiesterase enzymes of the guinea pig. *European Journal of Pharmacology,* 486**,** 67-74.

TADDEI, M. L., GIANNONI, E., FIASCHI, T. & CHIARUGI, P. 2012. Anoikis: an emerging hallmark in health and diseases. *Journal of Pathology,* 226**,** 380-393.

TADINI-BUONINSEGNI, F., SMEAZZETTO, S., GUALDANI, R. & MONCELLI, M. R. 2018. Drug Interactions With the Ca2+-ATPase From Sarco(Endo)Plasmic Reticulum (SERCA). *Frontiers in Molecular Biosciences,* 5**,** 8.

TAKAHASHI, K., TANABE, K., OHNUKI, M., NARITA, M., ICHISAKA, T., TOMODA, K. & YAMANAKA, S. 2007. Induction of pluripotent stem cells from adult human fibroblasts by defined factors. *Cell,* 131**,** 861-872.

TALLAWI, M., RAI, R., BOCCACCINI, A. R. & AIFANTIS, K. E. 2015. Effect of Substrate Mechanics on Cardiomyocyte Maturation and Growth. *Tissue Engineering Part B-Reviews,* 21**,** 157-165.

TAMARIZ, L. J. & BASS, E. B. 2004. Pharmacological rate control of atrial fibrillation. *Cardiology clinics,* 22**,** 35-45.

TEERLINK, J. R., CLARKE, C. P., SAIKALI, K. G., LEE, J. H., CHEN, M. M., ESCANDON, R. D., ELLIOTT, L., BEE, R., HABIBZADEH, M. R., GOLDMAN, J. H., SCHILLER, N. B., MALIK, F. I. & WOLFF, A. A. 2011. Dose-dependent augmentation of cardiac systolic function with the selective cardiac myosin activator, omecamtiv mecarbil: a first-in-man study. *Lancet,* 378**,** 667-675.

TEMMA, K., AKERA, T., CHUGUN, A., KONDO, H., HAGANE, K. & HIRANO, S. 1993. COMPARISON OF CARDIAC ACTIONS OF DOXORUBICIN, PIRARUBICIN AND ACLARUBICIN IN ISOLATED GUINEA-PIG HEART. *European Journal of Pharmacology,* 234**,** 173-181.

TERAMURA, S. & YAMAKADO, T. 1998. Calcium sensitizers in chronic heart failure: inotropic interventions-reservation to preservation. *Cardiologia (Rome, Italy),* 43**,** 375-85.

TERRENOIRE, C., WANG, K., TUNG, K. W. C., CHUNG, W. K., PASS, R. H., LU, J. T., JEAN, J. C., OMARI, A., SAMPSON, K. J., KOTTON, D. N., KELLER, G. & KASS, R. S. 2013. Induced pluripotent stem cells used to reveal drug actions in a long QT syndrome family with complex genetics. *Journal of General Physiology,* 141**,** 61-72.

TERTOOLEN, L. G. J., BRAAM, S. R., VAN MEER, B. J., PASSIER, R. & MUMMERY, C. L. 2018. Interpretation of field potentials measured on a multi electrode array in pharmacological toxicity screening on primary and human pluripotent stem cell-derived cardiomyocytes. *Biochemical and Biophysical Research Communications,* 497**,** 1135-1141.

THAVANDIRAN, N., DUBOIS, N., MIKRYUKOV, A., MASSE, S., BECA, B., SIMMONS, C. A., DESHPANDE, V. S., MCGARRY, J. P., CHEN, C. S., NANTHAKUMAR, K., KELLER, G. M., RADISIC, M. & ZANDSTRA, P. W. 2013. Design and formulation of functional pluripotent stem cell-derived cardiac microtissues. *Proceedings of the National Academy of Sciences of the United States of America,* 110**,** E4698-E4707.

TILLEY, D. G. 2011. G Protein–Dependent and G Protein–Independent Signaling Pathways and Their Impact on Cardiac Function. *Circulation Research,* 109**,** 217-230.

TODAKA, K., WANG, J., YI, G. H., STENNETT, R., KNECHT, M., PACKER, M. & BURKHOFF, D. 1996. Effects of levosimendan on myocardial contractility and oxygen consumption. *The Journal of pharmacology and experimental therapeutics,* 279**,** 120-7.

TOLMAN, K. G. 2002. The liver and lovastatin. *The American Journal of Cardiology,* 89**,** 1374-1380.

TORRETTI, J., WEINSTEI.E, EPSTEIN, F. H., HENDLER, E. & LONGNECK.RE 1972. FUNCTIONAL SIGNIFICANCE OF NA-ATPASE, K-ATPASE IN KIDNEY - EFFECTS OF OUABAIN INHIBITION. *American Journal of Physiology,* 222**,** 1398-&.

TRAISTER, A., LI, M., AAFAQI, S., LU, M. L., ARAB, S., RADISIC, M., GROSS, G., GUIDO, F., SHERRET, J., VERMA, S., SLORACH, C., MERTENS, L., HUI, W., ROY, A., DELGADO-OLGUIN, P., HANNIGAN, G., MAYNES, J. T. & COLES, J. G. 2014. Integrin-linked kinase mediates force transduction in cardiomyocytes by modulating SERCA2a/PLN function. *Nature Communications,* 5**,** 11.

TREPAT, X., DENG, L., AN, S. S., NAVAJAS, D., TSCHUMPERLIN, D. J., GERTHOFFER, W. T., BUTLER, J. P. & FREDBERG, J. J. 2007. Universal physical responses to stretch in the living cell. *Nature,* 447**,** 592-+.

TULLOCH, N. L., MUSKHELI, V., RAZUMOVA, M. V., KORTE, F. S., REGNIER, M., HAUCH, K. D., PABON, L., REINECKE, H. & MURRY, C. E. 2011. Growth of Engineered Human Myocardium With Mechanical Loading and Vascular Coculture. *Circulation Research,* 109**,** 47-U195.

TUTTLE, R. R. & MILLS, J. 1975. Dobutamine: development of a new catecholamine to selectively increase cardiac contractility. 36**,** 185-196.

TZATZALOS, E., ABILEZ, O. J., SHUKLA, P. & WU, J. C. 2016. Engineered heart tissues and induced pluripotent stem cells: Macro- and microstructures for disease modeling, drug screening, and translational studies. *Advanced drug delivery reviews,* 96**,** 234-44.

UZUN, A. U., MANNHARDT, I., BRECKWOLDT, K., HORVATH, A., JOHANNSEN, S. S., HANSEN, A., ESCHENHAGEN, T. & CHRIST, T. 2016. Ca2+-Currents in Human Induced Pluripotent Stem Cell-Derived Cardiomyocytes Effects of Two Different Culture Conditions. *Frontiers in Pharmacology,* 7**,** 14.

VALENTIN, J.-P., BIALECKI, R., EWART, L., HAMMOND, T., LEISHMANN, D., LINDGREN, S., MARTINEZ, V., POLLARD, C., REDFERN, W. & WALLIS, R. 2009. A framework to assess the translation of safety pharmacology data to humans. *Journal of Pharmacological and Toxicological Methods,* 60**,** 152-158.

VAN MEER, B. J., DE VRIES, H., FIRTH, K. S. A., VAN WEERD, J., TERTOOLEN, L. G. J., KARPERIEN, H. B. J., JONKHEIJM, P., DENNING, C., IJZERMAN, A. P. & MUMMERY, C. L. 2017. Small molecule absorption by PDMS in the context of drug response bioassays. *Biochemical and Biophysical Research Communications,* 482**,** 323-328.

VAN MEER, B. J., KROTENBERG, A., SALA, L., DAVIS, R. P., ESCHENHAGEN, T., DENNING, C., TERTOOLEN, L. G. J. & MUMMERY, C. L. 2019. Simultaneous measurement of excitation-contraction coupling parameters identifies mechanisms underlying contractile responses of hiPSC-derived cardiomyocytes. *Nature Communications,* 10**,** 9.

VAN MEER, B. J., TERTOOLEN, L. G. J. & MUMMERY, C. L. 2016. Concise Review: Measuring Physiological Responses of Human Pluripotent Stem Cell Derived Cardiomyocytes to Drugs and Disease. *Stem Cells,* 34**,** 2008-2015.

VANBOXTEL, C. J., OLSON, R. D., BOERTH, R. C. & OATES, J. A. 1978. DOXORUBICIN - INOTROPIC EFFECTS AND INHIBITORY ACTION ON OUABAIN. *Journal of Pharmacology and Experimental Therapeutics,* 207**,** 277-283.

VASSALLE, M. 1971. AUTOMATICITY AND AUTOMATIC RHYTHMS. *American Journal of Cardiology,* 28**,** 245-&.

VEERMAN, C. C., KOSMIDIS, G., MUMMERY, C. L., CASINI, S., VERKERK, A. O. & BELLIN, M. 2015. Immaturity of Human Stem-Cell-Derived Cardiomyocytes in Culture: Fatal Flaw or Soluble Problem? *Stem Cells and Development,* 24**,** 1035-1052.

VETULLI, H. M., ELIZARI, M. V., NACCARELLI, G. V. & GONZALEZ, M. D. 2018. Cardiac automaticity: basic concepts and clinical observations. *Journal of Interventional Cardiac Electrophysiology,* 52**,** 263-270.

VOLLERT, I., SEIFFERT, M., BACHMAIR, J., SANDER, M., EDER, A., CONRADI, L., VOGELSANG, A., SCHULZE, T., UEBELER, J., HOLNTHONER, W., REDL, H., REICHENSPURNER, H., HANSEN, A. & ESCHENHAGEN, T. 2014. In Vitro Perfusion of Engineered Heart Tissue Through Endothelialized Channels. *Tissue Engineering Part A,* 20**,** 854-863.

VOZZI, C., DUPONT, E., COPPEN, S. R., YEH, H. I. & SEVERS, N. J. 1999. Chamber-related differences in connexin expression in the human heart. *Journal of Molecular and Cellular Cardiology,* 31**,** 991-1003.

WAGNER, S., MAIER, L. S. & BERS, D. M. 2015. Role of Sodium and Calcium Dysregulation in Tachyarrhythmias in Sudden Cardiac Death. 116**,** 1956-1970.

WALKER, D. K., ACKLAND, M. J., JAMES, G. C., MUIRHEAD, G. J., RANCE, D. J., WASTALL, P. & WRIGHT, P. A. 1999. Pharmacokinetics and metabolism of sildenafil in mouse, rat, rabbit, dog and man. *Xenobiotica,* 29**,** 297-310.

WALLIS, R., GHARANEI, M. & MADDOCK, H. 2015. Predictivity of in vitro non-clinical cardiac contractility assays for inotropic effects in humans - A literature search. *Journal of Pharmacological and Toxicological Methods,* 75**,** 62-69.

WANG, X. F., LIN, G., MARTINS-TAYLOR, K., ZENG, H. & XU, R. H. 2009. Inhibition of Caspase-mediated Anoikis Is Critical for Basic Fibroblast Growth Factor-sustained Culture of Human Pluripotent Stem Cells. *Journal of Biological Chemistry,* 284**,** 34054-34064.

WANG, Y. X. & KORTH, M. 1995. EFFECTS OF DOXORUBICIN ON EXCITATION-CONTRACTION COUPLING IN GUINEA-PIG VENTRICULAR MYOCARDIUM. *Circulation Research,* 76**,** 645-653.

WATANABE, K., UENO, M., KAMIYA, D., NISHIYAMA, A., MATSUMURA, M., WATAYA, T., TAKAHASHI, J. B., NISHIKAWA, S., MUGURUMA, K. & SASAI, Y. 2007. A ROCK inhibitor permits survival of dissociated human embryonic stem cells. *Nature Biotechnology,* 25**,** 681-686.

WEINBERGER, F., MANNHARDT, I. & ESCHENHAGEN, T. 2017. Engineering Cardiac Muscle Tissue A Maturating Field of Research. *Circulation Research,* 120**,** 1487-1500.

WEISS, J. N., QU, Z., CHEN, P.-S., LIN, S.-F., KARAGUEUZIAN, H. S., HAYASHI, H., GARFINKEL, A. & KARMA, A. 2005. The Dynamics of Cardiac Fibrillation. *Circulation,* 112**,** 1232-1240.

WHITING, B., WILLIAMS, R. L., LORENZI, M., VARADY, J. C. & ROBINS, D. S. 1981. EFFECT OF NAPROXEN ON GLUCOSE-METABOLISM AND TOLBUTAMIDE KINETICS AND DYNAMICS IN MATURITY ONSET DIABETICS. *British Journal of Clinical Pharmacology,* 11**,** 295-302.

WILLIAMS, R. S. & BISHOP, T. 1981. Selectivity of Dobutamine for Adrenergic Receptor Subtypes. *Journal of Clinical Investigation,* 67**,** 1703-1711.

WINSLOW, R. L., HINCH, R. & GREENSTEIN, J. L. 2005. Mechanisms and models of cardiac excitation-contraction coupling. *Tutorials in Mathematical Biosciences Ii,* 1867**,** 97-131.

WIT, A. L. & CRANEFIELD, P. F. 1977. Triggered and automatic activity in the canine coronary sinus. *Circulation research,* 41**,** 434-45.

WITCHEL, H. J., PABBATHI, V. K., HOFMANN, G., PAUL, A. A. & HANCOX, J. C. 2002. Inhibitory actions of the selective serotonin re-uptake inhibitor citalopram on HERG and ventricular L-type calcium currents. *Febs Letters,* 512**,** 59-66.

WORTSMAN, J., FRANK, S. & CRYER, P. E. 1984. ADRENOMEDULLARY RESPONSE TO MAXIMAL STRESS IN HUMANS. *American Journal of Medicine,* 77**,** 779-784.

WU, X., SUN, Z., FOSKETT, A., TRZECIAKOWSKI, J. P., MEININGER, G. A. & MUTHUCHAMY, M. 2010. Cardiomyocyte contractile status is associated with differences in fibronectin and integrin interactions. *American Journal of Physiology-Heart and Circulatory Physiology,* 298**,** H2071-H2081.

XU, C. H., POLICE, S., HASSANIPOUR, M., LI, Y., CHEN, Y. H., PRIEST, C., O'SULLIVAN, C., LAFLAMME, M. A., ZHU, W. Z., VAN BIBER, B., HEGEROVA, L., YANG, J. W., DELAVAN-BOORSMA, K., DAVIES, A., LEBKOWSKI, J. & GOLD, J. D. 2011. Efficient generation and cryopreservation of cardiomyocytes derived from human embryonic stem cells. *Regenerative Medicine,* 6**,** 53-66.

XUE, Y. T., CAI, X. J., WANG, L. L., LIAO, B. J., ZHANG, H., SHAN, Y. L., CHEN, Q. Y., ZHOU, T. C., LI, X. R., HOU, J. D., CHEN, S. B., LUO, R. P., QIN, D. J., PEI, D. Q. & PAN, G. J. 2013. Generating a Non-Integrating Human Induced Pluripotent Stem Cell Bank from Urine-Derived Cells. *Plos One,* 8**,** 7.

YANG, X., PABON, L. & MURRY, C. E. 2014a. Engineering Adolescence Maturation of Human Pluripotent Stem Cell-Derived Cardiomyocytes. *Circulation Research,* 114**,** 511-523.

YANG, X., RODRIGUEZ, M., PABON, L., FISCHER, K. A., REINECKE, H., REGNIER, M., SNIADECKI, N. J., RUOHOLA-BAKER, H. & MURRY, C. E. 2014b. Tri-iodo-L-thyronine promotes the maturation of human cardiomyocytes-derived from induced pluripotent stem cells. *Journal of Molecular and Cellular Cardiology,* 72**,** 296-304.

YOKOO, N., BABA, S., KAICHI, S., NIWA, A., MIMA, T., DOI, H., YAMANAKA, S., NAKAHATA, T. & HEIKE, T. 2009. The effects of cardioactive drugs on cardiomyocytes derived from human induced pluripotent stem cells. *Biochemical and Biophysical Research Communications,* 387**,** 482-488.

YOKOSHIKI, H. & SPERELAKIS, N. 2003. Vasodilating mechanisms of levosimendan. *Cardiovascular Drugs and Therapy,* 17**,** 111-113.

YOU, J., MOON, H., LEE, B. Y., JIN, J. Y., CHANG, Z. E., KIM, S. Y., PARK, J., HWANG, Y.-S. & KIM, J. 2014. Cardiomyocyte sensor responsive to changes in physical and chemical environments. *Journal of biomechanics,* 47**,** 400-9.
ZHANG, G. Q., WEI, H., LU, J., WONG, P. & SHIM, W. 2013. Identification and Characterization of Calcium Sparks in Cardiomyocytes Derived from Human Induced Pluripotent Stem Cells. *Plos One,* 8.
ZHANG, X.-D., COULIBALY, Z. A., CHEN, W. C., LEDFORD, H. A., LEE, J. H., SIRISH, P., DAI, G., JIAN, Z., CHUANG, F., BRUST-MASCHER, I., YAMOAH, E. N., CHEN-IZU, Y., IZU, L. T. & CHIAMVIMONVAT, N. 2018. Coupling of SK channels, L-type Ca2+ channels, and ryanodine receptors in cardiomyocytes. *Scientific Reports,* 8.
ZHANG, Y., MIGNONE, J. & MACLELLAN, W. R. 2015. CARDIAC REGENERATION AND STEM CELLS. *Physiological Reviews,* 95**,** 1189-1204.
ZHAO, Y., RAFATIAN, N., FERIC, N. T., COX, B. J., ASCHAR-SOBBI, R., WANG, E. Y., AGGARWAL, P., ZHANG, B., CONANT, G., RONALDSON-BOUCHARD, K., PAHNKE, A., PROTZE, S., LEE, J. H., HUYER, L. D., JEKIC, D., WICKELER, A., NAGUIB, H. E., KELLER, G. M., VUNJAK-NOVAKOVIC, G., BROECKEL, U., BACKX, P. H. & RADISIC, M. 2019. A Platform for Generation of Chamber-Specific Cardiac Tissues and Disease Modeling. *Cell,* 176**,** 913-+.
ZHUANG, J. P., YAMADA, K. A., SAFFITZ, J. E. & KLEBER, A. G. 2000. Pulsatile stretch remodels cell-to-cell communication in cultured myocytes. *Circulation Research,* 87**,** 316-322.
ZIMAN, A. P., LETICIA GOMEZ-VIQUEZ, N., BLOCH, R. J. & LEDERER, W. J. 2010. Excitation-contraction coupling changes during postnatal cardiac development. *Journal of Molecular and Cellular Cardiology,* 48**,** 379-386.
ZUPPINGER, C. 2016. 3D culture for cardiac cells. *Biochimica Et Biophysica Acta-Molecular Cell Research,* 1863**,** 1873-1881.

Appendix – Publications

Articles

Saleem, U., van Meer, B.J., Katili, P.A., Mohd Yusof, N.A.N, Mannhardt, I., Garcia, A.K., Tertoolen, L., de Korte, T., Vlaming, M.L.H., McGlynn, K., et al. (2019). Blinded, multi-centre evaluation of drug-induced changes in contractility using human induced pluripotent stem cell-derived cardiomyocytes. (Manuscript submitted to Toxicological Sciences)

de Korte, T., Katili, P.A., Mohd Yusof, N.A.N., van Meer, B.J., Saleem, U., Burton, F.L., Smith, G.L., Clements, P., Mummery, C.L., Eschenhagen, T., et al. (2019). Unlocking Personalized Biomedicine and Drug Discovery with Human Induced Pluripotent Stem Cell-Derived Cardiomyocytes: Fit for Purpose or Forever Elusive? Annual review of pharmacology and toxicology. (IF: 13.295 (2018))

Mosqueira, D., Mannhardt, I., Bhagwan, J.R., Lis-Slimak, K., Katili, P.A., Scott, E., Hassan, M., Prondzynski, M., Harmer, S.C., Tinker, A., et al. (2018). CRISPR/Cas9 editing in human pluripotent stemcell-cardiomyocytes highlights arrhythmias, hypocontractility, and energy depletion as potential therapeutic targets for

hypertrophic cardiomyopathy. European Heart Journal 39, 3879-+. (IF: 23.425 (2018))

Conference abstracts

Katili, P.A., Hoang, M.D., Hortigon, M., Rodriguez, V.Z., Smith, G., Denning, C., George, V.T. Mature cardiomyocytes on engineered 3D substrates for modelling and modulating cardiac hypertrophy. Heart Failure Association of the European Society of Cardiology Winter Meeting 2017. Les Diablerets, Switzerland. January 2017.